



HAL
open science

Probing entanglement on quantum platforms using randomized measurements

Aniket Rath

► **To cite this version:**

Aniket Rath. Probing entanglement on quantum platforms using randomized measurements. Physics [physics]. Université Grenoble Alpes [2020-..], 2023. English. NNT : 2023GRALY072 . tel-04523142

HAL Id: tel-04523142

<https://theses.hal.science/tel-04523142>

Submitted on 27 Mar 2024

HAL is a multi-disciplinary open access archive for the deposit and dissemination of scientific research documents, whether they are published or not. The documents may come from teaching and research institutions in France or abroad, or from public or private research centers.

L'archive ouverte pluridisciplinaire **HAL**, est destinée au dépôt et à la diffusion de documents scientifiques de niveau recherche, publiés ou non, émanant des établissements d'enseignement et de recherche français ou étrangers, des laboratoires publics ou privés.

THÈSE

Pour obtenir le grade de

DOCTEUR DE L'UNIVERSITÉ GRENOBLE ALPES

École doctorale : PHYS - Physique

Spécialité : Physique Théorique

Unité de recherche : Laboratoire de Physique et de Modélisation des Milieux Condensés

**Sonder l'intrication sur des plateformes quantiques à l'aide de
mesures aléatoires**

**Probing entanglement on quantum platforms using randomized
measurements**

Présentée par :

Aniket RATH

Direction de thèse :

Cyril BRANCIARD

CHARGE DE RECHERCHE HDR, CNRS DELEGATION ALPES

Directeur de thèse

Benoit VERMERSCH

MAITRE DE CONFERENCES HDR, UNIVERSITE GRENOBLE ALPES

Co-directeur de thèse

Rapporteurs :

ANTONIO ACIN DALMASCHIO

PROFESSEUR, INSTITUTE OF PHOTONIC

SHANNON WHITLOCK

PROFESSEUR DES UNIVERSITES, UNIVERSITE DE STRASBOURG

Thèse soutenue publiquement le **14 novembre 2023**, devant le jury composé de :

FRANCK BALESTRO,

PROFESSEUR DES UNIVERSITES, UNIVERSITE GRENOBLE
ALPES

Président

ANTONIO ACIN DALMASCHIO,

PROFESSEUR, INSTITUTE OF PHOTONIC

Rapporteur

SHANNON WHITLOCK,

PROFESSEUR DES UNIVERSITES, UNIVERSITE DE
STRASBOURG

Rapporteur

LEONARDO MAZZA,

MAITRE DE CONFERENCES HDR, UNIVERSITE PARIS-SACLAY

Examineur

CECILIA LANCIEN,

CHARGE DE RECHERCHE, CNRS DELEGATION ALPES

Examinatrice



Abstract

There have been recently significant progress in quantum technologies to realize physically diverse quantum computation and simulation platforms. The aim of this thesis is to develop theoretical approaches based on measurement protocols to experimentally characterize quantum entanglement generated in these state-of-art quantum technological platforms. In the past few years, protocols belonging to the *randomized measurement toolbox* (RM toolbox) have shown to have the ability to measure bipartite entanglement (entanglement between two parts of a quantum system). These protocols have been implemented in several experimental platforms consisting of quantum simulators and quantum computers beyond the regime of full state tomography. In this manuscript, we principally report the development of new approaches based on the RM toolbox to provide experimental groups with advanced tools and methods to probe new fundamental quantities of interest related to entanglement prepared in large quantum platforms.

The first objective of this thesis is to provide a new protocol to optimize the existing RM protocol by reducing statistical errors in the estimated quantities. This is done with two approaches: (i) via importance sampling of randomized measurements and (ii) by implementing common randomized measurements. These techniques automatically enable us to implement the RM toolbox to estimate properties associated to entanglement on larger experimental platforms. Then, a central part of this work proposes an alternate effective protocol to measure an important quantity known as the *quantum Fisher information* (QFI) that enables us to characterize the multipartite entanglement content of the underlying quantum state and is a fundamental quantity in quantum metrology. This novel protocol is based on estimating the QFI via the RM toolbox, as a converging series of lower bound polynomials of the density matrix.

Additionally, the manuscript also focuses on solving a practical bottleneck of the current RM toolbox caused by the over-burdening classical cost to post-process experimental RM data to evaluate unbiased estimations of relevant quantities. This motivates the introduction of the *batch shadow formalism* that circumvents this problem and provides an efficient data treatment technique with rigorous performance guarantees to get estimates of quantities accessible from experimental RM data. Lastly, owing to these developments of the RM toolbox, the manuscript reports estimation of some quantities that were accessed for the first time by experimental implementation of this toolbox on two different architectures of quantum platform consisting of superconducting qubits and trapped ions.

Keywords: *Randomized measurements, Entanglement, Quantum Fisher information, Classical shadow formalism, Experimental protocols.*

Résumé

La technologie quantique a fait des progrès significatifs dans la réalisation de diverses plateformes de calcul et de simulation quantiques. L'objectif de cette thèse est de développer des approches théoriques pour comprendre le rôle de l'intrication dans les systèmes quantiques, et de proposer des protocoles de mesure pour sonder expérimentalement ces concepts dans ces plateformes technologiques quantiques courantes. Ces dernières années, des protocoles appartenant aux *mesures aléatoires* (randomized measurement toolbox or RM toolbox) ont montré leur capacité à mesurer l'intrication bipartite (intrication entre deux parties d'un système quantique). Ces protocoles ont été mis en œuvre dans plusieurs plateformes expérimentales composées de simulateurs et d'ordinateurs quantiques. Ce manuscrit rapporte principalement le développement de nouvelles approches basées sur cette toolbox afin de fournir aux groupes expérimentaux des outils avancés de mesure de l'intrication en mesurant des nouvelles quantités fondamentales d'intérêt liées à l'intrication préparée dans les plateformes quantiques.

Le premier objectif de cette thèse est de fournir un nouveau protocole pour optimiser le protocole RM existant en réduisant les erreurs statistiques dans l'estimation des quantités. Ceci est fait avec deux approches : (i) via l'échantillonnage d'importance des unitaires aléatoires locales et (ii) en mettant en œuvre des mesures aléatoires communes (common randomized measurements). Ces techniques nous permettent d'implémenter automatiquement la boîte à outils RM (RM toolbox) pour estimer les propriétés associées à l'intrications sur de plus grandes plateformes expérimentales. Ensuite, une partie centrale de ce travail propose un protocole alternatif efficace pour mesurer une quantité fondamentale en métrologie quantique connue comme *information quantique de Fisher* (quantum Fisher information) qui nous permet de caractériser le contenu de l'intrication multipartite de l'état quantique. Ce protocole est basé sur l'estimation de l'information quantique de Fisher via la boîte à outils RM, en tant qu'une série convergente de polynômes de la matrice de densité.

En outre, le manuscrit se concentre également sur la résolution d'un problème pratique de la boîte à outils RM actuelle, causé par le coût classique excessif du post-traitement des données RM expérimentales afin d'évaluer des estimations non biaisées des quantités d'intérêt. Cela motive l'introduction du *formalisme de batch shadows* et fournit une technique de traitement des données efficace avec des garanties de performance rigoureuses pour obtenir des estimations des quantités accessibles à partir des données RM expérimentales. Enfin, en raison de ces développements de la boîte à outils RM, le manuscrit discute également des quantités qui ont été accessibles pour la première fois par la mise en œuvre expérimentale de cette boîte à outils sur deux architectures différentes de plateforme quantique composée de qubits supraconducteurs et d'ions piégés.

Mots-clés : Mesures aléatoires, intrication, information quantique de Fisher, formalisme de classical shadows, protocoles expérimentaux.

Acknowledgments

Firstly, I would like to offer the work that I have carried out during my PhD thesis and its fruitful outcomes at the lotus feet of the Mother and Sri Aurobindo. Without their divine grace and guidance, this work would not have been possible.

Having successfully completed my PhD thesis and looking back at the journey of the last three years, I feel extremely grateful and thankful to all the people that have been part of this valuable experience with me. First of all, I would like to express my gratitude to all the members of my jury starting with the Referees, Antonio Acin and Shannon Whitlock for accepting to evaluate my thesis manuscript and the Examiners, Leonardo Mazza, Cécilia Lancien and Franck Balestro for participating and sharing their important feedbacks regarding my thesis work.

I started to carry out my research work in this field during my Master's second year internship with Benoît Vermersch. Though the internship took place during the difficult Covid period in 2020, Benoît's guidance made me really passionate to pursue this line of research for my thesis as well. Then, I was very fortunate to get the opportunity to carry out my thesis in Grenoble as a result of a joint project between my two supervisors Benoît Vermersch and Cyril Branciard.

The success of my PhD work would not be possible without the guidance of my two gurus Benoît and Cyril. Both granted me the freedom to work independently at my own pace. They always found the time for me to clarify concepts, to discuss in detail my analytical and numerical computations and to devise plans for future projects. Additionally, they have instilled in me a profound commitment to be rigorous and methodical in my research endeavors, and have greatly shaped my current way of coherent scientific presentation and writing. I am immensely grateful for having them as my PhD supervisors.

During the course of my PhD work, I have been fortunate to collaborate with wonderful researchers. I have thoroughly enjoyed working with some of the PhD students and Post-Docs from whom I learnt a lot of minute technical details about my subject and who have helped me in understanding concepts in areas not within my expertise. My first project on importance sampling of randomized measurements lead to collaboration with the group of Peter Zoller. I would like to thank him for his inputs and ideas that improved significantly our project. I would equally like to thank Andreas Elben who helped me with some of the difficult technical calculations in this project and collaborations in other projects as well. I would like to also thank Anna Minguzzi for guiding me along with Benoît during my master's internship and providing her expertise on quantum metrology and ultra cold atoms for the quantum Fisher information project.

I enjoyed working a lot with Vitto (Dr. Vittorio Vitale from SISSA) who has shared a lot of my academic joys and pains till date. We have been very good work buddies and have tackled many problems together as a team. With our regular discussions, he has equally helped me broaden my expertise in the field. I would also like to thank Richard Kueng for his guidance in some of the technical aspects related to classical shadows. Along with that, I equally enjoyed working and discussing with

the group of Pasquale Calabrese, especially Sara and Filiberto. I would like to thank Petar Jurcevic for his experimental collaboration with the IBM quantum hardware. Lastly, would like to thank both Lata and Manoj from whom I have learnt valuable concepts from both the theoretical and experimental side, especially on the physics of the trapped ion quantum simulators. I would also like to thank them for having a fruitful collaboration for the Mpemba project.

Working at the lab once the Covid restrictions were lifted was always a pleasure. I have shared my office with wonderful people and have thoroughly enjoyed the experience during the PhD. At first, I worked the major part of my PhD in the old LPMMC building with an office which was also the common library space. It was shared among wonderful friends Romuald, Côme and other interns. Later in 2022, our office shifted to the new building G-411. I have enjoyed immensely working here till today and had amazing friends Francesco, Victor, Vittorio and Matteo along with me that made each day at work a very pleasant experience. Especially, I would dearly miss the company of Francesco and Vitto that filled the day with jokes, laughter and pure entertainment. I shall cherish all the experiences and wonderful memories that we had together starting from H2 lunches, post-work apéros, crazy late-night parties to some wonderful holiday trips. I would like to thank you all for sharing this wonderful journey with me. I would like to also thank all my other LPMMC colleagues and friends that I had over these past three years. Definitely a special mention goes to Anastasia for her mentorship and immediate help and advice on any topic, to Amit and Giovanni for hosting all the LPMMC parties and barbeques and lastly to Piero and Kosta with whom I have shared a lot jokes and funny moments over these past years.

I would also like to thank my other friends in Europe, Utsarg, Nayana, Pritam, Chetna, Praveen and Saptarshi, who have always been my well wishers and with whom I have shared exciting and fun holiday periods. I also wanted to thank my friend Dr. Nagesh with whom I have shared nice experiences starting from our Master's in Dijon to moving and staying together in Grenoble during the Covid period, to sharing our PhD experiences, enjoying holiday trips together and playing PUBG regularly during the weekends. I would like to thank one of my very good friend and well wisher, Mira, who has been always eager to help me and with whom I have had enriching discussions regarding my thesis work and other general topics as well. I would really like to thank Sap (Saptarshi) who has been and continues to be a big brother to me. He has guided, advised and helped me in all aspects since I have set foot in France. Lastly, I am also very thankful to all my friends, classmates, teachers and well-wishers in Pondicherry, Dijon and Grenoble.

Since my childhood, Bapa (my father) has been my role model and inspiration to learn more about Physics and finally pursue a PhD in it. He along with Aai (my grandma) and Aji (my grandpa) have been my guardian angels. They would have been extremely proud of this work that I have completed and achieved now. I would like to dedicate my entire PhD work to them and I am grateful for all the love and support that they have given to me. I am grateful to Mausai (my aunt), Mausai (my uncle) and Sidd (my brother) for their love, support and good wishes. Lastly, my heartfelt gratitude goes to Maa (my mother) who being far physically has always loved, supported and encouraged me throughout my studies abroad and has sacrificed and contributed immensely in making me the person that I am today. I am immensely thankful to all of you for all your good wishes and blessings and for

everything you have done for me. This has lead me to be where I am today.

Table of Contents

Introduction / Introduction en français	10
1 Introduction to entanglement quantifiers	20
1.1 Bipartite entanglement in pure states	21
1.2 Entanglement entropies	22
1.2.1 Entanglement detection with entropies	23
1.3 Mixed state entanglement	23
1.3.1 Positive-partial transpose condition	24
1.3.2 CCNR criterion	25
1.3.3 Operator entanglement	25
1.4 Multipartite entanglement	27
1.4.1 Quantum Fisher information	28
1.4.2 Connection with quantum metrology	28
2 Introduction to randomized measurements	30
2.1 How are measurements done?	31
2.2 Estimation of properties with tomography	32
2.3 Estimation of the purity	34
2.3.1 Estimation of the purity using physical copies	34
2.4 Estimation of the purity using Random measurements	35
2.4.1 Short mathematical background	36
2.4.2 The RM protocol and its derivation	38
2.4.3 Fidelity estimations from random measurements	41
2.4.4 Post-processing and additional features of the RM protocol	42
2.5 The classical shadow formalism	45
2.5.1 Randomized measurement tomography	45
2.5.2 Classical Shadows	46
2.5.3 Estimation of quantum properties with classical shadows	48
2.6 Current challenges and outline	51
3 Optimizing randomized measurements protocol with importance sampling	53
3.1 The main idea: approximate then select	54
3.2 The optimized classical-quantum protocol	56
3.2.1 The importance sampling protocol	58
3.3 Analytical estimations of statistical errors	60
3.3.1 Variance of uniform sampling for a pure product state	61
3.3.2 Variance of importance sampling for a pure product state	63
3.4 Numerical study and performance highlights	64
3.4.1 Estimation with perfect sampler	65
3.4.2 Machine-learning sampling for product and GHZ states	66

3.4.3	Sampling from MPS approximations	68
3.4.4	Importance sampling illustration for the toric code experiment	70
3.5	Conclusion	73
4	Estimation of the quantum Fisher information with classical shadows	75
4.1	Construction of the lower bounds of QFI	77
4.1.1	Convergence and other properties	78
4.2	Protocol to measure QFI and its error analysis in qubit platforms	80
4.2.1	Error analysis of a generic multi-copy functional	81
4.2.2	Sample complexity for lower bounds F_n	85
4.2.3	Numerical illustrations	87
4.3	Experimental measurement of the QFI on a quantum device	88
4.3.1	Robust estimation of quantum properties in a nutshell	89
4.3.2	Experimental Results	89
4.4	Conclusion	92
5	Observation of the entanglement barrier using batch shadows	94
5.1	Batch shadow formalism	96
5.1.1	General variance treatment of batch shadow estimator	98
5.1.2	Sample complexity calculations to estimate Rényi 2-OE	100
5.1.3	Numerical investigations	104
5.2	Experimental observation of the entanglement barrier	105
5.2.1	Mixed state entanglement conditions and experimental detection	107
5.3	Conclusion	111
6	Common randomized measurements	112
6.1	Main idea & the protocol	113
6.1.1	The common randomized measurement protocol	114
6.1.2	CRM protocol beyond the classical shadows regime	115
6.2	Performance illustrations of the CRM protocol	116
6.2.1	Direct fidelity estimation	117
6.2.2	Purity estimations: common randomized vs importance sampling	119
6.2.3	Higher order estimations: common randomized vs standard shadows	120
6.3	Conclusion	122
7	Conclusions and perspectives / Conclusions et perspectives en français	124
8	Résumé en français	130
	Appendices	136
A	Alternate expressions for the lower bounds and the quantum Fisher information	137
B	Variance computation for the batch shadow estimator	140

C Properties of classical shadows with local Pauli measurements	143
Bibliography	146

Introduction / Introduction en français

The early period of last century comprised of the ‘first quantum revolution’ that consisted of researchers trying to understand the intrinsic nature of quantum mechanics. Several of the founding experiments at that time began by manipulating *single quantum* particles at the atomic scale. Currently, with rapid advancements on the experimental front, we enter into the era of the second quantum revolution [22]. Over the past few years, current experiments have the capability to program coherent interactions between tens to hundreds of particles that can be arranged and manipulated in various tunable geometries. With these operations, one can create highly complex and correlated quantum matter states on diverse quantum platforms such as Rydberg atoms [70, 110], trapped ions [43, 83], superconducting qubits [18, 1], ultra-cold atoms in optical lattices [69] and quantum dots [12].

Originally as suggested by Feynman in Ref. [38]: “Let the computer itself be built of quantum mechanical elements which obey quantum mechanical laws”, these quantum technological platforms made up of the building blocks known as *qubits*, now present for us a rich playground for practical applications in the current era dubbed as the Noisy-Intermediate Scale Quantum (NISQ) era [97]. These imperfect and noisy devices are prospective candidates for *quantum computation* [25] that could potentially out-perform classical computer in certain specific ‘hard’ tasks, *quantum simulation* [46] of fundamental models of condensed matter and high-energy physics, *quantum communication* [49] and *quantum metrology* [47, 94]. Currently, we can greatly feel an active drive to develop further these various quantum technologies as investments starting from public to private organizations have started to surge. Our hope is to develop practical commercial quantum technology that will help solve today’s real world problems.

A key resource that is often generated by coherent interactions between particles in these quantum devices and that is completely absent in their classical counterparts is *quantum entanglement* [62]. It describes the extent to which a many-body quantum state can not be described as a classical product state [53]. This elementary quantum property has its imprint in several fields of study starting from quantum information and computation [53] to condensed matter and high energy physics [46]. There has been a significant interest to constantly characterize and estimate entanglement produced in today’s noisy quantum platforms in full generality, independent of the platform’s architecture and the prepared many-body state. Estimating entanglement properties naturally helps benchmark the quantum platform and also could provide interesting signatures of universal properties related to entanglement [27].

To estimate properties associated to entanglement for an unknown quantum state prepared in quantum devices presents an outstanding technological challenge as the quantum state of N qubits lives in an exponentially large Hilbert space of dimension 2^N . There exists experimental methods such as quantum state tomography (QST) that can reconstruct an unknown quantum state ρ [52, 21] prepared in an

experiment. A main drawback of this method is that the required number measurements to overcome statistical errors scale exponentially with the number of qubits N , i.e it scales as 2^{3N} [54]. The consequence of such an overload of measurements and exponential resources required for classical postprocessing of the experimental results greatly restricts the investigation of properties of interest in larger quantum platforms. In particular, this technique can potentially probe properties of quantum system in the range of 6 – 8 qubits.

In recent years, new advanced protocols by the name of *randomized measurement toolbox* (RM toolbox) [31] have been developed by theorists to assist the constant experimental progress. This protocol is based on executing on a prepared quantum state of interest, single qubit (or global) random unitary operations that are sampled from an appropriate unitary ensemble followed by fixed computational basis measurements. This procedure, repeated many times for different sets of unitaries and recorded measurements makes up a data-set. This quantum to classical translation via the RM protocol maps succinctly a vast amount of information contained in the multi qubit quantum state to some compact representation in the form of classical data. Then, efficient classical post-processing of this collected data follows to give us access to properties of interest of the quantum system.

One of the main advantages of this method is that it offers a reduced measurement budget compared to QST to measure quantities relevant to entanglement. To overcome statistical errors that are caused by finite measurement statistics, the required number of measurements for randomized measurements scale as $2^{\alpha N}$ with $\alpha \in [1, 1.5]$ [29, 11, 125, 32]. This allows the RM protocol to be implemented on current quantum hardware beyond the regime of QST and has been experimentally demonstrated to access many interesting properties of quantum many-body states associated to entanglement such as entanglement entropies [11, 111, 135, 60], negativities [34, 86], scrambling [72] and topological invariants [33, 17]. Additionally, this method also allows experimentalists to benchmark their prepared quantum states by measuring the fidelity (through state overlap) of an experimental quantum state with respect to a corresponding state calculated or modelled classically, e.g on a high-performance cluster [32, 73] or realized on another quantum platform as demonstrated in [142]. Thus these results suggest that the RM protocol can be a method of reference to probe properties of interest associated to entanglement in quantum simulators and quantum computers.

Since the development of the RM protocol, there have been some pertinent challenges and questions that have been asked. In this manuscript, we shall provide solutions to some relevant and practical problems in this context. Below, we summarize and divide the challenges tackled by this manuscript that broadly make up the following research objectives of this thesis:

1. *Optimization:* Currently, the RM protocol still suffers from an exponential scaling of the required number of measurements to fight against statistical errors in the estimation of the quantities. Though this method can be applied to probe system-sizes beyond QST, the increasing demand to benchmark quantum properties in larger quantum devices still presents a challenge. The first research axis focuses on rendering the current RM protocol more efficient. We provide a key solution by developing a more optimized version of the current RM protocol. This consequently allows us to implement the protocol to inves-

tigate quantum properties created in larger experimental setups as discussed in Chapter. 3 and Chapter. 6.

2. *Probe new quantities:* Until present, quantum entanglement between two parties (bipartite entanglement) has been extensively probed in quantum experiments. The extension of the RM toolbox to estimate quantities related to multipartite entanglement and other novel quantities of interest that can be accessed using the same framework of the RM toolbox, has been another research direction that has been greatly explored during this thesis in Chapter. 4 and Chapter. 5.
3. *Measurement budget analysis:* Estimating the sample complexity (required number of measurements) becomes crucial in understanding the required investments in terms of experimental resources and time. In this context, we develop in detail a generalized and formal study comprised of both analytical and numerical techniques to obtain the required number of measurements to estimate arbitrary quantities of interest accessible using the RM toolbox in Chapter. 4.
4. *Effective data post-processing methods:* Probing properties generated in large system sizes with the RM protocol consequently presents post-processing overload of collected experimental data. A significant effort of this thesis focuses on solving this practical issue. We develop a new efficient formalism that is supported equally by compact classical routines for a fast treatment of the experimental data generated by the RM protocol in Chapter. 5.
5. *Experimental realization of the protocol:* Lastly, development of experimental protocols from the theory side has its ultimate impact when they are verified on real experimental devices. We report the implementation of some of our novel proposed methods on experimental platforms to measure new quantities of interest for the first time as shown in Chapter. 4 and Chapter. 5.

Structure of the manuscript — This manuscript is self-contained and comprises a total of seven chapters including the conclusion. The first two chapters will provide the required background to quantum entanglement and the RM toolbox. In Chapter. 1, we start by introducing the notion of quantum entanglement. We define a list of important *entanglement quantifiers* that shall be discussed throughout the course of this manuscript. These quantities can certify or quantify the presence of different kinds of entanglement for example in *pure* or *mixed* states or in a scenario of entanglement between two parties—*bipartite entanglement* or entanglement among multiple parties—*multipartite entanglement*.

The introductory chapter on entanglement is followed by Chapter. 2, where we shall review in detail the *randomized measurement toolbox* [31] and additionally derive the *classical shadow formalism* [64] which forms a key component of the RM toolbox. We shall show in particular that with this framework, we can access quantities expressed as expectation values of multi-copy operators directly from the RM data generated by the experiment. These two chapters set us up for the subsequent chapters that shall discuss and elaborate on the results developed during the course of this thesis and have lead to published works.

The following chapters of the thesis follow a format that is article-based. They sequentially include the following list of completed works that have been re-worked and modified to avoid repetitions and to finally achieve a coherent manuscript:

- *Aniket Rath, Rick van Bijnen, Andreas Elben, Peter Zoller, and Benoît Vermersch.* Importance sampling of randomized measurements for probing entanglement. *Phys. Rev. Lett.*, *127:200503*, Nov 2021 (Chapter. 3 and Ref. [99]).
- *Aniket Rath, Cyril Branciard, Anna Minguzzi, and Benoît Vermersch.* Quantum Fisher information from randomized measurements. *Phys. Rev. Lett.*, *127:260501*, Dec 2021 (Chapter. 4 and in Ref. [100])
- *Vittorio Vitale, Aniket Rath, Petar Jurcevic, Andreas Elben, Cyril Branciard, and Benoît Vermersch.* Estimation of the quantum Fisher information on a quantum processor, *arXiv:2307.16882*, 2023 (Chapter. 4 and in Ref. [129])
- *Aniket Rath, Vittorio Vitale, Sara Murciano, Matteo Votto, Jérôme Dubail, Richard Kueng, Cyril Branciard, Pasquale Calabrese, and Benoît Vermersch.* Entanglement barrier and its symmetry resolution: Theory and experimental observation. *PRX Quantum*, *4:010318*, Feb 2023 (Chapter. 5 and in Ref. [101]).
- *Benoît Vermersch, Aniket Rath, Bharathan Sundar, Cyril Branciard, John Preskill, and Andreas Elben.* Enhanced estimation of quantum properties with common randomized measurements, *arXiv:2304.12292*, 2023 (Chapter. 6 and in Ref. [126]).

Chapter. 3 centers around the optimization problem related to the randomized measurement protocol which is detailed in Ref. [99]. We consider the case where we are interested to estimate the purity of an unknown quantum state from randomized measurement data. The purity of a quantum state can be used to detect entanglement and can quantify it for pure states. The aim is to develop a new framework that enables us to decrease statistical errors in estimating the purity compared to the initial proposed protocol in Ref. [11]. This would then allow us to measure the purity in much larger quantum system compared to the current system sizes that we can address. The main idea that we develop in this chapter is to use an *approximate prior knowledge* on the prepared quantum state of the experiment and implement based on this knowledge *importance sampling* of random unitaries. In the chapter, we show analytical evidence of reduction of statistical errors and provide multiple numerical case studies by simulating the protocol classically.

The results of Chapter. 4 are based on Ref. [100] and the last section of this chapter is based on a recently completed work [129]. It comprises in designing a method adapted in the framework of the RM toolbox to probe multipartite entanglement in quantum platforms and also experimentally verify the proposal on a superconducting qubit device. We aim here to estimate the *quantum Fisher information* (QFI), a quantity that can witness multipartite entanglement via the *entanglement depth* present in the underlying quantum system [122, 67]. As the highly non-linear expression of the QFI cannot be estimated without employing quantum state tomography, in our work, we propose an alternate expression to measure the QFI by constructing a converging polynomial series of lower bounds as a function of the density matrix.

These lower bounds can be estimated using the classical shadow formalism of the RM toolbox [64] for system sizes beyond the regime of QST. Additionally, in this chapter, we also derive a general framework that provides rigorous bounds on the required number of measurements to evaluate arbitrary functions accessible by the classical shadow formalism with a given accuracy and confidence interval. In the last section of Chapter. 4, we discuss a recently completed work [129] where we apply our theoretical proposal and other advanced techniques of the RM toolbox to estimate experimentally the QFI using the converging series of lower bounds in a superconducting qubit device for system size upto 13 qubits. On this platform, we prepare GHZ states and the ground state of the transverse field Ising model at the critical point using the quantum adiabatic optimization algorithm [37].

In Chapter. 5, we present the results from Ref. [101]. Here, we provide a new formalism of classical shadows that we dub *batch classical shadows*. It enables us to effectively post-process estimations of quantities of interest from the RM dataset which were not accessible by previous methods. The bottleneck that crippled previous methods involved an expensive cost of classical data-treatment for the classical shadow formalism which is solved by the batch shadow formalism. We also developed a general framework to assess the required number of measurements to estimate functions of interest using this new formalism. The development of this framework was extremely useful in firstly observing an interesting quantum property associated with the *operator entanglement* known as *the entanglement barrier* [130] from existing experimental data. Secondly, it also enabled us to successfully estimate higher order lower bounds of the QFI from experimental data as stated earlier.

Lastly, Chapter. 6 is based on the work of Ref. [126]. We develop a new variant of the RM protocol that we coin *common randomized measurements* (CRM) in order to boost estimation of expectation values of multi-copy operators that can be accessed from the classical shadow formalism. We define a new kind of classical shadow known as common randomized shadows (CR shadows). This framework also uses an approximate prior knowledge on the prepared state of the experiment to enhance estimations of the quantities of interest. We perform multiple numerical case studies to demonstrate the advantages of the developed framework compared to the standard classical shadow formalism [64].

Particularly, Chapter. 3 and 6 contain additional relevant studies that have not been explicitly mentioned in their respective publications. We include a note at the beginning of each of these chapters to describe the correspondence between its content and the respective publication. We end the thesis with conclusions and perspectives on our work.

Introduction en français

Le début du siècle dernier a été marqué par la "première révolution quantique", au cours de laquelle les chercheurs ont tenté de comprendre la nature intrinsèque de la mécanique quantique. Plusieurs des expériences fondatrices de l'époque ont commencé par la manipulation de *particules quantiques uniques* à l'échelle atomique. Aujourd'hui, grâce aux progrès rapides réalisés sur le front expérimental, nous entrons dans l'ère de la deuxième révolution quantique [22]. Au cours des dernières années, les expériences actuelles ont permis de programmer des interactions cohérentes entre des dizaines ou des centaines de particules qui peuvent être

disposées et manipulées dans diverses géométries accordables. Ces opérations permettent de créer des états de matière quantique hautement complexes et corrélés sur diverses plateformes quantiques telles que les atomes de Rydberg [70, 110], les ions piégés [43, 83], les qubits supraconducteurs [18, 1], les atomes ultrafroids dans des réseaux optiques [69] et les boîtes quantiques (quantum dots) [12].

A l'origine, comme suggéré par Feynman dans Ref. [38]: "Que l'ordinateur lui-même soit construit à partir d'éléments mécaniques quantiques qui obéissent aux lois de la mécanique quantique", ces plateformes technologiques quantiques composées de blocs de construction connus sous le nom de *qubits* nous offrent aujourd'hui un riche terrain de jeu pour des applications pratiques dans l'ère actuelle appelée "ère quantique à échelle intermédiaire et bruitée" (NISQ) [97]. Ces dispositifs imparfaits et bruyants sont des candidats potentiels pour *le calcul quantique* [25] qui pourrait potentiellement surpasser les ordinateurs classiques dans certaines tâches "difficiles" spécifiques, la *simulation quantique* [46] des modèles fondamentaux de la matière condensée et de la physique des hautes énergies, la *communication quantique* [49] et la *métrologie quantique* [47, 94]. Actuellement, nous sentons une volonté active de développer davantage ces diverses technologies quantiques, car les investissements des organisations publiques et privées ont commencé à augmenter. Nous espérons développer une technologie quantique commerciale pratique qui contribuera à résoudre les problèmes du monde réel d'aujourd'hui.

L'intrication quantique est une ressource clé qui est souvent générée par des interactions cohérentes entre les particules dans ces dispositifs quantiques et qui est totalement absente dans ses homologues classiques [62]. Il décrit la mesure dans laquelle un état quantique à plusieurs corps ne peut pas être décrit comme un état produit classique [53]. Cette propriété quantique élémentaire est cruciale dans plusieurs domaines d'étude, depuis l'information et l'informatique quantiques [53] jusqu'à la matière condensée et la physique des hautes énergies [46]. La caractérisation de l'intrication produite dans les plateformes quantiques bruitées d'aujourd'hui ont suscité un intérêt considérable, en toute généralité, indépendamment de l'architecture de la plateforme quantique et de l'état préparé de nombreux corps. L'estimation des propriétés de l'intrication permet naturellement d'évaluer la performance de la plateforme quantique et pourrait également fournir des signatures intéressantes de propriétés universelles liées à l'intrication [27].

L'estimation des propriétés associées à l'intrication pour un état quantique inconnu préparé dans des dispositifs quantiques représente un défi technologique exceptionnel car l'état quantique de N qubits vit dans un espace de Hilbert exponentiellement grand de dimension 2^N . Il existe des méthodes expérimentales telles que la tomographie d'états quantiques (QST) qui peut reconstruire un état quantique inconnu ρ [52, 21] préparé lors d'une expérience. L'un des principaux inconvénients de cette méthode est que le nombre de mesures nécessaires pour surmonter les erreurs statistiques augmente de façon exponentielle avec le nombre de qubits N , c'est-à-dire qu'il s'élève à 2^{3N} [54]. La conséquence d'une telle surcharge de mesures et des ressources exponentielles requises pour le post-traitement classique des résultats expérimentaux limite considérablement l'étude des propriétés intéressantes dans les grandes plateformes quantiques. En particulier, cette technique peut potentiellement sonder les propriétés de systèmes quantiques de l'ordre de 6 à 8 qubits.

Ces dernières années, de nouveaux protocoles avancés appelés "randomized measurement toolbox" (RM toolbox) [31] ont été mis au point par des théoriciens pour

faciliter les progrès expérimentaux constants. Ce protocole est basé sur l'exécution, sur un état quantique d'intérêt préparé, d'opérations unitaires aléatoires sur chaque qubit, échantillonnées à partir d'un ensemble unitaire approprié, suivies de mesures projectives dans une base fixe. Cette procédure, répétée de nombreuses fois pour différents ensembles unitaires et de mesures enregistrées, constitue un ensemble de données. Cette conversion du quantique au classique via le protocole RM permet de transposer succinctement une grande quantité d'informations contenues dans l'état quantique à qubits multiples en une représentation compacte sous forme de données classiques. Ensuite, un post-traitement classique efficace de ces données collectées permet d'accéder aux propriétés intéressantes du système quantique.

L'un des principaux avantages de cette méthode est qu'elle offre un budget de mesure réduit par rapport à la QST pour mesurer les quantités pertinentes pour l'intrication. Pour surmonter les erreurs statistiques causées par des statistiques de mesure finies, le nombre requis de mesures de l'intrication est réduit à $2^{\alpha N}$ avec $\alpha \in [1, 1.5]$ [29, 11, 125, 32]. Cela permet d'implémenter le protocole RM sur les plateformes quantique actuel au-delà du régime de la QST. Il a été démontré expérimentalement qu'elle permet d'accéder à de nombreuses propriétés intéressantes des états quantiques à plusieurs corps associés à l'intrication, telles que les entropies d'intrication [11, 111, 135, 60], les négativités [34, 17], l'embrouillage (scrambling) [72] et les invariants topologiques [33, 17]. En outre, cette méthode permet également aux expérimentateurs d'évaluer leurs états quantiques préparés en mesurant la fidélité d'un état quantique expérimental par rapport à un état correspondant calculé ou modélisé classiquement, par exemple sur un cluster à haute performance [32] ou réalisé sur une autre plateforme quantique. Ces résultats suggèrent donc que le protocole RM peut être une méthode de référence pour sonder les propriétés intéressantes dans les simulateurs quantiques et les ordinateurs quantiques.

Depuis le développement du protocole RM, certains défis et questions pertinents ont été posés. Dans ce manuscrit, nous apporterons des solutions à certains problèmes pertinents et pratiques dans ce contexte. Nous pouvons résumer et diviser les défis abordés par ce manuscrit qui constituent globalement les objectifs de recherche suivants de cette thèse :

1. *Optimisation*: Actuellement, le protocole RM souffre toujours d'une échelle exponentielle du nombre de mesures nécessaires pour lutter contre les erreurs statistiques dans l'estimation des quantités. Bien que cette méthode puisse être appliquée pour sonder des systèmes de plus grande taille par rapport à la QST, la demande croissante d'étalonnage des propriétés quantiques dans des dispositifs quantiques de plus grande taille constitue toujours un défi. Le premier axe de recherche se concentre sur l'amélioration de l'efficacité du protocole RM actuel. Nous apportons une solution clé en développant une version plus optimisée du protocole RM actuel. Cela nous permet de mettre en œuvre le protocole pour étudier les propriétés quantiques créées dans des dispositifs expérimentaux plus importants, comme indiqué dans les chapitres 3 et au chapitre 6.
2. *Sonder de nouvelles quantités* : Jusqu'à présent, l'intrication quantique entre deux parties (intrication bipartite) a été largement étudiée dans les expériences quantiques. L'extension de la boîte à outils RM pour estimer les quantités

liées à l'intrication multipartite et d'autres nouvelles quantités intéressantes auxquelles on peut accéder en utilisant le même cadre de la boîte à outils RM, a été une autre direction de recherche qui a été largement explorée au cours de cette thèse dans les chapitres. 4 et au chapitre. 5.

3. *Analyse du budget de mesure* : L'estimation de la complexité de l'échantillon (nombre requis de mesures) devient cruciale pour comprendre les investissements requis en termes de ressources expérimentales et de temps. Dans ce contexte, nous développons en détail une étude généralisée et formelle comprenant à la fois des techniques analytiques et numériques pour obtenir le nombre requis de mesures pour estimer des quantités arbitraires d'intérêt accessibles en utilisant le formalisme RM dans le chapitre. 5.
4. *Méthodes efficaces de post-traitement des données* : L'étude des propriétés générées dans des systèmes de grande taille à l'aide du protocole RM entraîne une surcharge de post-traitement des données expérimentales collectées. Un effort important de cette thèse se concentre sur la résolution de ce problème pratique. Nous développons un nouveau formalisme efficace qui est soutenu également par des routines classiques compactes pour un traitement rapide des données expérimentales générées par le protocole RM dans le chapitre. 5.
5. *Réalisation expérimentale du protocole* : Enfin, le développement de protocoles expérimentaux à partir de la théorie nécessite sa "cerise sur le gâteau". Ceci est réalisé par la mise en œuvre des nouvelles méthodes proposées sur des plateformes expérimentales réelles et la mesure de nouvelles quantités d'intérêt, comme le montrent les chapitres. 4 et au chapitre. 5.

Structure du manuscrit — Ce manuscrit est autonome et comprend un total de sept chapitres. Les deux premiers chapitres fournissent le contexte nécessaire à l'intrication quantique et à la boîte à outils RM. Dans le chapitre. 1, nous commençons par introduire la notion d'intrication quantique. Nous définissons un certain nombre de *quantificateurs d'intrication* importants qui seront discutés tout au long de ce manuscrit. Ces quantités peuvent certifier ou quantifier la présence de différents types d'intrication, par exemple dans des états *purs* ou *mixtes* ou dans un scénario d'intrication entre deux parties, *d'intrication bipartite* ou d'intrication entre plusieurs parties, *d'intrication multipartite*.

Le chapitre d'introduction sur l'intrication est suivi du chapitre. 2. Nous examinerons en détail la *boîte à outils des mesures aléatoires* (RM toolbox) [31] et déduirons en outre le *formalisme de classical shadows* [64], qui constitue un élément clé de la boîte à outils des mesures aléatoires. Nous montrerons en particulier qu'avec ce cadre, nous pouvons accéder à des quantités exprimées en tant que valeurs d'espérance d'opérateurs multicopies directement à partir des données RM générées par l'expérience. Ces deux chapitres nous préparent pour les chapitres suivants qui discuteront et développeront les résultats développés au cours de cette thèse et qui ont conduit à des travaux publiés.

Les chapitres suivants de la thèse suivent un format basé sur des articles. Ils comprennent la liste suivante de travaux réalisés :

- *Aniket Rath, Rick van Bijnen, Andreas Elben, Peter Zoller, and Benoît Vermersch*. Importance sampling of randomized measurements for probing entanglement. *Phys. Rev. Lett.*, 127:200503, Nov 2021 (Chapter. 3).

- *Aniket Rath, Cyril Branciard, Anna Minguzzi, and Benoît Vermersch.* Quantum Fisher information from randomized measurements. *Phys. Rev. Lett.*, 127:260501, Dec 2021 (Chapter. 4)
- *Vittorio Vitale, Aniket Rath, Petar Jurcevic, Andreas Elben, Cyril Branciard, and Benoît Vermersch.* Estimation of the quantum Fisher information on a quantum processor, *arXiv:2307.16882*, 2023 (Chapter. 4)
- *Aniket Rath, Vittorio Vitale, Sara Murciano, Matteo Votto, Jérôme Dubail, Richard Kueng, Cyril Branciard, Pasquale Calabrese, and Benoît Vermersch.* Entanglement barrier and its symmetry resolution: Theory and experimental observation. *PRX Quantum*, 4:010318, Feb 2023 (Chapter. 5).
- *Benoît Vermersch, Aniket Rath, Bharathan Sundar, Cyril Branciard, John Preskill, and Andreas Elben.* Enhanced estimation of quantum properties with common randomized measurements, *arXiv:2304.12292*, 2023 (Chapter. 6).

Le chapitre. 3 est centré sur le problème d’optimisation lié au protocole de mesure aléatoire qui est détaillé dans Ref. [99]. Nous considérons le cas où nous sommes intéressés à estimer la pureté d’un état quantique inconnu à partir de données de mesures aléatoires. L’objectif est de développer un nouveau cadre qui nous permet de réduire les erreurs statistiques dans l’estimation de la pureté par rapport au protocole initial proposé dans Ref. [11]. Cela nous permettrait alors de mesurer la pureté dans des systèmes quantiques beaucoup plus grands que les tailles de systèmes actuelles que nous pouvons traiter. L’idée principale que nous développons dans ce chapitre est d’utiliser *une connaissance préalable approximative* de l’état quantique préparé de l’expérience et de mettre en œuvre, sur la base de cette connaissance, *l’échantillonnage préférentiel* d’unitaires aléatoires. Dans ce chapitre, nous montrons des preuves analytiques de la réduction des erreurs statistiques et fournissons plusieurs études de cas numériques en simulant le protocole de manière classique.

Les résultats du chapitre. 4 sont basés sur Ref. [100] et la dernière section de ce chapitre est basée sur un travail récemment achevé [129]. Il s’agit de concevoir une méthode adaptée dans le cadre de la boîte à outils RM pour sonder l’intrication multipartite dans les plateformes quantiques et de vérifier expérimentalement la proposition sur un dispositif de qubit supraconducteur. Nous visons ici à estimer l’information quantique de Fisher (QFI), une quantité qui peut témoigner du degré d’intrication multipartite présent dans le système sous-jacent [67, 122]. Comme l’expression hautement non linéaire de la QFI ne peut être estimée sans utiliser la tomographie d’état quantique, nous proposons dans notre travail une expression alternative pour mesurer la QFI en construisant une série polynomiale convergente de limites inférieures en tant que fonction de la matrice de densité. Ces limites inférieures peuvent être estimées en utilisant le formalisme de *classical shadows* de la boîte à outils RM [64] pour des tailles de système dépassant le régime de la QST. En outre, dans ce chapitre, nous dérivons également un cadre général qui fournit des bornes rigoureuses sur le nombre requis de mesures pour évaluer des fonctions arbitraires accessibles par le formalisme de classical shadows avec une précision et un intervalle de confiance donnés.

Dans la dernière section du chapitre. 4, nous discutons d’un travail récemment achevé [129] dans lequel nous appliquons notre proposition théorique pour estimer

expérimentalement le QFI en utilisant la série convergente de limites inférieures dans un dispositif de qubits supraconducteurs pour une taille de système allant jusqu'à 13 qubits. Sur cette plateforme, nous préparons l'état GHZ et l'état fondamental du modèle d'Ising à champ transverse au point critique en utilisant l'algorithme d'optimisation adiabatique quantique.

Dans le chapitre. 5 nous présentons les résultats de Ref. [101]. Nous proposons ici un nouveau formalisme des classical shadows que nous appelons *batch shadows*. Il nous permet d'effectuer efficacement des estimations a posteriori des quantités d'intérêt à partir de l'ensemble de données RM qui n'étaient pas accessibles par les méthodes précédentes. Le goulot d'étranglement qui paralysait les méthodes précédentes impliquait un coût élevé de traitement des données classiques du formalisme de classical shadows. Nous avons également mis au point un cadre général permettant d'évaluer le nombre de mesures nécessaires pour estimer les fonctions d'intérêt à l'aide du nouveau formalisme de batch shadows. Le développement de ce cadre a été extrêmement utile pour observer une propriété quantique intéressante associée à *d'intrication de l'opérateur*, connue sous le nom de *barrière d'intrication* [130], à partir de données expérimentales existantes. Deuxièmement, il nous a également permis d'estimer avec succès des limites inférieures d'ordre supérieur de la QFI à partir de données expérimentales, comme indiqué précédemment.

Enfin, le chapitre. 6 est basé sur les travaux de Ref. [126]. Nous développons une nouvelle variante du protocole RM que nous appelons *mesures aléatoires communes* (CRM) afin d'améliorer l'estimation des valeurs d'espérance des opérateurs multicopies qui peuvent être accessibles à partir du formalisme de classical shadows. Nous définissons un nouveau type de classical shadows appelée *common randomized shadows* (CR shadows). Ce cadre utilise également une connaissance préalable approximative de l'état préparé de l'expérience pour améliorer les estimations des quantités d'intérêt. Nous réalisons plusieurs études de cas numériques pour démontrer les avantages du cadre développé par rapport au formalisme standard de classical shadows [64].

En particulier, les chapitres. 3 et 6 contiennent des études pertinentes supplémentaires qui n'ont pas été explicitement mentionnées dans leurs publications respectives. Nous incluons une note au début de chacun de ces chapitres pour décrire la correspondance entre son contenu et la publication correspondante.

1

Introduction to entanglement quantifiers

The present chapter introduces the required theoretical background to understand the quantities of interest for this manuscript that certify entanglement in quantum many-body systems.

Contents

1.1	Bipartite entanglement in pure states	21
1.2	Entanglement entropies	22
1.2.1	Entanglement detection with entropies	23
1.3	Mixed state entanglement	23
1.3.1	Positive-partial transpose condition	24
1.3.2	CCNR criterion	25
1.3.3	Operator entanglement	25
1.4	Multipartite entanglement	27
1.4.1	Quantum Fisher information	28
1.4.2	Connection with quantum metrology	28

Entanglement is a vital resource and plays a key role in various applications starting from quantum cryptography [28], quantum teleportation [4], quantum metrology [94] and in quantum computation and simulation [97]. There are various quantities starting from Bell inequalities [10], entanglement witnesses [120], entropic quantities and non-linear functionals of the quantum state that certify the presence of entanglement in a quantum state [53]. In this chapter, we shall aim at providing a brief theoretical overview of some important entanglement quantifiers among the vast zoo of quantities that certify entanglement. In particular, we will mainly focus on introducing the background of the quantities that shall be relevant to this manuscript and will be discussed in detail in subsequent chapters. Namely, we will mainly devote our attention on quantifiers that describe bipartite entanglement (entanglement between two constituents of the system) in the context of both pure and mixed quantum systems and also in the multipartite scenario (entanglement between multiple parties of the system).

1.1 Bipartite entanglement in pure states

Consider a quantum system that comprises of two parts A and B as illustrated in Fig. 1.1. The full system is described by a quantum state in a d dimensional Hilbert space $\mathcal{H}_{AB}(d)$

$$|\psi_{AB}\rangle = \sum_{i,j} \Psi_{ij} |i_A\rangle \otimes |j_B\rangle \quad (1.1)$$

where $\{|i_A\rangle\}$ and $\{|i_B\rangle\}$ are orthonormal bases spanning the Hilbert spaces of sub-systems A and B given by $\mathcal{H}_A(d_A)$ and $\mathcal{H}_B(d_B)$ with dimensions d_A and d_B respectively. We assume here that the wave function $|\psi_{AB}\rangle$ is pure; that is, the state of the environment $|\psi_E\rangle$ can be factorized with respect to the state of the system that we are interested in. We define a separable state if a given state $|\psi_{AB}\rangle$ obeys a product decomposition [53] as follows

$$|\psi_{AB}\rangle = |\psi_A\rangle \otimes |\psi_B\rangle. \quad (1.2)$$

On the contrary, a state that fails to be represented as above is called an *entangled state* that shares entanglement between the parts A and B . In particular, such an entangled state cannot be prepared using local operations on sub-systems A and B aided by classical communication (LOCC operations). Additionally, we can define the Schmidt decomposition of this state into orthonormal base $|a_\ell\rangle \in \mathcal{H}_A(d_A)$ and $|b_\ell\rangle \in \mathcal{H}_B(d_B)$ such that [53]

$$|\psi_{AB}\rangle = \sum_{\ell=1}^R w_\ell |a_\ell\rangle |b_\ell\rangle \quad (1.3)$$

with $\{w_\ell\}_\ell$ being the Schmidt spectrum that obeys $\sum_\ell w_\ell^2 = 1$ with $w_\ell \geq 0$ and $R \leq \min\{d_A, d_B\}$ is the Schmidt rank of the state $|\psi_{AB}\rangle$. Interestingly, this decomposition also validates the presence of entanglement: Entangled states have a Schmidt rank $R > 1$, that is, there exists at least two non-zero values for w_ℓ in the Schmidt

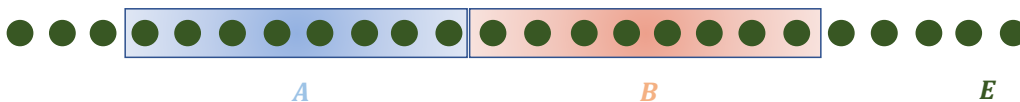


Figure 1.1: *Bipartite quantum system* — This figure illustrates a quantum system where each green circle represents a local system. The full system is comprised of a sub-system A (blue) and sub-system B (red). The rest of the constituents form the environment E .

decomposition of the state $|\psi_{AB}\rangle$. A pure product state *always* has a single Schmidt value that results in $R = 1$. Additionally, the Schmidt decomposition allows us to introduce a set of important quantities that can also quantify the amount of entanglement in the system of interest.

1.2 Entanglement entropies

One can obtain a reduced density matrix (RDM) that describes all the properties of the state in region A (or conversely in B) by tracing out the degrees of freedom of the complement system (B in this case). This operation, that is achieved by taking the partial trace gives

$$\rho_A = \text{Tr}_B(\rho_{AB}) = \text{Tr}_B(|\psi_{AB}\rangle\langle\psi_{AB}|) = \sum_{\ell=1}^R w_\ell^2 |a_\ell\rangle\langle a_\ell| \quad (1.4)$$

where we have the density matrix of the full system $\rho_{AB} = |\psi_{AB}\rangle\langle\psi_{AB}|$ which is an operator that is positive and semi-definite. The square singular values w_ℓ^2 define the eigenvalues λ_ℓ of the RDM. One can define an entropy of entanglement famously known as the *von Neumann entropy*

$$S_{\text{vN}}(\rho_A) = - \sum_{\ell=1}^R \lambda_\ell \log \lambda_\ell = -\text{Tr}(\rho_A \log \rho_A) \quad (1.5)$$

and additionally the *Rényi entropies*

$$S_n(\rho_A) = \frac{1}{1-n} \log \sum_{\ell=1}^R (\lambda_\ell)^n = \frac{1}{1-n} \log \text{Tr}(\rho_A^n). \quad (1.6)$$

More generally, one can recover the von Neumann entropy from Rényi entropies given by $\lim_{n \rightarrow 1} S_n = S_{\text{vN}}$. Importantly, for pure states described in the joint system $A \cup B$, the above entropies satisfy the appropriate conditions to be considered as *entanglement measures*, i.e they quantify the amount of entanglement in the system and vanish for separable states. They are *entanglement monotones*, that is they do not increase under LOCC operations [62]. Additionally, these set of entropies have a range of important applications in understanding universal behaviors in many-body physics [27]. They also quantify the complexity to classically simulate quantum

many-body systems with numerical methods such as tensor network algorithms [113]. Let us now show how entanglement entropies detect entanglement of a quantum system.

1.2.1 Entanglement detection with entropies

Let us fall back on the entanglement Schmidt criteria obtained from the Schmidt decomposition. As states with a Schmidt rank $R = 1$ are product states, this implies that there exists a unique singular value $w_\ell = 1$ (also a unique eigenvalue $\lambda_\ell = 1$). Computing the RDM of the sub-system A as done in Eq. (1.4) shows that the reduced state ρ_A has a *purity* $\text{Tr}(\rho_A^2) = 1$ and is therefore a pure state. The von Neumann or Rényi entropy of a reduced state on A is $S_{\text{vN}}(\rho_A) = S_n(\rho_A) = 0$. This immediately gives rise to the following statement based on the Schmidt criterion: A pure state defined on the system $A \cup B$ is entangled between A and B *if and only if* the von Neumann or Rényi entropy of the reduced systems A (respectively B) is nonzero [53].

Additionally, we observe from Eq. (1.6) that if $R > 1$, the purity of the reduced state $\text{Tr}(\rho_A^2) < 1$. This can be easily noted from the fact that the purity $\text{Tr}(\rho_A^2)$ can be equivalently expressed using Eq. (1.4) as

$$\text{Tr}(\rho_A^2) = \sum_{\ell=1}^R w_\ell^4 = \sum_{\ell=1}^R \lambda_\ell^2. \quad (1.7)$$

When $R > 1$, $\forall \ell : \lambda_\ell < 1$ as it satisfies $\sum_{\ell=1}^R \lambda_\ell = 1$. This results in $\sum_{\ell} \lambda_\ell^2 = \text{Tr}(\rho_A^2) < 1$. Thus in an analogous manner, we can state that the RDMs of entangled states are mixed when compared to the pure state ρ_{AB} : $\text{Tr}(\rho_A^2) < 1 = \text{Tr}(\rho_{AB}^2)$ and conversely the entropy of the reduced states are larger than entropy of the full system $S_2(\rho_A) > S_2(\rho_{AB}) = 0$. We note that the purity and the second Rényi entropy will be the main quantities of interest in Chapters. 2 - 3 where we describe methods to measure them in order to validate the presence of entanglement in experimentally prepared quantum states. Note additionally that these conditions can also be used to detect entanglement in mixed quantum state ($\text{Tr}(\rho_{AB}^2) < 1$) as long as we satisfy the condition shown earlier ($\text{Tr}(\rho_A^2) < \text{Tr}(\rho_{AB}^2)$). A drawback of these conditions is that though they are powerful to assert bipartite entanglement in pure quantum states, they are weaker conditions to detect bipartite entanglement for generic mixed states. We shall discuss in the subsequent section the appropriate quantities to address this issue.

1.3 Mixed state entanglement

Pure states are in general hard to realize in experimental platforms. The system or sub-system of interest is always coupled to an external environment. The description of the quantum state in such a scenario is more appropriately captured by the density matrix ρ_{AB} . In general, such states have a global purity $\text{Tr}(\rho_{AB}^2)$ less than one. Generic separable states can be constructed in terms of convex weights

p_ℓ and product states $\rho_A^{(\ell)} \otimes \rho_B^{(\ell)}$ acting on sub-system A and B respectively. We can define such a separable state by [53]

$$\rho_{AB} = \sum_{\ell} p_{\ell} \rho_A^{(\ell)} \otimes \rho_B^{(\ell)}. \quad (1.8)$$

These separable states could be classically correlated as one can prepare them only using LOCC operations but do not possess quantum correlations among the two parties. To certify entanglement for generic mixed states, one could already start with the purity or entropic condition mentioned in the previous section which remains valid in this situation as well [62]. A draw back of the latter is that the entropic condition is weak to detect entanglement present in generic mixed states. There are entangled states that are *not* detected by this condition. So, now let us discuss some more advanced tests that can typically better confirm the presence of entanglement in such mixed states.

1.3.1 Positive-partial transpose condition

The positive-partial transpose condition is based on a mathematical operation known as the *partial transpose*. To better understand this operation, let us expand for concreteness the density matrix ρ_{AB} in the bases $\{|i_A\rangle\}$ and $\{|i_B\rangle\}$ as given in Eq. (1.1)

$$\rho_{AB} = \sum_{i_A, j_A}^{d_A} \sum_{i_B, j_B}^{d_B} (\rho_{AB})_{(i_A j_A, i_B j_B)} |i_A\rangle\langle j_A| \otimes |i_B\rangle\langle j_B|. \quad (1.9)$$

The partial transposition consists in executing the transposition of the density matrix with respect to a given sub-system. Without loss of generality, the partial transposition performed with respect to the sub-system A can be noted by

$$\rho_{AB}^{T_A} = \sum_{i_A, j_A}^{d_A} \sum_{i_B, j_B}^{d_B} (\rho_{AB})_{(j_A i_A, i_B j_B)} |i_A\rangle\langle j_A| \otimes |i_B\rangle\langle j_B| \quad (1.10)$$

where we have exchanged the indices i_A and j_A . The density matrix ρ_{AB} is said to be *positive-partial transpose* (PPT) if $\rho_{AB}^{T_A}$ is positive semi-definite $\rho_{AB}^{T_A} \geq 0$, that is, its spectrum does not contain any negative eigenvalues. The negation of PPT is said to be *negative partial transpose* (NPT). This definition is followed by an entanglement criterion known as the PPT criterion or the Peres-Horodecki criterion [91] which states that: A bipartite separable state ρ_{AB} is PPT. More precisely, for a given state ρ_{AB} , if the spectrum of $\rho_{AB}^{T_A}$ contains a negative eigenvalue, then the state is necessarily entangled across the partition A and B [61].

The PPT criterion is also associated to an entanglement monotone known as the *negativity* [128] $\mathcal{N} = \sum_{\ell | \lambda_{\ell}' < 0} |\lambda_{\ell}'|$ and is defined by the spectrum λ_{ℓ}' of $\rho_{AB}^{T_A}$. It simply quantifies entanglement through the amount the PPT criterion is violated [128]. One may now wonder if the PPT condition detects all possible separable states? This is the case only for low dimensional systems. It has been shown that a state defined in $\mathcal{H}_A(2) \otimes \mathcal{H}_B(2)$ or $\mathcal{H}_A(2) \otimes \mathcal{H}_B(3)$ is separable if and only if it is PPT [61]. Though this condition is capable of detecting entanglement for many generic mixed states, there exists a class of entangled states known as *bound entangled* that can not be detected via this criterion [53]. Now let us move our focus to another entanglement detection condition known as the CCNR criteria for mixed quantum states that can detect some of the bound entangled states [53].

1.3.2 CCNR criterion

The *computable cross norm* or *realignment* criterion [107, 108] provides a simple test to certify entanglement for generic mixed states and in particular in a small window of entangled states that are not sensitive to the PPT criterion. The criteria states that if ρ_{AB} is separable then

$$\|\mathcal{R}(\rho_{AB})\|_1 \leq 1, \quad (1.11)$$

where we define the trace norm $\|X\|_1 = \text{Tr}(\sqrt{XX^\dagger})$ and the realignment operation as $[\mathcal{R}(\rho_{AB})]_{(i_A i_B, j_A j_B)} := (\rho_{AB})_{i_A j_A, i_B j_B}$ that re-shapes the original $d_A d_B \times d_A d_B$ density matrix ρ_{AB} into a *realigned* matrix of dimension $d_A^2 \times d_B^2$. This criterion can be further enhanced and generalized into the *enhanced realignment criterion* [140]. It states that, if a state ρ_{AB} is separable then

$$\|\mathcal{R}(\rho_{AB} - \rho_A \otimes \rho_B)\|_1 \leq \sqrt{1 - \text{Tr}(\rho_A^2)} \sqrt{1 - \text{Tr}(\rho_B^2)}. \quad (1.12)$$

where ρ_A and ρ_B are the RDMs on sub-systems A and B respectively. We note that the presence of bipartite entanglement between sub-systems A and B is confirmed when Eq. (1.11) or Eq. (1.12) are violated. Note that in Chapter. 5, we shall also introduce new variants of conditions based on the CCNR and the enhanced CCNR to detect entanglement in mixed quantum states.

Alternately, we can obtain the CCNR criterion by performing an *operator Schmidt decomposition* [53] of ρ_{AB} acting on a Hilbert space $\mathcal{H}_A(d_A) \otimes \mathcal{H}_B(d_B)$

$$\frac{\rho_{AB}}{\sqrt{\text{Tr}(\rho_{AB}^2)}} = \sum_{\ell} \mu_{\ell} O_{A,\ell} \otimes O_{B,\ell} \quad (1.13)$$

where we have the *operator* Schmidt coefficients μ_{ℓ} that are real and positive and the operators $O_{A,\ell}$ and $O_{B,\ell}$ that form an orthonormal basis on the operator space of sub-system A and B respectively. The LHS of Eq. (1.13) is appropriately normalized to ensure that $\sum_{\ell} \mu_{\ell}^2 = 1$. The CCNR criterion is equivalently expressed in terms of the operator Schmidt values, that is, a separable state ρ_{AB} satisfies [53]

$$\sum_{\ell} \mu_{\ell} \leq \frac{1}{\sqrt{\text{Tr}(\rho_{AB}^2)}}. \quad (1.14)$$

As seen previously, from the Schmidt decomposition of pure states, we defined a set of entropic quantities, namely the von Neumann and the Rényi entropies. We shall detail in the next section, how we can define in a similar spirit, entropic quantities based on the operator Schmidt coefficients obtained from the operator Schmidt decomposition.

1.3.3 Operator entanglement

The operator Schmidt decomposition can be more easily related to the standard Schmidt decomposition for pure states. Let us consider the state $\varrho_{AB} = \frac{\rho_{AB}}{\sqrt{\text{Tr}(\rho_{AB}^2)}}$. The connection between the two decompositions can be understood when we vectorize the operator ϱ_{AB} using the known Choi-Jamiołkowski isomorphism [71, 16]:

$$\varrho_{AB} = \sum_{i,j} (\varrho_{AB})_{i,j} |i\rangle\langle j| \quad \mapsto \quad |\varrho_{AB}\rangle = \sum_{ij} (\varrho_{AB})_{i,j} |i\rangle |j\rangle. \quad (1.15)$$

The vectorized operator state $|\varrho_{AB}\rangle$ now lives in a doubled Hilbert space $\mathcal{H}_{AB}(d) \otimes \mathcal{H}_{AB}(d)$. The operator Schmidt decomposition can be viewed as applying the Schmidt decomposition on the pure vectorized operator state $|\varrho_{AB}\rangle$ and then returning to the operator space [53]. With the operator Schmidt coefficients μ_ℓ , we define the *Rényi α -operator entanglement entropy* (Rényi α -OE) as

$$S^{(\alpha)}(\rho_{AB}) = \frac{1}{1-\alpha} \log \sum_{\ell=1}^{\text{srank}(\rho_{AB})} (\mu_\ell^2)^\alpha \quad (1.16)$$

and correspondingly the (Shannon) *operator entanglement entropy* [138, 136, 98, 95] which is the same in the limit of $\alpha \rightarrow 1$

$$S(\rho_{AB}) = - \sum_{\ell=1}^{\text{srank}(\rho_{AB})} \mu_\ell^2 \log \mu_\ell^2 \quad (1.17)$$

with $\text{srank}(\rho_{AB})$ being the operator Schmidt rank. We remark as previously done, that if the state obeys $S(\rho_{AB}) = 0$, then it can be expressed in an operator product form on subsystem A and B like $\rho_{AB} = \rho_A \otimes \rho_B$ and is said to be *operator separable*. On the contrary, when $S(\rho_{AB}) > 0$, ρ_{AB} is operator entangled. Importantly, it is worth noting the distinction of a quantum system being “operator” or “state” entangled. We emphasize on the fact that a quantum system can be operator entangled ($S(\cdot) > 0$) while being *not* entangled with respect to the definition of the standard terminology given for separable mixed states as defined in Eq. (1.8). In particular, Chapter. 5 shall discuss a method to measure the second operator Rényi entropy and reveal an interesting quantum many-body property associated with this quantity known as the *entanglement barrier* [26, 130].

Entanglement witnesses

Taking a short detour, in a simpler scenario, for *any* entangled state, one can construct an *entanglement witness* that is expressed as an expectation value of certain observables in order to detect entanglement [120]. This constructed observable \mathcal{W} , is designed to provide a negative outcome, only if the state being measured is entangled. In other words, if the measured value of the entanglement witness is below a certain threshold i.e $\text{Tr}(\mathcal{W}\rho) < 0$, it implies the presence of entanglement. Famous entanglement witnesses known as *Bell inequalities* [10] can assert the presence of *non-local correlations* in a prepared quantum state and thus also validate the presence of entanglement. To their advantage these quantities can be probed with minimal assumptions on the operations performed by the measurement device or the quantum state being measured: these are said to be *device-independent* entanglement witnesses. They simply focus on the correlations between measurement outcomes, making them experimentally accessible and applicable to a wide range of quantum systems. Note additionally that not *all* entangled states violate Bell inequalities [132, 53]. However, as mentioned earlier, every entangled state can be detected by a certain entanglement witness though it is not obvious to propose the right witness for a given unknown entangled state.

1.4 Multipartite entanglement

Let us now discuss the nature and structure of entanglement present amongst more than two parties. In recent years, there has been a significant interest to analyze the rich multipartite structure of quantum states. The characterization of multipartite entanglement allows us to have a fine-grained understanding of the structure of quantum states at the most fundamental level.

Let us consider a pure multipartite quantum state $|\psi\rangle$ constituted of N particles. It is easy to see that in the case when $N = 2$, we can classify the state either to be entangled or separable while $N > 2$ requires further finer investigation. We define a *fully separable* or *1-producible* state if we can decompose the quantum state $|\psi\rangle$ as a N -fold tensor product of states [53]

$$|\psi\rangle = \bigotimes_{i=1}^N |\phi_i\rangle, \quad (1.18)$$

where $|\phi_i\rangle$ describes the state of the i^{th} particle. In the case of mixed states, we can obtain a fully separable state in terms of a statistical mixture of fully separable pure states

$$\rho = \sum_j p_j |\psi_j\rangle\langle\psi_j| \quad (1.19)$$

with $p_j \geq 0$ and $\sum_j p_j = 1$. Clearly, upon examination, there exist many possible tensor product structures of such a multipartite state. One may either wonder about the number of particles that are entangled in state $|\psi\rangle$ or the number of decomposable separable partitions of the state $|\psi\rangle$. Both these questions can be addressed by the notion of *producibility* vs *separability* [53].

Firstly, we can introduce the notion of *k-producibility* that corresponds to a division of the multipartite state described by the largest non-separable set of at most k particles. More formally these states can be defined as

$$|\psi_{k\text{-prod}}\rangle = |\phi_{N_1}\rangle \otimes |\phi_{N_2}\rangle \otimes \cdots \otimes |\phi_{N_L}\rangle, \quad (1.20)$$

where N_l denotes the number of particles in the state $|\phi_{N_l}\rangle$ that satisfies $N_l \leq k$ for all values of l and $\sum_l N_l = N$. On the other hand, the notion of *m-separability* describes multipartite content in terms of a decomposition of the state in m possible separable blocks,

$$|\psi_{m\text{-sep}}\rangle = |\phi_{N_1}\rangle \otimes |\phi_{N_2}\rangle \otimes \cdots \otimes |\phi_{N_m}\rangle \quad (1.21)$$

where a given block l contains N_l particles with $\sum_l N_l = N$. There exists $\frac{m^N}{m!}$ possible manner to decompose m blocks from a total set of N particles.

We can observe that the two notions of *k-producibility* and *m-separability* describe different potential decompositions of the multipartite state $|\psi\rangle$ and provide a finer knowledge on the structure of entanglement. In two extreme cases, both these notions converge to the same multipartite description of the state, i.e $|\psi_{N\text{-sep}}\rangle = |\psi_{1\text{-prod}}\rangle$ describes the fully separable state as in Eq. (1.18). On the other hand, quantum states that are *not* $|\psi_{2\text{-sep}}\rangle$ or *not* $|\psi_{(N-1)\text{-prod}}\rangle$ describe a well-known class of states that are *genuinely multipartite entangled* (GME) and constitute all N particles to be entangled with each other. Note, additionally that we can define mixed *k-producible* or *m-separable* states as statistical mixtures via

convex combinations of at most k -producible or at least m -separable pure states respectively. Let us now discuss a particular quantity that is relevant to detect multipartite entanglement in quantum states.

1.4.1 Quantum Fisher information

The *quantum Fisher information* (QFI) being a fundamental quantity of relevance shares an important association with detecting multipartite entanglement in quantum systems. Its applications range from quantum metrology [8, 9, 94], many-body physics [131, 81], resource theory [74] to quantum information. The explicit expression of the QFI is defined in function of the eigenvalues λ_i of the density matrix $\rho = \sum_i \lambda_i |i\rangle\langle i|$ and an Hermitian operator \mathcal{A}

$$F_Q = 2 \sum_{(i,j), \lambda_i + \lambda_j > 0} \frac{(\lambda_i - \lambda_j)^2}{\lambda_i + \lambda_j} |\langle i | \mathcal{A} | j \rangle|^2. \quad (1.22)$$

When the state is pure $\rho = |\psi\rangle\langle\psi|$, the QFI is simply four times the variance of the operator \mathcal{A} : $F_Q = 4 (\langle\psi| \mathcal{A}^2 |\psi\rangle - \langle\psi| \mathcal{A} |\psi\rangle^2)$. Considering N spin 1/2 particles or qubits and $\mathcal{A} = \frac{1}{2} \sum_{l=1}^N \sigma_\nu^{(l)}$ with $\nu = x, y, z$ that defines the Pauli matrices, the QFI is directly linked to detecting entanglement in generic states ρ as all separable states obey $F_Q \leq N$ [93]. Thus $F_Q > N$ implies the presence of entanglement in the state ρ . The maximum attainable value of QFI is upper bounded by $F_Q \leq N^2$.

The deep relation of QFI and multipartite entanglement comes from the fact that it can witness the *entanglement depth* of a quantum state. The entanglement depth defines the number of particles that are non-trivially entangled in the state, i.e if a quantum state is *not* k -producible, then it contains an entanglement depth of *at least* $k + 1$. We can certify the entanglement depth of a given state with violations of certain bounds on the QFI (that form entanglement witnesses) [122, 67]. In particular, the entanglement depth is closely related to the producibility nature of the state as it consists of characterizing the number of entangled particles. Consider a k -producible state, then the following inequality holds:

$$F_Q \leq \Gamma(N, k) \equiv \left\lfloor \frac{N}{k} \right\rfloor k^2 + \left(N - \left\lfloor \frac{N}{k} \right\rfloor k \right)^2. \quad (1.23)$$

If $F_Q > \Gamma(N, k)$, then the quantum state is *not* k -producible and hence contains an entanglement depth $\geq k + 1$ [122, 67]. Apart for the QFI validating the presence of multipartite entanglement, let us also discuss some of its pertinent entanglement properties associated with quantum metrology.

1.4.2 Connection with quantum metrology

Quantum metrology is the field that focuses on obtaining enhanced estimations of unknown parameters from standard measurements [47]. Consider the estimation accuracy $\Delta\theta$ of an unknown parameter θ encoded in a quantum state $\rho(\theta)$ that is estimated by performing M measurements. The accuracy heavily depends and is always bounded by the inverse of the QFI of the quantum state $\rho(\theta)$ given by $\Delta\theta \geq \frac{1}{\sqrt{F_Q M}}$ which is called the Cramer-Rao bound [93]. Typically, the maximum phase accuracy provided by separable (or classical) states is limited by the

standard shot-noise limit $\Delta\theta = \frac{1}{\sqrt{NM}}$ [47]. Enhanced accuracies can be achieved for k -partite entangled (quantum) states given by $\Delta\theta = \frac{1}{\sqrt{kNM}}$ as the bound in Eq. (1.23) increases monotonically with the entanglement depth k [93]. In the case when the achieved value of QFI of a quantum state is saturated to N^2 , one attains the ultimate Heisenberg limit of sensitivity $\Delta\theta = \frac{1}{N\sqrt{M}}$ [93].

Interestingly, while entanglement remains extremely resourceful for quantum technological applications, it has been rigorously argued that not *all* entangled states are meaningful for enhanced metrological tasks [93, 94]. It has been shown that the states that obey $F_Q > N$ are *necessary and sufficient* to achieve higher sensitivities beyond the shot-noise limit [93]. Thus, as seen before, along with certifying entanglement, the previous inequality is central to identify quantum states that are more suited for applications in quantum metrology. Moreover, the usefulness of the states in terms of estimation accuracy is proportional to the value of QFI. In particular, states with larger entanglement depth provide higher accuracy as the bound in Eq. (1.23), increases proportionally with k : $F_Q \leq kN$ [122, 67]. The ultimate precision is provided by a genuinely multipartite entangled state that has an entanglement depth of $k = N$ with an associated QFI value of N^2 . Due to its great pertinence in various branches of quantum theory, we shall discuss at length in Chapter. 4, how to access the QFI in quantum platforms and demonstrate its estimation on a superconducting quantum device.

With this we end the introduction on the entanglement quantifiers around which this manuscript is centered. In the following chapter, we shall elaborate on methods to measure some of the previous quantities and quantify entanglement on experimental quantum hardware. In particular, we shall discuss and introduce the central method: the *randomized measurement toolbox* [31]. So stay tuned!

2

Introduction to randomized measurements

This chapter provides the necessary formal background to the randomized measurement toolbox which shall be the central measurement technique addressed in the subsequent chapters to measure interesting quantities associated with entanglement.

Contents

2.1	How are measurements done?	31
2.2	Estimation of properties with tomography	32
2.3	Estimation of the purity	34
2.3.1	Estimation of the purity using physical copies	34
2.4	Estimation of the purity using Random measurements	35
2.4.1	Short mathematical background	36
2.4.2	The RM protocol and its derivation	38
2.4.3	Fidelity estimations from random measurements	41
2.4.4	Post-processing and additional features of the RM protocol	42
2.5	The classical shadow formalism	45
2.5.1	Randomized measurement tomography	45
2.5.2	Classical Shadows	46
2.5.3	Estimation of quantum properties with classical shadows	48
2.6	Current challenges and outline	51

We are currently in the era where we have at our disposal noisy intermediate-scale quantum devices that range from tens to hundreds of qubits [97]. Lately, characterizing quantum properties prepared in these systems, independently of the architecture of the platform has raised a significant interest among theorists as well as experimentalists building such devices. In particular, measuring properties and quantities associated to entanglement, as introduced in the previous chapter, becomes relevant to understand the most elementary quantum property that can be used to benchmark the performance of quantum computers and simulators. What are the methods that help us measure physical properties embedded in these large Hilbert spaces? In this chapter, we shall present and discuss three potential candidates that address this problem and probe properties associated to entanglement prepared on a quantum hardware. In particular, we shall introduce the central method of this manuscript known as the *randomized measurement toolbox* (RM toolbox) [31] and shall re-derive the formalism in the context of measuring the purity of an unknown quantum state in generic quantum platforms made up of qubits. In addition, we will also discuss a vital addition to the RM toolbox known as the *classical shadow formalism* [64]. This formalism provides us with estimations of additional quantities of interest based on the randomized measurement framework. Before getting into the details of the toolbox, let us start by briefly discussing how a measurement procedure is done in common experimental setups.

2.1 How are measurements done?

Let us first describe the standard measurement procedure that are routinely done in quantum devices. We consider here for simplicity quantum devices made up of qubits. In such platforms, measurements typically consists of local operations performed to collapse the prepared state ρ in a fixed computational basis. The computational basis in general is defined as measuring each qubit locally along the z axis. Thus, after the local measurement operation, the state of each individual qubit either collapses to the state $|0\rangle\langle 0|$ or $|1\rangle\langle 1|$ associated to the bit-string 0 or 1 respectively. In the case of a N -qubit state, the set of observed bit-strings can possibly take 2^N different values. The probability to observe a given bit-string $\mathbf{s} = (s_1, \dots, s_N)$ with $s_i \in \{0, 1\}$ is given by the Born's rule

$$P(\mathbf{s}) = \text{Tr}(|\mathbf{s}\rangle\langle \mathbf{s}| \rho) = \langle \mathbf{s} | \rho | \mathbf{s} \rangle \quad (2.1)$$

where $|\mathbf{s}\rangle = |s_1\rangle \otimes \dots \otimes |s_N\rangle$. To estimate the probabilities experimentally requires repeating the measurement step multiple times. We prepare the state of interest ρ in the experiment and collect bit-string measurements $s^{(m)}$ from a finite number of repetitions $m = 1, \dots, N_M$ of the experiment. From this data, we can provide the estimated probability $\hat{P}(\mathbf{s})$ by counting the number of occurrence of the bit-string \mathbf{s} :

$$\hat{P}(\mathbf{s}) = \sum_{m=1}^{N_M} \frac{\delta_{s^{(m)}, \mathbf{s}}}{N_M}. \quad (2.2)$$

In the limit when $N_M \rightarrow \infty$, the estimated probability converges to the exact theoretical value of the probability given by the Born's rule $\mathbb{E}_{\text{QM}}[\hat{P}(\mathbf{s})] = P(\mathbf{s})$, where $\mathbb{E}_{\text{QM}}[\cdot]$ is the *quantum mechanical average* over the projective measurements.

These probabilities additionally can be used to extract expectation values of local observables that are diagonal in the computational basis. We can estimate, for example, the total transverse magnetization in the system given by $O = \frac{1}{2} \sum_{j=1}^N Z_j$, with Z_j being the Pauli- z matrix acting on the j^{th} qubit, directly from the measured bit-strings as given by

$$\langle O \rangle = \text{Tr}(O\rho) = \sum_{\mathbf{s}} \text{Tr}(|\mathbf{s}\rangle\langle\mathbf{s}| \rho) \langle \mathbf{s} | O | \mathbf{s} \rangle = \sum_{\mathbf{s}} P(\mathbf{s}) \langle \mathbf{s} | O | \mathbf{s} \rangle. \quad (2.3)$$

The above quantity can be *directly* linked to the measurement data obtained from the experiment using Eq. (2.2). An obvious question that arises is how do we compute the expectation value of observables that are not diagonal in the computational basis, like observables related to Pauli- x or Pauli- y operators X or Y respectively. In these cases, the experimental platforms need to implement a unitary transformation prior to the measurement operation. More specifically, in-order to measure the observable X_j , we need to perform a local Hadamard transformation $H_j = \frac{1}{\sqrt{2}} \begin{pmatrix} 1 & 1 \\ 1 & -1 \end{pmatrix}$ prior to the measurement. This transforms the computation basis of the j^{th} qubit to eigenbasis $|+\rangle$ and $|-\rangle$ of Pauli- x . Similarly, to measure expectation value of Y_j , one needs to execute a local transformation of $H_j S_j^\dagger = \frac{1}{\sqrt{2}} \begin{pmatrix} 1 & -i \\ 1 & +i \end{pmatrix}$ with $S_j = \begin{pmatrix} 1 & 0 \\ 0 & -i \end{pmatrix}$ being the single qubit phase gate prior to the measurement of the qubit. These transformations are done locally depending on the observable at question that needs to be measured and are easily executed in current devices. The expectation value of generic observable made up of local Pauli matrices can be directly calculated in a similar fashion as shown in Eq. (2.3). With this background, we can now discuss the existing methods that can be used to measure entanglement related quantities.

2.2 Estimation of properties with tomography

Quantum state tomography (QST) has been one of the “go to” methods to probe properties of quantum states prepared in experiments [54]. Suppose, we prepare an unknown N -qubit quantum state ρ in the experiment. The main objective of this algorithm is to reconstruct the quantum state ρ by performing repeated single copy measurements. To be more concrete, we can summarize QST as follows: A density matrix ρ defined on $\mathcal{H}(d)$ ($d = 2^N$) can always be expanded as a sum over N -fold tensor product of Pauli matrices [53]

$$\rho = \frac{1}{2^N} \sum_{\mathcal{P}} \text{Tr}(\rho \mathcal{P}) \mathcal{P} \quad (2.4)$$

where $\mathcal{P} = \bigotimes_{i=1}^N \mathcal{P}_i$ with $\mathcal{P}_i \in \{\mathbb{1}, X, Y, Z\}$ is a single qubit Pauli matrix. We note that the sum in the above equation runs over all possible combinations of single qubit Pauli matrices on N qubits. This results with a total number of summands

given by 4^N . Thus the central objective of QST is to measure each Pauli string \mathcal{P} and estimate its associated weight $\text{Tr}(\rho\mathcal{P})$. The weight $\text{Tr}(\rho\mathcal{P})$ is equivalent to the estimation of an expectation value of the prepared state ρ with respect to a given Pauli string \mathcal{P} and can be easily performed for each \mathcal{P} as detailed in previous section. Once we have reconstructed the quantum state, we can probe all its associated properties related to entanglement from the same measurement data. The main catch of this method is that it requires an expensive measurement budget. The required number of measurements to overcome statistical errors that occur as we repeat the experiment a finite number of times, scale exponentially with respect to the system size N . More concretely, it has been shown that to achieve an accuracy ε in trace distance for a quantum state of rank R , requires a number of single copy measurements that scales as $M = \mathcal{O}(2^N R^2/\varepsilon^2)$ [54]. In the case of an unknown quantum state of full rank, the sample complexity (required number of measurements) scales as $M = \mathcal{O}(2^{3N}/\varepsilon^2)$ and becomes prohibitively expensive. Additionally, the task to classically post-process the measurement data can be over-burdening due to an exponential increase of the required classical memory as a function of N . These reasons limit the use of QST on system sizes up to 8 – 10 qubits [116].

There have also been alternative proposals that take into consideration some suitable assumptions on the quantum state and provide sample complexity improvements for QST. These include the following short list:

- QST using *compressed sensing* [52] can help reduce the required number of measurements for state reconstruction. This method is effective when the investigated density matrix has a *low rank* (close to a pure state) as the measurements could only be done within the rank of the density matrix.
- Under the assumption that the quantum state can be well approximated by a matrix product state (MPS) of low bond dimension, that is, it has a low level of entanglement, one can use the technique of *MPS tomography* [21, 77]. This method is efficient as the number of measurements scale polynomially as a function of the system size N .
- *Neural network tomography* can be used to train few parameters of a classical neural network model which can in turn represent the quantum state in terms of an efficient ansatz [121, 13].

As QST is in general an expensive tool to implement in terms of the measurement cost and the classical treatment of the measurement data; one may consider looking for alternative approaches that do not require an explicit reconstruction of the state and can be applied to investigate properties of arbitrary quantum states of interest without prior assumptions on their structure. In particular, in order to measure properties of the quantum states for larger systems, we may want to develop methods that *directly* give access to these estimates from the data acquired from the experiment. Importantly, these approaches should be practical and can be readily implemented on current quantum hardware with cheap post-processing methods of the experimental data. In this context, let us now describe alternate approaches to estimate state-agnostically a simple non-linear quantity of the quantum state as introduced in the previous chapter: *the purity*.

2.3 Estimation of the purity

The purity of the quantum state $p_2 = \text{Tr}(\rho^2)$ is a simple but fundamental quantity that not only asserts the presence of entanglement in a quantum state ρ , but also relates more importantly to the second Rényi entropy $S_2(\rho) = -\log \text{Tr}(\rho^2)$ (in Eq. (1.6)). Firstly, as we have seen earlier in Chapter. 1 (Sec. 1.2.1), measuring the purity (or second Rényi entropy) can immediately detect the presence of entanglement in the quantum system. This quantity can also reveal interesting properties of entanglement in terms of its scaling with respect to the (sub-)system sizes as described by an area law [27] (the entanglement entropy grows with the area of the (sub-)system) or volume law (the entanglement entropy grows with the volume of the (sub-)system), universal signatures of quantum phase transitions [66] and finally topological order [75] created by long-range entanglement that is characterized by the topological entanglement entropy [75, 57]. In addition, the purity provides a simple figure of merit to benchmark the quality of state produced after executing an algorithm on noisy quantum processors. A purity close to one can immediately suggest a well executed quantum circuit or quantum dynamics that has not been affected drastically by errors and decoherence in the experiment. First, let us begin by reviewing other methods to access the purity of a quantum state ρ .

2.3.1 Estimation of the purity using physical copies

The purity can be alternately formulated in terms of a linear observable over two copies of the quantum state ρ

$$p_2 = \text{Tr}(\rho^2) = \text{Tr}(\mathbb{S}\rho \otimes \rho) \quad (2.5)$$

where the swap operator \mathbb{S} is defined on $\mathcal{H}(d) \otimes \mathcal{H}(d)$ and acts on two copies of the state $|i_1\rangle$ and $|i_2\rangle$ as $\mathbb{S}|i_1\rangle \otimes |i_2\rangle = |i_2\rangle \otimes |i_1\rangle$. The above expression can be readily seen as

$$\text{Tr}(\mathbb{S}\rho \otimes \rho) = \sum_{j_1, j_2} \langle j_2, j_1 | \rho \otimes \rho | j_1, j_2 \rangle = \sum_{j_1, j_2} \langle j_2 | \rho | j_1 \rangle \langle j_1 | \rho | j_2 \rangle = \text{Tr}(\rho^2). \quad (2.6)$$

From the above equation, the purity can be measured as the expectation value of the swap operator. This formalism requires at first the realization of two *identical physical copies* $\rho \otimes \rho$ of the quantum state in the experiment and then to perform joint entangling operations between the two independent copies (or Bell measurements) to estimate the expectation value of the swap operator [68, 6]. One of the first measurement of the purity up to six atoms using this protocol was demonstrated in a platform composed of ultra-cold bosonic gas [68]. These impressive experiments consisted in demonstrating entanglement dynamics between two phases of the Bose-Hubbard model. The ground state prepared at large interaction strengths of this model which is described by a Mott insulator (product state with $S_2(\rho) = 0$) melted into a super-fluid state (entangled state with $S_2(\rho) > 0$) at smaller values of the interaction strength. More advanced recent experiments on neutral atom quantum platform have demonstrated this method's applicability to measure $S_2(\rho)$ up to eight qubits [6].

One of the main technological challenges of this protocol is that it requires physical copies of the state that can be created and coherently manipulated in noisy

quantum platforms. For this reason, one may be limited by the system size of the experimental platform at hand or could potentially find it practically difficult, based on the architecture layout of the platform, to implement joint-entangling measurement operations. So, a more practical question that can be asked is the following: Given a single copy of a quantum hardware, can we estimate the purity of the state realized in this system with a direct method that would scale more favorably compared to QST? The answer to this question directly leads us to introduce the central method of this manuscript known as the *randomized measurement toolbox* (RM toolbox) [31]. It was originally inspired by the two copy estimation of the purity in Eq. (2.5) [30] and provided a protocol that can be easily implemented in current experiments with repeated single copy operations that are done in the case of QST.

In summary, a quick overview of the following section goes as follows: We shall begin by providing some historical background that inspired the creation of the current RM protocol. To understand and appreciate the details of the RM protocol, we will present a short mathematical background to summarize the necessary tools at play. Following this, we will provide the full derivation of the protocol as presented in [30] and discuss further some of its key features that include the required number of measurements to overcome statistical errors, classical data treatment to obtain estimations from experimental data and some of its robustness characteristics.

2.4 Estimation of the purity using Random measurements

The main intuition of the RM toolbox [31] is to replace the method employing entangling measurements on multiple physical copies of the state by *an estimate of the statistics of finite rounds of randomized experiments* performed only on single copies of the state at a given instance. The historical background of this method was first presented by van Enk and Benakeer [36]. They claimed that non-linear properties of the state ρ such as trace moments $p_n = \text{Tr}(\rho^n)$ can be estimated directly without the use of multiple copies or state reconstruction in the case of a single multi-level system ($N = 1$). The additional ingredient that they introduced was to use *random unitaries* chosen from an appropriate ensemble prior to the projective measurements on the system. This step repeated multiple times on single copies for different unitaries yields a collection of random measurements that can provide estimation of moments p_n . Inspired by their work, further works [29, 124, 30, 11] developed this formalism to be applicable for many-body systems ($N > 1$) with random unitaries that can be applied locally on each individual constituent or globally on the whole quantum state as preferred by the constraints of the experimental setup [124].

We shall now detail in the following subsections the formalism of the randomized measurement toolbox that can estimate the purity using statistical correlations of the random measurement data. We will begin by giving the reader a short theoretical background on some useful mathematical tools in this context.

2.4.1 Short mathematical background

Let us consider for simplicity a quantum system composed of N -qubits and the set $\mathcal{U}(d)$ containing all the unitary matrices defined on the full space of these N qubits with $d = 2^N$. We consider *Haar random unitaries* that are sampled according to the distribution of the Haar measure on this unitary group [20]. The Haar measure defines an unique measure that remains invariant under group multiplication: For $U, V \in \mathcal{U}(d)$, the ensemble average over the Haar measure of a function $f(V)$ defined on $\mathcal{U}(d)$ satisfies

$$\int_{\text{Haar}} dV = 1 \quad (2.7)$$

and

$$\int_{\text{Haar}} dV f(V) = \int_{\text{Haar}} dV f(UV) = \int_{\text{Haar}} dV f(VU). \quad (2.8)$$

The group $\mathcal{U}(d)$ that respects the Haar measure is called a *circular unitary ensemble* (CUE). We can estimate averages, according to the Haar measure, for an operator O that acts on the same space. This action is described by a quantum channel $\Phi(O)$

$$\Phi(O) = \int_{\text{Haar}} dV V^\dagger O V \quad (2.9)$$

where the operator O is averaged or *twirled* over all possible choice of unitaries $V \in \mathcal{U}(d)$. Twirling an operator in simple terms can be seen as a “sandwich” of the operator O between V^\dagger and V that is averaged over the different choices of unitaries V . One can also compute averages over higher order moments of the unitaries V . We can now consider an operator O that acts on $\mathcal{H}(d)^{\otimes t}$. Twirling the operator over t -copies which is also known as a *t -fold Haar twirl* $\Phi^{(t)}(O)$ can be defined as

$$\Phi^{(t)}(O) = \int_{\text{Haar}} dV (V^\dagger)^{\otimes t} O V^{\otimes t}. \quad (2.10)$$

To sample random unitaries V acting on $\mathcal{H}(d)$ from the CUE is a hard task to implement on realistic quantum platforms as it demands an exponential resource with the system size N . For example, to generate a Haar random unitary V that acts on N qubits requires a quantum circuit made up of $\mathcal{O}(N^2 2^{2N})$ number of single and two qubit gates [35]. This makes sampling a large number of unitaries practically unfeasible. Instead, to compute averages of higher order moments over the Haar measure, one could restrict the unitaries to form a finite set $\{V_i\}$ with $i = 1, \dots, K$. The set $\{V_i\}$ is said to be a *unitary t -design* [51] if and only if

$$\forall O : \frac{1}{K} \sum_{i=1}^K V_i^{\dagger \otimes t} O V_i^{\otimes t} = \Phi^{(t)}(O) = \int_{\text{Haar}} dV V^{\dagger \otimes t} O V^{\otimes t} \equiv \mathbb{E}_V [V_i^{\dagger \otimes t} O V_i^{\otimes t}], \quad (2.11)$$

that is, the average over this discrete set is equal to an average over all possible unitaries according to the Haar measure for multi-copy polynomials of V of degree t . We have also added the short hand notation $\mathbb{E}_V[\cdot]$ to denote the average over the unitaries. Moreover, if a set is an unitary t -design then it is automatically an unitary t' -design for $t' < t$. For example, the Clifford group is known to be a 2-design as it is a 3-design [143] but does not satisfy the necessary relations to be

a 4–design [144]. The set of unitary t –designs bring practical values as they can be efficiently realized with local random circuits and in quantum simulators having generic local interactions.

To explicitly evaluate the t –fold twirling of an operator O as described before, we can use the mathematical identity in the form of Schur-Weyl duality [106]

$$\Phi^{(t)}(O) = \sum_{\pi, \sigma \in \mathcal{S}_t} C_{\pi, \sigma} W_{\pi} \text{Tr}(W_{\sigma} O) \quad (2.12)$$

where W_{π} is a t –copy permutation operator belonging to the symmetric group \mathcal{S}_t and π denotes the permutation of the index that acts as $j \mapsto \pi(j)$. Its action is defined as

$$W_{\pi} |i_1, \dots, i_t\rangle = |i_{\pi(1)}, \dots, i_{\pi(t)}\rangle, \quad \forall |i_1, \dots, i_t\rangle \in \mathcal{H}(d)^{\otimes t} \quad \text{and for } \pi \in \mathcal{S}_t, \quad (2.13)$$

where the $|i_m\rangle$ are the basis states defined in the Hilbert space $\mathcal{H}(d)$ with an implicit tensor product over the qubits. The matrix C is called the Weingarten matrix whose coefficients $C_{\pi, \sigma} = \text{Wg}(\pi\sigma^{-1})$ can be calculated using the Weingarten function Wg [19]. For example, we show the explicit expressions for the cases of $t = 1, 2$, which will come in our use in later computations.

We can explicitly express the t –fold twirling by using Eq. (2.12) and replacing the appropriate identity for the Weingarten matrix. The 1–fold twirling identity for an operator O in $\mathcal{H}(d)$ can be written as

$$\Phi^{(1)}(O) = \frac{\mathbb{1}}{d} \text{Tr}(O) \quad (2.14)$$

while, the 2–fold twirling identity for an operator $O \in \mathcal{H}(d)^{\otimes 2}$ writes as

$$\Phi^{(2)}(O) = \frac{1}{d^2 - 1} \left(\mathbb{1} \text{Tr}(O) + \mathbb{S} \text{Tr}(\mathbb{S} O) - \frac{1}{d} \mathbb{S} \text{Tr}(O) - \frac{1}{d} \mathbb{1} \text{Tr}(\mathbb{S} O) \right). \quad (2.15)$$

The above equation is a result of an expansion of the sum in Eq. (2.12) with respect to the elements $\pi, \sigma \in \mathcal{S}_t$. We note here that the permutation operator $W_{(1,2)} = \mathbb{1}$ and $W_{(2,1)} = \mathbb{S}$ defined on the space $\mathcal{H}(d)^{\otimes 2}$ respectively. Also for the sake of completeness of the above result, we have $\text{Wg}(\mathbb{1}) = \frac{1}{d}$ for $t = 1$ and $\text{Wg}(\mathbb{1}^{\otimes 2}) = \frac{1}{d^2 - 1}$, $\text{Wg}(\mathbb{S}) = \frac{-1}{d(d^2 - 1)}$ for $t = 2$.

Twirling for local unitaries

Consider now for simplicity unitaries belonging to $\mathcal{H}(d)$ defined as $V = \bigotimes_{i=1}^N V_i$, where each V_i is a *local random unitary* sampled from the CUE defined on the unitary group $\mathcal{U}(2)$ that acts of the i^{th} qubit. As we shall see later on, the algebra that we present here for the local unitaries are well motivated as they can be effectively implemented in most of the current experimental qubit platforms.

When we have an operator O of the form $O = \bigotimes_{i=1}^N O_i$, the t –fold twirling can be similarly computed in terms of tensor product of permutation operators π_i and σ_i that act locally on each qubit. This explicitly writes as

$$\Phi_N^{(t)} \left(\bigotimes_{i=1}^N O_i \right) = \bigotimes_{i=1}^N \Phi_1^{(t)}(O_i) = \bigotimes_{i=1}^N \sum_{\pi_i, \sigma_i \in \mathcal{S}_t} C_{\pi_i, \sigma_i} W_{\pi_i} \text{Tr}(W_{\sigma_i} O_i) \quad (2.16)$$

where \mathcal{S}_t is the symmetric group. The same calculation for t -fold twirling ($t = 1, 2$) in the case of a single qubit product operator O_i gives

$$\Phi_1^{(1)}(O_i) = \frac{\mathbb{1}_i}{2} \text{Tr}(O_i) \quad (2.17)$$

for the 1-fold twirling and

$$\Phi_1^{(2)}(O_i) = \frac{1}{3} \left(\mathbb{1}_i \text{Tr}(O_i) + \mathbb{S}_i \text{Tr}(\mathbb{S}_i O_i) - \frac{1}{2} \mathbb{S}_i \text{Tr}(O_i) - \frac{1}{2} \mathbb{1}_i \text{Tr}(\mathbb{S}_i O_i) \right) \quad (2.18)$$

for the 2-fold twirling. We have used here the fact that local Hilbert space dimension of each qubit is $d = 2$ and the operators $W_{(1,2)_i} = \mathbb{1}_i$ and $W_{(2,1)_i} = \mathbb{S}_i$ act on the i^{th} qubit.

This summarizes the required mathematical background to address and understand the details of the RM toolbox formalism to measure the purity. In the next sub-section we shall describe and derive the estimation of the purity from random measurements.

2.4.2 The RM protocol and its derivation

In this section we shall re-derive the formalism of the randomized measurement toolbox (RM toolbox) based on the prior work of [30], to estimate the purity of a quantum state. The RM protocol introduced in [29, 11, 125, 32], are based on applying random unitaries U sampled from at least an unitary 2-design or CUE. In particular, we shall be more interested in the case where we want to estimate the purity of a N -qubit quantum state prepared in a quantum device that has the capability to perform independent local random operations on each individual qubit. The only requirements from the experimental side for the RM protocol is firstly to be able to rotate randomly each individual qubit independently on the Bloch sphere and secondly to be able to measure the state of each qubit in a fixed computational basis. These requirements are generally easily satisfied in many of the current available quantum devices.

Protocol

We illustrate the randomized measurement protocol in Fig. 2.1. We prepare a N -qubit state of interest ρ . This is followed by local random operations $U = U_1 \otimes \cdots \otimes U_N$ that are applied on the quantum state where single qubit random unitaries U_i are sampled from at least a 2-design. The rotated state $U\rho U^\dagger$ is then locally projected for each qubit on a fixed computational basis state $|\mathbf{s}\rangle = |s_1, \dots, s_N\rangle$. We independently repeat this procedure of single copy measurements for N_U distinct random unitaries $U^{(r)}$ with $r = 1, \dots, N_U$ and for each of the applied unitary $U^{(r)}$, subsequently record N_M bit-string outcomes $\mathbf{s}^{(r,m)} = (s_1^{(r,m)}, \dots, s_N^{(r,m)})$ with the additional label $m = 1, \dots, N_M$ running over the number of projective measurements performed. The total number of experimental runs is then given by $M = N_U N_M$, which is the product of the number of applied unitaries and the number of projective measurements performed for each unitary. This provides a data set collected from the experiment in the form of bit-strings that implicitly carry information about the prepared quantum state ρ and also the applied random unitaries $U^{(r)}$.

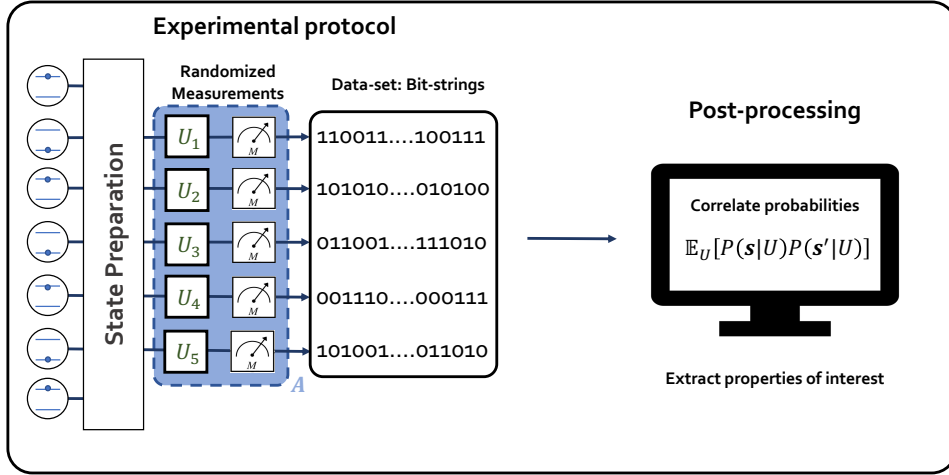


Figure 2.1: *Randomized measurement protocol* — The figure describes the randomized measurement protocol. We prepare a state of interest in the experiment. We apply a set of random unitaries sampled from a suitable ensemble followed by measurements in a fixed computational basis. The data-set comprises of the bit-strings that implicitly carry the knowledge of the unitaries and the prepared state. Fast data post-processing allow us to extract some non-linear quantities of interest from this experimental data.

From this data, one can estimate the probability given by the Born's rule to observe a spin configuration $|\mathbf{s}\rangle$ after the applied random rotation U

$$P(\mathbf{s}|U) = \text{Tr} (|\mathbf{s}\rangle\langle\mathbf{s}| U \rho U^\dagger) = \langle\mathbf{s}| U \rho U^\dagger |\mathbf{s}\rangle. \quad (2.19)$$

The main intuition of the derivation as mentioned in [30] is to compute the average over the random unitaries $\mathbb{E}_U[\cdot]$ of *second order correlations* of the outcome probabilities obtained from the RM data-set. As a first observation that was made in [30], we note that the ensemble average over the unitaries of the cross-correlation of the outcome probabilities can be written as an expectation value of an operator O and the twirled state $\Phi^{(2)}(\rho^{\otimes 2})$. Defining such an operator O that is diagonal in the computational basis $O = \sum_{\mathbf{s}, \mathbf{s}'} O_{\mathbf{s}, \mathbf{s}'} |\mathbf{s}\rangle\langle\mathbf{s}| \otimes |\mathbf{s}'\rangle\langle\mathbf{s}'|$ and by recalling the action of the 2-fold twirl (Eq. (2.10) for $t = 2$), we have

$$\begin{aligned} \text{Tr} (O \Phi^{(2)}(\rho^{\otimes 2})) &= \text{Tr} (O \Phi^{(2)\dagger}(\rho^{\otimes 2})) = \text{Tr} \left(\sum_{\mathbf{s}, \mathbf{s}'} O_{\mathbf{s}, \mathbf{s}'} |\mathbf{s}, \mathbf{s}'\rangle\langle\mathbf{s}, \mathbf{s}'| \mathbb{E}_U [U^{\otimes 2}(\rho \otimes \rho) U^{\dagger \otimes 2}] \right) \\ &= \sum_{\mathbf{s}, \mathbf{s}'} O_{\mathbf{s}, \mathbf{s}'} \text{Tr} (\mathbb{E}_U [|\mathbf{s}\rangle\langle\mathbf{s}| \otimes |\mathbf{s}'\rangle\langle\mathbf{s}'| U^{\otimes 2} \rho^{\otimes 2} (U^\dagger)^{\otimes 2}]) \\ &= \sum_{\mathbf{s}, \mathbf{s}'} O_{\mathbf{s}, \mathbf{s}'} \mathbb{E}_U [\text{Tr} (|\mathbf{s}\rangle\langle\mathbf{s}| U \rho U^\dagger) \text{Tr} (|\mathbf{s}'\rangle\langle\mathbf{s}'| U \rho U^\dagger)] \\ &= \sum_{\mathbf{s}, \mathbf{s}'} O_{\mathbf{s}, \mathbf{s}'} \mathbb{E}_U [P(\mathbf{s}|U)P(\mathbf{s}'|U)] \end{aligned} \quad (2.20)$$

where we have used the fact that the 2-fold twirling channel is Hermitian-preserving and obeys self-duality: $\Phi^{(2)}(\cdot) = \Phi^{(2)\dagger}(\cdot)$. Most importantly, we see that the RHS of

the above expression is what we can estimate from the experimental data consisting of bit-strings. We remark that the operator O can be viewed as a *virtual* two copy observable. It is virtual in the sense that the average over the applied unitaries taken for the cross-correlations of the bit-string probabilities *effectively* provides a two copy observable. In the experiment, we do not have two *physical* copies of the state but rather only perform single copy measurements. Thus from the self-duality of the channel we get

$$\mathrm{Tr} (O \Phi^{(2)} (\rho^{\otimes 2})) = \mathrm{Tr} (\Phi^{(2)} (O) \rho \otimes \rho). \quad (2.21)$$

We begin to notice that the final form of the above expression starts to resemble close to a form of the purity that we have defined earlier in Eq. (2.5). So in-order to directly relate the cross-correlations of the probabilities that are accessed from the experimental measurement data to the purity, we equate

$$p_2 = \mathrm{Tr}(\rho^2) = \mathrm{Tr}(\mathbb{S}\rho \otimes \rho) = \mathrm{Tr} (\Phi^{(2)} (O) \rho \otimes \rho) = \sum_{\mathbf{s}, \mathbf{s}'} O_{\mathbf{s}, \mathbf{s}'} \mathbb{E}_U [P(\mathbf{s}|U)P(\mathbf{s}'|U)]. \quad (2.22)$$

Thus the main goal now is to find the appropriate operator O and its coefficients $O_{\mathbf{s}, \mathbf{s}'}$ that satisfy $\Phi^{(2)} (O) = \mathbb{S}$.

Purity estimator for local random unitaries

Our starting point consists in noting that the swap operator acting on $\mathcal{H}(d) \otimes \mathcal{H}(d)$ can be expressed as

$$\mathbb{S} = \sum_{\mathbf{s}, \mathbf{s}'} |\mathbf{s}'\rangle\langle\mathbf{s}| \otimes |\mathbf{s}\rangle\langle\mathbf{s}'| = \bigotimes_{i=1}^N \sum_{s_i, s'_i} |s'_i\rangle\langle s_i| \otimes |s_i\rangle\langle s'_i| = \mathfrak{s}^{\otimes N} \quad (2.23)$$

where $\mathfrak{s} = \sum_{s, s'} |s'\rangle\langle s| \otimes |s\rangle\langle s'|$ is the swap operator defined on $\mathcal{H}(2) \otimes \mathcal{H}(2)$ and acts on 2-copies of a single qubit. Thus considering the same structure for our operator $O = o^{\otimes N}$ that acts locally on each site, we have

$$\Phi^{(2)} (O) = \Phi_N^{(2)} (o^{\otimes N}) = \left(\Phi_1^{(2)} (o) \right)^{\otimes N} = \mathfrak{s}^{\otimes N}. \quad (2.24)$$

Then, using the identity presented in Eq. (2.18), it is sufficient to determine the local two copy single qubit operator $o = \sum_{s, s'}^2 o_{s, s'} |s\rangle\langle s| \otimes |s'\rangle\langle s'|$ along with its coefficients that satisfy

$$\Phi_1^{(2)} (o) = \frac{1}{3} \left(\mathbb{1} \mathrm{Tr}(o) + \mathfrak{s} \mathrm{Tr}(\mathfrak{s}o) - \frac{1}{2} \mathfrak{s} \mathrm{Tr}(o) - \frac{1}{2} \mathbb{1} \mathrm{Tr}(\mathfrak{s}o) \right) = \mathfrak{s} \quad (2.25)$$

that act on two copies of the single qubit. This implies

$$\mathrm{Tr}(o) - \frac{1}{2} \mathrm{Tr}(\mathfrak{s}o) = 0 \quad \text{and} \quad \mathrm{Tr}(\mathfrak{s}o) - \frac{1}{2} \mathrm{Tr}(o) = 3, \quad (2.26)$$

which requires the following equations to hold:

$$\mathrm{Tr}(o) = \sum_{s, s'} o_{s, s'} = 2 \quad \text{and} \quad \mathrm{Tr}(\mathfrak{s}o) = \sum_s o_{s, s} = 4. \quad (2.27)$$

The simple choice of $o_{s,s'}$ that satisfies the above equations was found in Ref. [30, 11] as $o_{s,s'} = 2 \times (-2)^{-D[s,s']}$ where D is the Hamming distance which is one if $s \neq s'$ and zero if $s = s'$. By replacing the coefficient $O_{s,s'} = 2^N \prod_{i=1}^N (-2)^{-D[s_i,s'_i]} = 2^N \times (-2)^{-D[s,s']}$ in Eq. (2.22) we can re-express the purity of a quantum state as

$$p_2 = \text{Tr}(\mathbb{S}\rho \otimes \rho) = 2^N \sum_{\mathbf{s}, \mathbf{s}'} (-2)^{-D[\mathbf{s}, \mathbf{s}']} \mathbb{E}_U [P(\mathbf{s}|U)P(\mathbf{s}'|U)]. \quad (2.28)$$

The above equation is an important relation that relates directly the quantity of interest (in this case the purity) to estimations of spin probabilities that can be computed from the data of the RM protocol. Analogously, the Rényi entropy can be simply estimated by taking the negative logarithm of the above expression. We also remark that the estimator of purity provided here does not require explicitly the knowledge of the applied unitary as one only needs to construct probabilities from the collected bit-strings of the RM data.

2.4.3 Fidelity estimations from random measurements

In addition, the expression of the purity in Eq. (2.28) with a slight modification can also be used to estimate fidelities between two quantum states ρ_1 and ρ_2 that are prepared in two separate quantum platforms. To illustrate the idea briefly, which can directly be derived using a similar reasoning as before; we consider a scenario where two quantum devices independent of the type of architecture, would like to realize the same state ρ . As both the platforms will suffer from different types of errors during the state preparation, they will end up generating two different states ρ_1 and ρ_2 in each platform respectively. The fidelity can be used as a metric to understand the overlap between the two prepared states. In the particular case of pure quantum states, the fidelity can be defined as an overlap $\mathcal{F}_{\text{pure}}(|\psi_1\rangle, |\psi_2\rangle) = |\langle \psi_1 | \psi_2 \rangle|^2$ where $|\psi_1\rangle$ and $|\psi_2\rangle$ denote the pure states prepared on device 1 and 2 respectively. For mixed states, we can consider the fidelity defined as [79]

$$\mathcal{F}(\rho_1, \rho_2) = \frac{\text{Tr}(\rho_1 \rho_2)}{\max\{\text{Tr}(\rho_1^2), \text{Tr}(\rho_2^2)\}}. \quad (2.29)$$

In order to estimate this quantity, the main intuition given in [32] is that the overlap is expressed in terms of the swap operator $\text{Tr}(\rho_1 \rho_2) = \text{Tr}(\mathbb{S}\rho_1 \otimes \rho_2)$. Though one can directly measure the overlap by performing joint measurements on the two platforms simultaneously, it becomes quite evident that this method is highly impractical when the two states are prepared on two different architectures of quantum platforms located in two distinct locations. We can employ an alternative method based on the purity formula obtained above, where we can cross-correlate the probabilities estimations from the two devices to realize an effective virtual swap operator [32]. In the protocol, we apply *the same* set of N_U unitaries and record N_M bit-string measurements for each of them. We calculate the probabilities $P_1(\mathbf{s}|U)$ and $P_2(\mathbf{s}'|U)$ after having applied the unitary U on platform 1 and 2 respectively by

$$P_i(\mathbf{s}|U) = \text{Tr}(|\mathbf{s}\rangle\langle \mathbf{s}| U \rho_i U^\dagger) = \langle \mathbf{s} | U \rho_i U^\dagger | \mathbf{s} \rangle \quad (2.30)$$

with $i = 1$ or 2 . Cross-correlating these probabilities as done previously to derive the purity of the state [30], we finally obtain

$$\text{Tr}(\rho_1 \rho_2) = \text{Tr}(\mathbb{S}\rho_1 \otimes \rho_2) = 2^N \sum_{\mathbf{s}, \mathbf{s}'} (-2)^{-D[\mathbf{s}, \mathbf{s}']} \mathbb{E}_U [P_1(\mathbf{s}|U)P_2(\mathbf{s}'|U)]. \quad (2.31)$$

The major advantage of this formula is that one can estimate fidelities between two experimental platforms *directly* by sharing the experimental data classically (over the internet for example) [32]. Quantum platforms all around the world can be benchmarked against one another or against a theoretical state with this method.

Let us now move the discussion to detail how to treat the experimental data in the post-processing phase of the RM protocol. We shall also highlight some of the important features that provide an advantage to estimate the purity (or overlap) from the RM protocol compared to other proposed methods.

2.4.4 Post-processing and additional features of the RM protocol

Post-processing

As we have seen previously, the RM protocol consists of applying N_U different local random unitaries $U^{(r)}$ and recording N_M bit-string measurements for each of them. The experimental data obtained after executing the RM protocol consists of a collection of bit-strings $\mathbf{s}^{(r,m)} = (s_1^{(r,m)}, \dots, s_N^{(r,m)})$ with $s_i^{(r,m)} \in \{0, 1\}$ that are labeled by $r = 1, \dots, N_U$ and $m = 1, \dots, N_M$. Each of the bit-string $\mathbf{s}^{(r,m)}$ is a random variable that is distributed according to the Born's rule $P(\mathbf{s}|U^{(r)})$ as defined in Eq. (2.19). With this data-set, we can provide an estimator $\hat{P}(\mathbf{s}|U^{(r)})$ that gives the estimated probability to observe the bit-string \mathbf{s} after having applied the unitary $U^{(r)}$

$$\hat{P}(\mathbf{s}|U^{(r)}) = \sum_{m=1}^{N_M} \frac{\delta_{\mathbf{s}^{(r,m)}, \mathbf{s}}}{N_M} \quad (2.32)$$

where we simply count the number of occurrences of the bit-string $\mathbf{s}^{(r,m)} = \mathbf{s}$. In the limit when $N_M \rightarrow \infty$, the estimated probability converges to the exact theoretical value of the probability given by the Born's rule $\mathbb{E}_{\text{QM}} [\hat{P}(\mathbf{s}|U^{(r)})] = P(\mathbf{s}|U^{(r)})$. To estimate the purity as given in Eq. (2.28) (or analogously for the overlap between two quantum states as in Eq. (2.31)), we need an estimate of the cross-correlation of the probabilities. We note importantly that $\mathbb{E}_{\text{QM}} [\hat{P}(\mathbf{s}|U^{(r)})\hat{P}(\mathbf{s}'|U^{(r)})] \neq P(\mathbf{s}|U^{(r)})P(\mathbf{s}'|U^{(r)})$ and has a bias of $\mathcal{O}(1/N_M)$ [124]. Thus, if one naively averages the cross-correlations of the estimated probabilities respectively for \mathbf{s} and \mathbf{s}' , one would obtain a biased estimator of the purity. In order to provide unbiased estimates of polynomial functionals, we use the theory of U-statistics [59]. The U-statistics estimator can be formulated by summing all possible *different pairs* of bit-strings [124] recorded for a single unitary $U^{(r)}$. This gives for an applied unitary $U^{(r)}$

$$P(\mathbf{s}|U^{(r)})P(\mathbf{s}'|U^{(r)}) = \mathbb{E}_{\text{QM}} \left[\frac{1}{N_M(N_M - 1)} \sum_{m \neq m'} \delta_{\mathbf{s}, \mathbf{s}^{(r,m)}} \delta_{\mathbf{s}', \mathbf{s}^{(r,m')}} \right], \quad (2.33)$$

which leads to the final estimator of the purity \hat{p}_2 by replacing the U-statistics estimator of cross-correlation of the probabilities in Eq. (2.28)

$$\hat{p}_2 = \frac{2^N}{N_U N_M (N_M - 1)} \sum_{r=1}^{N_U} \sum_{m \neq m'}^{N_M} (-2)^{-D[\mathbf{s}^{(r,m)}, \mathbf{s}^{(r,m')}]}. \quad (2.34)$$

This unbiased estimator guarantees that $\mathbb{E}[\hat{p}_2] = p_2$ with $\mathbb{E}[\cdot] = \mathbb{E}_U \mathbb{E}_{\text{QM}}[\cdot]$ [30]. Additionally, for later convenience we can alternately define the estimator of the purity as:

$$\hat{p}_2 = \frac{1}{N_U} \sum_{r=1}^{N_U} \hat{X}_2(U^{(r)}) \quad \text{with} \quad \hat{X}_2(U^{(r)}) = \frac{2^N}{N_M(N_M - 1)} \sum_{\substack{m \neq m' \\ m, m'=1}}^{N_M} (-2)^{-D[\mathbf{s}^{(r,m)}, \mathbf{s}^{(r,m')}]} \quad (2.35)$$

that satisfies

$$\mathbb{E}_{\text{QM}}[\hat{X}_2(U^{(r)})] = X_2(U^{(r)}) = 2^N \sum_{\mathbf{s}, \mathbf{s}'} (-2)^{-D[\mathbf{s}, \mathbf{s}']} P(\mathbf{s}|U^{(r)}) P(\mathbf{s}'|U^{(r)}) \quad (2.36)$$

with $p_2 = \mathbb{E}_U[X_2(U^{(r)})]$. The above expression for the estimator of the purity already provides us some intuition on potential advantages of the RM protocol. The estimate can be computed effectively on a classical device as it can be heavily parallelized on multiple classical processors. It can be computed on the fly and does not require storing large matrices in classical memory as in the case with QST. Importantly, we notice that the knowledge of the applied unitary in the experiment does not explicitly enter the post-processing of the RM data. This feature allows this RM protocol to possess some additional robustness features in the estimation of the purity [11, 32]. We shall also see in the next section, that adding the knowledge of the applied unitaries we can define new estimators from the RM data-set. In summary, it provides a direct method to connect the measurement data with the quantity of interest such as the purity.

Statistical errors

The experiment for the RM protocol is always executed for a finite number of runs $M = N_U N_M$ due to time and energy constraints of the concerned quantum platform. From the collected data the estimator \hat{p}_2 can be constructed as shown earlier. This estimator differs from the true value of the purity p_2 of the underlying state due to *statistical errors*. Statistical errors are induced due to a finite application of random unitaries N_U followed by finite number of measurements N_M . It can be characterized by the average relative statistical error $\mathcal{E} = \overline{|\hat{p}_2 - p_2|}/p_2$, where $(\overline{\cdot})$ represents an average performed over multiple numerically simulated independent experimental runs of the RM protocol using the same measurement budget M . One may wonder about the sample complexity of the RM protocol to provide estimates of the purity with a certain accuracy. In other words, what is the required number of measurements in terms of N_U and N_M to achieve a desired precision of the purity? Does the RM protocol provide any sample complexity advantages compared to the method of QST introduced earlier? Various prior studies and numerical simulations [29, 11] have addressed this question and have shown that the total number of randomized measurements $M = N_U N_M$ scales as $2^{\alpha N}$ with $\alpha \in [1, 1.5]$ [29, 11, 125, 32] for most generic quantum states. The scaling of the required number of measurements, as a function of the system-size N , is one of the key advantages of the RM protocol. Though the method still scales exponentially with respect to N , it is significantly better when compared to QST (that scales as $M \sim 2^{3N}$ [54]). The direct consequence of this result is that we can expect to go beyond and measure

the purity (and also the second Rényi entropy or benchmark quantum states with the fidelity) for larger systems that are not accessible by QST.

Experimental implementations of the RM protocol

Since the RM protocol provides an easy method to measure the purity of the quantum state in current NISQ platforms, several experiments realizing the RM protocol have been carried out on different quantum platforms ranging from trapped ions [11], superconducting qubits [142, 111, 60] to nitrogen vacancy (NV) spin center [134]. Let us summarize and name a few pertinent ones below that measured interesting entanglement properties connected to many-body physics. The first experiment demonstrating the implementation of the RM protocol was realized on an ion trap quantum simulator [11]. They measured purities (and second Rényi entropy) of system sizes up to 10 qubits and demonstrated generation of entanglement for a many-body system undergoing a quench dynamics. We shall discuss some of the details of this experiment later in the manuscript as it contains a rich amount of physics in terms of entanglement dynamics. Further experiments have been performed to measure fidelities between multiple pairs of quantum states that are realized on different quantum computing platforms [134]. These experiments successfully measured the fidelities upto 13 qubits between multiple superconducting devices of IBM and other architectures such as trapped ion platforms of IonQ. Experiments were also conducted on Google's Sycamore superconducting chip to measure second Rényi entropy via the purity [111, 60]. In the first experiment, they realized the ground state of the toric code [111]. To demonstrate that the toric code ground state has topological properties or formally said to have a topological order, they measured a quantity known as the topological entanglement entropy (TEE) [57, 75]. The TEE can be expressed in terms of second Rényi entropies of certain sub-partitions of the considered system [57] and was measured for a partition size up to 9 qubits. The second more recent experiment was conducted to understand the scaling of the entanglement entropy in measurement-induced circuits [60]. They demonstrated using the second Rényi entropy the area and volume law scaling in 2D shallow circuits.

In summary, the RM protocol turns to be a cheaper method to implement on current available experimental devices in comparison to the standard QST. It gives access to properties of prepared quantum many-body states such as purities, state-fidelities, etc. With the current scalings of the required number of measurements, one can envisage applying this protocol to probe purities of (sub-)systems consisting up to 15 qubits. In the next chapter, one of the original contributions of this manuscript shall address and propose a method to extend the applicability of the RM protocol to measure purity in quantum systems of larger system-sizes. Now, one may wonder if we can estimate additional quantities such as higher order polynomials of the density matrix or expectation value of additional arbitrary multi-copy operators other than the purity using the same RM framework? This particularly could be of interest to detect entanglement in the quantum system. To address this problem, recent developments have introduced extensions to the RM toolbox. Particularly, in the following section we shall derive and introduce the classical shadow framework [64].

2.5 The classical shadow formalism

In the previous section, we have described how the randomized measurement (RM) protocol provides a direct method to estimate the purity of an unknown quantum state [29, 11, 125, 32]. The common notion that links these prior works is that the quantity of interest was directly extracted from the measured bit-strings after applying random unitary operations. The knowledge of the random unitaries applied in the experiment were not involved explicitly in the estimation of these quantities. The estimator of the purity discussed in the previous section was *unitary agnostic* as it did not require the explicit knowledge of the unitaries applied in the experiment. It is natural to think that the knowledge of the unitaries used in the experiment forms also a key part of the experimental RM data-set. One may wonder if we can extend the RM toolbox's capabilities by utilizing this knowledge.

This was indeed the case when the *classical shadow formalism* was introduced [64]. The classical shadows formalism is an important extension of the RM toolbox that uses the exact same experimental procedure as before. It consists of a simple additional ingredient that explicitly incorporates the knowledge of the applied unitaries during the data-treatment phase to provide estimations of the quantities of interest. The main feature of this method is that it opens up the possibilities to measure additional quantities of interest from the same data-set provided by the randomized measurement framework. In particular, one can evaluate higher order polynomials and expectation values of arbitrary linear and multi-copy operators $O^{(n)}$ that act on $\mathcal{H}(d)^{\otimes n}$ with $n \in \mathbb{N}^*$. These quantities can be expressed as $\text{Tr}(\rho^n)$ and $\text{Tr}(O^{(n)}\rho^{\otimes n})$ respectively.

In this section, we shall re-derive the classical shadow formalism inspired by the formalism of the *randomized measurement tomography* as described in [30, 87]. In the following sections, we shall show firstly that using the knowledge of the unitaries and the measured bit-strings from the experiment, the RM tomography formalism allows us to reconstruct the underlying density matrix. From this expression, we shall establish the connection to the more familiar expression of the classical shadows given in [64]. Then we will detail some of its properties and describe how it can be used to evaluate expectation values of multi-copy operators.

2.5.1 Randomized measurement tomography

Consider a N -qubit quantum state prepared on a quantum device. We can write the state in the two copy space $\mathcal{H}(d) \otimes \mathcal{H}(d)$ with $d = 2^N$ as

$$\rho = \text{Tr}_2(\mathbb{S}(\mathbb{1} \otimes \rho)) \quad (2.37)$$

where we take the partial trace with respect to the second copy and introduce the swap operator \mathbb{S} . Once we have the swap operator visible, we can use the same thread of reasoning to replace it with a virtual operator acting on two copies. The key idea again as proposed in [30] is to find an operator O such that $\Phi^{(2)}(O) = \mathbb{S}$. From Sec. 2.4.2 (Eq. (2.28)), we know that such an operator exists and can be

written as

$$\begin{aligned}
 O &= \sum_{\mathbf{s}, \mathbf{s}'} O_{\mathbf{s}, \mathbf{s}'} |\mathbf{s}\rangle\langle\mathbf{s}| \otimes |\mathbf{s}'\rangle\langle\mathbf{s}'| = 2^N \sum_{\mathbf{s}, \mathbf{s}'} (-2)^{-D[\mathbf{s}, \mathbf{s}']} |\mathbf{s}\rangle\langle\mathbf{s}| \otimes |\mathbf{s}'\rangle\langle\mathbf{s}'| \\
 &= 2^N \bigotimes_{i=1}^N \sum_{s_i, s'_i} (-2)^{-D[s_i, s'_i]} |s_i\rangle\langle s_i| \otimes |s'_i\rangle\langle s'_i|
 \end{aligned} \tag{2.38}$$

where D represents the Hamming distance. We can replace the swap operator in Eq. (2.37) by the twirled operator $\Phi^{(2)}(O) = \mathbb{E}_U[(U^\dagger)^{\otimes 2} O U^{\otimes 2}]$

$$\begin{aligned}
 \rho &= \text{Tr}_2(\Phi^{(2)}(O)(\mathbb{1} \otimes \rho)) \\
 &= 2^N \text{Tr}_2 \left(\mathbb{E}_U \left[(U^\dagger)^{\otimes 2} \sum_{\mathbf{s}, \mathbf{s}'} (-2)^{-D[\mathbf{s}, \mathbf{s}']} |\mathbf{s}, \mathbf{s}'\rangle\langle\mathbf{s}, \mathbf{s}'| U^{\otimes 2} \right] (\mathbb{1} \otimes \rho) \right) \\
 &= 2^N \sum_{\mathbf{s}, \mathbf{s}'} (-2)^{-D[\mathbf{s}, \mathbf{s}']} \mathbb{E}_U [U^\dagger |\mathbf{s}\rangle\langle\mathbf{s}| U \text{Tr}(|\mathbf{s}'\rangle\langle\mathbf{s}'| U \rho U^\dagger)] \\
 &= 2^N \sum_{\mathbf{s}, \mathbf{s}'} (-2)^{-D[\mathbf{s}, \mathbf{s}']} \mathbb{E}_U [P(\mathbf{s}'|U) U^\dagger |\mathbf{s}\rangle\langle\mathbf{s}| U]
 \end{aligned} \tag{2.39}$$

where we have explicitly expanded the trace operation and used the trace cyclicity property $\text{Tr}(AB) = \text{Tr}(BA)$. We have also used the short-hand notation $|\mathbf{s}, \mathbf{s}'\rangle\langle\mathbf{s}, \mathbf{s}'| = |\mathbf{s}\rangle\langle\mathbf{s}| \otimes |\mathbf{s}'\rangle\langle\mathbf{s}'|$ for convenience. The above expression reconstructs the underlying density matrix using the randomized measurement data. The experimental protocol can be described as given below. After having prepared the N -qubit quantum state on the device, we perform randomized measurements by employing N_U local random unitaries $U^{(r)}$ followed by N_M bit-string measurements $\mathbf{s}^{(r,m)} = (s_1^{(r,m)}, \dots, s_N^{(r,m)})$ with $r = 1, \dots, N_U$ and $m = 1, \dots, N_M$. The data post-processing uses the full knowledge of the RM data-set that includes the registered bit-strings and the applied unitaries to construct the density matrix. The estimator $\hat{\rho}$ of ρ can be obtained from analyzing the experimental data as

$$\hat{\rho} = \frac{2^N}{N_U} \sum_{r=1}^{N_U} \sum_{\mathbf{s}, \mathbf{s}'} (-2)^{-D[\mathbf{s}, \mathbf{s}']} \hat{P}(\mathbf{s}'|U^{(r)}) U^{(r)\dagger} |\mathbf{s}\rangle\langle\mathbf{s}| U^{(r)} \tag{2.40}$$

where we estimate the probabilities $\hat{P}(\mathbf{s}'|U^{(r)}) = \frac{1}{N_M} \sum_{m=1}^{N_M} \delta_{\mathbf{s}', \mathbf{s}^{(r,m)}}$. The reconstructed density matrix averaged over the applied unitaries and the projective measurements satisfies $\mathbb{E}[\hat{\rho}] = \rho$. The famous classical shadow formalism introduced in [64] can be derived based on the randomized tomography formulation as we show in the next section

2.5.2 Classical Shadows

The name classical shadows was first given in Ref. [64] and quite accurately captures the essence of the formalism. The derivation of this formalism will automatically clarify many of its advantages as its name suggests. To begin its derivation, let us consider the expression from the randomized tomography of Eq. (2.40) in the specific regime where we perform N_U random transformations $U^{(r)}$ with $r = 1, \dots, N_U$

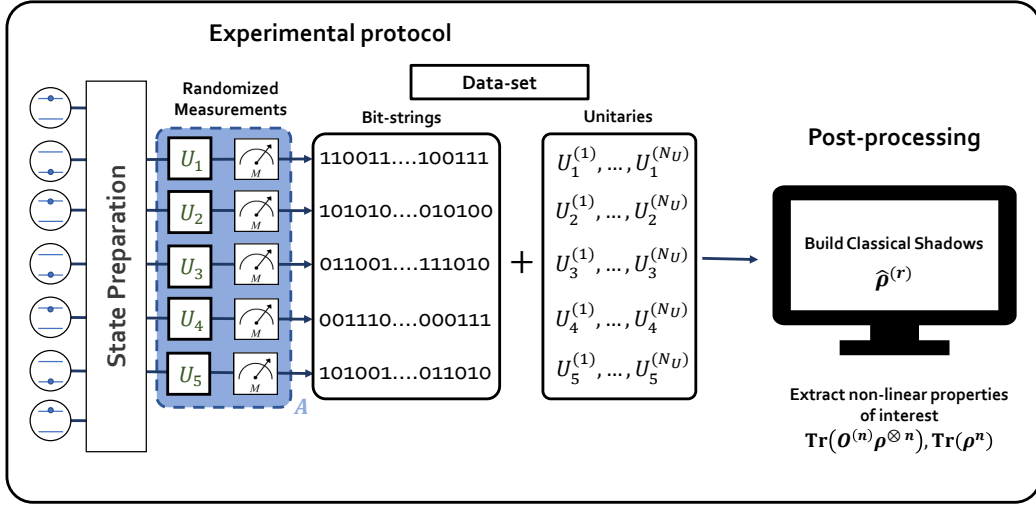


Figure 2.2: *Protocol for classical shadow formalism* — The figure describes the randomized measurement protocol to construct classical shadows. As we see, the experimental protocol does not change when compared with Fig. (2.1). The additional ingredient that is introduced is to use along with the bit-string measurements, the knowledge of the unitaries applied in the experiment. Post-processing classically this experimental data-set, we can construct classical shadows to predict non-linear properties of the underlying quantum state.

followed by a *single* projective measurement ($N_M = 1$) $\mathbf{s}^{(r)} = (s_1^{(r)}, \dots, s_N^{(r)})$. As illustrated in Fig. 2.2, the experimental data-set consists of the measured bit-strings and *also* the applied unitaries. For a single applied unitary $U^{(r)}$ and the corresponding measured bit-string $\mathbf{s}^{(r)} = (s_1^{(r)}, \dots, s_N^{(r)})$, we can construct an operator $\hat{\rho}^{(r)}$ that depends on the applied unitary rotation $U^{(r)}$ from Eq. (2.40) that has the following form

$$\hat{\rho}^{(r)} = 2^N \sum_{\mathbf{s}, \mathbf{s}'} (-2)^{-D[\mathbf{s}, \mathbf{s}']} \delta_{\mathbf{s}', \mathbf{s}^{(r)}} U^{(r)\dagger} |\mathbf{s}\rangle \langle \mathbf{s}| U^{(r)} = 2^N \sum_{\mathbf{s}} (-2)^{-D[\mathbf{s}, \mathbf{s}^{(r)}]} U^{(r)\dagger} |\mathbf{s}\rangle \langle \mathbf{s}| U^{(r)} \quad (2.41)$$

As the Hamming distance $D[\mathbf{s}, \mathbf{s}'] = \sum_{i=1}^N D[s_i, s'_i]$, the applied unitary $U^{(r)} = U_1^{(r)} \otimes \dots \otimes U_N^{(r)}$ and the projected state $|\mathbf{s}\rangle = |s_1, \dots, s_N\rangle$ can all be expressed locally for each qubit, we can write

$$\hat{\rho}^{(r)} = \bigotimes_{i=1}^N \hat{\rho}_i^{(r)} = 2^N \bigotimes_{i=1}^N \sum_{s_i} (-2)^{-D[s_i, s_i^{(r)}]} U_i^{(r)\dagger} |s_i\rangle \langle s_i| U_i^{(r)}. \quad (2.42)$$

Without loss of generality, focusing on the expression of the operator $\hat{\rho}_i^{(r)}$ of a single qubit at site i , we can decompose the sum over the bit-string s_i for the two cases when $s_i = s_i^{(r)}$ and $s_i \neq s_i^{(r)}$. This gives

$$\begin{aligned} \hat{\rho}_i^{(r)} &= 2U_i^{(r)\dagger} \left| s_i^{(r)} \right\rangle \left\langle s_i^{(r)} \right| U_i^{(r)} - U_i^{(r)\dagger} \left(\mathbb{1} - \left| s_i^{(r)} \right\rangle \left\langle s_i^{(r)} \right| \right) U_i^{(r)} \\ &= 3U_i^{(r)\dagger} \left| s_i^{(r)} \right\rangle \left\langle s_i^{(r)} \right| U_i^{(r)} - \mathbb{1} \end{aligned} \quad (2.43)$$

where we have used the fact that when $s_i \neq s_i^{(r)}$, we have the complementary bit-string which can be expressed as $\mathbb{1} - \left| s_i^{(r)} \right\rangle \left\langle s_i^{(r)} \right|$. Combining all these results together we finally obtain the standard formula of a classical shadow [64]

$$\hat{\rho}^{(r)} = \bigotimes_{i=1}^N \hat{\rho}_i^{(r)} = \bigotimes_{i=1}^N \left(3U_i^{(r)\dagger} \left| s_i^{(r)} \right\rangle \left\langle s_i^{(r)} \right| U_i^{(r)} - \mathbb{1} \right) \quad (2.44)$$

that equally fulfills $\mathbb{E}[\hat{\rho}^{(r)}] = \rho$. This expression is a special case of Eq. (2.40) obtained for a single applied unitary $U^{(r)}$ from the RM tomography formalism as explained in the previous section. The term ‘‘classical shadow’’ can be better understood from Eq. (2.44): We construct an operator in the *classical* post-processing stage, using the knowledge of the applied unitary and the measurement outcome, that records some information of the prepared many-body quantum state ρ in terms of a *classical snapshot*. With the collection of the classical snapshots $\hat{\rho}^{(r)}$ for $r = 1, \dots, N_U$, we can infer properties of the quantum state as $\mathbb{E}[\hat{\rho}^{(r)}] = \rho$ is satisfied [30, 64]. Additionally, we observe from Eq. (2.44) that to classically store these snapshots requires low memory on a device due to its sparse tensor product structure. A single snapshot can be described by $4N$ complex numbers with the storage that does not scale exponentially with the system size N as in the case of QST. This enables these snapshots to be efficiently computed and stored in classical memory from the RM data-set. One may wonder how this framework differs from that of QST as we can reconstruct the state from these classical snapshots. More importantly, how many measurements do we require to overcome statistical errors for this particular framework? We shall see in the following section that we can again directly evaluate expectation values of linear and multi-copy operators without requiring an explicit construction of the quantum state. Additionally, this framework also allows us to provide rigorous performance guarantees in terms of sample complexity.

2.5.3 Estimation of quantum properties with classical shadows

In this section, we will elaborate on estimations of multi-copy observables $f_n = \text{Tr}(O^{(n)}\rho^{\otimes n})$ that can be extracted from the classical shadow formalism. Instead of measuring directly multi-copy expectation values using physical copies in the experiment (which can be currently a challenge), the classical shadow framework provides unbiased estimations using repeated single copy randomized measurements.

Given a collection of N_U classical shadows $\hat{\rho}^{(r)}$ constructed using Eq. (2.44), we can provide an unbiased estimator of the function \hat{f}_n using U-statistics [59]. This is achieved by replacing each copy of the density matrix in the multi-copy function f_n by a different classical shadow and computing the average over all possible such choices to pick n different shadows from a total collection of N_U shadows. This is explicitly expressed as

$$\hat{f}_n = \frac{1}{n!} \binom{N_U}{n}^{-1} \sum_{r_1 \neq \dots \neq r_n} \text{Tr} \left(O^{(n)} \hat{\rho}^{(r_1)} \otimes \hat{\rho}^{(r_2)} \otimes \dots \otimes \hat{\rho}^{(r_n)} \right). \quad (2.45)$$

where $\rho^{\otimes n}$ is replaced by $\hat{\rho}^{(r_1)} \otimes \hat{\rho}^{(r_2)} \otimes \dots \otimes \hat{\rho}^{(r_n)}$ with $r_1 \neq \dots \neq r_n$. Here we use the key identity that the average over the applied unitaries and the measurement

for all shadows gives $\mathbb{E}[\hat{\rho}^{(r_i)}] = \rho$. Then the properties of U-statistics [59] ensure that \hat{f}_n is an unbiased estimator of f_n , i.e. $\mathbb{E}[\hat{f}_n] = f_n$. As one sees, we do not reconstruct the quantum state explicitly as done in the case of QST but perform a multi-linear operation on the fly to obtain estimators of quantities during the post-processing phase. Within the construction of the current formalism, such estimators can be evaluated with classical post-processing of RM-data using CPU or GPU processors with the computational time scaling as $\mathcal{O}(N_U^n)$ without needing to store exponentially large density matrices. Analogous to the unitary agnostic estimator of the purity discussed earlier in Eq. (2.28), the work of [64] proposed an alternate estimator of the purity constructed from the classical shadow framework expressed as

$$p_2 = \frac{1}{2!} \binom{N_U}{2}^{-1} \sum_{r_1 \neq r_2} \text{Tr}(\hat{\rho}^{(r_1)} \hat{\rho}^{(r_2)}). \quad (2.46)$$

Note that both the unitary agnostic [30, 11] and the shadow estimator [64] of the purity can be constructed from the same experimental RM data-set. It is still not clear which among the two estimators of the purity provides a better estimation for a generic quantum state. In particular, for a fixed measurement budget $M = N_U N_M$, the shadow estimator achieves better accuracy when $N_U \gg N_M$ while the unitary agnostic estimator functions better in the regime where $N_U < N_M$ [31]. As the shadow estimator uses the knowledge of the random unitary in the data treatment phase, it might be less robust to errors induced in the random unitaries compared to the unitary agnostic estimator of the purity. On the other hand, the shadow estimator allows generalizations to evaluate higher moments of the density matrix $p_n = \text{Tr}(\rho^n)$, that can be effectively computed classically by evaluating overlaps between all the distinct shadows using local site contractions. Until now, functions of order $n \leq 3$ have been successfully extracted from experimental RM data [34]. As shown, the main advantage of this framework is that it provides a method to access arbitrary functions $O^{(n)}$ with $n \geq 1$ from the same RM data-set collected from the experiment.

Measure first, ask questions later — The former phrase has been coined in the review [31] and aptly captures the usefulness of the classical shadow formalism. As classical shadows provide a rich collection of non-linear quantities that can be accessed from the experimental data of randomized measurements, it can give theorists as well as experimentalists the liberty to choose the quantum properties to be investigated *after* having performed the experiment. A concrete example is the re-analysis of the RM experimental data of [11] that was carried out to investigate entanglement in mixed states generated by a quench dynamics [34].

Using simple functions such as moments of the partially transposed density matrix $\text{Tr}([\rho_{AB}^{T_A}]^n)$ with $n = \mathbb{N}^*$, the authors in Ref. [34] derived a slightly weaker condition called “ p_3 -PPT” based on the original PPT criterion shown in Chapter. 1 as follows

$$\rho_{AB} \text{ is separable} \implies \rho_{AB} \in \text{PPT} \implies \text{Tr}([\rho_{AB}^{T_A}]^3) \geq \text{Tr}([\rho_{AB}^{T_A}]^2)^2. \quad (2.47)$$

The violation of this condition detects entanglement between the constituents A and B of the quantum system. They successfully measured the two quantities in the above inequality by re-analyzing the same data-set of [11] and validated the presence of entanglement in mixed sub-systems of interest. In a similar spirit, we shall derive

in Chapter. 5, a weaker variant of the CCNR (also enhanced CCNR) condition that can be estimated using the same experimental data [11]. Especially in Chapters. 4 - 5, we will exploit these features of classical shadows to measure non-linear quantities of interest like the QFI and the operator entanglement by adapting them to the RM framework. This framework allows the same RM data-set to be recycled in-order to estimate different quantities that become relevant at a later time.

Performance guarantees

The work of [64] provided rigorous performance guarantees in terms of sample complexity for the classical shadow framework to evaluate different estimations, particularly in the regime where we make only a single projective measurement ($N_M = 1$). Thus the total budget simplifies to $M = N_U$. Consider an Hermitian operator O that acts on a N -qubit state ρ . One can estimate the expectation value of this operator $f_1 = \text{Tr}(O\rho)$ from M constructed classical shadows given by

$$\hat{f}_1 = \frac{1}{M} \sum_{r=1}^M \text{Tr}(O\hat{\rho}^{(r)}). \quad (2.48)$$

The convergence of the estimator \hat{f}_1 to its true value $f_1 = \mathbb{E}_U[\hat{f}_1]$ is governed by the variance $\text{Var}[\hat{f}_1] = \mathbb{E}_U[\hat{f}_1^2] - \mathbb{E}_U[\hat{f}_1]^2$, where the variance is estimated over the applied unitaries. To estimate $|\hat{f}_1 - f_1| < \epsilon$ for a given accuracy ϵ and with a certain confidence δ , one can firstly use the well known Chebyshev's inequality that bounds the probability of the estimator \hat{f}_1 being in a certain confidence interval:

$$\Pr \left[|\hat{f}_1 - f_1| \geq \epsilon \right] \leq \frac{\text{Var}[\hat{f}_1]}{\epsilon^2} = \frac{\text{Var}[\text{Tr}(O\hat{\rho})]}{M\epsilon^2} \quad (2.49)$$

with $\hat{\rho}$ being a single shot shadow. Here we have used the fact that the shadows $\hat{\rho}^{(r)}$ from Eq. (2.48) are independent, thus we have $\text{Var}[\hat{f}_1] = \frac{1}{M} \text{Var}[\text{Tr}(O\hat{\rho})]$. A key result introduced in [64], provides an upper bound on the single shot variance. This can be cast into the following concrete statement

Fact 1. [64, Proposition. 3] *Given a linear function $f_1 = \text{Tr}(O\rho)$ defined by an Hermitian operator O that acts on a N -qubit state ρ , the single-shot variance in function of the shadow $\hat{\rho}$ obeys the following bound*

$$\text{Var}[\text{Tr}(O\hat{\rho})] \leq 2^N \text{Tr}(O^2). \quad (2.50)$$

The above fact is an important identity that shall be used and generalized further in our work in the subsequent chapters. Using this identity, we want to ensure that Eq. (2.49) is upper-bounded by the confidence level δ . The above variance bound and the Chebyshev's inequality allows us to express concrete lower bound to the sample complexity $M = N_U$ to achieve a fixed accuracy ϵ with confidence level of at least $1 - \delta$ given by

$$M \geq \frac{2^N \text{Tr}(O^2)}{\epsilon^2 \delta}. \quad (2.51)$$

Thus, by performing measurements greater than the above bound would guarantee that the estimation of f_1 is evaluated with a confidence level of $1 - \delta$ while

respecting $|\hat{f}_1 - f_1| < \epsilon$. Additionally, the same collection of shadows can also be used to estimate arbitrary many linear observables of interest. This could be of interest to certify entanglement using entanglement witnesses [42, 53], to measure fidelities with respect to target pure states $|\psi\rangle$ [41] or estimate ground state energy of molecules [63]. These estimators also satisfy rigorous sample complexity bounds as developed in [64, Theorem. 1]. Moreover, these sample complexity results have been extended only for a few non-linear functionals such as the purity $\text{Tr}(\rho_{AB}^2)$ and $\text{Tr}([\rho_{AB}^{T_A}]^3)$ in [34, Lemma. 2 and Lemma. 3 respectively]. These results state that in the limit of large number of measurements M which is analogous to a regime where ϵ is small, the required number of measurements to evaluate these functions scale $\propto 2^N$.

2.6 Current challenges and outline

In this chapter, we introduced the full framework of the RM toolbox that provides estimations of quantum properties of interest from experimental data. Its strength mainly lies in its simple applicability and lower required number of measurements compared to other existing measurement techniques. In particular, the arrival of the classical shadow formalism played a key role in further enriching the pertinence of the RM toolbox and is currently an active topic of research and study. Our work detailed in this manuscript equally aims at providing solutions to some of the existing problems faced by the current construction of the RM toolbox that we will briefly overview in this section.

Firstly, the RM toolbox suffers from exponential scalings, that is, the required number of measurements scale exponentially with the number of qubits N . Due to the fast progress in current experimental devices, it becomes important to have methods to be able to measure the purity in these larger systems. As a concrete example, with the current framework we can not measure the purity in the regime of 25 – 30 qubits and are limited in the regime of 10 – 15 qubits due to statistical errors. In Chapter. 3, we shall provide a potential solution to this problem by improving the current protocol in order to fight statistical errors and correspondingly reduce the required number of measurement and the associated exponential scaling. The optimized protocol shall implement importance sampling to select the few best unitaries needed to be applied in the experiment.

Secondly, let us now move our attention to the classical shadow formalism of the RM toolbox. Though with this method we can measure arbitrary multi-copy functions using the RM data, we lack sample complexity bounds that would provide rigorous performance guarantees for them. More importantly, the U-statistics estimator to evaluate a given arbitrary order functional has *practical limitations* as post-processing such estimators for higher order functions requires an expensive data-treatment. Additionally, can we measure quantities that do not explicitly express as multi-copy functions? How can we improve estimation accuracy for multi-copy functions using classical shadows?

We address these problems systematically from Chapter. 4 on-wards where we

shall focus on further developing the classical shadow formalism. In Chapter. 4, we will provide a structured method to estimate an important non-linear quantity known as the *quantum Fisher information* that can not be cast directly as a multi-copy function. Our strategy would be to devise a series of multi-copy functionals that converge to the true value of the QFI and evaluate them using the classical shadow formalism. This will then motivate us to formulate sample complexity bounds for arbitrary such multi-copy functions. Additionally, the last section of this chapter, we also discuss a recent work that demonstrates the first experimental measurement of the QFI via the lower bounds that have been derived in that chapter.

In Chapter. 5, we will provide a practical solution to estimate functions of arbitrary order by introducing the *batch shadow formalism*. We will show analytically the performance of this formalism compared to the existing one. This will enable us to measure the operator entanglement entropy that is difficult to access with the current U-statistics estimator. By re-analysing the experimental data of [11] we shall unveil interesting entanglement properties associated to it such as the *entanglement barrier*. Lastly, in Chapter. 6, we will show how to again tackle statistical errors by boosting the estimation of multi-copy estimators using the notion of *common random numbers*. With this we shall propose a modified protocol that we call *common randomized measurements*.

3

Optimizing randomized measurements protocol with importance sampling

This chapter is based on the published work: *Aniket Rath, Rick van Bijnen, Andreas Elben, Peter Zoller, and Benoît Vermersch*. Importance sampling of randomized measurements for probing entanglement. *Phys. Rev. Lett.*, 127:200503, Nov 2021 (Ref. [99]) and includes an additional study presented in Sec. 3.4.4.

We develop here a new protocol based on importance sampling of local random unitaries to reduce the statistical errors in the estimation of the purity. I actively contributed in the development of this protocol and numerically benchmarked its performance for the various case studies presented here. My contribution also consisted in writing the related portions of the manuscript of Ref. [99].

Contents

3.1	The main idea: approximate then select	54
3.2	The optimized classical-quantum protocol	56
3.2.1	The importance sampling protocol	58
3.3	Analytical estimations of statistical errors	60
3.3.1	Variance of uniform sampling for a pure product state	61
3.3.2	Variance of importance sampling for a pure product state	63
3.4	Numerical study and performance highlights	64
3.4.1	Estimation with perfect sampler	65
3.4.2	Machine-learning sampling for product and GHZ states	66
3.4.3	Sampling from MPS approximations	68
3.4.4	Importance sampling illustration for the toric code experiment	70
3.5	Conclusion	73

In the previous chapter, we discussed how we can measure the purity of an unknown quantum state by implementing randomized measurements in an experiment. The measurement budget $M = N_U N_M$, where N_U are the number of applied local random unitaries and N_M the number of measurements performed for each applied unitary, defines the total number of repetitions performed in the experiment. However, as experiments are repeated for a finite measurement budget, this leads to *statistical errors* in the estimation of the purity. In particular, the required number of measurements in the case of randomized measurements for a given tolerance of statistical error scale *exponentially* ($M \sim 2^{aN}$ with $a \in [1, 1.5]$) with respect to the number of qubits N [29, 11, 125, 32]. This typically restricts our access to estimate the purity in experiments for (sub-)system sizes in the regime of 10 – 15 qubits.

The growth of current experimental platforms necessitates the development of methods in order to benchmark the entanglement generation in such quantum devices beyond the current restrictive regime. In this chapter, we will propose a protocol based on randomized measurements that will enable us to measure the purity of quantum states in significantly larger (sub-)system sizes N . This is achieved by reducing predominantly the statistical errors that governs the estimation of the purity from finite set of measurements.

We organize this chapter as follows: firstly, we describe the crucial ingredient that is central to the effectiveness of the new randomized measurement protocol that we propose here. This is followed by practical details that gives the necessary tools to implement the new protocol. We will also provide some analytical calculations that guarantee its performance compared to the old protocol. And lastly, we will spend a vast majority of the chapter illustrating its performance on different quantum states with numerical simulations and various case studies.

3.1 The main idea: approximate then select

The previous version of the randomized measurement protocol introduced in the earlier works of [30, 11] was based on a *state-agnostic* method to measure the purity. It implemented a set of random unitaries that were always chosen uniformly from the Haar measure irrespective of the state prepared in the experiment. But in typical experimental scenarios, the first step always consists of deciding the perfect state ρ that we aim to prepare on the quantum device. In certain scenarios, these prepared quantum states can be well approximated using classical simulation [89]. Thus our main proposal here consists of two main steps. First we use this valuable *prior knowledge* to construct a classical representation of the experimental quantum state. The prior classical state can be considered as an *approximation* to the realized experimental state due to unknown decoherence effects or other fundamental reasons that limit classical representations of quantum states. Second, based on the prior knowledge, we prepare the right *selection* of local random unitaries for the experiment that would help reduce statistical errors. These unitaries are sampled according to an appropriate probability distribution defined in function of

the approximate classical state at hand and exploit the structure of the underlying quantum state.

Let us now concretely discuss the new optimized protocol and why it becomes more effective compared to the old protocol in order to reduce statistical errors. Our starting point is to view the purity estimator introduced in former works of [30, 11] and as mentioned in Eq. (2.28) as a Monte Carlo integration performed over the unitaries that are distributed *uniformly* according to the Haar measure dU which writes as $p_2 = \mathbb{E}[X_2(U)] = \int X_2(U)dU$. In principle, one can define the purity estimator for unitaries that are sampled from a given distribution $p(U)$ as

$$p_2 = \mathbb{E}_{p(U)} \left[\frac{X_2(U)}{p(U)} \right] \equiv \int \left(\frac{X_2(U)}{p(U)} \right) p(U)dU \quad (3.1)$$

where we recall the function $X_2(U)$ as given in Eq. (2.36) is expressed in function of the Born probability $P(\mathbf{s}|U) = \langle \mathbf{s} | U \rho U^\dagger | \mathbf{s} \rangle$ for a given random unitary U and the measured bit-string $|\mathbf{s}\rangle = |s_1, \dots, s_N\rangle$. We also define $\mathbb{E}_{p(U)}[\cdot]$ as the average over the unitaries sampled according to a chosen distribution $p(U)dU$. For example, for a function $g(U)$ we have $\mathbb{E}_{p(U)}[g(U)] = \int g(U) p(U)dU$. When the unitaries are sampled *uniformly* from the Haar measure as done earlier, we have $p(U) = 1$ and we recover our previous expression as mentioned in Eq. (2.28) and in Refs. [30, 11]. Analogously, randomized measurements involves evaluating the above integral with finite number of applied unitaries N_U where the estimated function $\hat{X}_2(U^{(r)})$ is evaluated from experimental data for each unitary $U^{(r)}$ with $r = 1, \dots, N_U$. The associated estimator of the purity can be given by

$$\hat{p}_2 = \frac{1}{N_U} \sum_{r=1}^{N_U} \frac{\hat{X}_2(U^{(r)})}{p(U^{(r)})}. \quad (3.2)$$

The function $X_2(U)$ defined earlier depends on the quantum state and the applied local random unitaires ($U = \bigotimes_{i=1}^N U_i$). It turns out naturally that, for a given quantum state, this multi-variate function could present a complex multi-dimensional landscape consisting of minima and maxima as a function of U . In order to effectively evaluate a Monte Carlo integral of this complex function, the wise choice is to perform an *importance sampling* of the random unitaries $p(U) = p_{\text{IS}}(U)$ that would prioritize the *important* regions of the function and exploit its inherent structure. This is the main intuition that we borrow from Monte Carlo integration strategies [96]. It makes a more intelligent choice of the sampling probability distribution $p(U)$ compared to a blind uniform sampling in order to boost the estimations obtained from Monte Carlo integrals in question.

The choice of the appropriate distribution function $p_{\text{IS}}(U)$ impacts directly the statistical errors of the estimation of the purity. To achieve optimal performances, we can naively choose the distribution function to follow in a consistent manner the structure of the function to be integrated. It should sample predominantly local random unitaries distributed near the vicinity of the maxima of the function $X_2(U)$ and conversely sample less frequently in the regions close to the minima of the function. In this way, we anticipate that the required number of random unitaries N_U is significantly reduced in comparison to the uniform case. Considering the above requirements, the best candidate of such a sampling function follows naturally and

boils down to be

$$p_{\text{IS}}(U) = \frac{|[X_2(U)]_{\text{IS}}|}{\int |[X_2(U)]_{\text{IS}} dU|}, \quad (3.3)$$

for some function $[X_2(U)]_{\text{IS}}$ that aims at approximating $X_2(U)$. Let us now discuss in the following section the details of the importance sampling protocol and provide the recipe to obtain and build the function $[X_2(U)]_{\text{IS}}$.

3.2 The optimized classical-quantum protocol

As we have seen, in order to perform importance sampling we require a priori a classical representation of the quantum state that we intend to prepare in the experiment. Let us define this classical approximate state to be σ . We emphasize again that σ could be an approximation of the true state realized in the experimental setup. One may consider these classical representations belonging to families of mean-field states or variational tensor-network states such as matrix-product-states (MPS), projected-entangled pair states (PEPS) [127] that can model in certain scenarios the underlying quantum state prepared in the experiment. In particular, let us focus on an approximate theory representation of the quantum state that can be obtained using a class of states known as Matrix-Product-States. These states are commonly found in condensed matter problems [113]. We can define a MPS wave-function describing a N -qubit state

$$|\psi_\chi\rangle = \sum_{\substack{s_1, \dots, s_N \\ \ell_1, \dots, \ell_{N-1}}} [A_1]_{s_1}^{(\ell_1)} [A_2]_{s_2}^{(\ell_1, \ell_2)} \dots [A_N]_{s_N}^{(\ell_{N-1})} |\mathbf{s}\rangle, \quad (3.4)$$

where $|\mathbf{s}\rangle = |s_1\rangle \otimes \dots \otimes |s_N\rangle$ denotes the physical indices of the tensor, and the bond index ℓ_i can have a maximum dimension given by the *bond dimension* χ . The bond dimension is a key parameter that describes the amount of entanglement that is captured by the MPS. A MPS of bond dimension χ can at most have an entanglement entropy $\propto \log(\chi)$. For instance, such states can adequately describe many-body ground states of gapped Hamiltonians [27] or low depth random quantum circuits [39]. Truncation of the bond-dimension at a given value of χ provides an approximation of the quantum state. The choice of a MPS state is more physically inspired in terms of finding a valid approximation of the underlying quantum state. The importance sampling function $[X_2(U)]_{\text{IS}}$ can be *directly* constructed from the probabilities $P_\chi(\mathbf{s}|U)$ for a given random unitary U from the approximate MPS state $\sigma = |\psi_\chi\rangle\langle\psi_\chi|$ at hand via classical simulations. With this we can build the importance sampling function $[X_2(U)]_{\text{IS}}$ as given in Eq. (2.36).

Alternately, in the case where RM-data generated from prior quantum experiments that realized the same quantum state are available, we can implement powerful existing machine learning (ML) methods. The goal is to train a ML model to fit a function that closely mimics the desired multi-variate function $X_2(U)$ for any given unitary U . This is done by defining a training set that consists of evaluating $X_2(U)$ for various different random unitaries U . The training involves providing as input to the neural network numerous samples of unitaries U and their associated

function $X_2(U)$ for each unitary U as the desired output of the network. Following the successful training procedure of the ML algorithm, we obtain a compact classical representation of $[X_2(U)]_{\text{IS}}$ in terms of a saved neural network model. This procedure enables us to convert a costly classical computation (of the training the samples) into a classical model $[X_2(U)]_{\text{IS}}$. In both of these scenarios, one could boost the estimation of the purity by avoiding uniform sampling and rather using the classical representation or available experimental data-set to build the importance sampling function.

This pre-processing step using tensor-network or machine-learning performed on a classical device provides the importance sampling function to sample the required unitaries to be applied on the quantum experiment. Hence, the new protocol relies on the assistance of a classical device to optimize the randomized measurement protocol for the quantum device. Before recapping the details of the importance sampling algorithm, let us briefly discuss how we can alternately parameterize the local random unitaries to make the sampling task more convenient.

Parametrization of the local random unitaries

In order sample unitaries effectively from an appropriate importance sampling distribution, we firstly need to parameterize the local random unitary. In the protocol, local random unitaries $U = \bigotimes_{i=1}^N U_i$ are sampled from the Haar measure $dU = \prod_{i=1}^N dU_i$. Each of the single qubit unitary U_i with $i = 1, \dots, N$ is a 2×2 matrix sampled from the Haar measure dU_i on the unitary group $\mathcal{U}(2)$ and belongs to the CUE. We can define such a single qubit unitary given in [24, Eq. (3.17)] as

$$U_i = \begin{bmatrix} \cos \phi_i e^{i\alpha_i} & \sin \phi_i e^{i\psi_i} \\ -\sin \phi_i e^{-i\psi_i} & \cos \phi_i e^{-i\alpha_i} \end{bmatrix} \quad (3.5)$$

where $\phi_i \in [0, \pi/2]$; α_i & $\psi_i \in [0, 2\pi]$ with the single qubit Haar measure given as follows [24]

$$dU_i = 2 \cos \phi_i \sin \phi_i d\phi_i \frac{d\alpha_i}{2\pi} \frac{d\psi_i}{2\pi}. \quad (3.6)$$

We can alternately write the Haar measure by defining $\sin^2 \phi_i = \xi_i$ which leads to

$$dU_i = d\xi_i \frac{d\alpha_i}{2\pi} \frac{d\psi_i}{2\pi} \quad (3.7)$$

where $\xi_i \in [0, 1]$. Such a local random unitary U_i can be experimentally realized by combining random rotations along y and z axes of the Bloch sphere as given by

$$U_i = R_z(\gamma_i) R_y(\theta_i) R_z(\varphi_i) \quad (3.8)$$

where $R_\beta(\theta) = e^{-i\sigma^\beta \theta/2}$, σ^β with $\beta = y, z$ are the Pauli matrices and $\theta \in [0, 2\pi]$ is the random rotation angle. By equating the matrix elements of Eq. (3.5) and Eq. (3.8) gives the relation between the parametrized unitary angles in function of the rotation angles and the corresponding Haar distribution measures

$$\begin{cases} \xi_i = \sin^2(\theta_i/2) \\ \psi_i = (\varphi_i - \gamma_i)/2 + \pi \\ \alpha_i = -(\varphi_i + \gamma_i)/2 \end{cases} \implies \begin{cases} d\xi_i = \sin(\frac{\theta_i}{2}) \cos(\frac{\theta_i}{2}) d\theta_i \\ d\psi_i = (d\varphi_i - d\gamma_i)/2 \\ d\alpha_i = -(d\varphi_i + d\gamma_i)/2 \end{cases} \quad (3.9)$$

As each of the qubit is projected along the computational z -basis, we can ignore the last R_z rotation of U_i in Eq. (3.8) by putting $\gamma_i = 0$. We see firstly, from Eq. (3.9), that sampling φ_i uniformly in $[0, 2\pi]$ leads to α_i and ψ_i being distributed uniformly. Secondly, sampling ξ_i uniformly in $[0, 1]$ leads to an uniform sampling of θ_i . Thus for uniformly sampling local random unitaries for each qubit according to the Haar measure, it suffices to randomly sample: ξ_i relating the z rotation $R_y(\theta_i)$ and φ_i connecting the local unitary angles ψ_i and α_i . Thus we finally can express each local random unitary as $U_i = R_y(\theta_i)R_z(\varphi_i)$ which is parameterized by two rotation angles. The multi-variate function $X_2(U)$ is finally expressed in terms of $2N$ angles θ_i and φ_i with $i = 1, \dots, N$.

3.2.1 The importance sampling protocol

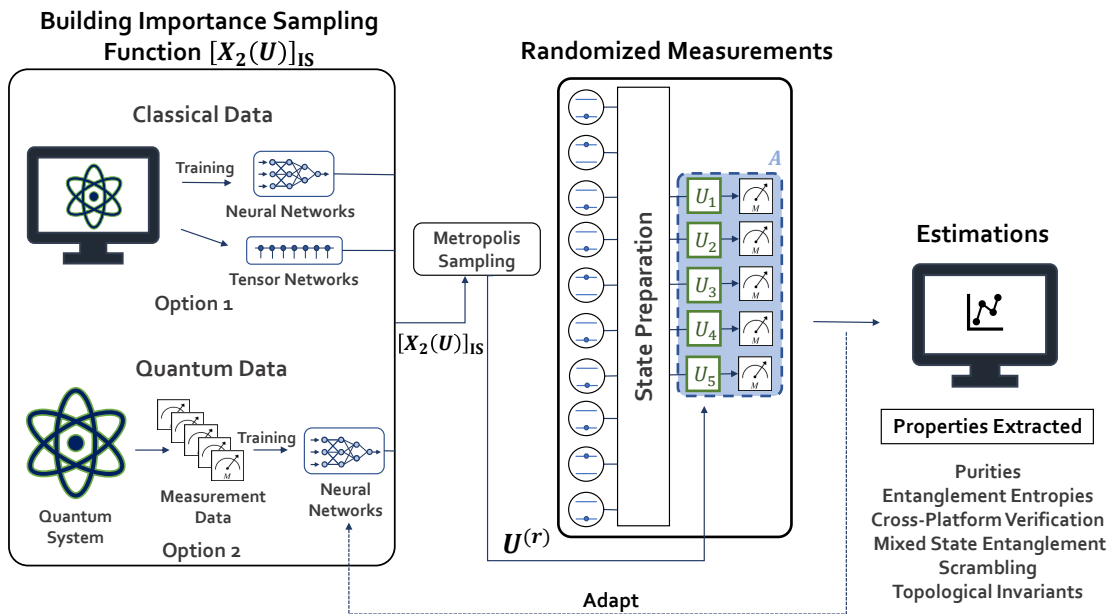


Figure 3.1: *Importance sampling randomized measurement protocol* — The figure describes the full protocol that implements importance sampling of random unitaries in an experiment to measure properties of the quantum state. It starts with a classical pre-processing step that builds the sampling function $[X_2(U)]_{IS}$. In the second step, local random unitaries are sampled from this function and are executed on the quantum hardware. The final step realizes a fast post-processing of the experimental data to extract purities and other properties of interest. Additionally, the samples obtained from the experiment can be fed-back to improve the classical function for future experiments.

We describe here the importance sampling protocol. As summarized in Fig. 3.1, we start by a pre-processing phase where we build the importance sampling function $[X_2(U)]_{IS}$ from the proposed methods of preference as described above. This step involves having an *approximate prior knowledge* of the quantum state of interest prepared on the quantum hardware or prior experimental samples at hand. At the end of this step, we obtain a classical representation of the state and the sampling function $[X_2(U)]_{IS}$. In the second step, we would like to sample N_U unitaries from the importance sampling distribution $p_{IS}(U)$ defined in Eq. (3.3). We achieve the sampling by implementing the metropolis algorithm [96].

This algorithm is based on the acceptance-rejection procedure which starts by sampling uniformly the $2N$ angles that defines a single random unitary acting on the N -qubit state from a proposal distribution. The proposal distribution most often is taken to be uniformly distributed in the given interval of parameters. The algorithm has a fixed target distribution $[X_2(U)]_{\text{IS}}$ according to which it aims to generate samples of unitaries. As this algorithm is based on an iterative procedure of ‘accept and reject’, it accepts a new candidate unitary only if it satisfies a certain criteria¹. If the criteria is not satisfied it rejects the candidate sample and repeats the previous check with a newly picked unitary from the proposal distribution. At the end of running this algorithm one finds a collection of N_S samples that contains N_U distinct unitaries. This is due to the fact that the algorithm does not choose another unitary until the criteria is fulfilled which causes it to repeat some of the previously sampled unitaries. We thus define $n^{(r)}$ as the number of occurrence of the sampled unitary $U^{(r)}$ from total collection of N_S samples (that include repetition of the same samples within it).

Once the sampling is done, we perform for each of the unitaries $U^{(r)}$ with $r = 1, \dots, N_U$, a total of N_M projective measurements on the quantum device, where we record the bit-strings $\mathbf{s}^{(r,m)}$ with $m = 1, \dots, N_M$. Finally, by post-processing the data-set of the bit-strings, we can obtain an unbiased importance sampling estimate of the purity given by

$$[p_2]_{\text{IS}} = \frac{1}{N_S} \sum_{r=1}^{N_U} \frac{n^{(r)} \hat{X}_2(U^{(r)})}{p_{\text{IS}}(U^{(r)})}. \quad (3.10)$$

Let us try to give an idea about the relevant measurement budget ($N_U N_M$) to implement importance sampling for experiments. When we consider the regime of $N_M \gg 1$ and that the classical state σ closely approximates the experimentally prepared state ρ i.e $\rho \approx \sigma$, we have for a given unitary $X_2(U^{(r)}) \approx [X_2(U^{(r)})]_{\text{IS}}$. Thus we observe that the ratio in above expression becomes constant and we can intuitively see that the estimator has less statistical fluctuations. The only deviations are due to the shot noise (finite number of measurements N_M). Hence the relevant measurement budget ($N_U N_M$) to be considered for importance sampling is of sampling a fixed, smaller number of unitaries and performing a large number of projective measurements $N_M \gg 1$ to account for shot-noise fluctuations. This also becomes pertinent for experimental platforms that have a significant calibration time such as trapped ions [11]. The few chosen unitaries can be very well calibrated and would induce less errors in the estimates. Additionally, increasing the number of measurements in these quantum experiments is easier compared to increasing the number of unitaries.

In order to provide a concrete assessment on the improvement that importance sampling provides when compared to uniform sampling, we will discuss in the subsequent sections analytical estimation of the statistical errors governed by the variance of the purity estimator obtained for both uniform and importance sampling. In particular, we will be interested to determine the scaling of the variance as a function of the system-size N as it directly quantifies the statistical error and the scalability of

¹Given an initial chosen unitary $U^{(0)}$, a candidate unitary $U^{(\text{cand})}$ is accepted if $\beta < \alpha$, where β is chosen from a uniform random distribution between $[0, 1]$ and $\alpha = \min \left\{ 1, \frac{|[X_2(U^{(\text{cand})})]_{\text{IS}}|}{|[X_2(U^{(0)})]_{\text{IS}}|} \right\}$, otherwise it is rejected.

the RM protocol. We shall back our analytical predictions with numerical simulations of the randomized measurement protocol by performing different case studies in the upcoming sections.

3.3 Analytical estimations of statistical errors

In this section, we will provide the variance of the estimator of the purity in the case of uniform and importance sampling for finite number measurements N_U and N_M . We consider here for simplicity that we have collected N_U independent unitaries $U^{(r)}$ sampled either from the importance sampling distributed $p_{\text{IS}}(U) = \frac{|[\hat{X}_2(U)]_{\text{IS}}|}{\int |[\hat{X}_2(U)]_{\text{IS}}| dU}$ or the uniform distribution $p_{\text{uni}}(U) = 1$ and collect a set of N_M bit-strings $\mathbf{s}^{(r,m)}$ for each of them. We can construct for a given unitary $U^{(r)}$ the estimator as a function of the observed bit-strings after applying the same unitary as given in Eq.(2.35)

$$\hat{X}_2(U^{(r)}) = \frac{2^N}{N_M(N_M - 1)} \sum_{m' \neq m} (-2)^{-D[\mathbf{s}^{(r,m')}, \mathbf{s}^{(r,m)}]}. \quad (3.11)$$

The quantum mechanical average over the measurements of the above estimator gives

$$\mathbb{E}_{\text{QM}}[\hat{X}_2(U^{(r)})] = X_2(U^{(r)}). \quad (3.12)$$

The unbiased estimator of the purity \hat{p}_2 for a generic distribution $p(U)$ can be given by recalling Eq. (3.2) as

$$\hat{p}_2 = \frac{1}{N_U} \sum_{r=1}^{N_U} \frac{\hat{X}_2(U^{(r)})}{p(U^{(r)})} \quad (3.13)$$

with

$$\mathbb{E}[\hat{p}_2] \equiv \mathbb{E}_{p(U)}[\mathbb{E}_{\text{QM}}[\hat{p}_2]] = p_2 = \text{Tr}(\rho^2). \quad (3.14)$$

Here $\mathbb{E}[\cdot]$ includes the expectation over the unitaries from a distribution $p(U)$ and the quantum mechanical average over the measurements. The key quantity that governs the statistical errors in our protocol is given by the variance of \hat{p}_2 . We can express the variance of the estimator \hat{p}_2 as

$$\text{Var}[\hat{p}_2] = \frac{1}{N_U} \text{Var} \left[\frac{\hat{X}_2(U^{(r)})}{p(U^{(r)})} \right] = \frac{1}{N_U} \left(\mathbb{E} \left[\left(\frac{\hat{X}_2(U^{(r)})}{p(U^{(r)})} \right)^2 \right] - \mathbb{E} \left[\frac{\hat{X}_2(U^{(r)})}{p(U^{(r)})} \right]^2 \right) \quad (3.15)$$

where $\text{Var}[\mathbf{X}] = \mathbb{E}[\mathbf{X}^2] - \mathbb{E}[\mathbf{X}]^2$ and we note additionally that for $r = 1, \dots, N_U$, each of the random unitaries are sampled independently. From this property, we obtain that $\text{Var}[\hat{p}_2] = 1/N_U \text{Var} \left[\frac{\hat{X}_2(U^{(r)})}{p(U^{(r)})} \right]$. As we show in our work [99, Appendix. E], we have the following proposition that summarizes our findings

Proposition 1. *The variance of \hat{p}_2 for a general distribution $p(U)$ is given by*

$$\text{Var}[\hat{p}_2] = \frac{1}{N_U} \left(\frac{(N_M - 3)(N_M - 2)}{N_M(N_M - 1)} \Gamma^{(4)} + \frac{4(N_M - 2)}{N_M(N_M - 1)} \Gamma^{(3)} + \frac{2}{N_M(N_M - 1)} \Gamma^{(2)} - \text{Tr}(\rho^2)^2 \right). \quad (3.16)$$

where, the coefficients $\Gamma^{(k)}$ are given by

$$\Gamma^{(k)} = \mathbb{E}_{p(U)} \left[\frac{\text{Tr} (O^{(k)}(U\rho U^\dagger)^{\otimes k})}{p(U)^2} \right] = \int_{\text{Haar}} \frac{\text{Tr} (O^{(k)}(U\rho U^\dagger)^{\otimes k})}{p(U)^2} p(U) dU \quad (3.17)$$

and the k -copy operators $O^{(k)}$ are expressed as

$$O^{(4)} = O \otimes O; \quad O^{(3)} = (\mathbb{1} \otimes O)(O \otimes \mathbb{1}); \quad O^{(2)} = O^2 \quad (3.18)$$

with the operator O diagonal in the computational basis as

$$O = 2^N \sum_{\mathbf{s}, \mathbf{s}'} (-2)^{-D[\mathbf{s}, \mathbf{s}']} |\mathbf{s}\rangle\langle\mathbf{s}| \otimes |\mathbf{s}'\rangle\langle\mathbf{s}'| = 2^N \bigotimes_{i=1}^N \sum_{s_i, s'_i} (-2)^{-D[s_i, s'_i]} |s_i\rangle\langle s_i| \otimes |s'_i\rangle\langle s'_i|. \quad (3.19)$$

Additionally, we can express the 2-copy operator O in an alternate form to simplify our following calculations:

$$O = 2^N \sum_{\mathbf{s}, \mathbf{s}'} (-2)^{-D[\mathbf{s}, \mathbf{s}']} |\mathbf{s}\rangle\langle\mathbf{s}| \otimes |\mathbf{s}'\rangle\langle\mathbf{s}'| = \frac{1}{2^N} \bigotimes_{i=1}^N [(\mathbb{1}_i \otimes \mathbb{1}_i) + (3Z_i \otimes Z_i)]. \quad (3.20)$$

where Z_i is the Pauli- z operator acting on the i^{th} qubit. The above expression can be verified by expanding for a single qubit the RHS of the equation. Furthermore, we note, as further detailed in our work [99, Appendix. B], the function $X_2(U) = \text{Tr}[O(U\rho U^\dagger)^{\otimes 2}]$ is bounded by $1/2^N \leq X_2(U) \leq 4^N$ and is thus a positive function. Let us now illustrate the concrete expression of the variance of the purity for the two sampling methods.

3.3.1 Variance of uniform sampling for a pure product state

Consider without loss of generality a N -qubit pure product state $\rho = |0\rangle\langle 0|^{\otimes N}$. We sample local random unitaries $U = \bigotimes_{i=1}^N U_i$ uniformly from the Haar measure by taking $p(U) = p_{\text{uni}}(U) = 1$. Our goal is to compute explicitly all the terms $\Gamma^{(k)} = \mathbb{E}_{p(U)}[\Gamma^{(k)}(U)]$ in Eq. (3.16). The computation becomes easy as we note that the sampled unitaries U , the operator $O^{(k)} = \bigotimes_{i=1}^N O_i^{(k)}$ (noting the form of O in Eq. (3.20)) and the state ρ can be described locally for each qubit. This implies that we have

$$\Gamma^{(k)}(U) = \frac{\text{Tr} \left(O^{(k)}(U |0\rangle\langle 0|^{\otimes N} U^\dagger)^{\otimes k} \right)}{p_{\text{uni}}(U)^2} = \prod_{i=1}^N \text{Tr} \left(O_i^{(k)}(U_i |0\rangle\langle 0| U_i^\dagger)^{\otimes k} \right) \quad (3.21)$$

where we have taken $p_{\text{uni}}(U) = 1$ and have defined

$$O_i^{(4)} = O_i \otimes O_i, \quad O_i^{(3)} = (O_i \otimes \mathbb{1}_i)(\mathbb{1}_i \otimes O_i), \quad O_i^{(2)} = (O_i)^2 \quad (3.22)$$

with $O_i = \frac{1}{2}(\mathbb{1}_i \otimes \mathbb{1}_i)(3Z_i \otimes Z_i)$ such that $O = \bigotimes_{i=1}^N O_i$. Computing the expressions of $\Gamma^{(k)}(U)$ for each qubit leads to the following:

$$\Gamma^{(2)}(U) = \frac{1}{4^N} \prod_i (10 + 6 \operatorname{Tr}(|0\rangle\langle 0| U_i^\dagger Z_i U_i)^2) \quad (3.23)$$

$$\Gamma^{(3)}(U) = \frac{1}{4^N} \prod_i (1 + 15 \operatorname{Tr}(|0\rangle\langle 0| U_i^\dagger Z_i U_i)^2) \quad (3.24)$$

$$\Gamma^{(4)}(U) = \frac{1}{4^N} \prod_i (1 + 3 \operatorname{Tr}(|0\rangle\langle 0| U_i^\dagger Z_i U_i)^2)^2. \quad (3.25)$$

We further notice that the term $\operatorname{Tr}(|0\rangle\langle 0| U_i Z_i U_i^\dagger) = \langle 0| U_i Z_i U_i^\dagger |0\rangle$ is bounded in $[-1, 1]$. As the local unitaries are distributed by the Haar measure and each individual qubit is measured in the z -basis, we can also parameterize them using two rotation angles θ_i and ϕ_i as $U_i = R_y(\theta_i)R_z(\phi_i)$ as shown in Sec. 3.2. By simple replacement we get

$$\begin{aligned} \operatorname{Tr}(|0\rangle\langle 0| U_i^\dagger Z_i U_i) &= \operatorname{Tr}(|0\rangle\langle 0| R_z(\phi_i)^\dagger R_y(\theta_i)^\dagger Z_i R_y(\theta_i) R_z(\phi_i)) \\ &= \operatorname{Tr}(|0\rangle\langle 0| R_y(\theta_i)^\dagger Z_i R_y(\theta_i)) \end{aligned} \quad (3.26)$$

where we have used the relation for matrices A, B : $(AB)^\dagger = B^\dagger A^\dagger$ and the trace cyclicity $\operatorname{Tr}(AB) = \operatorname{Tr}(BA)$. We also note that $R_z(\phi_i) |0\rangle\langle 0| R_z(\phi_i)^\dagger = |0\rangle\langle 0|$. This expression shows that the unitary only depends on the R_y rotation. Using (3.5) and (3.9), we can rewrite $\langle 0| U_i Z_i U_i^\dagger |0\rangle = \cos \theta_i = 1 - 2\xi_i$ with ξ_i being uniformly distributed in $[0, 1]$. Then, the Haar measure simplifies to $dU = \prod_{i=1}^N dU_i = \prod_{i=1}^N d\xi_i$. By a simple replacement $z_i = 1 - 2\xi_i \implies d\xi_i = -dz_i/2$, we can compute $\Gamma^{(k)}$ by performing the Haar integral locally for each qubit due to the independence of the local random unitaries over each qubit site. We get

$$\begin{aligned} \Gamma^{(2)} &= \int dU \Gamma^{(2)}(U) = \left[\frac{1}{8} \int_{-1}^1 dz (10 + 6z^2) \right]^N = 3^N \\ \Gamma^{(3)} &= \int dU \Gamma^{(3)}(U) = \left[\frac{1}{8} \int_{-1}^1 dz (1 + 15z^2) \right]^N = \left(\frac{3}{2} \right)^N \\ \Gamma^{(4)} &= \int dU \Gamma^{(4)}(U) = \left[\frac{1}{8} \int_{-1}^1 dz (1 + 3z^2)^2 \right]^N = \left(\frac{6}{5} \right)^N. \end{aligned}$$

We can thus summarize our results by the following Lemma:

Lemma 1 (Uniform sampling). *Consider a N -qubit pure product state ρ and local random unitaries U_i sampled uniformly from the Haar measure with $p(U) = p_{\text{uni}}(U) = 1$. Then, we find*

$$\Gamma^{(4)} = \left(\frac{6}{5} \right)^N; \quad \Gamma^{(3)} = \left(\frac{3}{2} \right)^N; \quad \Gamma^{(2)} = 3^N. \quad (3.27)$$

The computation of the variance for uniform sampling shows explicitly the exponential scaling with respect to the system size N associated with randomized measurements as these coefficients enter explicitly the expression of the variance as given in Eq. (3.16). Let us now move on to a similar case study done for importance sampling.

3.3.2 Variance of importance sampling for a pure product state

We consider here without loss of generality the N -qubit pure product state $\rho = |0\rangle\langle 0|^{\otimes N}$ and random unitaries $U = \bigotimes_{i=1}^N U_i$ sampled from the importance sampling distribution $p(U) = p_{\text{IS}}(U) = \frac{[X_2(U)]_{\text{IS}}}{\int [X_2(U)]_{\text{IS}} dU}$. In particular, to find the optimal variance scaling for importance sampling, we consider here a perfect sampler given by $[X_2(U)]_{\text{IS}} = X_2(U)$. We firstly note that we can express $X_2(U)$ as

$$\begin{aligned} X_2(U) &= \text{Tr} (O(U\rho U^\dagger)^{\otimes 2}) = \frac{1}{2^N} \prod_{i=1}^N \text{Tr} \left((\mathbb{1}_i \otimes \mathbb{1}_i + 3Z_i \otimes Z_i)(U_i |0\rangle\langle 0| U_i^\dagger)^{\otimes 2} \right) \\ &= \frac{1}{2^N} \prod_{i=1}^N \left(1 + 3 \langle 0| U_i^\dagger Z_i U_i |0\rangle^2 \right). \end{aligned} \quad (3.28)$$

In a similar manner as done for the uniform sampling case in the previous section, we would like to compute the function $\Gamma^{(k)} = \mathbb{E}_{p(U)}[\Gamma^{(k)}(U)] = \int \Gamma^{(k)}(U)p(U)dU$. We have, replacing the expression of the importance sampling distribution in Eq. (3.21),

$$\Gamma^{(k)}(U) = \left[\int X_2(U)dU \right]^2 \frac{\prod_{i=1}^N \text{Tr} \left(O_i^{(k)}(U_i |0\rangle\langle 0| U_i^\dagger)^{\otimes k} \right)}{X_2(U)^2}. \quad (3.29)$$

We note that for a pure product state that is considered here $\int X_2(U)dU = p_2 = 1$. Borrowing the notations and definitions that were introduced in the previous subsection, we can compute the terms $\Gamma^{(k)}$ by performing the Haar integrals for each qubit. This results in

$$\begin{aligned} \Gamma^{(2)} &= \int \Gamma^{(2)}(U)X_2(U)dU = \left[\frac{1}{4} \int_{-1}^1 dz \frac{10 + 6z^2}{1 + 3z^2} \right]^N = \left(1 + \frac{4\pi}{3\sqrt{3}} \right)^N \\ \Gamma^{(3)} &= \int \Gamma^{(3)}(U)X_2(U)dU = \left[\frac{1}{4} \int_{-1}^1 dz \frac{(1 + 15z^2)}{1 + 3z^2} \right]^N = \left(\frac{5}{2} - \frac{2\pi}{3\sqrt{3}} \right)^N \\ \Gamma^{(4)} &= \int \Gamma^{(4)}(U)X_2(U)dU = \left[\frac{1}{4} \int_{-1}^1 dz \frac{(1 + 3z^2)^2}{1 + 3z^2} \right]^N = 1^N. \end{aligned}$$

We can then summarize our findings as follows

Lemma 2 (Importance sampling with perfect sampler). *Consider a N -qubit pure product state ρ and local random unitaries $U = \bigotimes_{i=1}^N U_i$ sampled from an importance sampling distribution $p(U) = p_{\text{IS}}(U) = \frac{X_2(U)}{\int X_2(U)dU}$ according to the Haar measure. Then, we find*

$$\Gamma^{(4)} = 1^N; \quad \Gamma^{(3)} = \alpha^N; \quad \Gamma^{(2)} = \beta^N \quad (3.30)$$

with $\alpha = \frac{5}{2} - \frac{2\pi}{3\sqrt{3}} \approx 1.29$, and $\beta = 1 + \frac{4\pi}{3\sqrt{3}} \approx 3.42$.

The analytical expressions derived in Lemma. 1 and Lemma. 2 show that in the case of importance sampling, the $\Gamma^{(k)}$ terms for $k = 3, 4$ have reduced exponentials as a function of system size compared to that of uniform sampling for a pure

product state. As the variance can be directly related to the statistical error of the estimation of the purity, we can concur that the number of measurements for importance sampling will scale more favourably in comparison to the uniform sampling. To highlight this explicitly we can use our analytical calculations presented here to understand the scaling of the number of measurements as a function of the system size N . For a given value of statistical error \mathcal{E} (which we define in this case by the relation $\text{Std}[\hat{p}_2] = \sqrt{\frac{\pi}{2}}\mathcal{E}$), we can extract analytically the optimal required number of measurements $N_U N_M$ by using Eq. (3.16) in the case of uniform and importance sampling.

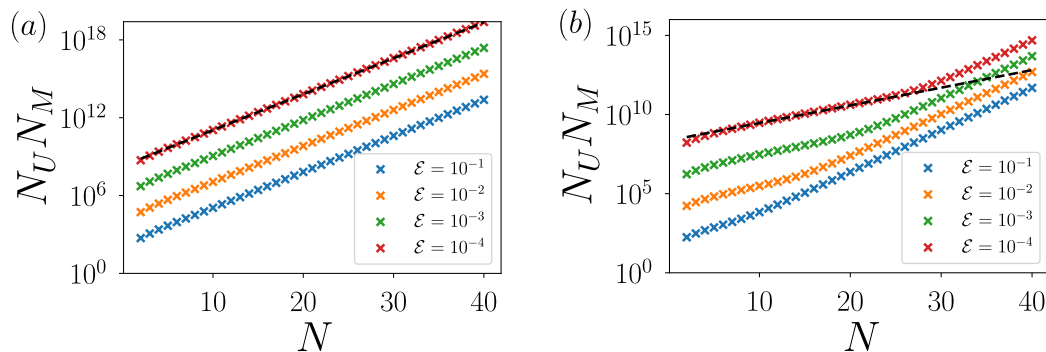


Figure 3.2: *Measurement budget scaling for product states* — Panel (a) for uniform and (b) for importance sampling, show the required number of measurements for different accuracy regimes (in function of \mathcal{E}) for different system-sizes N . The black dashed line is a guide $\propto 2^{aN}$ for the asymptotic scaling in the limit $\mathcal{E} \rightarrow 0$, with $a = 0.92$ for uniform sampling and $a = 0.37$ for importance sampling.

Our results illustrated in Fig. 3.2(a-b) show that the required number of measurements scales as 2^{aN} . Additionally, we confirm the existence of two distinct regimes for importance sampling: For a threshold value of $N \leq N_c$, the scaling for importance sampling is greatly reduced with an associated exponent $a = 0.37$. When $N > N_c$, we observe a scaling exponent of $a = 0.88$. We can relate the observation of these two regimes to the dominance of $\Gamma^{(k)}$ terms in Lemma. 2. When $N < N_c$, the terms $\Gamma^{(k)}$ for $k = 3, 4$ are dominant, while $N > N_c$ is mainly dominated by larger value of $\Gamma^{(2)}$ in the asymptotic limit. Moreover, we do not observe this feature in the case of uniform sampling that has a constant scaling exponent of $a = 0.92$. This behaviour shows that the relevant regime $N < N_c$ increases as a function of the inverse of the statistical error \mathcal{E} . This means that importance sampling provides striking performance to evaluate the purity in the high accuracy regime ($\mathcal{E} \rightarrow 0$) in comparison to uniform sampling.

In order to confirm and complement our analytical studies we shall now provide numerical evidence of the same for different states.

3.4 Numerical study and performance highlights

In this section, we shall complement our analytical findings of Lemma. 1 and Lemma. 2 by numerical simulations of the randomized measurement protocol in

order to gauge the performance of importance sampling compared to uniform sampling. In particular, we shall study different states ranging from product states, GHZ states, random states and also entangled state produced in a quantum simulation experiment [11] along with a case study of the experiment in [111]. We assess the performance of the importance sampling with respect to uniform sampling by computing the *average statistical error* which is given by $\mathcal{E} = |\hat{p}_2 - p_2|/p_2$, where p_2 is the true value of the purity of the quantum state of interest and \hat{p}_2 is an estimation either provided by importance sampling (using Eq. (3.10)) or uniform sampling (using Eq. (2.34)). The statistical error \mathcal{E} in the following case studies is computed by averaging $\langle \cdot \rangle$ over 100 independently simulated experimental runs of the RM protocol.

3.4.1 Estimation with perfect sampler

We start by simulating the RM protocol for a N -qubit pure product state $\rho = |0\rangle\langle 0|^{\otimes N}$. Here to understand the optimal performance provided by importance sampling, we consider the approximate state to model perfectly the experimental state, i.e. $\rho = \sigma$. So we sample random unitaries from the ideal theory state, i.e. $p_{\text{IS}}(U) = \frac{X_2(U)}{\int X_2(U)dU}$, where we take $[X_2(U)]_{\text{IS}} = X_2(U)$. For our first set of numerical simulations, we simulate the randomized measurements using various different values of the number of unitaries N_U and the corresponding bit-string measurements N_M . From these simulations, we extract the minimal measurement budget M by finding numerically the best combination of N_U and N_M to obtain a fixed level of statistical error \mathcal{E} . In particular, as mentioned earlier, for importance sampling done from a perfect sampler ($[X_2(U)]_{\text{IS}} = X_2(U)$), the optimal measurement budget is obtained for $N_U = 1$ and $N_M \gg 1$ as from Eq. (3.13), we have $\hat{p}_2 = \left(\int X_2(U)dU\right) \frac{\hat{X}_2(U^{(1)})}{X_2(U^{(1)})} = p_2 \frac{\hat{X}_2(U^{(1)})}{X_2(U^{(1)})}$. In this limit of $N_M \gg 1$: $\frac{\hat{X}_2(U^{(1)})}{X_2(U^{(1)})} \sim 1$ and thus \hat{p}_2 is close to the value of p_2 .

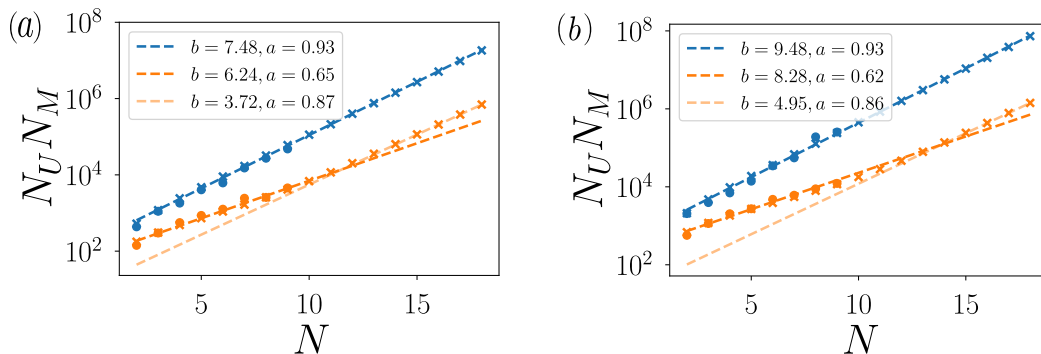


Figure 3.3: *Statistical error scaling for product states* — Panel (a-b) shows the scaling of the total required number of measurements $N_U N_M$ as a function of the system-size N for product states to reach a given value of the statistical error $\mathcal{E} = 0.1$ (for panel (a)) and $\mathcal{E} = 0.05$ (for panel (b)). The number of measurements scale as 2^{b+aN} .

Fig. 3.3(a-b) show the optimal budget $N_U N_M$ as a function of the system-size for two different values of \mathcal{E} . We have plotted the estimate of the purity in blue and orange for uniform and importance sampling respectively. The circles describe the numerical simulations and the cross the analytical prediction as shown in the previous section. In general, the number of measurements $N_U N_M$ scales exponentially

2^{b+aN} as a function of the system-size N for both the sampling methods. Interestingly, we observe that importance sampling provides a reduced exponent $a \approx 0.65$ in comparison to uniform sampling which has $a \approx 0.93$. Additionally, the prefactor 2^b is always reduced for importance sampling with respect to uniform sampling.

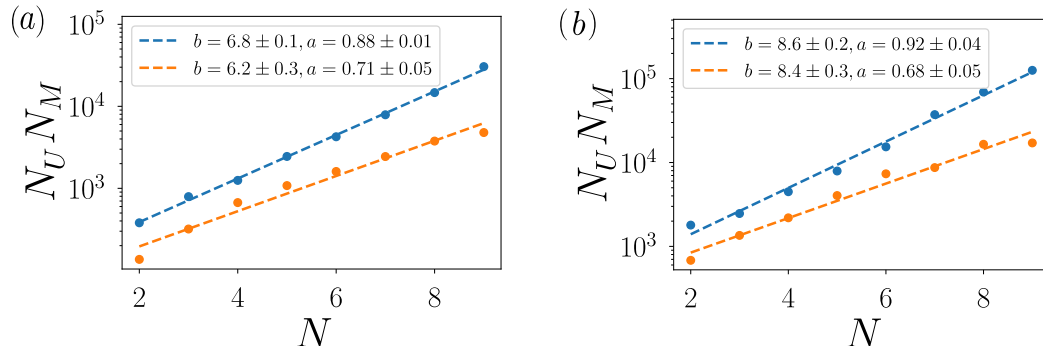


Figure 3.4: *Statistical error scaling for GHZ states* — Panels (a-b) show the scaling of the total number of measurements $N_U N_M$ as a function of the system-size for a fixed error of $\mathcal{E} = 0.1$ and $\mathcal{E} = 0.05$ in panels (a) and (b) respectively. We observe, in general, a reduced exponent for the measurement scaling for importance sampling in comparison to uniform sampling.

Moving to the case where we consider entangled GHZ states $|\psi_{\text{GHZ}}^{(N)}\rangle = (|0\rangle^{\otimes N} + |1\rangle^{\otimes N})/\sqrt{2}$, we observe as shown in Fig. 3.4 similar performances from our numerical simulations with importance sampling (in orange) providing improved estimations compared to uniform sampling (in blue) as given by their respective scaling exponents.

Random states — Additionally, we also simulate the RM protocol for N -qubit random states defined as $|\psi\rangle = U_{\text{CUE}} |0\rangle^{\otimes N}$ where U_{CUE} is a unitary sampled from the CUE of dimension $d = 2^N$. We again perform importance sampling from a perfect sampler $[X_2(U)]_{\text{IS}} = X_2(U)$. In Fig. 3.5(a-b), we plot the extracted optimal measurement budget $M = N_U N_M$ for a fixed level of statistical error (in blue for uniform and orange for importance sampling respectively). We observe that importance sampling does not provide additional scaling improvements with respect to the system size N . We only gain in terms of the pre-factor 2^b that reduces the number of measurements when compared with uniform sampling. One of the potential reasons of this behaviour could be due to a lack of substantial peaks in the multi-variate function $X_2(U)$ around which importance sampling could prioritize the unitaries.

3.4.2 Machine-learning sampling for product and GHZ states

In this section, we demonstrate importance sampling performed from a trained machine-learning (ML) model that samples unitaries from the distribution $p_{\text{IS}}(U)$. We consider a collection of classical data obtained by performing randomized measurements without shot-noise, i.e we take $N_M \rightarrow \infty$. The neural network model is trained by feeding the $2N$ input angles corresponding to the random unitary U and the output being its associated function $X_2(U)$. For product state, we easily obtain a trained deep neural network (DNN) that fits the function $X_2(U)$ with a mean absolute error below five percent. For this task, we use optimized routines of the library TensorFlow-Keras for which we take a total of $N_{\text{samples}} = 10^5$ training samples. Further details on the training parameters are provided in [99, Appendix. C] for the

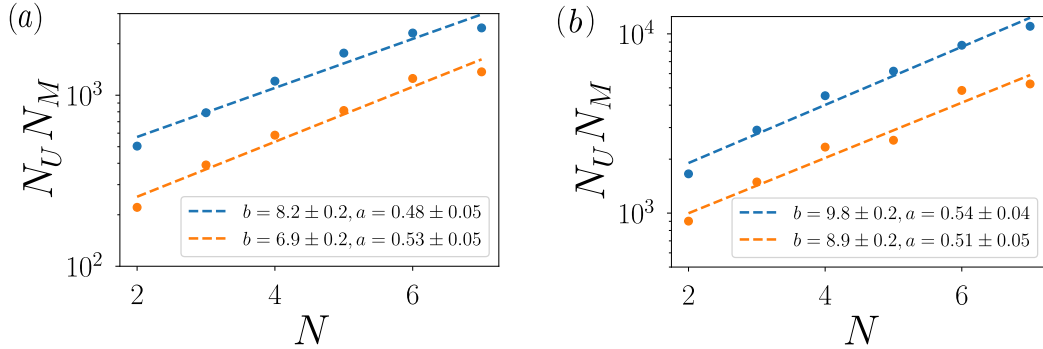


Figure 3.5: *Statistical error scaling for random states* — Panels (a-b) show the scaling of the total number of measurements $N_U N_M$ as a function of the system-size for a fixed error of $\mathcal{E} = 0.1$ and $\mathcal{E} = 0.05$ in panels (a) and (b) respectively.

interested readers. In the case of the GHZ state $|\psi_{\text{GHZ}}^{(N)}\rangle$, we train the DNN model to learn the intrinsic correlations present in it so that the neural network model is able to sample the required correlated random unitaries that are more effective than the uniform ones. Once we obtain the model with an adequate fit below the error threshold of choice, we save them and re-use the same for later sampling task.

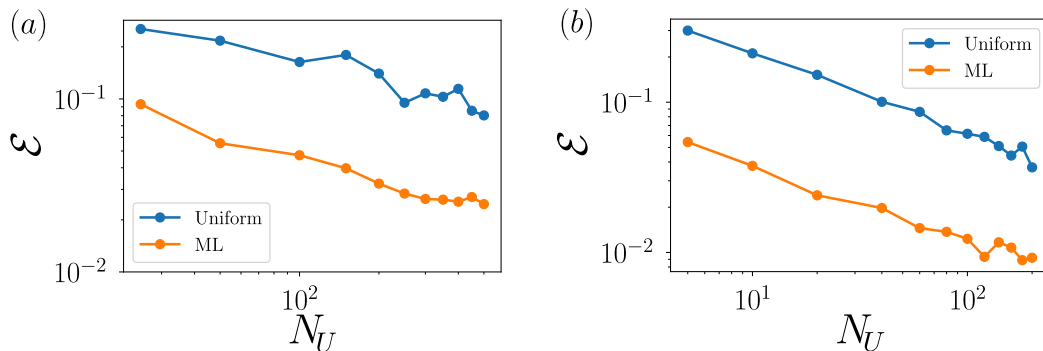


Figure 3.6: *Error scaling as function of the number of unitaries* — Panel (a) for 10-qubit product state and (b) for 5-qubit GHZ state, show the statistical error scaling as a function of the applied number unitaries N_U . The importance sampling is performed from a trained DNN model. We fix the number of measurements to be $N_M = 10^3$.

Error scaling with the number of unitaries — We illustrate the result of the statistical error scaling for both the sampling methods as a function of the number of unitaries for a 10 qubit product state in Fig. 3.6(a) and a 5 qubit GHZ state in Fig. 3.6(b). Though errors in both cases scale as $1/\sqrt{N_U}$ as dictated by standard Monte-Carlo error decay, we see that importance sampling out-performs standard uniform sampling by decreasing the statistical errors effectively by a factor of five. As shown, this implies that to achieve a fixed accuracy in terms of \mathcal{E} , importance sampling requires less measurement compared to standard uniform sampling.

Error scaling with the number of projective measurements — Additionally, performing similar simulations for both product and GHZ states for fixed values of N_U , we can see the behavior of the error as a function of the number of measurements N_M . We plot in Fig. 3.7(a-d), the average statistical error in function of re-scaled units of $N_M/2^{aN}$, where a is adjusted to make all the points for different system sizes, collapse onto a single curve. As the plots suggest, the scaling exponent for importance

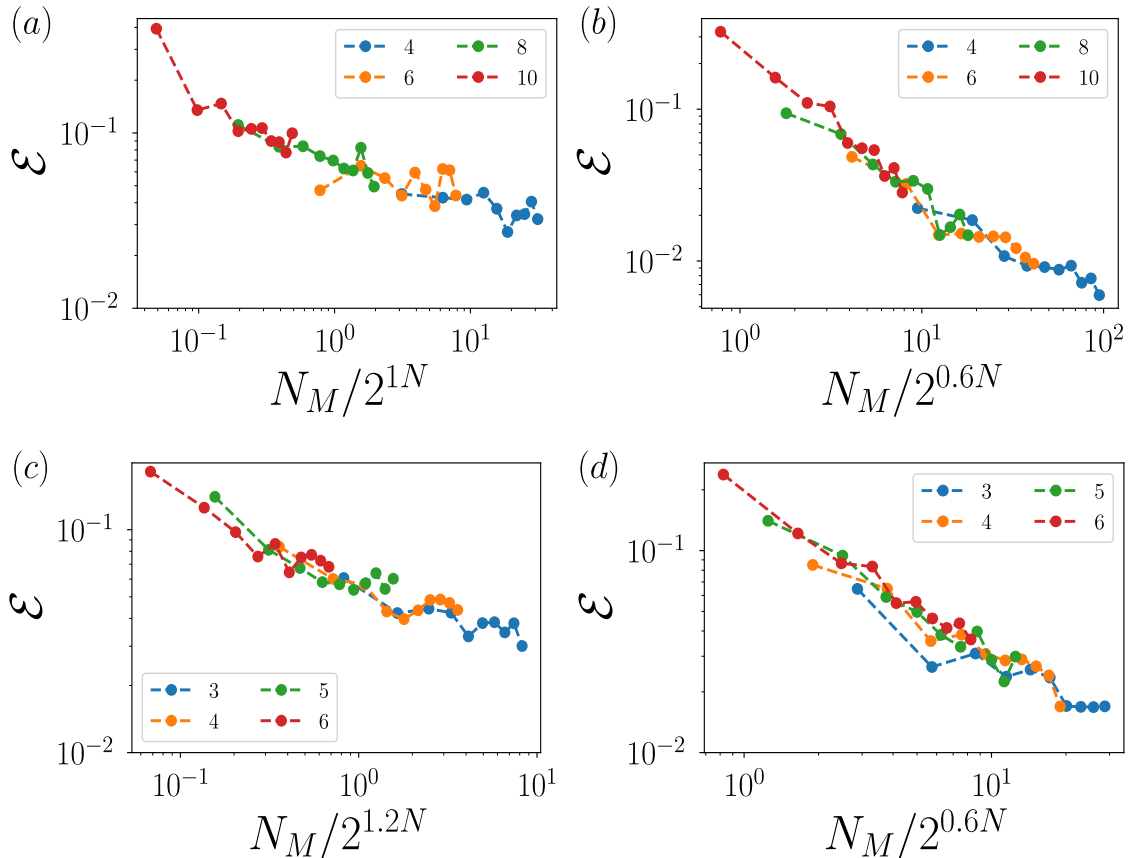


Figure 3.7: *Error scaling as function of the number of measurements* — Panel (a-b) for product state with $N_U = 500$ and (c-d) GHZ state with $N_U = 200$ show the statistical error scaling as a function the rescaled units $N_M/2^{aN}$. For panels (a) and (c), the unitaries are sampled uniformly and for panel (b) and (d) the unitaries are sampled from the trained DNN model.

sampling is roughly reduced by half when compared to uniform sampling. It is important to note, compared to the previous case, that here importance sampling not only reduces the required number of unitaries N_U but also provides a reduction to the number of measurements N_M . This is due to the fact that the unitaries sampled according to the importance sampling distribution are chosen close to the maxima of the multi-variate function $X_2(U)$ where fluctuations due to shot-noise are smaller compared to other regions of the function.

3.4.3 Sampling from MPS approximations

We now move to an example of an entangled state prepared in a quantum simulation experiment that implemented the randomized measurements protocol for the first time [11]. This experimental state was realized on a trapped-ion quantum simulator, by quenching an initial N -qubit Néel state $|\psi_0\rangle = |01\rangle^{\otimes N/2}$ with a long-range H_{XY} Hamiltonian for different amounts of time. The 10 qubit state realized after quenching for a total of $t = 5$ ms had an experimental purity value $p_2 \approx 0.62$ which indicates that the realized state was not pure and suffered from decoherence. We consider here a scenario where we would like to perform importance sampling without the knowledge of the decoherence parameter in a given experiment. This could be due to a lack of knowledge on all the decoherence mechanisms affecting

the quantum device. To perform importance sampling we consider two methods. First, we train our neural network model by considering samples taken from the perfect pure state at $t = 5$ ms by modelling classically the same experiment without decoherence. Second, we use the more physically inspired approach to create an approximation of the prepared state using a MPS. From the MPS we can build the importance sampling function as described in the earlier sections.

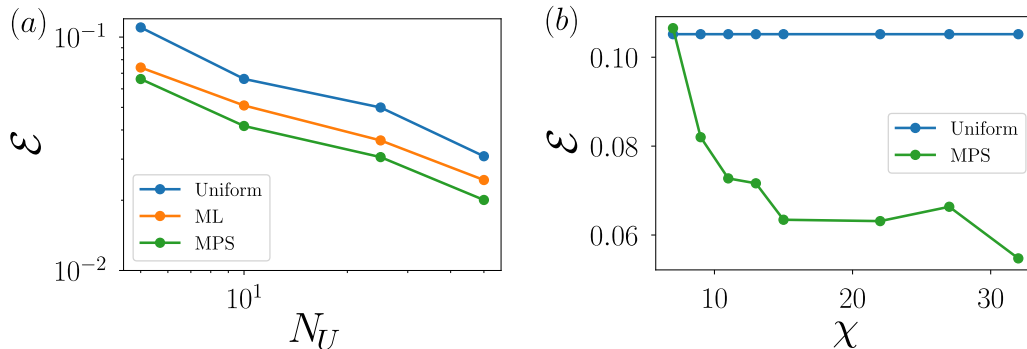


Figure 3.8: *Purity estimation using importance sampling from ML and MPS for entangled 10-qubit state* — Panel (a) shows the statistical error scaling as a function of the number of unitaries N_U for a fixed value of $N_M = 7500$ for uniform sampling (blue) and importance sampling done with a CNN model (orange) and an MPS approximation of the state of bond-dimension $\chi = 15$ (green). Panel (b) highlights the error reduction as a function of the bond dimension χ used of the MPS sampler for a fixed measurement budget of $N_U = 5$ and $N_M = 75000$.

Fig. 3.8(a-b) shows the result of the numerical investigation. In particular, for the neural network model that we use in this case, we specifically consider training a convolutional neural network (CNN) that can potentially capture some quasi-translational invariant features of the function. We remark from Fig. 3.8(a) that the CNN model outperforms the uniform sampling. The MPS state $|\psi_\chi\rangle$ for $\chi = 15$ with a fidelity $\langle\psi_\chi|\rho|\psi_\chi\rangle = 0.7$ compared to the experimental state ρ already outperforms the ML sampling. Interestingly, when we plot the statistical error for a fixed measurement budget ($N_U N_M$) as a function of the bond dimension χ of the MPS (Fig. 3.8(b)), we observe that as the MPS starts to describe the entanglement content of the experimental state more accurately with an increase of the bond-dimension, the statistical errors reduce. This is due to the fact that the approximate state σ approaches ρ when χ is increased. We also observe an interesting trade-off between classical and quantum resources involved. To obtain a better importance sampler that enables the reduction of the measurement budget on the experimental side requires increasing the bond-dimension that uses more classical resources and run-time.

Optimization for mixed state sub-systems — Additionally, we show that importance sampling can be implemented to probe sub-systems of interest of a quantum state ρ . This, in particular, is relevant to effectively establish the presence of entanglement in the system as done in [53, 11] or to measure for instance the topological entanglement entropy expressed as a function of Rényi entropies of sub-partitions [57, 111]. We shall perform a case study on the latter experiment in the next section to illustrate a strategy of importance sampling to measure multiple sub-system purities. Importance sampling becomes more relevant in these scenarios as the probabilities obtained from the bit-string measurements on a highly mixed

state takes values in a much reduced interval [30]. Here we will be interested to probe the purity of the half-system reduced state $\rho_A = \text{Tr}_B(\rho)$ of the entangled quenched state discussed previously [11]. In particular, we shall effectively consider a half-system prepared at $t = 5$ ms and $t = 7.5$ ms for a total system of 10 and 20 qubits respectively. For the 10 qubit system, the half-system purity was found to be $\text{Tr}(\rho_A^2) = 0.16$. We trained the CNN model to build the fit function from samples obtained from the 5-qubit half-system. In the case of the MPS, we considered $\rho_{\text{red}} = \text{Tr}_B(|\psi_\chi\rangle\langle\psi_\chi|)$ with $\chi = 15$ as the approximation to the reduced experimental state for importance sampling.

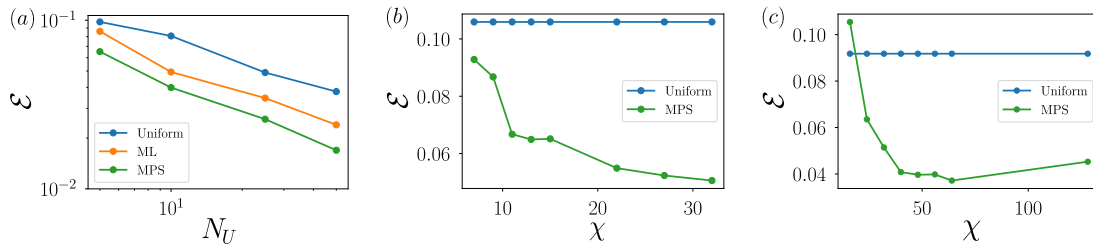


Figure 3.9: *Purity estimation using importance sampling from ML and MPS constructed from mixed states* — Panels (a-b) show the average statistical error \mathcal{E} for a 5-qubit reduced state taken from a total system of 10 qubits. Panel (a) shows the error scaling as a function of N_U for importance sampling done from a CNN model and an MPS approximation of bond-dimension $\chi = 15$. We fix the value of $N_M = 7500$. Panel (b) shows the estimation error as a function of the bond-dimension of the MPS approximation used. We fix $N_U = 5$ and $N_M = 7500$. Panel (c) illustrates the statistical error as a function of χ for a 10-qubit reduced state taken from a total system of 20 qubits for $N_U = 5$ and $N_M = 10^5$.

Fig. 3.9(a) illustrates similar results where statistical errors are reduced by importance sampling. Again we observe the MPS approximation outperforming our trained CNN model for the mixed state. In Fig. 3.9(b) we show the decay of the statistical errors as a function of varying bond-dimension χ . In the case of the 10-qubit half-system, we considered the full 20-qubit state $\rho = |\psi\rangle\langle\psi|$ to be a pure state which was described by an MPS of bond-dimension $\chi = 256$. This reduced state had a purity value of $\text{Tr}(\rho_A^2) = 0.103$. To perform importance sampling we consider states of the form $\rho_{\text{red}} = \text{Tr}_B(|\psi_\chi\rangle\langle\psi_\chi|)$ for various values of the bond-dimension χ . We show in Fig. 3.9(c), the reduction of error as a function of the MPS approximation considered for importance sampling. The MPS representation with $\chi = 24$ having a fidelity $\mathcal{F}(\rho_A, \rho_{\text{red}}) = 0.87$ performs better than the uniform sampler (second point in Fig. 3.9(c)). As a general remark, we observe that MPS approximations are well suited and powerful for the importance sampling task and perform better compared to trained machine-learning models.

3.4.4 Importance sampling illustration for the toric code experiment

In this section, we shall highlight the performance of importance sampling for an experiment that measured the topological entanglement entropy (TEE) using randomized measurements [111]. The experiment prepared a 31-qubit toric code ground state $|G\rangle$ on the Sycamore quantum processor made up of superconducting qubits. They demonstrated the first measurement of TEE revealing topological order in

their quantum platform. This was achieved by measuring with uniform sampling the purity in the high accuracy regime of partitions up to 9 qubits. In our case study, we intend to illustrate the estimation of the TEE for a 9 qubit sub-partition for both uniform and importance sampling and gauge their performance.

We consider the 9-qubit partition to be divided into 3 different sub-systems A , B and C respectively as shown in Fig. 3.10. The TEE can be formally defined in terms of the sub-system second Rényi entropies as [75, 57]

$$\begin{aligned} S_2^{\text{topo}} &= S_2^{(A)} + S_2^{(B)} + S_2^{(C)} - S_2^{(AB)} - S_2^{(BC)} - S_2^{(AC)} + S_2^{(ABC)} \\ &= -\log \frac{[p_2]_A + [p_2]_B + [p_2]_C + [p_2]_{ABC}}{[p_2]_{AB} + [p_2]_{BC} + [p_2]_{AC}} \end{aligned} \quad (3.31)$$

where AB indicates the union of the sub-systems A and B and $[p_2]_\Gamma = \text{Tr}(\rho_\Gamma^2)$ is the purity of the sub-system Γ . The original experiment implemented local haar random unitaries that were sampled uniformly to evaluate all sub-system purities. The full state being entangled comprises of sub-systems that are mixed. The total measurement budget used to estimate the TEE for a 9 qubit sub-system was $M = N_U N_M = 1000 \times 10000$.

As the experiment a priori intends to realize the ground state of the toric code, we can use this available knowledge to our benefit in order to perform importance sampling of the local random unitaries. We obtain the reduced density matrix of the 9-qubit partition by modelling the full ground state of the toric code using a MPS [113]. From this modelled state, we can obtain the theoretical 9-qubit reduced state ρ_{ABC} tracing over the remaining set of qubits. This state allows us to calculate the ideal values of the purities. We find that the sub-system consisting of 3 qubits have a purity of $[p_2]_A = [p_2]_B = [p_2]_C = 0.125$, while the purities of the 6 qubit sub-systems AB , AC and BC are given as $[p_2]_{AB} = 0.0156$, $[p_2]_{AC} = 0.0312$ and $[p_2]_{BC} = 0.0624$ respectively. The full 9-qubit reduced state has a purity of $[p_2]_{ABC} = 0.0312$. From these values of the purities, we have $S_2^{\text{topo}}/\ln(2) = -1$ as measured in Ref. [111]. As we notice from the expression of Eq. (3.31), we can obtain the estimation of the purity for each sub-system by sampling the appropriate unitaries from the right distribution defined in terms of the state of the sub-system. Reducing the errors via importance sampling in the purity estimation of each of these highly mixed sub-systems will contribute in decreasing the statistical error in the estimation of S_2^{topo} .

We consider here importance sampling done from a perfect sampler, i.e $[X_2(U)]_{\text{IS}} = X_2(U)$. Importantly, we select unitaries from the ideal importance sampling distribution $X_2(U)$ that depends on the sub-system of interest in order to provide optimal estimation of its purity. Hence to evaluate S_2^{topo} effectively, we have to adapt the distribution function appropriately for all the sub-systems of interest as we shall explain next. In order to evaluate the purity of each sub-system with reduced error and provide an effective method to perform importance sampling, we propose to divide the full experiment in 4 batch experiments as shown in Fig. 3.10. For each batch $b = 1, \dots, 4$, we perform a total of $M^{(b)} = N_U^{(b)} N_M^{(b)}$ measurements. This gives the total number of measurements done in the full experiment as $M = \sum_b M^{(b)}$. We begin by the pre-processing step to prepare the local random unitaries for each batch experiment. As shown in Fig. 3.10, the four batches of experiments consist of

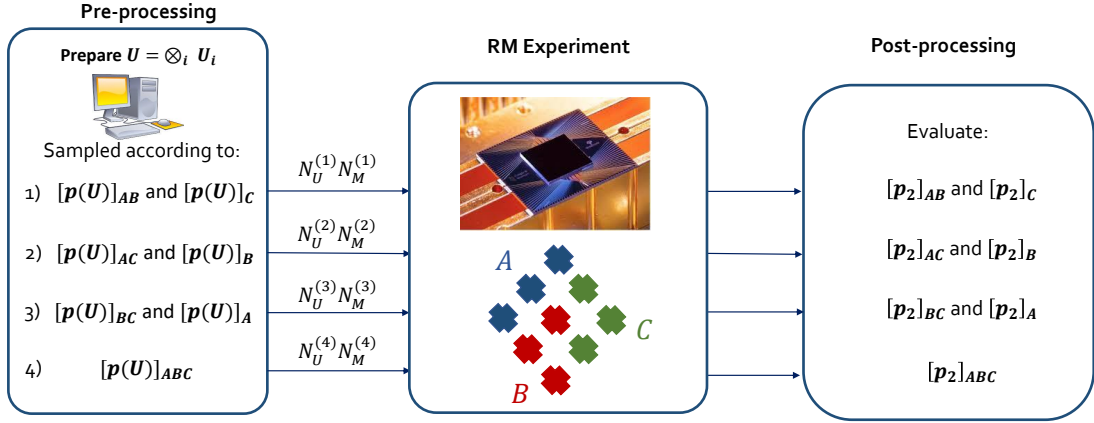


Figure 3.10: *Strategy to perform importance sampling for the toric code experiment [111] on the sycamore quantum processor [1]* — The figure describes the method to implement importance sampling in order measure S_2^{topo} . We divide the full experiment in total of four batch experiments. In each batch we sample unitaries according to the appropriate distributions as shown in the figure in order to estimate the purities of the concerned sub-systems. Combining all the estimations of the sub-system purities enables us to provide the importance sampled estimate of S_2^{topo} .

sampling unitaries from the following distribution:

$$[p(U)]_{\Gamma} = \frac{[X_2(U)]_{\Gamma}}{\int [X_2(U)]_{\Gamma} dU} \quad \text{and} \quad [p(U)]_{\bar{\Gamma}} = \frac{[X_2(U)]_{\bar{\Gamma}}}{\int [X_2(U)]_{\bar{\Gamma}} dU} \quad (3.32)$$

where $\Gamma \in \{AB, AC, BC, ABC\}$ and $\bar{\Gamma}$ describes the targeted sub-system and its complement.² Each of the functions $[X_2(U)]_{\Gamma}$ (or $[X_2(U)]_{\bar{\Gamma}}$) can be evaluated using the knowledge of sub-system density matrix ρ_{Γ} (or $\rho_{\bar{\Gamma}}$) as given in Eq. (2.28). We additionally remark that as we know the theoretical state, we can calculate the ideal value of the purity $[p_2]_{\Gamma} = \int [X_2(U)]_{\Gamma} dU$. Lastly, from each batch experiment, we get the estimated purities $[\hat{p}_2]_{\Gamma}$ and $[\hat{p}_2]_{\bar{\Gamma}}$ using Eq. (3.10).

We now present our results where we numerically simulated the randomized measurement protocol for the 9-qubit sub-system to estimate the TEE given by \hat{S}_2^{topo} . To gauge the performance, we compute the average statistical error $\mathcal{E} = \frac{|\hat{S}_2^{\text{topo}} - S_2^{\text{topo}}|}{S_2^{\text{topo}}}$ over 100 simulated experimental runs of protocol. We use in the case of uniform sampling the same measurement budget as done in the real experiment [111]. For importance sampling, we follow the procedure as shown in Fig. 3.10 and study two possible choices of measurement budget of the batch experiments. This aims at making a choice between having the same accuracy as uniform sampling with reduced measurements or an increased accuracy with similar number of measurements as performed in uniform sampling. In the first proposal, that we dub ‘IS₁’, we use $M^{(b)} = N_U^{(b)} \times N_M^{(b)} = 5 \times 20000$ for the first three batch experiments $b = 1, \dots, 3$. In the last batch experiment that evaluates the purity of the full 9 qubit sub-system, we use $M^{(4)} = N_U^{(4)} \times N_M^{(4)} = 20 \times 25000$. For the second proposal ‘IS₂’, we increase the number of unitaries and use $M^{(b)} = N_U^{(b)} \times N_M^{(b)} = 50 \times 20000$ for the

²When $\Gamma = ABC$, the complementary sub-system $\bar{\Gamma}$ is empty.

first three batch experiments $b = 1, \dots, 3$ and increase the number of measurements for the last batch experiment $M^{(4)} = N_U^{(4)} \times N_M^{(4)} = 20 \times 10^5$. The total measurement budget for ‘IS₁’ and ‘IS₂’ is given by $M = 8 \times 10^5$ and $M = 5 \times 10^6$ respectively. We note that both the importance sampling measurement budgets are *less* compared to the total measurement budget done in the case of uniform sampling. Now, we summarize our findings in the following table below:

	$[p_2]_A$	$[p_2]_B$	$[p_2]_C$	$[p_2]_{AB}$	$[p_2]_{AC}$	$[p_2]_{BC}$	$[p_2]_{ABC}$	S_2^{topo}
uniform	0.011%	0.012%	0.013%	0.37%	4.3%	4.25%	4.46%	9.67%
IS ₁	0.073%	0.078%	0.081%	2.51%	2.58%	3.18%	4.5%	9.74%
IS ₂	0.027%	0.025%	0.022%	0.76%	0.77%	1.05%	1.4%	3.04%

Table 3.1: *Performance highlight* — The above table illustrates the average statistical errors for evaluating the purities of each sub-system of the 9 qubit reduced state of $|G\rangle$ and its associated TEE S_2^{topo} .

We firstly observe that the 3-qubit sub-system purities are well estimated with uniform sampling as this state is completely mixed ($p_2 = 1/2^N$). The multi-variable function $[X_2(U)]_\Gamma$ with $\Gamma \in \{A, B, C\}$ presents a flat landscape without peak structure. Thus importance sampling does not provide additional enhancement of the estimation. Importantly, we remark that in the case of ‘IS₁’, the average statistical error of TEE is comparable to that of uniform sampling while the measurement budget is reduced by a factor of at least 10 with importance sampling ($M = 10^7$ for uniform compared to $M \sim 10^6$ for IS₁). In the second scenario with ‘IS₂’, using only half the amount of total measurements performed in the experiment ($M = 5 \times 10^6$ for IS₂ compared to $M = 10^7$ for uniform) we obtain a three-fold decrease of the statistical error to evaluate S_2^{topo} . Thus as we demonstrate again both the measurement cost and estimation accuracy are reduced for importance sampling when compared to uniform sampling. We note additionally that this proposed strategy can be implemented in the experiment, in the case where the experimental state is different than the classically modelled state used for importance sampling due to unknown decoherence effects (further numerically experiments concerning this scenario are presented in Chapter. 6).

3.5 Conclusion

In this chapter we proposed a new method taking advantage of importance sampling to optimize the randomized measurement protocol to estimate the purity of an unknown quantum state. It involves a procedure to parameterize the applied random unitaries, and a hybrid method to combine classical computational power with a quantum processor. We take advantage of the available approximate prior knowledge during the pre-processing stage of the protocol to select the best unitaries to perform randomized measurements in the experiment. The sampler to select the ‘important’ local unitaries can be built using classical representations such as tensor-

networks, of the underlying quantum state or training machine learning models using experimental data registered from prior experiments. From the various numerical case studies that we performed starting with product state to experimental states prepared in different quantum platforms, we observe that importance sampling allows us to significantly reduce the required number of measurements to estimate the purity for a fixed level of statistical error. The effective distribution of the measurement budget for implementing importance sampling consists of applying few unitaries $N_U \sim \mathcal{O}(10)$ and performing a large number of readout measurements $N_M \gg 1$. Our approach introduced here can be readily used on current experimental devices as well extend to probe in a similar fashion other quantum properties of interest such as fidelities [32], quantum scrambling [125] and topological invariants [33, 17] using randomized measurements.

As an additional remark, the importance sampling protocol is a powerful method that demonstrates the usefulness of using prior knowledge of the experimental state to boost estimation of the purity. Its only potential down side is that the right choice of the unitaries for the experiment are made prior to the data acquisition and depend on the (sub-)systems of interest to effectively enhance its estimation. This implies that it does not allow us to obtain enhanced estimation of the purity for all sub-systems of interest from the same experimental data. Additionally, this method currently only optimizes the estimation of purities (or state overlaps) in the framework of the RM toolbox. Can we extend these methods to reduce statistical errors in the estimation of other quantities of interest (other than the purity) that can be for example be accessed using the classical shadow formalism [64]? We shall address this challenge in Chapter. 6 of the manuscript, where we will introduce a new method that we call *common randomized measurements* to boost the estimation of the quantities of interest *without* involving the pre-processing step. In sharp contrast to the importance sampling method, the common randomized measurement protocol shall apply unitaries that are sampled *uniformly* in the experiment. With the same spirit of using approximate prior knowledge on the experimentally realized quantum state, we obtain enhanced estimations of quantum properties that can be accessed using the randomized measurement data solely through an effective post-processing method that we will detail in Chapter. 6. This method shall be applicable to reduce statistical errors for a wider class of quantities other than the purity accessed by RM data-set and can be readily tested on current experimental data.

In the upcoming chapters, we shall switch our focus towards the works that concern mainly to the classical shadow formalism. In particular, the next chapter shall propose a novel method to measure the quantum Fisher information using the RM toolbox and experimentally validate this method by measuring the QFI on a superconducting quantum processor. We shall also provide generalizations to existing performance guarantees for general quantities of interest that can be measured with the RM toolbox.

4

Estimation of the quantum Fisher information with classical shadows

This chapter is based on two published works: *Aniket Rath, Cyril Branciard, Anna Minguzzi, and Benoît Vermersch*. Quantum Fisher information from randomized measurements. *Phys. Rev. Lett.*, 127:260501, Dec 2021 (Ref. [100]) and *Vittorio Vitale, Aniket Rath, Petar Jurcevic, Andreas Elben, Cyril Branciard, and Benoît Vermersch*. Estimation of the quantum Fisher information on a quantum processor, *arXiv:2307.16882*, 2023 (Ref. [129]).

We present an operative method to estimate the quantum Fisher information (QFI) using a converging series of polynomials that can be estimated using the RM toolbox. This work is one of the central projects of my thesis. I have contributed to all the parts of the work (writing of the manuscript, analytical calculations, numerical investigations). The analytical calculations were done jointly with Benoît Vermersch and Cyril Branciard. In the later part of this chapter, we provide experimental measurements of the QFI on a quantum platform as given in Ref. [129] in which I developed the efficient numerical tools to analyze and extract relevant entanglement properties from the experimental data along with Vittorio Vitale and contributed to the writing of the manuscript along with other coauthors.

Contents

4.1	Construction of the lower bounds of QFI	77
4.1.1	Convergence and other properties	78
4.2	Protocol to measure QFI and its error analysis in qubit platforms	80
4.2.1	Error analysis of a generic multi-copy functional	81
4.2.2	Sample complexity for lower bounds F_n	85
4.2.3	Numerical illustrations	87
4.3	Experimental measurement of the QFI on a quantum device	88
4.3.1	Robust estimation of quantum properties in a nutshell	89

4.3.2 Experimental Results	89
4.4 Conclusion	92

As we have seen from Chapter. 1, the quantum Fisher information (QFI) is a prime example of a quantity that can certify for some applications, a potential quantum advantage compared to its classical counterparts [94]. For example, it is the central quantity related to quantum metrology [94, 93] as it validates states that have the adequate quantum resource to provide enhanced metrological sensitivities [94, 93]. Importantly, the quantum resource responsible in achieving improved metrological sensitivities consists of multipartite entanglement. The QFI additionally plays a significant role in highlighting various other quantum phenomena associated with multipartite entanglement in quantum many-body physics. It reveals universal properties of entanglement during phase transitions at finite temperature [137] or the role of multipartite entanglement in topological phase transition [92].

The current challenge that we address in this chapter is to measure the QFI for an unknown quantum state prepared on the quantum hardware comprised of qubits. The difficulty to estimate QFI arises from the fact that it is a *non-linear* function of the density matrix ρ and can not be cast into an observable that can be measured easily in experiments. Recall from Eq. (1.22) that the QFI is expressed in function of the eigenvalues of the density matrix $\rho = \sum_i \lambda_i |i\rangle\langle i|$ and an Hermitian operator \mathcal{A} as

$$F_Q = 2 \sum_{(i,j), \lambda_i + \lambda_j > 0} \frac{(\lambda_i - \lambda_j)^2}{\lambda_i + \lambda_j} |\langle i | \mathcal{A} | j \rangle|^2. \quad (4.1)$$

From this expression, we see that the only method that can estimate the QFI in a state-agnostic manner seems to be quantum state tomography (QST). As we have seen, this method has an expensive cost in terms of the required number of measurements to be executed on the quantum platform [54]. In this chapter, we will provide an alternate method to measure the QFI by constructing a polynomial series of the density matrix in the form of lower bounds that converge to the QFI. Each of the lower bounds can be measured in a state-agnostic manner using the classical shadow formalism [64] on current experimental devices with the same generated randomized measurement data. We highlight its convergence features along with rigorous sample complexity identities to estimate the required number of measurements to estimate them with a given accuracy and confidence interval. Lastly, we also describe the associated experimental estimation of the QFI via the RM toolbox for quantum states prepared on a superconducting quantum device.

4.1 Construction of the lower bounds of QFI

In this section, we shall introduce our systematic approach to construct the polynomial lower bounds of the QFI. We shall provide an alternate novel expression of the QFI and our bounds along with a convergence study of our bounds. Falling back on the inequality of Eq. (1.23) presented in the works of [122, 67], the QFI in particular detects the *entanglement depth* of a quantum state. For N qubits with collective spin operator $\mathcal{A} = \frac{1}{2} \sum_{l=1}^N \sigma_\mu^{(l)}$ where we define $\sigma_\mu^{(l)}$ as a Pauli matrix in an

arbitrary direction μ acting on the l^{th} spin, we find that if

$$F_Q > \Gamma(N, k) \equiv \left\lfloor \frac{N}{k} \right\rfloor k^2 + \left(N - \left\lfloor \frac{N}{k} \right\rfloor k \right)^2 \quad (4.2)$$

implies that the state is not k -producible and thus contains an entanglement depth of $k + 1$. Lower bounds of the QFI are useful to detect multipartite entanglement using the previous inequality. These include spin-squeezing inequalities that can be written simply in terms of an expectation value of an operator [93, 84, 119, 2, 7, 112], multiple coherences [45] and additional non-linear lower bounds to the QFI [104, 105, 139, 48, 3, 14]. These lower bounds however have a finite distance with respect to the QFI that limits the optimal detection of metrologically useful quantum states.

To construct the polynomial series of lower bounds that can be accessed by the classical shadow formalism, the key idea that we introduced in our work is to bound the fraction $\frac{(\lambda_i - \lambda_j)^2}{\lambda_i + \lambda_j}$ in Eq. (4.1) in terms of polynomials of the eigenvalues λ_i . We note that a function $g(x) = 1/x$ with $x \in [0, 1]$ can be expanded using the Taylor series as $\tilde{g}_n(x) = \sum_{\ell=0}^n (1-x)^\ell$ that satisfies: For $n \rightarrow \infty$, $\tilde{g}_n(x) \rightarrow g(x)$. Similarly, noting that the sum of eigenvalues are bounded as $0 < \lambda_i + \lambda_j \leq 1$, we have

$$\frac{1}{\lambda_i + \lambda_j} = \sum_{\ell=0}^{\infty} (1 - \lambda_i - \lambda_j)^\ell \geq \sum_{\ell=0}^n (1 - \lambda_i - \lambda_j)^\ell \quad (4.3)$$

for any $n \in \mathbb{N}$. Thus truncating the series at a finite value of n , we get the following expression for a generic lower bound

$$\begin{aligned} F_Q &= 2 \sum_{i,j} \sum_{\ell=0}^{\infty} (\lambda_i - \lambda_j)^2 (1 - \lambda_i - \lambda_j)^\ell |\langle i | \mathcal{A} | j \rangle|^2 \\ &\geq 2 \sum_{i,j} \sum_{\ell=0}^n (\lambda_i - \lambda_j)^2 (1 - \lambda_i - \lambda_j)^\ell |\langle i | \mathcal{A} | j \rangle|^2 = F_n. \end{aligned} \quad (4.4)$$

We can see that for any quantum state ρ and operator \mathcal{A} , we have $\forall n \in \mathbb{N}, F_{n+1} \geq F_n$ and that $F_n = F_Q$ when $n \rightarrow \infty$. In the two extreme cases when $\rho = |\psi\rangle\langle\psi|$ is pure or fully mixed $\rho = \mathbb{1}/2^N$, we have $F_n = F_Q, \forall n \in \mathbb{N}$. In the former case we have that $F_Q = F_n = 4(\langle\psi|\mathcal{A}^2|\psi\rangle - \langle\psi|\mathcal{A}|\psi\rangle^2)$ and in the latter $F_Q = F_n = 0$. Let us now move the discussion to the convergence of our lower bounds.

4.1.1 Convergence and other properties

In this section, we study the convergence features of the lower bounds F_n for a generic quantum state ρ that is neither pure nor fully mixed. Firstly, we notice that

$$\frac{1}{\lambda_i + \lambda_j} - \sum_{\ell=0}^n (1 - \lambda_i - \lambda_j)^\ell = \frac{(1 - \lambda_i - \lambda_j)^{n+1}}{\lambda_i + \lambda_j}. \quad (4.5)$$

In order to understand the convergence features of our bounds, we need to study the finite distance $\xi_n = F_Q - F_n$ between our bound F_n and the true value of the QFI F_Q . Using the previous equation, we have for any operator \mathcal{A}

$$\xi_n = F_Q - F_n = 2 \sum_{i,j:\lambda_i+\lambda_j>0} \frac{(\lambda_i - \lambda_j)^2}{\lambda_i + \lambda_j} (1 - \lambda_i - \lambda_j)^{n+1} |\langle i | \mathcal{A} | j \rangle|^2 = \mathcal{O}(\zeta^n) \quad (4.6)$$

where we define ζ as

$$\max_{i,j:\lambda_i+\lambda_j>0,\lambda_i\neq\lambda_j,\langle i|\mathcal{A}|j\rangle\neq 0} (1 - \lambda_i - \lambda_j). \quad (4.7)$$

When $n \rightarrow \infty$, we observe an exponential convergence of our bounds F_n to F_Q for any operator \mathcal{A} .

In order to illustrate this fact concretely, let us consider a quantum state defined as $\rho(p) = (1 - p) |\psi\rangle\langle\psi| + p\mathbb{1}/2^N$, where $|\psi\rangle$ is a pure state and $\mathbb{1}/2^N$ is the fully mixed state. The state $\rho(p)$ is mixed with global depolarizing noise of strength p . The distinct eigenvalues of $\rho(p)$ are $\lambda_1 = (1 - p) + p/2^N$ and $\lambda_2 = p/2^N$. We notice that for this specific state, all non-zero terms $(1 - \lambda_i - \lambda_j)$ in Eq. (4.6) are equivalent to $p - 2p/2^N$. With this remark, we can simplify the finite distance for $\rho(p)$ as

$$\xi_n = 2 \sum_{i,j:\lambda_i+\lambda_j>0} \frac{(\lambda_i - \lambda_j)^2}{\lambda_i + \lambda_j} (p - 2p/2^N)^{n+1} |\langle i|\mathcal{A}|j\rangle|^2 = F_Q (1 - 1/2^{N-1})^{n+1} p^{n+1}. \quad (4.8)$$

One can see, from the above expression, the exponential convergence of the lower bound F_n to the QFI with respect to the order n as the distance decays like $\xi_n \propto (1 - 1/2^{N-1})^{n+1} p^{n+1}$. In particular, for $\rho(p)$, the QFI is more directly given by [67] (replacing the eigenvalues in Eq. (4.1))

$$F_Q = 4 (\langle\psi|\mathcal{A}^2|\psi\rangle - \langle\psi|\mathcal{A}|\psi\rangle^2) \frac{(1 - p)^2}{1 - p + p/2^{N-1}} \quad (4.9)$$

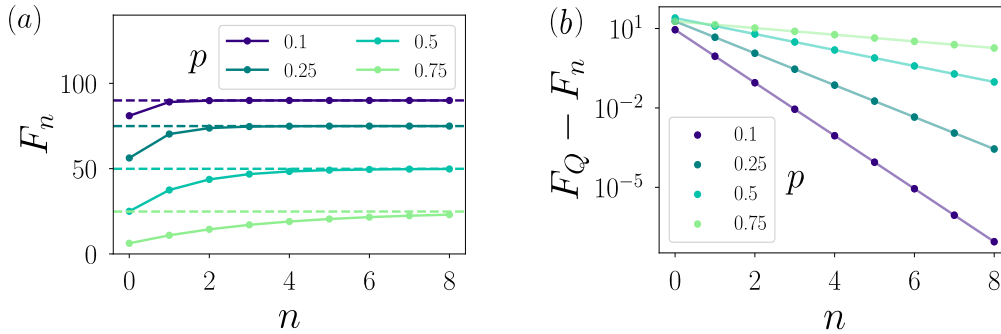


Figure 4.1: *Convergence of the lower bounds* — Panel (a) shows the QFI (dashed line) and its lower bounds F_n as a function of the order n (circle connected by solid lines) for a 10 qubit GHZ state that is mixed with different levels of depolarizing noise p (see legend). Panel (b) shows for the same state, the exponential convergence $\xi_n \propto (1 - 2^{-9})^n p^n$ for different values of p (see legend). Larger values of p show a slower convergence compared to smaller one.

Let us now illustrate this convergence for N -qubit noisy GHZ states that can be defined as $\rho(p) = (1 - p) |\psi_{\text{GHZ}}^{(N)}\rangle\langle\psi_{\text{GHZ}}^{(N)}| + p\mathbb{1}/2^N$ and the operator $\mathcal{A} = \sum_{l=1}^N \sigma_z^{(l)}$ with $|\psi_{\text{GHZ}}^{(N)}\rangle = (|0\rangle^{\otimes N} + |1\rangle^{\otimes N})/\sqrt{2}$. Fig. 4.1(a) shows the convergence of the lower bounds to the true value of the QFI for different values of noise strength p induced in the pure GHZ state. Secondly, Fig. 4.1(b) highlights the finite distance $F_Q - F_n$ for different values of p . From these plots we observe that when the state is more noisy (larger values of p), the convergence of the QFI is slower, so higher orders of the lower bounds need to be incorporated in order to estimate the value of the QFI.

Meanwhile it is also worth noting from Fig. 4.1(a-b) that highly noisy states have smaller values of QFI and turn out to be not so useful for metrological tasks.

We have shown earlier an alternate expression for the QFI in Eq. (4.4). It involves polynomials of the eigenvalues of the density matrix ρ that form a converging series of lower bounds to the QFI. One could naively think that the introduction of this alternate expression has no additional benefits as once again we need QST to estimate the eigenvalues to measure QFI. In Appendix. A, we bridge this gap and show that Eq. (4.4) can indeed be expressed firstly in terms of polynomials of the density matrix and secondly also in terms of a multi-copy operator. Both these forms then allow us to estimate these bounds using the classical shadow formalism. In particular, we can explicitly express the three lowest bounds F_0, F_1, F_2 as

$$\begin{aligned} F_0 &= 4\text{Tr}(\rho^2 \mathcal{A}^2 - \rho \mathcal{A} \rho \mathcal{A}) \\ F_1 &= 2F_0 - 4\text{Tr}(\rho^3 \mathcal{A}^2 - \rho^2 \mathcal{A} \rho \mathcal{A}) \\ F_2 &= 3F_1 - 3F_0 + 4\text{Tr}(\rho^4 \mathcal{A}^2 - \rho^2 \mathcal{A} \rho^2 \mathcal{A}). \end{aligned} \quad (4.10)$$

Let us now look at the experimental protocol that needs to be implemented on the quantum device to measure each of these lower bounds.

4.2 Protocol to measure QFI and its error analysis in qubit platforms

In the following section, we will detail the randomized measurement protocol that shall enable us to access the lower bounds F_n . In particular, we shall provide in the subsequent sections analytical estimations on the required number of measurements for a given tolerance of statistical error to estimate the lower bounds using randomized measurements.

For concreteness, the experimental protocol is described as follows. We prepare a N -qubit state of interest on the quantum device. We apply a set of N_U local random unitaries $U^{(r)} = U_1^{(r)} \otimes \dots \otimes U_N^{(r)}$ with $r = 1, \dots, N_U$ that are sampled from the circular unitary ensemble or at least a 2-design as described earlier in Sec. 2.4.2. These set of operations are followed by computational basis measurements that are repeated N_M times and for each applied unitary giving the bit-string outcomes $\mathbf{s}^{(r,m)} = (s_1^{(r,m)}, \dots, s_N^{(r,m)})$ with $m = 1, \dots, N_M$. The total number of repetitions performed in the experiment is given by $M = N_U N_M$. The data set generated by this protocol enables us to define for a single applied unitary $U^{(r)}$ a classical shadow as previously illustrated in Chapter. 2 (Eq. (2.40)) as follows [64]

$$\hat{\rho}^{(r)} = 2^N \sum_{\mathbf{s}, \mathbf{s}'} (-2)^{-D[\mathbf{s}, \mathbf{s}']} \hat{P}(\mathbf{s}' | U^{(r)}) U^{(r)\dagger} |\mathbf{s}\rangle \langle \mathbf{s}| U^{(r)} \quad (4.11)$$

where $\hat{P}(\mathbf{s}' | U^{(r)}) = \frac{1}{N_M} \sum_{m=1}^{N_M} \delta_{\mathbf{s}', \mathbf{s}^{(r,m)}}$ are the Born probabilities and D is the Hamming distance. In particular, when the random unitary $U^{(r)}$ is followed by a single projective measurement ($N_M = 1$), we can express the classical shadow in its more

standard form as given in [64] (Eq. (2.44) in Chapter. 2)

$$\hat{\rho}^{(r)} = \bigotimes_{i=1}^N \left[3 U_i^{(r)\dagger} \left| s_i^{(r)} \right\rangle \left\langle s_i^{(r)} \right| U_i^{(r)} - \mathbb{1}_2 \right]. \quad (4.12)$$

The classical shadows when averaged over the applied unitaries and performed measurements converge to the underlying density matrix prepared in the experiment $\mathbb{E}[\hat{\rho}^{(r)}] = \rho$. In order to build unbiased estimators for our lower bounds using these classical shadows, we use the U-statistics estimator [59] (Eq. (2.45) in Chapter. 2). We first note as shown in Appendix. A (Eq. (A.8)) that the lower bound F_n is described in terms of polynomial functions of order $q \in [2, n + 2]$ of the density matrix. Then the approach of U-statistics [59] computes the average over all possible combinations of q different classical shadows to estimate each polynomial order $q \in [2, n + 2]$. We can translate this idea explicitly to provide unbiased estimators of the three first bounds F_0, F_1, F_2 :

$$\begin{aligned} \hat{F}_0 &= 4 \beta_0^{-1} \sum_{r_1 \neq r_2} \text{Tr} \left(\hat{\rho}^{(r_1)} [\hat{\rho}^{(r_2)}, \mathcal{A}] \mathcal{A} \right), \\ \hat{F}_1 &= 2 \hat{F}_0 - 4 \beta_1^{-1} \sum_{r_1 \neq \dots \neq r_3} \text{Tr} \left(\hat{\rho}^{(r_1)} \hat{\rho}^{(r_2)} [\hat{\rho}^{(r_3)}, \mathcal{A}] \mathcal{A} \right), \\ \hat{F}_2 &= 3 \hat{F}_1 - 3 \hat{F}_0 + 4 \beta_2^{-1} \sum_{r_1 \neq \dots \neq r_4} \text{Tr} \left(\hat{\rho}^{(r_1)} \hat{\rho}^{(r_2)} [\hat{\rho}^{(r_3)} \hat{\rho}^{(r_4)}, \mathcal{A}] \mathcal{A} \right) \end{aligned} \quad (4.13)$$

with $\beta_j = (j + 2)! \binom{N_U}{j+2}$ and where $[\cdot, \cdot]$ denotes the commutator. Note that we can make a suitable choice of the operator \mathcal{A} during the post-processing phase. For example, in order to detect higher level of multipartite entanglement in the experiment using Eq. (4.2), the choice of the collective spin operator $\mathcal{A} = \sum_{l=1}^N \sigma_\mu^{(l)}$ can be adjusted based on the directions μ in order to maximize the QFI. More importantly, all the lower bounds can be accessed using the same RM data-set. The U-statistics estimator relates the experimental data directly to our lower bounds as given in Eq. (4.13). Additionally, we note that the computational cost to classically post-process the lower bound increases with the order n , as the number of summands β_j in the U-statistics expression increases rapidly with j . This means that estimating \hat{F}_2 is computationally more demanding than \hat{F}_1 compared to \hat{F}_0 . The solution to this practical problem shall be the main topic of discussion in Chapter. 5 where we shall introduce a new framework work to tackle this problem. Finally, the finite set of measurements M performed in the experiment induces statistical errors in the estimators of the lower bounds. These statistical errors play an important role in our ability to detect and validate experimentally the entanglement depth of an unknown quantum state with the help of the entanglement witnesses described in Eq. (4.2). In the subsequent sections, we shall analyse analytically the statistical errors and provide rigorous performance guarantees of our protocol to estimate the lower bounds of arbitrary order n .

4.2.1 Error analysis of a generic multi-copy functional

In this section, we consider that randomized measurements are performed using N_U unitaries followed by a single projective measurement $N_M = 1$. This results in a

total measurement budget of $M = N_U$ which is the optimal measurement budget split for the classical shadow formalism [31]. As we have stressed, the QFI can be estimated by measuring the converging polynomial series of bound until any order n . Not restricting only to the estimation of the QFI, we would like to develop here a general theory to study the performance guarantee by providing analytical estimation on the error bound for a general multi-copy functional f_q defined for a N -qubit state. This analysis will enable us to estimate the sample complexity, that is, the required number of measurements needed to be performed in an experiment to estimate a function to be ϵ close with a confidence level of δ . Moreover, these results will automatically translate to provide the same for our lower bounds. We recall that the general functional expressed in terms of the multi-copy operator $O^{(q)}$ acting on q copies of the density matrix ρ is given by

$$f_q = \text{Tr} \left(O^{(q)} \rho^{\otimes q} \right). \quad (4.14)$$

Its estimator constructed using M classical shadows is given by U-statistics as described in Chapter. 2 (Eq. (2.45)) and writes as

$$\hat{f}_q = \frac{1}{q!} \binom{M}{q}^{-1} \sum_{r_1 \neq \dots \neq r_q} \text{Tr} \left(O^{(q)} \bigotimes_{i=1}^q \hat{\rho}^{(r_i)} \right). \quad (4.15)$$

Using the Chebyshev's inequality, we can calculate the required sample complexity M to estimate f_q such that $|\hat{f}_q - f_q| < \epsilon$ with a confidence level of δ . It writes as given in Chapter. 2 (Eq. (2.49))

$$\Pr \left[|\hat{f}_q - f_q| \geq \epsilon \right] \leq \frac{\text{Var}[\hat{f}_q]}{\epsilon^2}. \quad (4.16)$$

As we see from the above equation, we need to compute the variance of the unbiased estimator \hat{f}_q . In the rest of section, we develop a framework to calculate and bound the variance of \hat{f}_q which governs the convergence of the estimator to its true value as $\mathbb{E}[\hat{f}_q] = f_q$. We can define the variance of the estimator of \hat{f}_q as

$$\text{Var} \left[\hat{f}_q \right] = \mathbb{E} \left[\hat{f}_q^2 \right] - \mathbb{E} \left[\hat{f}_q \right]^2 = \mathbb{E} \left[\hat{f}_q^2 \right] - f_q^2 \quad (4.17)$$

Expanding the estimator $\mathbb{E}[\hat{f}_q^2]$ using Eq. (4.15), we get

$$\text{Var} \left[\hat{f}_q^2 \right] = \frac{1}{q!^2} \binom{M}{q}^{-2} \sum_{r_1 \neq \dots \neq r_q} \sum_{r'_1 \neq \dots \neq r'_q} \mathbb{E} \left[\text{Tr} \left(O^{(q)} \bigotimes_{i=1}^q \hat{\rho}^{(r_i)} \right) \text{Tr} \left(O^{(q)} \bigotimes_{i=1}^q \hat{\rho}^{(r'_i)} \right) \right] - f_q^2 \quad (4.18)$$

Recalling that for any given random variables \mathbf{X} and \mathbf{Y} , the covariance is given by $\text{Cov}[\mathbf{X}, \mathbf{Y}] = \mathbb{E}[\mathbf{X}\mathbf{Y}] - \mathbb{E}[\mathbf{X}]\mathbb{E}[\mathbf{Y}]$, we can simplify the above expression as

$$\text{Var} \left[\hat{f}_q^2 \right] = \frac{1}{q!^2} \binom{M}{q}^{-2} \sum_{r_1 \neq \dots \neq r_q} \sum_{r'_1 \neq \dots \neq r'_q} \text{Cov} \left[\text{Tr} \left(O^{(q)} \bigotimes_{i=1}^q \hat{\rho}^{(r_i)} \right), \text{Tr} \left(O^{(q)} \bigotimes_{i=1}^q \hat{\rho}^{(r'_i)} \right) \right]. \quad (4.19)$$

The current task requires us to compute the sum in the above expression over two independent sets of q -uplets of indices $\{r_1, r_2, \dots, r_q\}$ and $\{r'_1, r'_2, \dots, r'_q\}$. This task can be broken down as follows:

- We start by summing over the number ℓ that denotes the indices that are in common between the two q -uplets.
- We perform the sum over these common indices denoting them into a single set of indices β_i that are present in the two q -uplets.
- We then sum over the remaining indices that are not common to each of the q -uplets. We denote these sets of indices as γ_i and γ'_i .
- To simplify the computation, we consider the above indices to be ordered, which allows us to sum over the all possible orderings of indices by introducing the permutation operators W_π, W_τ defined as $W_\pi = \sum_{i_1, \dots, i_q} |i_{\pi(1)}, \dots, i_{\pi(q)}\rangle \langle i_1, \dots, i_q|$ and equivalently for W_τ (referred in Chapter. 2, Eq. (2.13)).

We can summarize the listed steps by the following expression:

$$\text{Var}[\hat{f}_q] = \frac{1}{q!^2} \binom{M}{q}^{-2} \sum_{\ell=0}^q \sum_{\substack{\beta_1 < \dots < \beta_\ell \\ \neq \gamma_{\ell+1} < \dots < \gamma_q \\ \neq \gamma'_{\ell+1} < \dots < \gamma'_q}} \sum_{\pi, \tau} \text{Cov}[C_\pi, C_\tau] \quad (4.20)$$

with

$$C_\pi = \text{Tr}(O^{(q)} W_\pi \bigotimes_{i=1}^{\ell} \hat{\rho}^{(\beta_i)} \bigotimes_{j=\ell+1}^q \hat{\rho}^{(\gamma_j)} W_\pi^\dagger) = \text{Tr}(W_\pi^\dagger O^{(q)} W_\pi \bigotimes_{i=1}^{\ell} \hat{\rho}^{(\beta_i)} \bigotimes_{j=\ell+1}^q \hat{\rho}^{(\gamma_j)}) \quad (4.21)$$

and

$$C_\tau = \text{Tr}(O^{(q)} W_\tau \bigotimes_{i=1}^{\ell} \hat{\rho}^{(\beta_i)} \bigotimes_{j=\ell+1}^q \hat{\rho}^{(\gamma'_j)} W_\tau^\dagger) = \text{Tr}(W_\tau^\dagger O^{(q)} W_\tau \bigotimes_{i=1}^{\ell} \hat{\rho}^{(\beta_i)} \bigotimes_{j=\ell+1}^q \hat{\rho}^{(\gamma'_j)}). \quad (4.22)$$

We additionally note that the indices satisfy $\beta_i \neq \gamma_j, \beta_i \neq \gamma'_j, \gamma_i \neq \gamma'_j$ for all i, j . We see, by comparing the expression of C_π and C_τ that the indices γ_j or γ'_j appear only once in the expectation value composing the covariances. This leads to all $\hat{\rho}^{(\gamma_j)}$ and $\hat{\rho}^{(\gamma'_j)}$ terms to average to ρ as $\mathbb{E}[\hat{\rho}] = \rho$. All the different combinations of β indices give the same value, so we can simply write $\beta_i = i \forall i$. Counting the number of terms in the sum of the two q -uplets for different set of indices $\beta_1 < \dots < \beta_\ell$ ($\binom{M}{\ell}$ possible choices), $\gamma_{\ell+1} < \dots < \gamma_q$ ($\binom{M-\ell}{q-\ell}$ possible choices) and $\gamma'_{\ell+1} < \dots < \gamma'_q$ ($\binom{M-q}{q-\ell}$ possible choices), we get:

$$\text{Var}[\hat{f}_q] = \frac{\binom{M}{q}^{-2}}{q!^2} \sum_{\ell=0}^q \binom{M}{\ell} \binom{M-\ell}{q-\ell} \binom{M-q}{q-\ell} \text{Var} \left[\sum_{\pi} \text{Tr} (W_\pi^\dagger O^{(q)} W_\pi [\bigotimes_{i=1}^{\ell} \hat{\rho}^{(i)} \otimes \rho^{\otimes (q-\ell)}]) \right] \quad (4.23)$$

where we have simplified the expression of Eq. (4.20) using the fact that for dependent random variables \mathbf{X}_i we have

$$\text{Var} \left[\sum_i \mathbf{X}_i \right] = \sum_i \text{Var}[\mathbf{X}_i] + 2 \sum_{i < j} \text{Cov}[\mathbf{X}_i, \mathbf{X}_j] = \sum_{i,j} \text{Cov}[\mathbf{X}_i, \mathbf{X}_j]. \quad (4.24)$$

We can rewrite the trace term in the above expression for later convenience as a function of a multi-copy operator $O_\ell^{(q)}$ acting on ℓ copies of shadows $\hat{\rho}^{(\ell)}$

$$\text{Var}[\hat{f}_q] = \binom{M}{q}^{-2} \sum_{\ell=0}^q \binom{M}{\ell} \binom{M-\ell}{q-\ell} \binom{M-q}{q-\ell} \text{Var} \left[\text{Tr} \left(O_\ell^{(q)} \bigotimes_{i=1}^{\ell} \hat{\rho}^{(i)} \right) \right] \quad (4.25)$$

with ¹

$$O_\ell^{(q)} = \frac{1}{q!} \sum_{\pi} \text{Tr}_{\{\ell+1 \dots q\}} \left(W_{\pi}^{\dagger} O^{(q)} W_{\pi} [\mathbb{1}^{\otimes \ell} \otimes \rho^{\otimes (q-\ell)}] \right) = \text{Tr}_{\{\ell+1 \dots q\}} \left(\bar{O}^{(q)} [\mathbb{1}^{\otimes \ell} \otimes \rho^{\otimes (q-\ell)}] \right), \quad (4.26)$$

where we defined the “fully-scrambled” operator $\bar{O}^{(q)} = \frac{1}{q!} \sum_{\pi} W_{\pi}^{\dagger} O^{(q)} W_{\pi}$ for later convenience. Hence we have at our disposal an analytical expression of the variance for a generic estimator \hat{f}_q that can be evaluated knowing the operator $O^{(q)}$ and the state of interest ρ . Let us now show how we can bound such a general expression of the variance.

Variance bound

We note firstly that for $\ell = 0$, the above variance term is zero (so that the sum can be taken to start at $\ell = 1$). In order to bound the variance terms comprising of ℓ distinct copies of shadows, we start by reminding a key result proved in [64] (referred in Chapter. 2 in Fact. 1). It bounds the single-shot variance of a linear function $\text{Tr}(\tilde{O}_1 \hat{\rho}^{(1)})$ associated with the shadow $\hat{\rho}^{(1)}$ that acts on a N -qubit state:

$$\text{Var} \left[\text{Tr}(\tilde{O}_1 \hat{\rho}^{(1)}) \right] \leq 2^N \text{Tr}(\tilde{O}_1^2). \quad (4.27)$$

We can generalize this identity for a ℓ -order function with the operator \tilde{O}_ℓ acting on ℓ copies of shadows $\hat{\rho}^{(1)} \neq \dots \neq \hat{\rho}^{(\ell)}$ by considering the tensor product $\bigotimes_{i=1}^{\ell} \hat{\rho}^{(i)}$ as a single shadow in an augmented Hilbert space of dimension $2^{\ell N}$. This leads to the following general bound:

$$\text{Var} \left[\text{Tr} \left(\tilde{O}_\ell (\hat{\rho}^{(1)} \otimes \dots \otimes \hat{\rho}^{(\ell)}) \right) \right] \leq 2^{\ell N} \text{Tr}(\tilde{O}_\ell^2). \quad (4.28)$$

With this general condition and developing the binomial terms we can bound $\text{Var}[\hat{f}_q]$ from Eq. (4.25) as

$$\begin{aligned} \text{Var}[\hat{f}_q] &\leq \sum_{\ell=1}^q \frac{q!^2 (M-q)!^2 2^{\ell N}}{M! \ell! (q-\ell)!^2 (M-2q+\ell)!} \text{Tr}([O_\ell^{(q)}]^2) \\ &\leq \sum_{\ell=1}^q \frac{q!^2 2^{\ell N}}{\ell! (q-\ell)!^2 (M-\ell+1)^\ell} \text{Tr}([O_\ell^{(q)}]^2) \end{aligned} \quad (4.29)$$

where, we have isolated the dependency on M as finally we want to obtain a bound on M . The bound on $\text{Var}[\hat{f}_q]$ comprises of a sum of q different orders of contributions

¹One may note that the calculation of the operator $O_\ell^{(q)}$ can be simplified to a calculation of $\binom{q}{\ell}$ distinct rearrangements with each of the terms occurring $\frac{q!}{\ell!}$ times, and the partial trace being taken over the corresponding positions of ρ .

ℓ to the variance. Recalling the Chebyshev's inequality mentioned in Eq. (4.16), we write

$$\Pr \left[|\hat{f}_q - f_q| \geq \epsilon \right] \leq \frac{\text{Var}[\hat{f}_q]}{\epsilon^2} \leq \frac{1}{\epsilon^2} \sum_{\ell=1}^q \frac{q!^2 2^{\ell N} \text{Tr}([O_\ell^{(q)}]^2)}{\ell!(q-\ell)!^2 (M-\ell+1)^\ell}. \quad (4.30)$$

To ensure that $\Pr[|\hat{f}_q - f_q| \geq \epsilon] \leq \delta$, for a given confidence level $\delta \in [0, 1]$, we consider for simplicity that each term in the above sum is less than δ/q . This allows us to summarize our results with the following proposition

Proposition 2. *Consider a N -qubit state ρ and the associated multi-copy functional $f_q = \text{Tr}(O^{(q)} \rho^{\otimes q})$ defined in terms of the multi-copy operator $O^{(q)}$ that we want to estimate. For $\epsilon, \delta > 0$, it suffices*

$$M \geq \max_{1 \leq \ell \leq q} \left\{ \left(\frac{q q!^2}{\ell!(q-\ell)!^2} \frac{\text{Tr}([O_\ell^{(q)}]^2)}{\epsilon^2 \delta} \right)^{\frac{1}{\ell}} 2^N + \ell - 1 \right\} \quad (4.31)$$

number of measurements to ensure that the estimator \hat{f}_q defined in Eq. (4.15) is estimated such that $|\hat{f}_q - f_q| \leq \epsilon$ with a probability of at least $1 - \delta$.

The above expression provides the required measurement budget M to evaluate the estimator of an arbitrary order polynomial function with any defined accuracy ϵ and confidence level of $1 - \delta$. In particular, for each of the q possible values of ℓ the number of measurements is proportional to $\epsilon^{-2/\ell}$. We expect this to dictate different error decay regimes. In particular, this behavior have been shown through numerical simulations of the RM protocol for non-linear functions such as $\text{Tr}(\rho^2)$ and $\text{Tr}([\rho^{TA}]^3)$ in [34]. In the limit of $\epsilon \rightarrow 0$ (and for a fixed δ), the max in the above equation corresponds to $\ell = 1$ (linear contribution to the variance), with a required number of measurements $M \propto \epsilon^{-2}$. This proposition shall come in use in the subsequent section, where we will detail the sample complexity of our lower bounds.

4.2.2 Sample complexity for lower bounds F_n

Our previous variance computations for a generic function f_q allows us now to translate these findings to obtain the sample complexity of our lower bounds F_n . We start by recalling that the lower bound F_n contains polynomials of order up to $n+2$ (refer to Eq. (A.8)). The Cauchy-Schwarz inequality $\text{Cov}[\mathbf{X}_1, \mathbf{X}_2] \leq \sqrt{\text{Var}[\mathbf{X}_1]} \sqrt{\text{Var}[\mathbf{X}_2]}$ allows us to bound sum of dependent random variables \mathbf{X}_i as follows

$$\text{Var} \left[\sum_i \mathbf{X}_i \right] = \sum_i \text{Var}[\mathbf{X}_i] + 2 \sum_{i < j} \text{Cov}[\mathbf{X}_i, \mathbf{X}_j] \leq \left(\sum_i \sqrt{\text{Var}[\mathbf{X}_i]} \right)^2. \quad (4.32)$$

Using the above identity and the multi-copy expression of the lower bounds given in Eq.(A.11) of Appendix. A, we can write

$$\begin{aligned}\text{Var}[\hat{F}_n] &= \text{Var}\left[2\sum_{q=0}^n \binom{n+1}{q+1} (-1)^q \hat{f}_{q+2}\right] \leq 4\left[\sum_{q=0}^n \binom{n+1}{q+1} \sqrt{\text{Var}[\hat{f}_{q+2}]}\right]^2 \\ &\leq 4\left[(n+1)\max_{0\leq q\leq n} \binom{n+1}{q+1} \sqrt{\text{Var}[\hat{f}_{q+2}]}\right]^2 \\ &\leq 4(n+1)^2 \max_{0\leq q\leq n} \binom{n+1}{q+1}^2 \text{Var}[\hat{f}_{q+2}].\end{aligned}\quad (4.33)$$

Using now Eq. (4.29), we obtain

$$\text{Var}[\hat{F}_n] \leq 4(n+1)^2 \max_{0\leq q\leq n} \binom{n+1}{q+1}^2 \sum_{\ell=1}^{q+2} \frac{(q+2)!^2 2^{\ell N}}{\ell!(q+2-\ell)!^2 (M-\ell+1)^\ell} \text{Tr}([O_\ell^{(q+2)}]^2),\quad (4.34)$$

where $O_\ell^{(q+2)}$ is the ℓ -copy operator defined in Eq. (4.26), from the $(q+2)$ -copy operator $O^{(q+2)}$ defined in Eq. (A.12) of Appendix. A.

Using the Chebyshev's inequality, we can ensure that $\Pr[|\hat{F}_n - F_n| \geq \epsilon] \leq \delta$, for a given confidence level $\delta \in [0, 1]$, by taking for all values of q , each term in the above sum is less than $\delta/(q+2)$. This allows us to summarize the sample complexity bound for the lower bounds F_n with the following proposition

Proposition 3. *Consider a N -qubit state ρ and an Hermitian operator \mathcal{A} for which we want to estimate F_n . For $\epsilon, \delta > 0$, it suffices*

$$M \geq \max_{1\leq \ell\leq q+2\leq n+2} \left\{ \left(4(n+1)^2 \binom{n+1}{q+1}^2 \frac{(q+2)(q+2)!^2 \text{Tr}([O_\ell^{(q+2)}]^2)}{\ell!(q+2-\ell)!^2 \epsilon^2 \delta} \right)^{1/\ell} 2^N + \ell - 1 \right\}\quad (4.35)$$

number of measurements to ensure that the estimator \hat{F}_n is estimated such that $|\hat{F}_n - F_n| \leq \epsilon$ with a probability of at least $1 - \delta$.

The measurement budget M can now be evaluated by estimating $\text{Tr}([O_\ell^{(q+2)}]^2)$ (either analytically or numerically) which is expressed as a function of the state ρ and the operator \mathcal{A} . Analogous to the expression of Eq. (4.31), we could potentially expect for the above confidence interval bound, $n+2$ regimes where the measurements scale as $M \propto 2^N/\epsilon^{2/\ell}$ with $\ell = 1, \dots, n+2$.

For interested readers, we have explicitly detailed in our work [100], using the above proposition, the calculation of the sample complexity bounds for F_0 and F_1 respectively [100, Eq. G8 for F_0 and Eq. G12 for F_1]. To summarize our findings, the required number of measurements M scale as $\alpha 2^N$ with α being a factor that can be computed based on our framework provided here for any given state ρ and operator \mathcal{A} . In particular, when we consider GHZ states $\rho = |\psi_{\text{GHZ}}^N\rangle\langle\psi_{\text{GHZ}}^N|$ with $\mathcal{A} = \frac{1}{2} \sum_{l=1}^N \sigma_z^{(l)}$, in the limit when $\epsilon \rightarrow 0$ (when the dominant term in the variance is given by the linear one: $\text{Tr}([O_1^{n+2}]^2)$ with $n = 0, 1$) we find the sample complexities

as $M \geq 16 \frac{N^4}{\epsilon^2 \delta} 2^N$ and $M \geq 256 \frac{N^4}{\epsilon^2 \delta} 2^N$ for F_0 and F_1 respectively. These results present an interesting trade-off between detection of multipartite entanglement vs the experimental measurement cost. As n increases the lower bounds become tighter and are able to detect more multipartite entanglement content via the condition Eq. (4.2). On the other hand, higher bounds require more investment of measurements to overcome statistical errors. As we shall show in the next section, we can complement these analytical findings by numerical simulations of the randomized measurement protocol to estimate the lower bounds.

4.2.3 Numerical illustrations

In this section, we shall investigate the error scaling for our lower bounds F_0 and F_1 by numerically simulating the randomized measurement protocol. In particular, we consider the scenario where we perform a single computational basis measurement ($N_M = 1$) after applying the random unitary operation. The total measurement budget is simply given by $M = N_U$. We are interested in the average statistical error on the estimated bound \hat{F}_n given by $\mathcal{E} = |\hat{F}_n - F_n|/F_n$ with the average computed over 50 simulated experimental runs. We consider in our example N -qubit noisy GHZ states defined as $\rho(p) = (1 - p) |\psi_{\text{GHZ}}^N\rangle\langle\psi_{\text{GHZ}}^N| + p\mathbb{1}/2^N$ where p determines the strength of the global depolarization noise added to the ideal state and choose the Hermitian operator $\mathcal{A} = \frac{1}{2} \sum_{l=1}^N \sigma_z^{(l)}$.

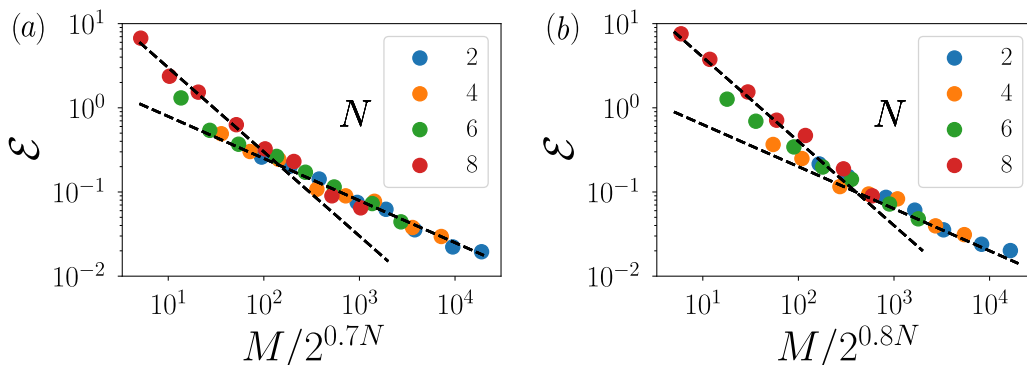


Figure 4.2: *Error scalings* — Panel (a) and (b) show the statistical error scaling for F_0 and F_1 respectively for a GHZ state mixed with depolarization strength of $p = 0.25$ for different values of N . The black dashed line are guide to the eye to highlight the different error decays $\propto 1/M$ and $1/\sqrt{M}$.

In fig. 4.2(a-b), we show the scaling of the average statistical error as a function of the re-scaled number of measurements $M/2^{aN}$ where we adjusted the coefficient a such that all the simulated data fall on a single curve. We see that the required number of measurements for $\mathcal{E} \sim 0.1$ scale as $2^{0.7N}$ for F_0 and $2^{0.8N}$ for F_1 . Interestingly, we also observe two error decay regimes, one $\propto 1/\sqrt{M}$ that represents the standard Monte-Carlo error decay and additionally a more rapid error decay $\propto 1/M$ that is prominent in the regime of low number of measurements that have a higher statistical error. These features become apparent from the expression of Proposition. 3 by simply inverting the relation $M \propto 1/\epsilon^{\frac{2}{\ell}}$ as we see that $\epsilon \propto M^{-\ell/2}$ with $\ell = 1, \dots, n + 2$.

Additionally, we complement these above numerical investigations by extracting the maximum value of the number of measurements M for different system sizes

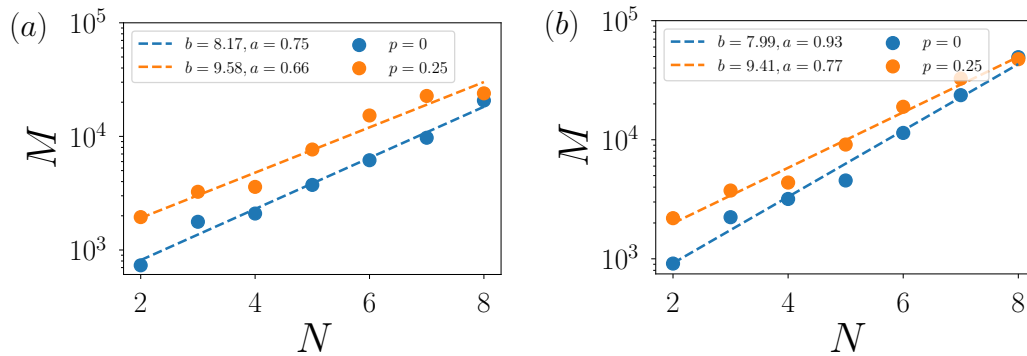


Figure 4.3: *Scaling of the required number of measurements* — Panel (a) and (b) provide the required number of measurements M to estimate F_0 and F_1 respectively for a fixed statistical error of $\mathcal{E} = 0.1$ for noisy GHZ states. We consider different values of p that adds depolarization noise to the ideal GHZ state. The circles represent the simulated data while the dashed lines provide the exponential fit 2^{b+aN} to understand the scaling of the measurements as a function of N .

N such that for each of them we obtain an average error $\mathcal{E} < 0.1$ using a linear interpolation function. This allows us to get fitted scaling exponents for M vs N . We plot these findings in Fig. 4.3(a-b), where the scaling exponents of the required number of measurements as a function of the system-size N agree with those found in the previous error scaling of Fig. 4.2. As shown by our analytical calculations in the previous section, we equally remark here that for a fixed level of statistical error \mathcal{E} , F_0 requires less measurements when compared to F_1 (as shown by the respective scaling exponents) at the cost of F_0 being less tight compared to F_1 in terms of measuring the QFI or detecting multipartite entanglement.

4.3 Experimental measurement of the QFI on a quantum device

In this section, we shall present a recently finished work [129] in which we provide an experimental measurement of QFI upto 13 qubits for quantum states prepared in a 33-qubit IBM superconducting device called ‘ibm_prague’ that is equipped with an ‘Egret r1’ quantum processor. Importantly, we use the converging polynomial series of lower bounds $F_0 \leq F_1 \leq \dots \leq F_n$ to estimate the QFI as introduced in Eq. (4.10) of this chapter by experimentally employing the randomized measurement protocol. Additionally, we combined a set of advanced methods of the RM toolbox to mitigate estimations of the converging lower bounds that are *robust* against errors caused uniquely during the RM protocol. Among these set of techniques, one of the main technical advancements that goes by the name of the *batch shadow formalism* that was developed during the course of this thesis [101], helped us post-process effectively the lower bounds from the generated experimental data-set. We leave the detailed discussion and development of the batch shadow formalism for the next chapter.

In the following subsections, we shall first present briefly the idea of the *robust shadows* proposed in Ref. [15, 76] that we implement in our experiments and then shall discuss the experimental results of the QFI for two prototypical examples of states realized on the noisy IBM quantum processor: (i) the GHZ state and (ii) the ground state of the transverse field Ising model (TFIM) prepared by the quantum approximate optimization algorithm (QAOA) at the critical point.

4.3.1 Robust estimation of quantum properties in a nutshell

As we continue to work in the NISQ era [97], the present quantum devices are prone to errors. This is due to a lack of total control over the operations performed on the device. This implies that errors are *also* induced during the RM protocol as the applied unitary and readout measurements could suffer from errors. These errors propagate to the estimations of quantities of interest extracted from the RM dataset. Within the framework of the RM toolbox, several recent works address this pertinent issue [15, 76]. In particular, Ref. [15] provides an experimentally-friendly method to mitigate the errors affecting the RM protocol under some verifiable and reasonable assumptions of the noise. In the classical shadow formalism, robust estimations can be obtained in the presence of an unknown noise channel. This is achieved via a calibration step, which uses a state that can be prepared with high fidelity. Under the assumption of local, gate-independent, time-stationary and Markovian noise, the RM-data obtained from such calibration provides a model to build robust classical shadows from randomized measurements.

Our experiments are thus divided in two steps (i) the calibration of randomized measurements (ii) randomized measurements on the state of interest ρ . Step (i), as suggested in Ref. [15, 76], requires realizing an experimental state with high fidelity (minimal state preparation errors). We fix the calibration step to be $|\mathbf{0}\rangle = |0\rangle^{\otimes N}$ that can be prepared with significantly high fidelity in our experimental platform. The calibration step requires us to perform randomized measurements on the state $|\mathbf{0}\rangle$. The data-set consisting of the applied ‘noisy’ unitaries and ‘noisy’ readout measurements collected in step (i) allow us to estimate the necessary noise parameter as shown in our work [129, Appendix. B2]. Using the RM data generated in step (ii) and the estimated noise parameter from step (i) we can construct in the post-processing stage a ‘robust shadow’ as given in our work [129, Appendix. B1]. Taking the U-statistics of the robust shadows allows us to obtain robust properties of multi-copy operators and equally the bounds of the QFI. Interestingly, in our work, we also verify some of the noise assumptions such as locality of the noise based on the calibration data of step (i).

4.3.2 Experimental Results

We present and discuss in this section the experimental results on the two type of states prepared in our quantum processor: (i) the GHZ state and (ii) the ground state of the TFIM at the critical point. Moreover, in our work, we propose and implement a new modified version of the robust protocol. The main intuition is to divide the full experimental run into multiple ‘iterations’ that consist of executing step (i) followed by step (ii) respectively. Assuming that the temporal fluctuations of the noise within a given iteration is negligible, calibration step in each iteration captures the specific

noise profile within that time window of the experiment. Thus consecutive iterations allows to account for the temporal variations in gate and readout errors. In each iteration, we implement a total of $N_U = 200$ number of unitaries for which we record $N_M = 1000$ bit-string measurements for both step (i) and step (ii). The number of such iteration runs are dictated by the total measurement budget which we fix with $N_U = 300 \cdot 2^{0.5N}$ and record $N_M = 1000$ bit-string measurements for each of them. This allows us to provide robust estimations of the lower bounds with statistical errors $\mathcal{E} \sim 10\%$.

GHZ state

GHZ states are ideal candidates for quantum metrology as they saturate the value of the QFI ($F_Q = N^2$) and, thus, can be used to reach higher sensitivities in parameter estimation that scale as $\sim N^{-1}$ (known as *Heisenberg limit*). By implementing the randomized measurements protocol, we experimentally estimate the QFI through the series of lower bounds as a function of different system sizes N . We witness the presence of multipartite entanglement with the help of entanglement witness given in Eq. (4.2) [122, 67, 102].

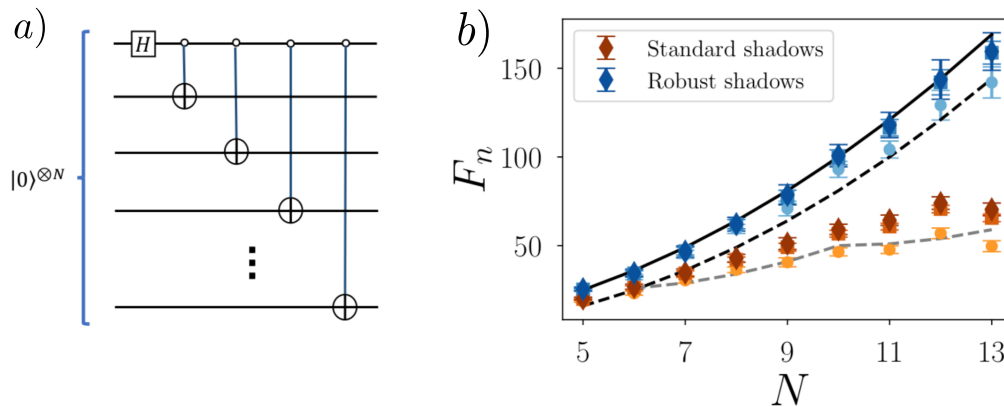


Figure 4.4: *Experimental results for the lower bounds of the QFI for the GHZ state* — Panel (a) shows the circuit implemented to prepare the GHZ state. In panel (b), we show F_2 , F_1 , F_0 (dark to light with diamond, square and circle respectively) as a function of the number of qubits N . The solid line is the exact value of the QFI $F_Q = N^2$ for pure GHZ states. The dashed black line corresponds to the entanglement witness $\Gamma(N, k = N - 1) = (N - 1)^2$ above which the state is considered to be genuinely multipartite entangled (GME). The dashed grey line corresponds to the entanglement witness $\Gamma(N, k = 5)$ above which we detect a state to be at least 6-partite entangled.

In Fig. 4.4, we show our experimental results. Fig. 4.4(a) shows the circuit used to prepare the GHZ state in our quantum processor. In Fig. 4.4(b) we show the experimental measurements F_2 , F_1 , and F_0 (dark to light) on the prepared GHZ state as a function of N . The black thick line provides the ideal scaling of the QFI ($F_Q = N^2$) for pure GHZ states. The black dashed line, instead, denotes the entanglement witness $\Gamma(N, k = N - 1)$ that scales as $(N - 1)^2$ above which we can consider our prepared states to be genuinely multipartite entangled (GME) with an entanglement depth of $k = N$. The experimental points correspond to the measured bounds for two different cases: Mitigated results through our calibration step in blue, raw data without performing the calibration step in orange. We observe that the mitigated data used to estimate F_n violates the necessary entanglement witness to

be GME for any size N . Thus all our prepared states have an entanglement depth of $k = N$. Hence, we demonstrate the presence of multipartite entanglement through the estimation of *converging* lower bounds to the QFI as proposed in this chapter. Importantly, we observe with the mitigation that the QFI for our experimental states grows $\sim N^2$. Additionally in our work, we also demonstrate the estimation of the lower bounds in the case when the calibration (step (i)) is done entirely at the beginning and is followed by the experiment (step (ii)). We observe clearly that our iterative experiment idea provides improved mitigated results compared to the latter method for larger system sizes.

Analysing the raw data (orange points in Fig. 4.4(b)) that are prone to errors during the RM protocol gives us lower estimations of the bounds. They do not violate the GME threshold and do not follow the expected scaling seen for the mitigated data points. This shows that the error mitigation in the measurement protocol is decisive and useful to estimate underlying properties of the prepared quantum states. In the case of the analysis of the raw data, we can assert from the witness bounds in Ref. [122, 67] that our prepared state contains an entanglement depth of $k = 6$ for $N \geq 6$.

Ground state of TFIM at the critical point

To complement the estimation of the QFI to more generic quantum many-body states, we study here the behaviour of the QFI at a critical point that also presents a rich structure of multipartite entanglement [115, 90, 44]. In particular, we consider the TFIM Hamiltonian

$$H = -J \sum_j Z_j Z_{j+1} - h \sum_j X_j, \quad (4.36)$$

where h is the transverse field and we set $J = 1$. It displays a quantum phase transition at $h = 1$ that manifests as a growth of multipartite entanglement that can be witnessed by the QFI [58]. We employ the classical simulations to optimize the parameters of the quantum adiabatic optimization algorithm [37] in order to realize the ground state at the critical point. Especially, as we shall see, we study the interplay between the depth d of the circuit realized and the approximation of the ground state.

The preparation of the state entails a series of unitary evolutions under the non-commuting terms in Eq. (4.36), i.e. $H_A = -J \sum_j Z_j Z_{j+1}$ and $H_B = -h \sum_j X_j$, that are applied to an initial quantum state $|\psi_0\rangle$. The final state after d layers can be written as:

$$|\psi(\boldsymbol{\delta}, \boldsymbol{\gamma})\rangle = \prod_{l=1}^d e^{-i\delta_l H_B} e^{-i\gamma_l H_A} |\psi_0\rangle \quad (4.37)$$

where the ‘angles’ δ_l and γ_l are variational parameters used in the l -th layer to minimise the final energy $\langle \psi(\boldsymbol{\delta}, \boldsymbol{\gamma}) | H | \psi(\boldsymbol{\delta}, \boldsymbol{\gamma}) \rangle$.

In Fig. 4.5(a) we show a sketch of the circuit used to prepare the desired state. In Fig. 4.5(b) we plot F_1 for different values of the depth d of the circuits as a function of the number of qubits N for the robust estimator. The solid black line represents the numerical exact value of the QFI. Our first observation consists in remarking that we generate and certify the presence of entanglement in all our prepared states

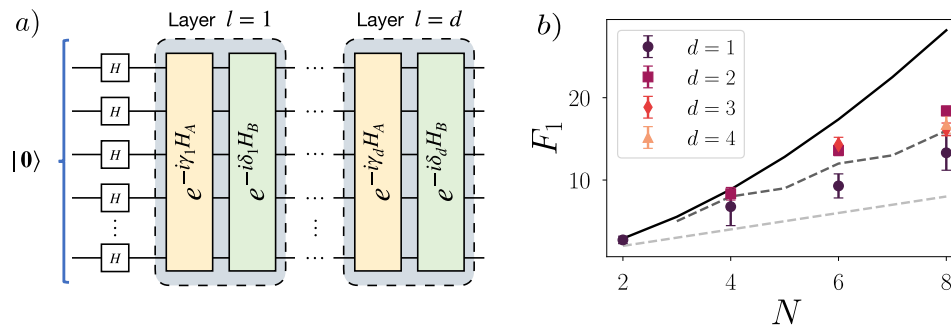


Figure 4.5: *Experimental results of the lower bound F_1 for the ground state of the TFIM at the critical point* — Panel (a) shows the sketch of the circuit used to variationally prepare the ground state. Panel (b) highlights the results for F_1 estimated with the robust estimator as a function of the number of qubits N , for different circuit depth d . The lines correspond to (solid black) exact QFI value, (dashed dark grey) detects entanglement depth $k = 3$ ($F_Q = \Gamma(N, 2)$), (dashed grey) detects entanglement ($F_Q = N$).

as $F_Q \geq F_1 \geq N$ within error bars for all values of depths d and system size N . The corresponding threshold is shown as a dashed grey line in the plot.

For all system-sizes, states prepared with a circuit depth of $d = 2$ have the highest measured value of F_1 compared to other circuit depths. As shown in Fig. 4.5(a), a further increase in the circuit depth d , incorporates more noisy gates that reduces the fidelity of the prepared state compared to its true target state. This results in a decrease of the QFI estimation compromised by the noisy state preparation that is captured very well in Fig. 4.5(b). We explicitly see for $d = 3, 4$, a compatible estimation of F_1 within error bars compared to the former case of $d = 2$ that shows a signature of noise and decoherence in the preparation of the state. In fact, in the ideal scenario, increasing the number of layers should guarantee better convergence to the target state resulting with a higher value of QFI.

Importantly, we establish the presence of multipartite entanglement via F_1 as we violate the entanglement witness $F_1 > \Gamma(N, k = 2)$. This confirms the presence of an entanglement depth of $k = 3$ for all prepared states of system-size $N > 2$, as the experimental points are above the witness depicted by the dashed dark grey line in Fig. 4.5(b). Thus our method allows to quantify the true metrological power in form of generating multipartite entanglement in variationally prepared noisy quantum states.

4.4 Conclusion

In this chapter, we presented an operative construction of monotonically increasing lower bounds that converge to the QFI. As the order of the bounds increase, they become more sensitive to detect the multipartite entanglement present in a quantum state. This helps in asserting and verifying quantum states capable of providing enhanced metrological sensitivities. These lower bounds are explicitly ex-

pressed as polynomials of the density matrix that enables us to measure them using the classical shadow formalism of the RM toolbox for any quantum state prepared on state-of-art quantum devices. To understand the behaviour of statistical errors caused by finite measurement statistics, we derive analytically the variance bounds for arbitrary multi-copy functionals of the density matrix that can be accessed using the RM data-set. This enabled us to extend our analytical calculations and make predictions on the required number of measurements to detect entanglement with a certain confidence interval using our lower bounds. Additionally in our work [100], we also extend our approach to measure the QFI in ensemble of collective spins that can be implemented using ultracold atoms or trapped ions platforms that are equally relevant for quantum metrological applications.

In the latter part of this chapter, we showed the first experimental measurement of the QFI on a quantum processor with up to 13 qubits based on the measurements of the converging series of polynomial lower bounds derived in this chapter. This work combined advanced methods of the randomized measurement that allowed us to mitigate drifting gate and readout errors. Additionally, the batch shadow framework, that shall be discussed at length in the following chapter, enabled us to effectively post-process unbiased estimators of the lower bounds using the experimental data. For our prepared GHZ states that employed the robust RM protocol, our estimators agree perfectly to the theoretically predicted value of $F_Q = N^2$ and validated that the prepared states were GME. Secondly, in the case of the variational preparation of the ground state of the critical TFIM, we observed an interesting trade-off by the estimation of the QFI: The theoretical approximation accuracy of the ground state increases with the circuit depth and is optimal at depth $d = N/2$, the best estimation of the theoretically predicted ground state QFI is obtained with a smaller circuit depth. This was attributed to the noise induced by an increase of the layers in the QAOA algorithm. More importantly, the advanced methods employed in this work are not only restricted to the measurement of the QFI but extend its use for estimating arbitrary non-linear multi-copy functionals of the density matrix.

Lastly, as we show, we can construct classical shadows from the RM data-set and measure order by order until the lower bound gets close enough to the desired value of the QFI. In practice, it becomes apparent quite easily that the classical post-processing of the experimental data to obtain the U-statistics estimator of higher order bounds soon becomes computationally unfeasible and impractical. This is due to the fact that the number of summands in the U-statistics estimator of the lower bounds increases rapidly with the order n . Moreover, we encounter this technical difficulty equally in the case when we want to estimate the operator entanglement using classical shadows. Motivated by this problem, in the following chapter, we shall present an effective solution for it by introducing the *batch shadow formalism*. It will enable us to post-process efficiently experimental data to give access to higher order estimation of the lower bounds and also observe interesting quantum properties associated to the operator entanglement.

5

Observation of the entanglement barrier using batch shadows

This chapter is based on the published work: *Aniket Rath, Vittorio Vitale, Sara Murciano, Matteo Votto, Jérôme Dubail, Richard Kueng, Cyril Branciard, Pasquale Calabrese, and Benoît Vermersch*. Entanglement barrier and its symmetry resolution: Theory and experimental observation. *PRX Quantum*, 4:010318, Feb 2023 (Ref. [101]).

In this work, we formally introduce the new batch shadow formalism and its properties to effectively post-process randomized measurement data to estimate multi-copy functionals. This enables us to re-analyze prior experimental data of [11] and observe the entanglement barrier. My main contribution consisted in developing the batch shadow formalism by deriving all its properties and obtaining the new entanglement criteria measurable using the RM protocol. The associated analytical calculations were performed jointly with Benoît Vermersch, Cyril Branciard and Richard Kueng. I also re-analyzed the experimental data to estimate the quantities of interest and engaged in writing the related portions of the manuscript along with other coauthors.

Contents

5.1	Batch shadow formalism	96
5.1.1	General variance treatment of batch shadow estimator	98
5.1.2	Sample complexity calculations to estimate Rényi 2-OE	100
5.1.3	Numerical investigations	104
5.2	Experimental observation of the entanglement barrier	105
5.2.1	Mixed state entanglement conditions and experimental detection	107
5.3	Conclusion	111

As seen from previous chapters, the addition of the classical shadow formalism to the RM toolbox extends access to many non-linear quantities of interest that can certify entanglement from the experimental RM data-set. More specifically, these quantities can be written as expectation values of multi-copy operator $O^{(n)}$ of the density matrix ρ , i.e $f_n = \text{Tr}(O^{(n)}\rho^{\otimes n})$. The U-statistics estimator links directly the RM data to the estimation of such functions. A key practical question that stands out is related to our ability to post-process the experimental data efficiently on a classical computer in order to obtain these estimators. The current U-statistics estimator presents a bottleneck for classical post-processing to extract the quantities of interest. Until now, functionals up to order $n \leq 3$ have been successfully extracted from experimental data [11, 34]. For $n > 3$, the post-processing time starts to increase significantly and becomes overburdening for classical devices. In this chapter, we will concretely address this problem by introducing a new framework of classical shadows that we dub *batch shadows*.

Our work, on the development of the batch shadow formalism originated from the inability to access a $n = 4$ order function. The function in particular that we were interested to estimate was the second Rényi operator entanglement entropy (or Rényi 2-OE). Recall from Chapter. 1 (Eq. (1.16)) that we can express the Rényi α -OE for a bipartite density matrix ρ_{AB} using the operator Schmidt coefficients μ_ℓ given as

$$S^{(\alpha)}(\rho_{AB}) = \frac{1}{1-\alpha} \log \sum_{\ell} (\mu_{\ell}^2)^{\alpha}. \quad (5.1)$$

To measure this quantity as constructed above requires an expensive measurement budget using quantum state tomography in order to access all the values of μ_{ℓ} . On the other hand, one can access moments of the Schmidt coefficients by reformulating them in terms of multi-copy observables in the form of trace polynomials $\text{Tr}(O^{(n)}\rho_{AB}^{\otimes n})$ [80]. This enables us to estimate them more easily compared to QST by employing the classical shadow formalism of the randomized measurement toolbox. In particular, a recent work showed that one can express the Rényi 2-OE as a ratio of a fourth order function (f_4) over a second order function (f_2) of ρ_{AB} [80]:

$$S^{(2)}(\rho_{AB}) = -\log \frac{f_4}{f_2} = -\log \frac{\text{Tr}(\mathcal{S} \rho_{AB}^{\otimes 4})}{\text{Tr}(\rho_{AB}^2)^2} = -\log \frac{\text{Tr} \left(\left[\mathbb{S}_{1,4}^{(A)} \otimes \mathbb{S}_{2,3}^{(A)} \otimes \mathbb{S}_{1,2}^{(B)} \otimes \mathbb{S}_{3,4}^{(B)} \right] \rho_{AB}^{\otimes 4} \right)}{\text{Tr}(\rho_{AB}^2)^2}. \quad (5.2)$$

where $\mathbb{S}_{a,b}^{(\Gamma)}$ is the two copy swap operator that acts on a^{th} and b^{th} copies of the sub-system Γ .

With this motivation, we organize this chapter as follows: We will first develop in detail the novel framework of batch shadows and perform a rigorous analysis on its statistical errors compared to the standard U-statistics estimator. This shall also be formally detailed in Appendix. B. Then, as an example, we will illustrate the required sample complexity to evaluate f_2 and f_4 with an error ϵ and confidence level δ . We will then apply this powerful framework to extract the Rényi 2-OE from existing experimental data of [11]. This shall enable us to observe interesting entanglement properties associated to this quantity such as the entanglement barrier that we will discuss in detail later in this chapter. Additionally, to the phenomenon of the entanglement barrier, we shall also show that the multi-copy observables f_2 and f_4 can be used to derive an entanglement condition based on the CCNR criteria

as given in Chapter. 1 (Sec:1.3.2) to detect mixed-state entanglement in quantum systems.

5.1 Batch shadow formalism

Our starting point is the RM data-set that consists of N_U distinct local random unitaries $U^{(r)} = \bigotimes_{i=1}^N U_i^{(r)}$ and N_M bit-string measurements recorded for each of them $\mathbf{s}^{(r,m)} = \left(s_1^{(r,m)}, \dots, s_N^{(r,m)} \right)$ with $r = 1, \dots, N_U$ and $m = 1, \dots, N_M$. From this data-set we can construct independent, unbiased estimators of the underlying quantum state in the form of classical shadows [64] as shown in previous chapters

$$\hat{\rho}^{(r,m)} = \bigotimes_{i=1}^N \left[3U_i^{(r)\dagger} \left| s_i^{(r,m)} \right\rangle \left\langle s_i^{(r,m)} \right| U_i^{(r)} - \mathbb{1} \right], \quad (5.3)$$

which give the underlying density matrix when averaged over the applied unitaries and measurements $\mathbb{E}[\hat{\rho}^{(r,m)}] = \rho$.

We recall that in order to measure functions $f_n = \text{Tr}(O^{(n)} \rho^{\otimes n})$, we use the U-statistics estimator \hat{f}_n given by [59]

$$\hat{f}_n = \frac{1}{n!} \binom{N_U}{n}^{-1} \sum_{r_1 \neq \dots \neq r_n} \text{Tr} \left[O^{(n)} \bigotimes_{i=1}^n \hat{\rho}^{(r_i)} \right], \quad (5.4)$$

where the sum ranges over all possible disjoint shadow indices $(r_1, \dots, r_n) \in \{1, \dots, N_U\}^{\times n}$ with $r_1 \neq \dots \neq r_n$. Additionally, we have also introduced here the classical shadow $\hat{\rho}^{(r)} = \frac{1}{N_M} \sum_m \hat{\rho}^{(r,m)}$ constructed by averaging over all measured bit-strings for an applied unitary $U^{(r)}$. The U-statistics estimator is an unbiased estimator, i.e., $\mathbb{E}[\hat{f}_n] = f_n$ [59, 100].

We observe for example that in order to estimate the U-statistics estimator of the purity ($\text{Tr}(\rho^2)$) with classical shadows, the moderate post-processing runtime scales quadratically $\mathcal{O}(N_U^2)$ with the number of unitaries N_U . Additionally, the runtime complexity further increases, as the required number of measurements M (in the regime of $M = N_U$ with $N_M = 1$) scale exponentially with respect to the system size N ($M \propto 2^N$) [34, 100]. In practice, the current optimal method to evaluate the U-statistics estimator of the purity \hat{f}_2 from a collection of N_U shadows writes as

$$\hat{f}_2 = \sum_{r_1 \neq r_2}^{N_U} \frac{\text{Tr}(\hat{\rho}^{(r_1)} \hat{\rho}^{(r_2)})}{N_U(N_U - 1)} = \frac{1}{N_U(N_U - 1)} \left[\text{Tr} \left(\sum_{r=1}^{N_U} \hat{\rho}^{(r)} \right)^2 - \text{Tr} \left(\sum_{r=1}^{N_U} \hat{\rho}^{(r)^2} \right) \right]. \quad (5.5)$$

This requires computing the sum and the squared sum over all the shadows and then computing the difference between them. This procedure requires two loops in the case when we do not store each classical shadow in classical memory. Similarly in the case of a third order function $f_3 = \text{Tr}(\rho^3)$, the U-statistics estimator is computed

as

$$\begin{aligned} \hat{f}_3 &= \sum_{r_1 \neq \dots \neq r_3}^{N_U} \frac{\text{Tr}(\hat{\rho}^{(r_1)} \hat{\rho}^{(r_2)} \hat{\rho}^{(r_3)})}{N_U(N_U - 1)(N_U - 2)} \\ &= \frac{\text{Tr} \left[\left(\sum_{r=1}^{N_U} \hat{\rho}^{(r)} \right)^3 - 3 \left(\sum_{r=1}^{N_U} \hat{\rho}^{(r)} \sum_{r=1}^{N_U} \hat{\rho}^{(r)^2} \right) + 2 \left(\sum_{r=1}^{N_U} \hat{\rho}^{(r)^3} \right) \right]}{N_U(N_U - 1)(N_U - 2)}. \end{aligned} \quad (5.6)$$

The same is visible for the above estimator that requires computing the sum, the squared sum and the cube of the sum in order to finally obtain the final U-statistics estimator.

Currently the above methods are restricted upto $n \leq 3$ and extending them to extract higher order functionals is not trivial and could be an interesting topic of study. As developing these methods for higher order functionals is not trivial, we are thus immediately exposed to the bottleneck of evaluating the U-statistics estimator. Naively, in the case of a function involving $n = 4$ copies of ρ , the number of summands to be calculated in Eq. (5.4) quickly becomes uncomputable for moderate system sizes as the runtime scales as $\mathcal{O}(M^4)$ without requiring to store exponentially large matrices in the classical memory. In general, for a generic function f_n , this underlying procedure quickly becomes unfeasible and impractical as it requires summing over all possible combinations of n distinct shadows $\hat{\rho}^{(r_1)}, \dots, \hat{\rho}^{(r_n)}$ for $r_i \in [1, \dots, M]$. Furthermore, its runtime scales with the number of terms involved in the sum of Eq. (5.4): $\mathcal{O}(M^n)$, a number that grows exponentially with the polynomial degree n . An additional bottleneck that plagues the post-processing is that the required number of measurements for the classical shadow formalism scales exponentially with respect to the systems-size N [31]. Thus one has to try to devise other alternatives to tackle this problem.

The main technical contribution of our work [101] addresses this pertinent practical issue. We propose another unbiased estimator of the same functional f_n by distributing our M shadows into $n' \geq n$ subsets, and first averaging the shadows in each subset. Each such defined subset is independent with respect to any other and can independently approximate ρ . More specifically, let us define the b^{th} *batch shadow* (denoted by a tilde rather than a hat) as

$$\tilde{\rho}^{(b)} = \frac{n'}{M} \sum_{t_b \in T_b} \hat{\rho}^{(t_b)} \quad \text{where} \quad T_b = \{1 + (b-1)M/n', \dots, bM/n'\} \quad (5.7)$$

for batches ranging from $b = 1, \dots, n'$ (for simplicity we assume n' divides M such that each subset contains M/n' original classical shadows). We note, as claimed above, that $\mathbb{E}[\tilde{\rho}^{(b)}] = \rho$ for every b . We then define the alternate unbiased estimator $\tilde{f}_n^{(n')}$ of f_n in a similar fashion to Eq. (5.4) by symmetrizing over n' batch shadows:

$$\begin{aligned} \tilde{f}_n^{(n')} &= \frac{(n' - n)!}{n!} \sum_{b_1 \neq \dots \neq b_n} \text{Tr} \left(O^{(n)} \bigotimes_{i=1}^n \tilde{\rho}^{(b_i)} \right) \\ &= \frac{(n' - n)!}{n!} \frac{n^n}{M^n} \sum_{b_1 \neq \dots \neq b_n} \sum_{t_{b_1} \in T_{b_1}, \dots, t_{b_n} \in T_{b_n}} \text{Tr} \left(O^{(n)} \bigotimes_{i=1}^n \hat{\rho}^{(t_{b_i})} \right). \end{aligned} \quad (5.8)$$

Again, by construction, $\mathbb{E}[\tilde{f}_n^{(n')}] = f_n$, i.e. the *batch shadow estimator* is unbiased. The principal advantage of introducing this batch estimator lies in the fact that, in the limit of $n' \ll M$, one can more efficiently post-process arbitrary n -order functionals $\tilde{f}_n^{(n')}$ compared to the basic U-statistics estimators \hat{f}_n . The evaluation of $\tilde{f}_n^{(n')}$ from the constructed batch shadows scales as $\mathcal{O}(n'^n)$. Thus by choosing $n' = n$ and assuming that $M \gg n^n$, we obtain the fastest estimator. The runtime scaling of this estimator becomes solely restricted by the time required to evaluate each batch shadow, resulting in an overall evaluation time of $\mathcal{O}(M)$. This is a drastic runtime improvement compared to the original U-statistics estimator in Eq. (5.4): $\mathcal{O}(M)$ steps (new) vs. $\mathcal{O}(M^n)$ steps (old).

We note that, by increasing n' the performance of $\tilde{f}_n^{(n')}$ improves in terms of convergence to the U-statistics estimator as more distinct ordered pairings of n different shadows $\hat{\rho}^{(r_1)}, \dots, \hat{\rho}^{(r_n)}$ are incorporated in the batch estimator that were not considered before. In the final limit of $n' = M$, we actually recover the full U-statistics estimator $\tilde{f}_n^{(M)} = \hat{f}_n$ which we have studied in detail in the previous chapter (Chapter. 4). Note also that, in contrast to the bare classical shadows $\hat{\rho}^{(r,m)}$, during the post-processing phase, the batch shadows $\tilde{\rho}^{(b)}$ are stored in memory as dense $2^N \times 2^N$ matrices. For typical memory available on current classical hardware, this limits our fast estimation methods to system sizes of up to $N \approx 15$ qubits.

In order to understand the trade-off in terms of performance of statistical errors vs computational feasibility of this new estimator $\tilde{f}_n^{(n')}$ compared with the standard U-statistics estimator \hat{f}_n , let us study its variance in the following section.

5.1.1 General variance treatment of batch shadow estimator

In this section, we would like to analytically benchmark the performance of the batch shadow estimator by studying its variance $\text{Var}[\tilde{f}_n^{(n)}]$. We remind again here that we work in the regime where we execute $M = N_U$ total measurements that are given by performing a single projective measurement ($N_M = 1$). Following a similar reasoning as done previously in Chapter. 4, we can gauge the performance by calculating the required number of measurements M to estimate f_n with an error $|\tilde{f}_n^{(n)} - f_n| \leq \epsilon$ and a certain confidence level using the Chebyshev's inequality:

$$\Pr[|\tilde{f}_n^{(n)} - f_n| \geq \epsilon] \leq \frac{\text{Var}[\tilde{f}_n^{(n)}]}{\epsilon^2}, \quad (5.9)$$

which leads us to now focus on the expression of $\text{Var}[\tilde{f}_n^{(n)}]$ for the batch shadow estimator. Now our goal is to compute this variance term and provide an upper bound to it. This shall be done with a similar spirit to the analytical calculations previously done in Chapter. 4 (in Sec. 4.2.1) which we detail for the interested readers in Appendix B. Recalling Eq. (B.4) from Appendix. B

$$\mathcal{V}_k = \text{Var} \left[\frac{1}{n!} \sum_{\pi} \text{Tr} \left(W_{\pi}^{\dagger} O^{(n)} W_{\pi} [\otimes_{i=1}^k \hat{\rho}^{(i)} \otimes \rho^{\otimes(n-k)}] \right) \right], \quad (5.10)$$

with W_{π} being the permutation operator that permutes the n shadows correspondingly as $W_{\pi} = \sum_{j_1, \dots, j_n} |j_{\pi(1)}\rangle\langle j_1| \otimes \dots \otimes |j_{\pi(n)}\rangle\langle j_n|$ (where the $|j_i\rangle$'s are orthonormal

basis states), we obtain the expression for $\text{Var}[\tilde{f}_n^{(n)}]$ as given in Eq. (B.5) of Appendix. B

$$\text{Var}[\tilde{f}_n^{(n)}] = \frac{n^2}{M} \mathcal{V}_1 + \frac{n^3(n-1)}{2M^2} (\mathcal{V}_2 - 2\mathcal{V}_1) + \mathcal{O}\left(\frac{1}{M^2}\right) \quad (5.11)$$

and additionally for any value of n' we obtain the expression of $\text{Var}[\tilde{f}_n^{(n')}]$ as given in Eq. (B.6) of Appendix. B

$$\text{Var}[\tilde{f}_n^{(n')}] = \frac{n^2}{M} \mathcal{V}_1 + \frac{n^2(n-1)^2 \frac{n'}{n'-1}}{2M^2} (\mathcal{V}_2 - 2\mathcal{V}_1) + \mathcal{O}\left(\frac{1}{M^2}\right). \quad (5.12)$$

Variance bounds for batch shadow estimators

We can provide bounds to the above variance expressions by using the fact that the variance of an average of random variables is upper-bounded by the average of the variances. This can be seen as follows: For K random variables C_i , one has, using the Cauchy–Schwarz inequality:

$$\begin{aligned} \left(\frac{1}{K} \sum_{i=1}^K C_i - \mathbb{E}\left[\frac{1}{K} \sum_{i=1}^K C_i\right]\right)^2 &= \left(\frac{\vec{\mathbf{1}}}{K} \cdot (\vec{C} - \mathbb{E}[\vec{C}])\right)^2 \\ &\leq \left\|\frac{\vec{\mathbf{1}}}{K}\right\|^2 \|\vec{C} - \mathbb{E}[\vec{C}]\|^2 = \frac{1}{K} \sum_{i=1}^K (C_i - \mathbb{E}[C_i])^2 \end{aligned} \quad (5.13)$$

with $\vec{C} = (C_1, \dots, C_K)$ and $\vec{\mathbf{1}} = (1, \dots, 1)$. Taking the expectation values on both sides gives $\text{Var}\left[\frac{1}{K} \sum_{i=1}^K C_i\right] \leq \frac{1}{K} \sum_{i=1}^K \text{Var}[C_i]$. This provides us the bound:

$$\begin{aligned} \mathcal{V}_k &= \text{Var} \left[\frac{1}{n!} \sum_{\pi} \text{Tr} \left(W_{\pi}^{\dagger} O^{(n)} W_{\pi} [\otimes_{i=1}^k \hat{\rho}^{(i)} \otimes \rho^{\otimes(n-k)}] \right) \right] \\ &\leq \overline{\mathcal{V}}_k = \frac{1}{n!} \sum_{\pi} \text{Var} \left[\text{Tr} \left(W_{\pi}^{\dagger} O^{(n)} W_{\pi} [\otimes_{i=1}^k \hat{\rho}^{(i)} \otimes \rho^{\otimes(n-k)}] \right) \right]. \end{aligned} \quad (5.14)$$

With this we can summarize and formalise the variance bound for arbitrary batch shadow estimator as follows.

Proposition 4. *Given a n^{th} order function $\text{Tr}(O^{(n)} \rho^{\otimes n})$ evaluated using the batch shadow estimator $\tilde{f}_n^{(n')}$ from a total of M measurements, its variance can be bounded as*

$$\text{Var}[\tilde{f}_n^{(n')}] \leq \sum_{j=1}^n \binom{n}{j} \frac{\binom{n'-n}{n-j}}{\binom{n'}{n}} \sum_{k=1}^j \left(\frac{n'}{M}\right)^k \left(1 - \frac{n'}{M}\right)^{j-k} \overline{\mathcal{V}}_k \quad (5.15)$$

and in particular for $n' = n$, the bound writes

$$\text{Var}[\tilde{f}_n^{(n)}] \leq \sum_{k=1}^n \binom{n}{k} \left(\frac{n}{M}\right)^k \left(1 - \frac{n}{M}\right)^{n-k} \overline{\mathcal{V}}_k. \quad (5.16)$$

One can further bound $\overline{\mathcal{V}_k}$ using the presented results of Chapter. 4 (Sec. 4.2.1, Eq. 4.28). This then, along with the Chebyshev bound, helps us obtain concrete sample complexity bounds to evaluate arbitrary functions $\tilde{f}_n^{(n')}$ for any chosen value of n' using batch shadows. In particular, we shall show an example of the sample complexity calculation for the batch shadow estimator of the purity in the upcoming sections.

More concretely, for comparison with the U-statistics estimator, Eq. (4.25), we can re-write the U-statistics estimator $\tilde{f}_n^{(M)} = \hat{f}_n$ as

$$\text{Var}[\hat{f}_n] = \sum_{k=1}^n \binom{n}{k} \frac{\binom{M-n}{n-k}}{\binom{M}{n}} \mathcal{V}_k = \sum_{k=1}^n \frac{\binom{n}{k}^2}{\binom{M}{k}} \left[\sum_{\ell=1}^k \binom{\ell}{k} (-1)^{\ell-k} \mathcal{V}_\ell \right]. \quad (5.17)$$

Computing the first and second order in $\frac{1}{M}$, we now obtain

$$\text{Var}[\hat{f}_n] = \frac{n^2}{M} \mathcal{V}_1 + \frac{n^2(n-1)^2}{2M^2} (\mathcal{V}_2 - 2\mathcal{V}_1) + \mathcal{O}\left(\frac{1}{M^2}\right). \quad (5.18)$$

We observe that the behavior for large M is dependent upon the relationship between n' and M . This dependence arises whether n' is treated as independent of M (as in the case of $n' = n$), or whether it is simply proportional to M (as observed in the limiting scenario of $n' = M$ as seen in standard U-statistics). Comparing Eq. (5.12) and Eq. (5.18), one finds that $\text{Var}[\tilde{f}_n^{(n')}$] and $\text{Var}[\hat{f}_n]$ have the same behavior of $\frac{n^2}{M} \mathcal{V}_1$ at first order in $\frac{1}{M}$ for any value of n' . This high accuracy regime results from large number of measurements M that is associated to the standard Monte-carlo error decay (as errors decays proportional to $\sqrt{\text{Var}[\hat{f}_n]} = \sqrt{\text{Var}[\tilde{f}_n^{(n')}]} \sim 1/\sqrt{M}$). At the second order, $\text{Var}[\tilde{f}_n^{(n')}]$ is only marginally larger (by a factor of $\frac{n'}{n'-1}$) than $\text{Var}[\hat{f}_n]$.

In summary, the key takeaway from this section is that the precision loss when utilizing our innovative batch shadow technique in place of the conventional U-statistics estimator for classical shadows is negligible. This conclusion remains valid regardless of the specific choice of n' , as our approach demonstrates comparable performance without significant compromise in accuracy. On the other hand, we evidently achieve exponential improvements in runtime of the classical treatment of the measurement data. We shall also confirm this fact by numerical simulations of the protocol.

In the following section, combining the general bounds on the batch shadow estimator and some new properties of classical shadows elaborated in Appendix. C, we can calculate the sample complexity bounds of the functions of interest.

5.1.2 Sample complexity calculations to estimate Rényi 2-OE

In this section, we aim to illustrate the principal steps of calculation for the sample complexity bound (required number of measurements) in order to evaluate the Rényi 2-OE using the batch shadow estimator introduced earlier. As we see from the expression of Rényi 2-OE given in Eq. (5.2), the numerator is expressed as a fourth order function $f_4 = \text{Tr}(\mathcal{S} \rho_{AB}^{\otimes 4})$ with the denominator expressed as the square of the purity $f_2 = \text{Tr}(\rho_{AB}^2)$. In order to improve on the existing sample complexity bounds derived for these quantities in previous works [34, 100, 80], we derive in

Appendix. C, novel variance bound relations based on *Pauli shadows* [65] that we shall use in the following. The combination of these relations along with the batch shadow formalism will give us rigorous analytical arguments on the required number of measurements to estimate f_2 and f_4 .

Sample complexity of f_2

In this section, we focus on illustrating the required number of measurements to estimate the purity $f_2 = \text{Tr}(\rho_{AB}^2)$ using the batch shadow estimator of Pauli shadows. As we will show here, we improve upon existing sample complexity bounds of previous works [34, 100] based on the geometric properties of Pauli shadows that are derived in Appendix. C.

The purity of a N -qubit quantum state ρ_{AB} can be expressed as:

$$f_2 = \text{Tr} \left(\mathbb{S}_{1,2}^{(AB)} \rho_{AB} \otimes \rho_{AB} \right) = \text{Tr}(\rho_{AB}^2), \quad (5.19)$$

where $\mathbb{S}_{1,2}^{(AB)}$ is the swap operator. As mentioned in Ref. [65], we can construct Pauli shadows by performing Pauli measurements that consist in applying M random unitaries $U^{(r)} = \bigotimes_{i=1}^N U_i^{(r)}$ (with $r = 1, \dots, M$) where each $U_i^{(r)}$ is uniformly sampled in the set $\mathcal{U}_{\text{cl}}(2) = \left\{ \mathbb{1}_2, \frac{1}{\sqrt{2}} \begin{pmatrix} 1 & 1 \\ 1 & -1 \end{pmatrix}, \frac{1}{\sqrt{2}} \begin{pmatrix} 1 & -i \\ 1 & +i \end{pmatrix} \right\}$ so that $U_i^\dagger Z U_i = Z, X, Y$. We also note that X, Y, Z are single qubit Pauli matrices. Note additionally that here $\mathcal{U}_{\text{cl}}(2)$ forms a discrete set taken from the single qubit Clifford gates (Hadamard and phase gate). The Pauli shadows can be constructed from the above data-set of Pauli measurements (unitaries and the measured bit-strings as done in Eq. (5.3)). Given M such Pauli shadows, the corresponding batch shadow estimator $\tilde{f}_2^{(2)}$ (with $n' = 2$) of the purity can be written as

$$\tilde{f}_2^{(2)} = \frac{1}{2!} \sum_{b_1 \neq b_2} \text{Tr} \left[\mathbb{S}_{1,2}^{(AB)} \bigotimes_{i=1}^2 \tilde{\rho}^{(b_i)} \right], \quad (5.20)$$

where each batch shadow $\tilde{\rho}^{(b)}$, for $b = 1, 2$ writes as

$$\tilde{\rho}^{(b)} = \frac{2}{M} \sum_{r=(b-1)M/2+1}^{bM/2} \hat{\rho}^{(r)}. \quad (5.21)$$

Our goal is to bound $\text{Var}[\tilde{f}_2^{(2)}]$ for Pauli shadows (this restriction is important, because we will use the introduced properties given in Appendix. C). We use Proposition. 4 to explicitly bound the variance of f_2 as

$$\text{Var}[\tilde{f}_2^{(2)}] \leq \frac{4}{M} \overline{\mathcal{V}}_1 + \frac{4}{M^2} (\overline{\mathcal{V}}_2 - 2\overline{\mathcal{V}}_1) \leq \frac{4}{M} \overline{\mathcal{V}}_1 + \frac{4}{M^2} \overline{\mathcal{V}}_2. \quad (5.22)$$

The next step consists of obtaining the bounds on the terms $\overline{\mathcal{V}}_k$. From the expression of Eq. (5.14), we notice that for $n = 2$, the two permutation operators that need to be considered are: $W_{(1,2)} = \mathbb{1} \otimes \mathbb{1}$ and $W_{(2,1)} = \mathbb{S}$. In each case, we find that $W_\pi^\dagger O^{(2)} W_\pi = \mathbb{S}$. Now recalling Lemma. 2 and Lemma. 3 from Appendix. C, we can compute the bounds on $\overline{\mathcal{V}}_1$ and $\overline{\mathcal{V}}_2$ respectively:

$$\overline{\mathcal{V}}_1 = \text{Var} \left[\text{Tr}(\mathbb{S}_{1,2}^{(AB)}(\hat{\rho} \otimes \rho_{AB})) \right] = \text{Var} \left[\text{Tr}(\hat{\rho} \rho_{AB}) \right] \leq \text{Tr}[\rho_{AB}^2] 2^N \leq 2^N, \quad (5.23)$$

$$\overline{\mathcal{V}}_2 = \text{Var} \left[\text{Tr}(\mathbb{S}_{1,2}^{(AB)}(\hat{\rho}^{(1)} \otimes \hat{\rho}^{(2)})) \right] = \text{Var} \left[\text{Tr}(\hat{\rho}^{(1)} \hat{\rho}^{(2)}) \right] \leq 8.5^N \leq 3^{2N}. \quad (5.24)$$

Then from Eq. (5.22), we obtain the following bound on $\text{Var}[\tilde{f}_2^{(2)}]$:

$$\text{Var}[\hat{f}_2^{(2)}] \leq \frac{4}{M} \overline{\mathcal{V}}_1 + \frac{4}{M^2} \overline{\mathcal{V}}_2 \leq \frac{4}{M} 2^N + \frac{4}{M^2} 3^{2N}. \quad (5.25)$$

Recalling the Chebyshev's inequality mentioned in Eq. (5.9), we conclude

$$\Pr \left[|\tilde{f}_2^{(2)} - f_2| \geq \epsilon \right] \leq \frac{\text{Var}[\tilde{f}_2^{(2)}]}{\epsilon^2} \leq \frac{4}{\epsilon^2} \left[\frac{2^N}{M} + \frac{3^{2N}}{M^2} \right]. \quad (5.26)$$

This allows us to formulate a concise sample complexity bound by taking the two terms in the above expression to be less than $\delta/2$

Proposition 5. *Suppose that we wish to estimate the purity $f_2 = \text{Tr}(\rho_{AB}^2) = \text{Tr}(\mathbb{S}_{1,2}^{(AB)} \rho_{AB}^{\otimes 2})$ of a N -qubit state ρ using the batch shadow estimator $\tilde{f}_2^{(2)}$ constructed from Pauli shadows. Then for $\epsilon, \delta \in (0, 1)$, a total of*

$$M \geq \max \left\{ 8 \frac{2^N}{\epsilon^2 \delta}, 2 \frac{3^{2N}}{\epsilon \sqrt{\delta}} \right\} \quad (5.27)$$

measurements suffices to ensure $\Pr \left[|\tilde{f}_2^{(2)} - f_2| \geq \epsilon \right] \leq \delta$.

We can compare the obtained sample complexity bound with previous bounds derived in the case of the U-statistics estimator $\hat{f}_2 = \tilde{f}_2^{(M)}$ of the purity using M Haar shadows [34, 100]. The previous sample complexity bound for the purity writes as

$$M \geq \max \left\{ 8 \frac{\text{Tr}(\rho_{AB}^2) 2^N}{\epsilon^2 \delta}, 2 \frac{2^{2N}}{\epsilon \sqrt{\delta}} + 1 \right\}. \quad (5.28)$$

We immediately notice the similarities between both these bounds, while the main striking difference is that using our key results on Pauli shadows as described previously, we were able to make the bound tighter (the exponential scaling improves from 4^N to 3^N). We also note that the scaling in terms of system size N is given by 3^N which is a strict improvement over general quantum state tomography. This kind of scaling for the purity is also observed for SIC POVM measurements on independent copies where the sample complexity bound scales as $M \propto 3^N / \epsilon^2 \delta$ [118]. But, when M becomes sufficiently large, the scaling in Eq. (5.25) is dominated by the first term ($k = 1$) which is $\propto 2^N / M$. This then produces a measurement complexity that scales as $M \propto 2^N / \epsilon^2 \delta$. From Eq. (5.28), we see similar scaling behavior in this limit $M \rightarrow \infty$ that reproduce an error decay rate proportional to $1/\sqrt{M}$ – the ultimate limit for any Monte Carlo averaging procedure.

Sample complexity of f_4

Let us now move on to compute the sample complexity bound of the function f_4 in the numerator of the Rényi 2-OE. We consider here the simplest batch shadow estimator $\tilde{f}_4^{(4)}$ of this function that can be evaluated from M Pauli shadows as:

$$\tilde{f}_4^{(4)} = \frac{1}{4!} \sum_{b_1 \neq \dots \neq b_4} \text{Tr} \left[\mathcal{S} \bigotimes_{i=1}^4 \tilde{\rho}^{(b_i)} \right] \quad (5.29)$$

where each batch shadow $\tilde{\rho}^{(b)}$, for $b = 1, \dots, 4$ is an average over $M/4$ Pauli shadows given as:

$$\tilde{\rho}^{(b)} = \frac{4}{M} \sum_{r=(b-1)M/4+1}^{bM/4} \hat{\rho}^{(r)} \quad (5.30)$$

and $\mathcal{S} = \mathbb{S}_{1,4}^{(A)} \otimes \mathbb{S}_{2,3}^{(A)} \otimes \mathbb{S}_{1,2}^{(B)} \otimes \mathbb{S}_{3,4}^{(B)}$. Our task is to bound the variance $\text{Var}[f_4^{(4)}]$. With the help of Proposition. 4, we can simply bound the corresponding variance as

$$\text{Var}[f_4^{(4)}] \leq \sum_{k=1}^4 \binom{4}{k} \left(\frac{4}{M}\right)^k \left(1 - \frac{4}{M}\right)^{4-k} \overline{\mathcal{V}}_k \leq \sum_{k=1}^4 \binom{4}{k} \left(\frac{4}{M}\right)^k \overline{\mathcal{V}}_k, \quad (5.31)$$

where each of the $\overline{\mathcal{V}}_k$ can be expressed from Eq. (5.14) as

$$\overline{\mathcal{V}}_k = \frac{1}{4!} \sum_{\pi} \text{Var} \left[\text{Tr} \left(\mathcal{S} W_{\pi} [\otimes_{i=1}^k \hat{\rho}^{(i)} \otimes \rho_{AB}^{\otimes(4-k)}] W_{\pi}^{\dagger} \right) \right]. \quad (5.32)$$

As we see, we now need to calculate the bounds on the term $\overline{\mathcal{V}}_k$ for each value of $k = 1, \dots, 4$. This mathematical step is illustrated in detail for interested readers in our work [101, Appendix C.4]. Summarizing our findings and putting all the pieces together, we obtain using Eq. (5.31)

$$\text{Var}[f_4^{(4)}] \leq \sum_{k=1}^4 \binom{4}{k} \frac{4^k}{M^k} \overline{\mathcal{V}}_k \leq \sum_{k=1}^4 \binom{4}{k} 4^k \frac{3^{kN}}{M^k} = \left(1 + 4 \frac{3^N}{M}\right)^4 - 1. \quad (5.33)$$

The Chebyshev's inequality in Eq. (5.9) helps us provide a sample complexity for this estimator that is summarized in the following proposition

Proposition 6. *Let ρ_{AB} be a bipartite quantum state on N qubits and suppose that we wish to estimate the non-linear function $f_4 = \text{Tr}(\mathcal{S} \rho_{AB}^{\otimes 4})$, with $\mathcal{S} = \mathbb{S}_{1,4}^{(A)} \otimes \mathbb{S}_{2,3}^{(A)} \otimes \mathbb{S}_{1,2}^{(B)} \otimes \mathbb{S}_{3,4}^{(B)}$, using the batch shadow estimator $f_4^{(4)}$ constructed from Pauli shadows. Then for $\epsilon, \delta > 0$, a total of*

$$M \geq 4 \frac{3^N}{(1 + \epsilon^2 \delta)^{\frac{1}{4}} - 1} \gtrsim 16 \frac{3^N}{\epsilon^2 \delta}, \quad (5.34)$$

measurements suffices to ensure $\text{Pr}[|f_4^{(4)} - f_4| \geq \epsilon] \leq \delta$.

This measurement cost scales (at worst) as 3^N in system size N . The variance bound obtained in Eq. (5.33) offers an exponential improvement over the best known scaling bound for the U-statistics estimate of f_4 in the case of Pauli shadows given in [80, Appendix. C, Eq. C36]. These improvements on the complexity bounds were achieved by exploiting the rich structure of Pauli basis measurements to produce powerful auxiliary statements, most notably Lemma. 1 and Lemma. 3 in Appendix. C. At the present stage, these auxiliary results are only valid for Pauli shadows and do not yet cover Haar shadows.

It is interesting to point out that the measurement complexity bound f_4 is always comparable in term of the scaling with the system-size N to the measurement complexity bound for f_2 (purity). Moving from a second-order function to a fourth

order function does not seem to incur a large penalty in measurement complexity. We equally note that, in the limit of $M \rightarrow \infty$, the dominant contribution to the variance is given by the linear term ($k = 1$) which scales $\propto 2^N/M$. Then, in this limit, it holds that the measurement bound scales as $2^N/\epsilon^2\delta$. Having discussed the sample complexity bounds, in the next section, we shall demonstrate numerically the error scaling of the batch shadow estimators for the function f_4 .

5.1.3 Numerical investigations

In this subsection, we would like to consecrate ourselves to support our analytical finding with numerical simulation of the protocol. We mainly would like to study error scalings and the performance of the batch shadow estimator $\tilde{f}_4^{(n')}$ by using random Pauli and Haar random shadows in the regime where $M \gg n'$ and compare it to the standard U-statistics estimator \hat{f}_4 . We consider a 4-qubit GHZ state and numerically simulate the protocol by applying M Haar random (CUE) unitaries U followed by fixed basis measurements to construct Haar random shadows (fixing $N_M = 1$). We equally construct numerically M Pauli shadows by choosing N random Pauli basis for each shadow. We calculate the average statistical error $\mathcal{E} = |\tilde{f}_4^{(n')} - f_4|/f_4$ for different values of n' and M by simulating the RM protocol 200 times. This is plotted in Fig. 5.1 for Pauli and Haar shadows respectively. We make two important observations:

- The error scaling characteristics of Pauli shadows, which require sampling from a fixed set of three measurement settings (x, y, z) , show similarities to those of Haar shadows that utilize an infinite number of measurement settings.
- The batch shadow estimator $\tilde{f}_4^{(n')}$ with $n' \sim 10$ has very close performance as that of the U-statistics estimator. This in general translates into huge runtime gain in terms of data treatment ($\mathcal{O}(10^4)$ compared to $\mathcal{O}(M^4)$) and allows us to process the quantities of interest for a larger set of measurement data. We clearly observed a limitation in post-processing the U-statistics estimator ($n' = M$) for a modest system size of $N = 4$ qubits. This constraint starts to be extremely prominent when the system size N increases. This is due to the fact that the number of measurements M scales exponentially with N as shown in the previous section.

To sum up this section, we introduced the batch shadow formalism and provided in Appendix. B and Appendix. C, the necessary analytical tools to compute sample complexity bounds for general multi-copy functionals of interest. In particular, we also derived new trace bounds identities of Lemma. 1 and Lemma. 3 for Pauli shadows. With the help of these results, we were able to obtain improved bounds on the required number of measurements to estimate the functions f_2 and f_4 . Supplementary numerical simulations of the protocol showed equally the advantages of using the batch shadow estimator compared to the standard U-statistics one. With all these tools at hand, let us now dive into the experimental observation of the entanglement barrier and its interesting properties realized on a trapped ion quantum simulator.

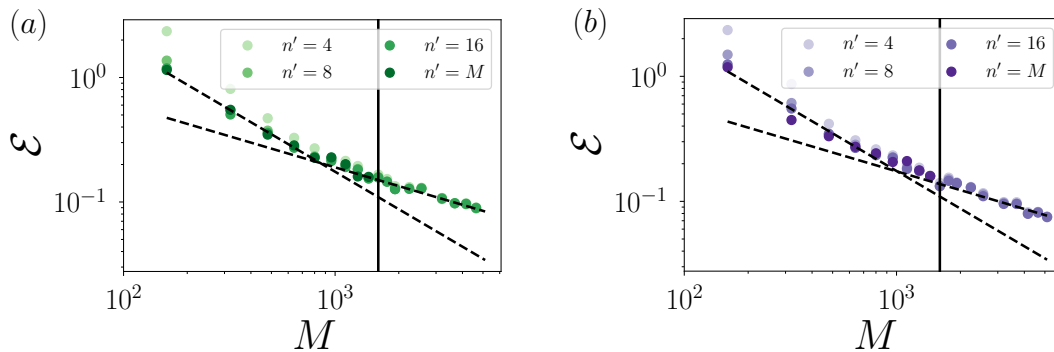


Figure 5.1: *Error scaling as a function of M* — Panels (a) for Pauli shadows and (b) for Haar shadows show the scaling of the average statistical error \mathcal{E} as a function of the number of measurements M for the functional $\tilde{f}_4^{(n')}$ calculated on a 4-qubit GHZ state for different values of n' . The black line marks the value of M until which we could simulate $\tilde{f}_4^{(M)}$. The dashed black lines highlight the different error scalings $\propto 1/M$ and $1/\sqrt{M}$.

5.2 Experimental observation of the entanglement barrier

Our main interest to measure the Rényi 2-OE follows from the fact that the operator entanglement (OE) of a reduced bipartite density matrix ρ_{AB} displays an interesting physical feature known as *the entanglement barrier* [130]. In this section, we will describe its relevance and observe the entanglement barrier by measuring the Rényi 2-OE with the help of the batch shadow formalism developed in this chapter. In particular, this novel method allows us to re-analyze the RM data of a prior experiment [11] and effectively estimate the Rényi 2-OE leading to its first experimental observation on a trapped ion quantum simulator.

The experimental platform in [11] consists of a linear string of trapped $^{40}\text{Ca}^+$ atoms where each individual ion encodes a single qubit. Coupling all ions off-resonantly with a laser beam subjects the ions to realize a long-range XY model in presence of a transverse field¹, whose effective Hamiltonian writes:

$$H_{XY} = \hbar \sum_{i < j} J_{ij} (\sigma_i^+ \sigma_j^- + \sigma_i^- \sigma_j^+) + \hbar B \sum_i \sigma_i^z, \quad (5.35)$$

where σ_i^+ (σ_i^-) are the spin-raising (lowering) operators with $i, j = 1, \dots, N$, J_{ij} the spin-spin coupling matrix and B the transverse magnetic field strength. The strength of the spin coupling follows an approximate power law behaviour that depends on the distance between the atoms $|i - j|$ given by $J_{ij} \sim J_{\max}/|i - j|^\alpha$ where the values of $J_{\max} = \max |J_{ij}|$ and α depend on the specifics of each experimental realization. For the experiments conducted with strings of 10 ions, $\alpha = 1.24$ and $J_0 = 420 \text{ s}^{-1}$. For the ones with 20 ions, $\alpha = 1.01$ and $J_0 = 370 \text{ s}^{-1}$.

The experiment in [11] performed a global quench dynamics using the H_{XY} Hamiltonian starting from an initial Néel state, $|\psi\rangle = |01\rangle^{\otimes N/2}$, with vanishing operator (and state) entanglement entropy. The global quench was followed by the implementation of the randomized measurement protocol involving a total of

¹in the regime of $B \gg \max |J_{ij}|$

$N_U = 500$ Haar random unitaries for which $N_M = 150$ bit-string measurements were collected for each applied unitary. For the 20 ion system, randomized measurements were performed on the central 10 ions of the chain.

We consider two bipartite reduced density matrices ρ_{AB} defined on the subsystems $A = [2, 3]$ and $B = [4, 5]$ and $A = [8, 9]$ and $B = [10, 11]$ for a total chain of 10 ions and 20 ions, respectively, where we have labelled the ions along the chain from 1 to N . Our observations remain unchanged for other partitions. Additionally, we can express Eq. (5.2) as a function of entropic quantities

$$S^{(2)}(\rho_{AB}) = -\log \frac{\text{Tr}(\mathcal{S} \rho_{AB}^{\otimes 4})}{\text{Tr}(\rho_{AB}^2)^2} = \tilde{S}^{(2)}(\rho_{AB}) - 2S_2(\rho_{AB}), \quad (5.36)$$

where we have defined the unnormalized Rényi 2-OE $\tilde{S}^{(2)}(\rho_{AB}) = -\log(\text{Tr}(\mathcal{S} \rho_{AB}^{\otimes 4}))$, and we note that $S_2(\rho_{AB})$ is the second Rényi entropy. We extracted Rényi 2-OE from the experimental data using the simplest batch shadow estimator with $n' = 4$ batches.

To further motivate the estimation of Rényi 2-OE, let us begin by briefly summarizing the phenomenon of the entanglement barrier. For a generic quantum dynamics starting from a product state with no entanglement (consequently no operator entanglement), the OE of a sub-system density matrix initially grows linearly as entanglement is generated from coherent interaction between particles. It then reaches a maximum height that is proportional to sub-system size that is equivalent to the state entanglement growing and saturating to a volume-law value. This value of the OE then decays at longer times of the dynamics. The decay at later times reflects the convergence of the reduced density matrix towards a simple stationary state [26], through the mechanism of thermalization [103, 85, 82, 23, 117]. This signature shape of the OE dynamics is most often interpreted as a ‘barrier’ in terms of our ability to represent efficiently the sub-system reduced density matrix all along the quantum evolution on classical hardware using algorithms such as tensor-networks [113]. In particular, the height of the ‘barrier’ or analogously the value of the OE attained provides an indication of the bond dimension of matrix product operator (MPO) required to simulate classically the reduced density matrix.

In Fig. 5.2(a), we observe the entanglement barrier for the considered partition of the 20 ion system. Firstly, the initial state at $t = 0$ ms starts from a product state of the type $\rho_{AB} = \rho_A \otimes \rho_B$ that has an associated Rényi 2-OE $S^{(2)}(\rho_{AB}) = 0$. As the quench dynamics begins, coherent interactions amongst the spins generate entanglement. We thus observe a barrier composed of a growth phase from $t > 0$ to $t \approx 3$ ms, and a decay phase from $t \approx 3$ ms to the last data point at $t = 10$ ms. The peak at $t \approx 3$ ms actually looks more like a double-peak with maxima at $t \approx 1.8$ ms and $t \approx 3.8$ ms. We interpret this as oscillations superimposed on the primary barrier, attributed to finite size effects due to the relatively small sizes of subsystems A and B . The initial growth phase during early times signifies the emergence of correlations between subsystems A and B , resulting from the coherent dynamics within the system. On the other hand, the subsequent decay phase reflects the trend of ρ_{AB} transitioning towards a thermal-like density matrix with small OE [26]. A comparison between Figures 5.2(a) and (b) reveals that no analogous barrier is observed in the smaller system of 10 ions. Particularly, the

decay phase is absent. This discrepancy is attributed to the finite size of the ion chain (10 compared to 20), and this aspect is elaborated in our work [101].

Alternatively, one can perceive the emergence of the barrier as being directly connected to the distribution of squared operator Schmidt values, denoted as μ_ℓ^2 according to Eq. (5.1). In the initial stages, the evolution originates from a pure product state, where a single Schmidt value differs from zero. The growth of entanglement is reflected in the increasing count of non-zero Schmidt coefficients, μ_ℓ . For long times, the system eventually locally tends to approach, in the case of the infinite temperature limit, to a density matrix that is proportional to the identity, $\rho_{AB} \propto \mathbb{1} = \mathbb{1}_A \otimes \mathbb{1}_B$. In this scenario, only a single Schmidt value differs from zero, leading to the vanishing of the value of OE.

The barrier can also be understood as a competition between the terms $\tilde{S}^{(2)}(\rho_{AB})$ and $S_2(\rho_{AB})$ in the respective regimes as shown in Fig. 5.2(c) [130]. In the growth phase, the unnormalised Rényi 2-OE $\tilde{S}^{(2)}(\rho_{AB})$ grows at a faster rate compared to the state entropy $2S_2(\rho_{AB})$. In the decay phase, this behavior is inverted. These general features are consistent with the theoretical predictions of different models shown in Refs. [26, 130, 5].

Overall Fig. 5.2(b) and (d) show excellent agreement of the experimental data with the numerically modeled results for the 10 ion experiment. On the other hand, it is quite surprising to see that even though the individual estimations of $\tilde{S}^{(2)}(\rho_{AB})$ and $S_2(\rho_{AB})$ from the 20 ion experiment as shown in Fig. 5.2(c) have systematic shifts of the experimentally measured values caused likely due to an imperfect modeling of decoherence during the experiment and the measurement protocol, the corresponding measured Rényi 2-OE shows quite good agreement with the theoretical model as in Fig. 5.2(a). This suggests a robustness feature of the Rényi 2-OE where errors in estimations of the two terms compensate each other. We also remark that the measured values of Rényi 2-OE are lower as shown in Fig. 5.2(a-b) from the numerical simulations of the experiment.

Additional to the entanglement barrier the quantities $\tilde{S}^{(2)}(\rho_{AB})$ and $S_2(\rho_{AB})$ expressed in function of multi-copy operators f_4 and f_2 respectively can serve to provide an entanglement condition for mixed states based on the CCNR (or enhanced CCNR) criteria. This shall be the topic of discussion of the next subsection.

5.2.1 Mixed state entanglement conditions and experimental detection

Firstly, let us start by a key result in entanglement theory by recalling that the operator Schmidt values for separable density matrix ρ_{AB} on a bipartite system $A \cup B$ obeys

$$\sum_{\ell=1}^R \mu_\ell \leq 1/\sqrt{\text{Tr}(\rho_{AB}^2)}, \quad (5.37)$$

see e.g. [53, Theorem 6] and also Eq. (1.11) in Chapter. 1. Here, $R \geq 1$ denotes the operator Schmidt rank and the Schmidt values μ_1, \dots, μ_R are non-negative ($\mu_\ell \geq 0$) and obey $\sum_{\ell=1}^R \mu_\ell^2 = 1$. Conversely, if Eq. (5.37) is violated, then ρ_{AB} is entangled across the bi-partition A and B . The main drawback to verify this condition is that it seems to rely on the explicit availability of an operator Schmidt decomposition and thus requires full quantum state tomography of the density matrix ρ_{AB} .

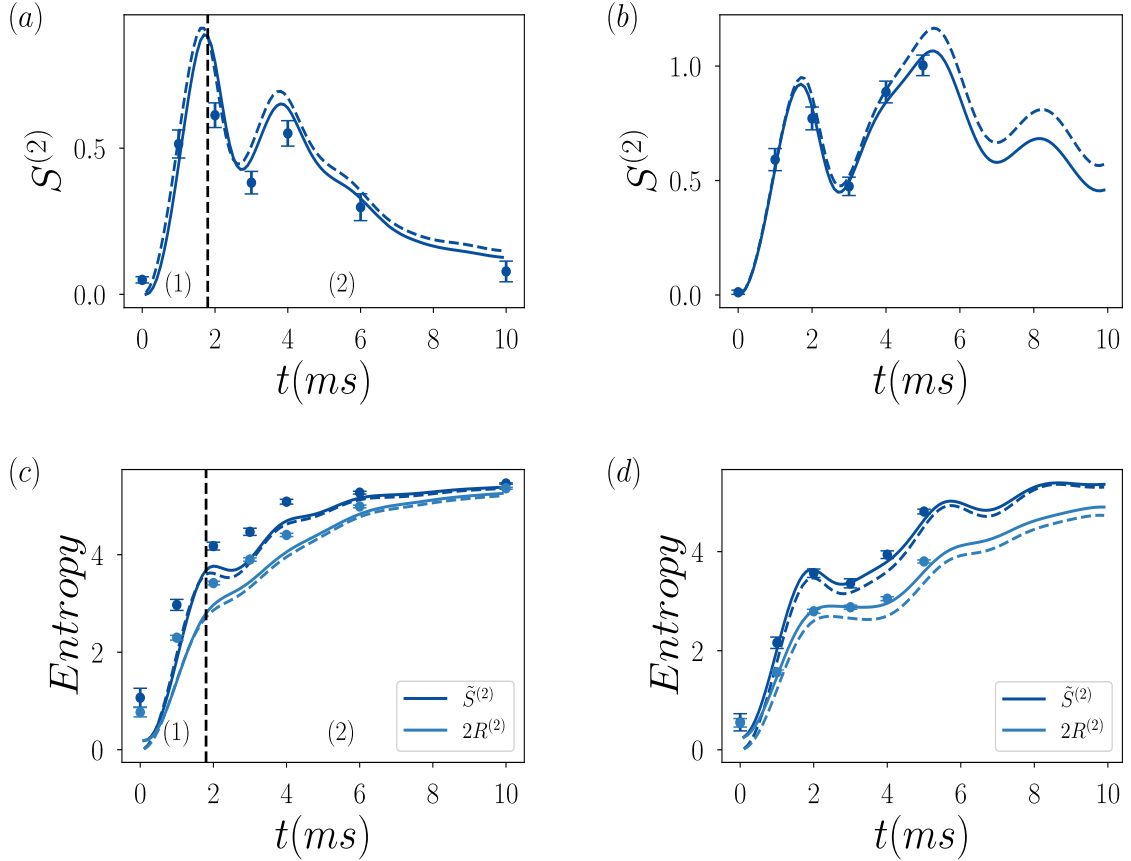


Figure 5.2: *Experimental observation of the entanglement barrier* — Panels (a-b) show the measured Rényi 2-OE and correspondingly, panels (c-d) the measured values of $\tilde{S}^{(2)}(\rho_{AB})$ and $S_2(\rho_{AB})$ relating to Rényi 2-OE as in Eq. (5.36) for a reduced density matrix of 4 ions from a total a system consisting of $N = 20$ (left panels) and $N = 10$ (right panels). We observe the two phases of the entanglement barrier that is separated by a black vertical dashed line for panels a) and c) given by: (1) the growth phase followed by (2) the decay phase. The points show experimental results with the error bars calculated with Jackknife resampling. Lines correspond to numerical simulations of the unitary dynamics (dashed) and including dissipation (solid).

As mentioned earlier in the chapter, this apparent drawback was recently overcome in Ref. [80]. There, the authors point out that sums of higher powers of Schmidt values can be reformulated in terms of linear observables in tensor products of the original density matrix ρ_{AB} .

$$\sum_{\ell=1}^R \mu_{\ell}^4 = \frac{\text{Tr}(\mathcal{S}\rho_{AB}^{\otimes 4})}{\text{Tr}(\rho_{AB}^2)^2} \quad \text{where} \quad \mathcal{S} = \mathbb{S}_{1,4}^{(A)} \otimes \mathbb{S}_{2,3}^{(A)} \otimes \mathbb{S}_{1,2}^{(B)} \otimes \mathbb{S}_{3,4}^{(B)}. \quad (5.38)$$

This is relevant, because we can estimate trace polynomials of the form $\text{Tr}(O^{(n)}\rho_{AB}^{\otimes n})$ by employing the classical shadow formalism of the RM toolbox [31]. It is important to remember now that we know how to directly estimate the RHS of Eq. (5.37), while we are not aware of a direct estimation protocol for the LHS of Eq. (5.37).

Let us consider a separable density matrix ρ_{AB} on a bipartite system $A \cup B$ as:

$$\frac{\rho_{AB}}{\sqrt{\text{Tr}[\rho_{AB}^2]}} = \sum_{\ell} \mu_{\ell} O_{A,\ell} \otimes O_{B,\ell}. \quad (5.39)$$

We can collect the operator Schmidt values in a vector l as $l = (\mu_1, \dots, \mu_R)$. Let us

note that the following inequality (Littlewood's inequality) based on vector norms holds

$$\|\ell\|_{p_\theta} \leq \|\ell\|_{p_1}^\theta \|\ell\|_{p_0}^{1-\theta}, \quad (5.40)$$

with $\theta \in [0, 1]$, and

$$\frac{1}{p_\theta} = \frac{\theta}{p_1} + \frac{1-\theta}{p_0}. \quad (5.41)$$

Here we have defined the vector norm (or ℓ_p norm) for a vector $\mathbf{x} = (x_1, \dots, x_n)$ as

$$\|\mathbf{x}\|_p = \left(\sum_{i=1}^n |x_i|^p \right)^{\frac{1}{p}}. \quad (5.42)$$

Choosing $\theta = 1/3$, $p_0 = 4$, $p_1 = 1$, we obtain $p_\theta = 2$, and

$$\|\ell\|_2 \leq \|\ell\|_1^{1/3} \|\ell\|_4^{2/3} \implies \|\ell\|_2^3 \leq \|\ell\|_1 \|\ell\|_4^2. \quad (5.43)$$

Therefore by simple manipulations and taking the squares of both sides of the equality, we can write the following conditions in terms of the vector norms of the operator Schmidt values of a separable density matrix:

$$\left(\frac{\|\ell\|_2^3}{\|\ell\|_4^2} \right)^2 \leq \|\ell\|_1^2 \leq 1/\text{Tr}(\rho_{AB}^2) \implies \text{Tr}(\rho_{AB}^2) \|\ell\|_2^6 \leq \|\ell\|_4^4 \quad (5.44)$$

where we have used the CCNR condition Eq. (1.11). Since

$$\|\ell\|_1 = \sum_{\ell=1}^R \mu_\ell, \quad \|\ell\|_2^6 = \left(\sum_{\ell=1}^R \mu_\ell^2 \right)^3 = 1, \quad \|\ell\|_4^4 = \sum_{\ell=1}^R \mu_\ell^4 = \frac{\text{Tr}(\mathcal{S}\rho_{AB}^{\otimes 4})}{\text{Tr}(\rho_{AB}^2)^2}, \quad (5.45)$$

we obtain the separability condition in terms of quantities that are accessible with randomized measurements from Eq. (5.44)

$$\text{Tr}(\rho_{AB}^2) \leq \frac{\text{Tr}(\mathcal{S}\rho_{AB}^{\otimes 4})}{\text{Tr}(\rho_{AB}^2)^2} \implies \text{Tr}(\rho_{AB}^2)^3 \leq \text{Tr}(\mathcal{S}\rho_{AB}^{\otimes 4}), \quad (5.46)$$

If this relation is violated, then we can confirm that the state ρ_{AB} must be entangled. In stark contrast to the original CCNR condition, both the expression on the left and the expression on the right of the above inequality are directly accessible in an experiment as we show in Fig. 5.3. From the above equation, we can also take logarithms and negate the sign to obtain an equivalent statement in terms of Rényi entropies.

Proposition 7 (Entanglement condition). *Let ρ_{AB} be a bipartite quantum state with Rényi 2-OE $S^{(2)}(\rho_{AB}) = -\log(\sum_{\ell} \mu_\ell^4)$ and Rényi 2-entropy $S_2(\rho_{AB}) = -\log(\text{Tr}(\rho_{AB}^2))$. Then, the relation*

$$S^{(2)}(\rho_{AB}) > S_2(\rho_{AB}) \quad (5.47)$$

implies that ρ_{AB} must be entangled (across the bipartition A vs B).

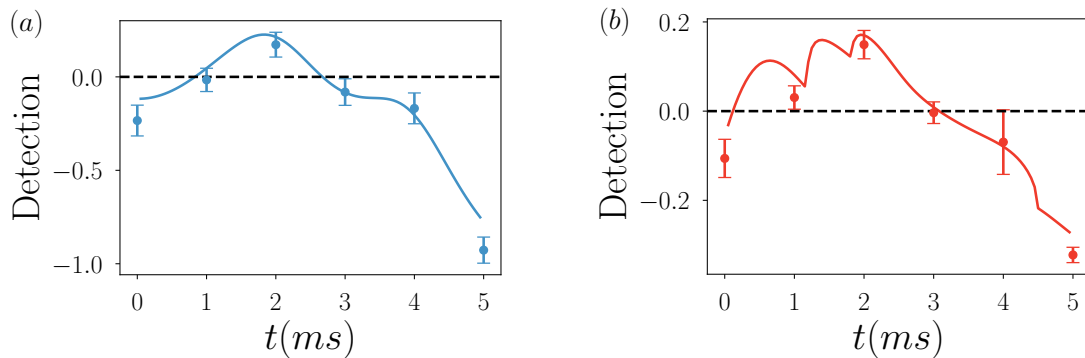


Figure 5.3: *Entanglement detection* — We consider a reduced density matrix ρ_{AB} defined on the subsystem $A = [1, 2]$ and $B = [3, 4]$ for the 10-ion experiment of Ref. [11]. In panel (a), we plot as detection on the vertical axis, the condition given in Proposition. 7 ($S^{(2)}(\rho_{AB}) - S_2(\rho_{AB})$), and similarly in panel (b) we use the optimal condition in Eq. (7) of [80] ($E_{2n}^{\pi}(\rho_{AB}) - 1$). We detect entanglement between the partitions A and B for various times t during the quench dynamics when we observe values greater than 0. The points show experimental results with the error bars calculated with Jackknife resampling. The solid lines correspond to numerical simulations of the unitary dynamics including dissipation.

Finally, we can substantially enhance the ability to detect entanglement by using the enhanced CCNR criteria. The key operation that it involves is to shift the original density matrix by

$$\rho'_{AB} \mapsto \rho_{AB} - \rho_A \otimes \rho_B, \quad (5.48)$$

where $\rho_A = \text{Tr}_B(\rho_{AB})$ and $\rho_B = \text{Tr}_A(\rho_{AB})$ are the reduced density matrices of ρ_{AB} . Note that this shifted density matrix ρ'_{AB} is not physical, because it has negative eigenvalues and a vanishing trace. Let us consider the vector $l' = (\mu'_1, \dots, \mu'_{R'})$ consisting of operator Schmidt decomposition of the shifted density matrix ρ'_{AB} . According to the enhanced realignment condition [53] and given in Eq. (1.12), we have

$$\frac{\|l'\|_2^3}{\|l'\|_4^2} \leq \|l'\|_1 \leq \frac{\sqrt{1 - \text{Tr}(\rho_A^2)} \sqrt{1 - \text{Tr}(\rho_B^2)}}{\sqrt{\text{Tr}([\rho'_{AB}]^2)}} \quad (5.49)$$

and using the same thread of calculations as done earlier we find

$$\sum_{\ell=1}^{R'} \mu_{\ell}^{\prime 4} \geq \frac{\text{Tr}([\rho'_{AB}]^2)}{(1 - \text{Tr}(\rho_A^2))(1 - \text{Tr}(\rho_B^2))} \implies \text{Tr}(\mathcal{S}(\rho'_{AB})^{\otimes 4}) \geq \frac{\text{Tr}([\rho'_{AB}]^2)^3}{(1 - \text{Tr}(\rho_A^2))(1 - \text{Tr}(\rho_B^2))}. \quad (5.50)$$

If this condition is violated, the underlying state must be entangled. Although it requires some additional work, the expression on both sides of this inequality can be re-expressed in terms of linear observables in tensor products of ρ_{AB} , which makes them experimentally accessible.

Moreover, entanglement conditions based on realignment moments have been introduced in [141]. In Figure 5.3, we employ batch shadow estimators to illustrate an example of entanglement detection in mixed states from the experimental data of Ref. [11] using Proposition. 7 and the optimal condition in Eq. (7) of [80], where we clearly observe an enhanced detection capability of the optimal condition. We additionally note that with the finite measurement statistics available from the experiment of Ref. [11], we were unable to extract experimentally, the enhanced

condition derived in Eq. (5.50) and its corresponding optimal condition [80, Eq. (8)] due to large error bars on the experimental data arising from the finite available measurement statistics.

5.3 Conclusion

This chapter was motivated by the prior technical difficulties associated to the RM toolbox to post-process classical shadows from RM data in order to measure quantities involving higher order multi-copy functions such as the QFI or the Rényi 2-OE. Our main technical contribution was to develop a method that we named the batch shadow formalism as a key addition to the RM toolbox. It offers an efficient solution to the pertinent post-processing problem that involves estimating higher order multi-copy functionals from RM data with close statistical performance when compared to the U-statistics estimator. The batch shadow estimator provides drastic runtime improvement compared to the original U-statistics estimator estimated using M classical shadows: $\mathcal{O}(M)$ steps (new) vs. $\mathcal{O}(M^n)$ steps (old). We develop this framework in detail and provide rigorous performance guarantees of it to understand the role of statistical errors involved in the estimates.

The batch shadow estimator enabled us to measure the Rényi 2-OE and consequently observe the entanglement barrier by re-processing existing experimental data. With our analytical framework of batch shadow estimators, we also establish improved sample complexity bounds to evaluate the Rényi 2-OE from batch shadows. To estimate the purity (f_2), Proposition. 5 provides an unconditional reduction from existing bounds of $4^N/\epsilon^2$ [34, 100]. Remarkably, we obtain the same scaling for the fourth order function f_4 , with similar polynomial improvements compared to previous bounds [80]. Additionally, we also derive and experimentally show simple mixed-state entanglement detection criteria according to the CCNR criterion that can be accessed from the RM data. In our accompanying paper [101], we also study the structure of the operator entanglement in the presence of certain symmetries in the system. We define symmetry resolved operator entanglement in presence of $U(1)$ symmetry in addition to the operator entanglement and experimentally measure them.

As an outlook to the batch shadow framework, we could aspire to devise alternate methods to make the post-processing task for classical shadows more scalable and efficient than current methods. In particular, we shall provide a partial solution to the problem in the following short chapter. The main idea is to address the measurement budget of classical shadows (or batch shadows) needed to evaluate multi-copy functions. We will introduce a framework known as *common randomized measurements* that shall help us decrease the measurement cost to estimate multi-copy functions compared to the old uniform sampling of randomized measurements. Thus we expect that by decreasing the measurement cost especially the required number of unitaries (N_U) shall simplify the post-processing cost of the concerned estimates.

6

Common randomized measurements

This chapter is based on the published work: *Benoît Vermersch, Aniket Rath, Bharathan Sundar, Cyril Branciard, John Preskill, and Andreas Elben*. Enhanced estimation of quantum properties with common randomized measurements, *arXiv:2304.12292, 2023* (Ref. [126]) and contains additional results as described in Sec. 6.1.2 and Sec. 6.2.2.

In this work, we introduce the new method that we call common randomized measurements that can reduce statistical errors in the estimation of multi-copy functionals using the classical shadow formalism. My contribution consisted in developing this method and performing the numerical analysis on direct fidelity estimation. I also participated in writing the manuscript along with other coauthors.

Contents

6.1	Main idea & the protocol	113
6.1.1	The common randomized measurement protocol	114
6.1.2	CRM protocol beyond the classical shadows regime	115
6.2	Performance illustrations of the CRM protocol	116
6.2.1	Direct fidelity estimation	117
6.2.2	Purity estimations: common randomized vs importance sampling	119
6.2.3	Higher order estimations: common randomized vs standard shadows	120
6.3	Conclusion	122

In this short chapter, we shall discuss a recently developed proposal to obtain enhanced estimations of quantities of interest from randomized measurement data [126]. As shown earlier in Chapter. 3, we proposed a method based on importance sampling of local random unitaries to reduce the exponential scaling of the required number of measurements to evaluate the purity of an unknown quantum state. This in particular provided improved performance that reduced the statistical error of the “unitary agnostic” estimate of the purity (refer to Eq. (2.28)). An important general question that we can ask now is that: How can we reduce the required number of measurements to evaluate the quantities that can be accessed using the classical shadows formalism? In particular, we are interested in reducing the statistical error in the estimation of the expectation of multi-copy operators (MCOs) $f_n = \text{Tr}(O^{(n)}\rho^{\otimes n})$ that equally suffer from exponential scalings of required measurements as a function of the system size N [31]. This issue has been addressed to reduce the statistical errors in the context of evaluating functions expressed as a single copy observable, i.e functions of the type $f_1 = \text{Tr}(O^{(1)}\rho)$ [63, 56, 55, 133, 123]. Here, our main goal is to provide a method to optimize all functions of interest for $n \geq 1$.

We organize this chapter as follows: We will provide the main idea of our proposal to boost estimations by reducing statistical errors of MCOs. It is inspired by *common random numbers* which is widely used in statistics for variance reduction and will help us introduce the *common randomized measurement* (CRM) protocol. Based on this idea, we will propose the construction of *boosted* estimators of multi-copy functionals using the common randomized (CR) shadows and additionally introduce a new CRM estimate for the unitary agnostic estimator for the purity. And finally we shall illustrate its performance to estimate many interesting quantum properties accessible from the RM data-set via numerical experiments.

6.1 Main idea & the protocol

Consider two random variables \mathbf{X} and \mathbf{Y} and suppose our ultimate goal is to estimate the expectation value of the random variable \mathbf{X} given by $\mathbb{E}[\mathbf{X}]$. We can obtain an estimate of the mean by simply averaging over K collected samples \mathbf{X}_i with $i = 1, \dots, K$. The statistical error associated to the estimator of the mean, as seen in the earlier chapters, can be quantified by the variance $\text{Var}[\mathbf{X}]$. Now, consider that we have at our disposal another random variable \mathbf{Y} which is *correlated* or *dependent* on the variable \mathbf{X} and whose average value $\mathbb{E}[\mathbf{Y}]$ is *known*. More explicitly, we can note that for all i , \mathbf{Y}_i is correlated to its partner \mathbf{X}_i . Then the idea of common random number suggests that $\mathbb{E}[\mathbf{X}]$ can be evaluated by averaging a new random variable $\mathbf{Z} = \mathbf{X} - \mathbf{Y} + \mathbb{E}[\mathbf{Y}]$ for *commonly* sampled variables $\{\mathbf{X}_i, \mathbf{Y}_i\}$ with the guarantee that $\mathbb{E}[\mathbf{Z}] = \mathbb{E}[\mathbf{X}]$. The advantage of doing so is understood when we compute the variance of the new variable \mathbf{Z} . We note that when the condition $\text{Cov}[\mathbf{X}, \mathbf{Y}] = \mathbb{E}[\mathbf{X}\mathbf{Y}] - \mathbb{E}[\mathbf{X}]\mathbb{E}[\mathbf{Y}] > \text{Var}[\mathbf{Y}]/2$ is satisfied, we can estimate $\mathbb{E}[\mathbf{X}]$ with a reduced variance given as

$$\text{Var}[\mathbf{Z}] = \text{Var}[\mathbf{X}] + \text{Var}[\mathbf{Y}] - 2\text{Cov}[\mathbf{X}, \mathbf{Y}] < \text{Var}[\mathbf{X}] \quad (6.1)$$

and this in return could potentially help decrease statistical errors in the estimation of $\mathbb{E}[\mathbf{X}]$. Let us now incorporate this idea and develop the necessary steps to implement common randomized measurements in practical scenarios to evaluate functions of interest more effectively.

6.1.1 The common randomized measurement protocol

The spirit of the common randomized measurement (CRM) protocol is consistent with the phrase “measure first, ask questions late” coined in [31]. The required additional ingredients to perform CRM come at play *only* during the post-processing phase of the protocol. Unlike in the case of importance sampling discussed in Chapter 3, the CRM protocol does not involve any pre-processing optimization step prior to the experimental execution. This presents a possible advantage over importance sampling, as CRM can be easily applied to both existing or future randomized measurement data to boost estimations of the properties that we would like to extract. We shall concretely illustrate this scenario in the subsequent section.

To delve in the details, let us consider for concreteness a N -qubit quantum state ρ prepared on a quantum device. As we have seen in all the previous chapters, we employ randomized measurements that consist of applying random unitaries $U^{(r)}$ with $r = 1, \dots, N_U$ and execute N_M bit-string measurements $\mathbf{s}^{(r,m)} = (s_1^{(r,m)}, \dots, s_N^{(r,m)})$ for each unitary with $m = 1, \dots, N_M$. This data set enables us to define N_U classical shadows as shown in the previous chapters

$$\hat{\rho}^{(r)} = 2^N \sum_{\mathbf{s}, \mathbf{s}'} (-2)^{-D[\mathbf{s}, \mathbf{s}']} \hat{P}_\rho(\mathbf{s}' | U^{(r)}) U^{(r)\dagger} |\mathbf{s}\rangle\langle\mathbf{s}| U^{(r)} \quad (6.2)$$

where $\hat{P}_\rho(\mathbf{s}' | U^{(r)}) = \sum_{m=1}^{N_M} \delta_{\mathbf{s}', \mathbf{s}^{(r,m)}} / N_M$ are the *experimentally estimated* Born probabilities and D is the Hamming distance. The average over the unitaries and the measured bit-strings of the classical shadows satisfies $\mathbb{E}[\hat{\rho}^{(r)}] = \rho$. Now, in order to enhance the estimations of MCOs, we utilize an approximate knowledge of the quantum state ρ prepared in our experiment as previously proposed in the importance sampling protocol [99]. This approximation is provided in terms of a classically representable state σ that theoretically models the experimental state or that can be also constructed from prior RM data. The main idea behind CRM is to classically simulate randomized measurements on the state σ using the *same* random unitaries that are applied in the experiment. In particular, we can define our CR shadows for an applied unitary $U^{(r)}$ as

$$\hat{\rho}_\sigma^{(r)} = \hat{\rho}^{(r)} - \sigma^{(r)} + \sigma \quad (6.3)$$

where we define the object $\sigma^{(r)}$ as

$$\sigma^{(r)} = 2^N \sum_{\mathbf{s}, \mathbf{s}'} (-2)^{-D[\mathbf{s}, \mathbf{s}']} P_\sigma(\mathbf{s}' | U^{(r)}) U^{(r)\dagger} |\mathbf{s}\rangle\langle\mathbf{s}| U^{(r)} \quad (6.4)$$

and $P_\sigma(\mathbf{s}' | U^{(r)}) = \langle\mathbf{s}' | U^{(r)} \sigma U^{(r)\dagger} | \mathbf{s}'\rangle$ is the *exact Born probability* calculated from the *fictitious* projective measurement of the state $U^{(r)} \sigma U^{(r)\dagger}$. Note that this operation is fictitious in the sense that it is performed numerically on a classical device—i.e we rotate and project the state σ with the same unitary $U^{(r)}$ applied in the experiment. This is the operation that allows us to correlate $\hat{\rho}^{(r)}$ and $\sigma^{(r)}$ while having the

knowledge of the mean $\mathbb{E}[\sigma^{(r)}] = \sigma$. Note also that the term $\sigma^{(r)}$ does not suffer from shot-noise due to finite number of measurements as we calculate the exact Born probabilities classically. Thus the average over the unitaries $\mathbb{E}[\sigma^{(r)}] = \mathbb{E}_U[\sigma^{(r)}] = \sigma$. This ultimately results in $\hat{\rho}_\sigma^{(r)}$ being an unbiased estimator of the prepared state ρ as $\mathbb{E}[\hat{\rho}_\sigma^{(r)}] = \rho - \sigma + \sigma = \rho$ for any chosen approximation σ . From this, we see the advantage of the CRM protocol as the data acquisition from the experiment is independent of the choice of the state σ .

To understand intuitively the strength of the CRM protocol, we consider the limit of large number of measurements $N_M \gg 1$. In this limit, if $\rho \approx \sigma$, then the classical shadow $\hat{\rho}^{(r)} \approx \sigma^{(r)}$. In this case, the random variables $\sigma^{(r)}$ and $\hat{\rho}^{(r)}$ (they share the same randomness as they depend on the same random applied unitary $U^{(r)}$) are strongly and positively correlated to one another. This in return reduces the variance of $\hat{\rho}^{(r)} - \sigma^{(r)}$ compared to that of standard classical shadows $\hat{\rho}^{(r)}$ calculated in the previous chapters.

In order to effectively evaluate enhanced estimations of MCOs $f_n = \text{Tr}(O^{(n)}\rho^{\otimes n})$, we can use the batch shadow estimator introduced in the previous chapter. We compute $b = 1, \dots, n'$ batch CR shadows $\tilde{\rho}_\sigma^{(b)} = n'/N_U \sum_{r=(b-1)N_U/n'}^{bN_U/n'} \hat{\rho}_\sigma^{(r)}$ by averaging N_U/n' CR shadows. This enables us to define an enhanced CR estimator $\tilde{f}_n^{(\text{CR})}$ by employing U-statistics [59]

$$\tilde{f}_{n,n'}^{(\text{CR})} = \frac{(n' - n)!}{n'} \sum_{b_1 \neq \dots \neq b_n} \text{Tr} [O^{(n)} (\tilde{\rho}_\sigma^{(b_1)} \otimes \dots \otimes \tilde{\rho}_\sigma^{(b_n)})] \quad (6.5)$$

with $\mathbb{E}[\tilde{f}_{n,n'}^{(\text{CR})}] = f_n$. Additionally, we observe that the adequate measurement budget ($M = N_U N_M$) for the CRM protocol is to take $N_M \gg N_U$ as for the effectiveness of the CR shadow one requires $\hat{\rho}^{(r)} \approx \sigma^{(r)}$ with them differing only due to the finite measurement statistics for a given unitary $U^{(r)}$. The time to post process the CR estimator firstly takes into account the additional routine to construct classically the approximation σ and its corresponding shadows $\sigma^{(r)}$ for $r = 1, \dots, N_U$. As in general, the number of unitaries used in this protocol is greatly reduced compared to the standard batch shadow estimator¹, the batch CR shadow estimator provides an *indirect* method to further reduce the classical post-processing cost to treat the RM data.

6.1.2 CRM protocol beyond the classical shadows regime

As we have seen before, using the RM data-set, we can estimate the purity of a quantum state using the unitary agnostic estimator described in Eq. (2.34) or using classical shadows as shown in Eq. (2.46). Here, we extend the CRM protocol to accommodate the estimation of the purity using the unitary agnostic estimator. We are mainly interested in this estimator as it can be effectively post-processed compared to the batch U-statistics estimator of CR shadows described in Eq. (6.1.1). In particular, with sharp contrast to the importance sampling protocol implemented

¹During the course of this work, we have developed routines that are well optimized and are ready to use to construct shadows for a large number of measurements N_M and do not pose a significant overhead.

for this estimator using σ in the *pre*-processing step of the protocol to sample the adequate unitary transformations, the CRM estimator of the purity shall use σ during the *post*-processing of the protocol to reduce the statistical error of the estimation of the purity. Recalling from Eq. (2.35) that the purity can be estimated using the RM experimental data-set performed on a state ρ as

$$\hat{p}_2 = \frac{1}{N_U} \sum_{r=1}^{N_U} \hat{X}_2^{(\rho)}(U^{(r)}) \quad \text{with} \quad \hat{X}_2^{(\rho)}(U^{(r)}) = \frac{2^N}{N_M(N_M - 1)} \sum_{\substack{m \neq m' \\ m, m'=1}}^{N_M} (-2)^{-D[\mathbf{s}^{(r,m)}, \mathbf{s}^{(r,m')}]} \quad (6.6)$$

with $\mathbb{E}[\hat{p}_2] = p_2$. Having at hand the approximation σ , allows us to classically simulate an estimator using Eq. (2.28) for the same applied unitary $U^{(r)}$ of the experiment:

$$X_2^{(\sigma)}(U^{(r)}) = 2^N \sum_{\mathbf{s}, \mathbf{s}'} (-2)^{-D[\mathbf{s}, \mathbf{s}']} P_\sigma(\mathbf{s}|U^{(r)}) P_\sigma(\mathbf{s}'|U^{(r)}) \quad (6.7)$$

with $P_\sigma(\mathbf{s}|U^{(r)}) = \langle \mathbf{s} | U^{(r)} \sigma U^{(r)\dagger} | \mathbf{s} \rangle$ being the exact Born probability and so that we have $\mathbb{E}_U[X_2^{(\sigma)}(U^{(r)})] = \text{Tr}(\sigma^2)$. As we see, the random variable $X_2^{(\sigma)}(U^{(r)})$ is positively correlated to $\hat{X}_2^{(\rho)}(U^{(r)})$, we can define a CR estimate of the purity as

$$\hat{p}_2^{(\text{CR})} = \frac{1}{N_U} \sum_{r=1}^{N_U} \left[\hat{X}_2^{(\rho)}(U^{(r)}) - X_2^{(\sigma)}(U^{(r)}) \right] + \text{Tr}(\sigma^2) \quad (6.8)$$

that satisfies

$$\mathbb{E} \left[\hat{p}_2^{(\text{CR})} \right] = \mathbb{E} \left[\hat{X}_2^{(\rho)}(U^{(r)}) - X_2^{(\sigma)}(U^{(r)}) + \text{Tr}(\sigma^2) \right] = p_2 - \text{Tr}(\sigma^2) + \text{Tr}(\sigma^2) = p_2. \quad (6.9)$$

Note again that in the limit $N_M \gg 1$, the closer the state σ approximates the prepared state ρ , the more correlated are the variables $\hat{X}_2^{(\rho)}(U^{(r)})$ and $X_2^{(\sigma)}(U^{(r)})$ that lead to variance reduction of the estimator $\hat{p}_2^{(\text{CR})}$ compared to \hat{p}_2 .

In the following section, we shall showcase the strengths of the CRM protocol in comparison to the standard RM protocol. In our work [126], we present a formal analysis on the variance study of the CRM estimator. Here in particular, we will compliment further our work with several case studies of examples starting from single-copy observables such as the direct fidelity estimation. We will then compare numerically the performance of CRM with respect to importance sampling to evaluate the purity and lastly we will establish the protocol's relevance to enhance the estimation of higher order functions of interest such as the lower bounds of the quantum Fisher information (QFI).

6.2 Performance illustrations of the CRM protocol

This section shall focus on providing some insights on the performance of the CRM protocol compared to that of the standard (or uniform) RM protocol. In

particular, we will be interested to observe the performance highlights for different types of quantities, starting from linear observables ($f_1 = \text{Tr}(O^{(1)}\rho)$), to the purity ($\text{Tr}(\rho^2)$) and higher order functions of the density matrix such as the bounds of the QFI (F_0 and F_1) introduced in Chapter. 4. For the purity evaluated for larger system-sizes with the ‘unitary-agnostic’ estimator, we shall study the error scalings of the CRM protocol compared to that of importance sampling introduced in Chapter. 3.

6.2.1 Direct fidelity estimation

Let us begin by providing an instructive analysis of the performance highlights of CRM shadows in the context of standard (single-copy) observables. For this case, many methods improving over standard classical shadows, e.g. Refs. [56, 55, 63, 133, 123] have been already developed. These methods rely on adapting randomized measurements performed on the experiment, eg using importance sampling of measurement settings, in a way that depends on the operator $O^{(1)}$. Here, instead, we build CR shadows from the data of standard classical shadows in an operator agnostic manner. We can boost the estimations of various observables from a single experimental data-set.

To demonstrate the explicit use of this feature, we consider here the example of direct fidelity estimation (DFE) [41, 114]. Here, one aims to estimate the fidelity \mathcal{F} of a prepared quantum state in the experiment ρ to a pure theoretical target state $|\phi\rangle$. The observable of interest is the projector on a theory state $O^{(1)} = |\phi\rangle\langle\phi|$, so that $\mathcal{F}_\phi = \langle O^{(1)} \rangle = \langle \phi | \rho | \phi \rangle$. In Refs [41, 114], DFE is realized by performing importance sampling of Pauli measurements according to the distribution of the theory state over Pauli strings. This means that an experimental data-set can be used to test *only* one theory state $|\phi\rangle$. In contrast, our approach allows to estimate the fidelity of a state with respect to arbitrary many theory states, from a single data-set. This could be of interest to check the overlap of the experimental state with multiple family of theory modelling such as mean-field approximations, stabilizer formalism [50], tensor-networks [113], etc. In addition, the CRM protocol allows us to choose the theory state after the experiment is performed. This for example is relevant in the case when a costly numerical computation triggered by an experimental result has to be run (in the spirit ‘measure first, ask question later’ of the RM toolbox [31]).

In our illustration, we consider a N -qubit ‘ideal’ state $|\psi\rangle$, prepared with a uni-dimensional random circuit composed of d alternated layers of single and two qubit Haar-random gates. These generated states are represented as Matrix-Product-States (MPS) using the PastaQ library [40]. We consider two scenarios: First in which the experimental state is prepared perfectly $\rho = |\psi\rangle\langle\psi|$, and secondly in which it is prepared with imperfect gates where each gate is subjected to local depolarization noise with probability p leading to a mixed prepared state ρ . We estimate the fidelities $\mathcal{F}_\phi = \text{Tr}(\sigma\rho) = \langle \phi | \rho | \phi \rangle$, for various approximations $\sigma = |\phi\rangle\langle\phi|$, which are obtained by truncating the exact output state of the noiseless quantum circuit $|\psi\rangle$ at different bond dimensions χ of the MPS. For estimating \mathcal{F}_ϕ , we use the density matrix σ as a prior to define the CR shadow as given in Eq. (6.3). We numerically simulate an experimental scenario in which we would like to benchmark multiple states σ with a fixed target state ρ prepared in the experiment. We collect a RM data-set consisting of Pauli measurements using N_U random unitaries

$U^{(r)} = \bigotimes_{i=1}^N U_i^{(r)}$ where each $U_i^{(r)}$ is uniformly sampled in $\left\{ \mathbb{1}_2, \frac{1}{\sqrt{2}} \begin{pmatrix} 1 & -1 \\ 1 & -1 \end{pmatrix}, \frac{1}{\sqrt{2}} \begin{pmatrix} 1 & -i \\ 1 & +i \end{pmatrix} \right\}$ so that $U_i^\dagger Z U_i = Z, X, Y$ with Z, X, Y being single qubit Pauli matrices. This is followed by N_M bit-string measurements performed on the ‘experimental’ state ρ (for both the ideal and noisy case)². From this data-set, the estimator of \mathcal{F}_ϕ can be evaluated from N_U CR shadows as

$$\widehat{\mathcal{F}}_\phi = \frac{1}{N_U} \sum_{r=1}^{N_U} \text{Tr}(\sigma \hat{\rho}_\sigma^{(r)}) = \frac{1}{N_U} \sum_{r=1}^{N_U} \text{Tr}(\sigma [\hat{\rho}^{(r)} - \sigma^{(r)} + \sigma]). \quad (6.10)$$

The standard (Pauli) shadow estimator can be simply computed by considering that $\sigma^{(r)} = \sigma = 0, \forall r$.³

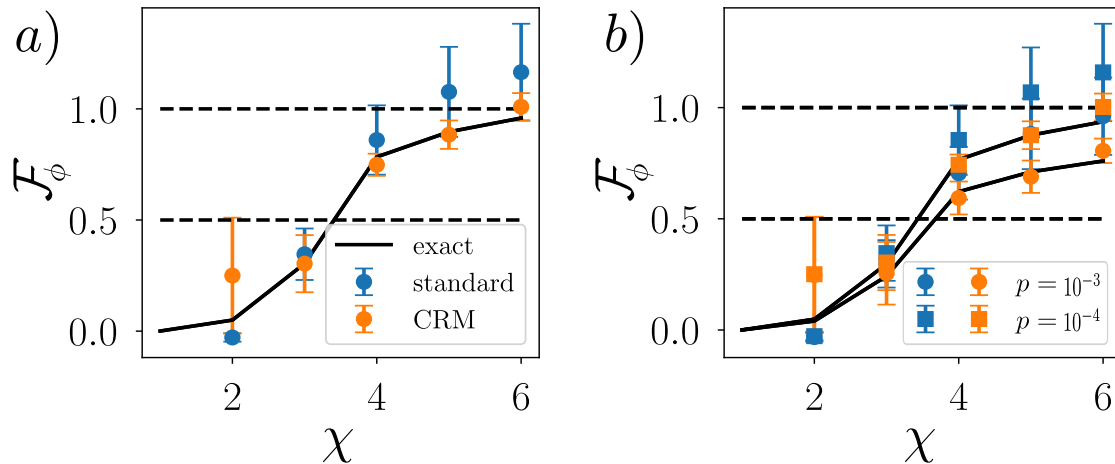


Figure 6.1: *Fidelity estimation in (noisy) random quantum circuits* — Panel a) shows the estimated fidelities $\widehat{\mathcal{F}}_\phi$ of the prepared state ρ and the theoretical prior states $\sigma = |\phi\rangle\langle\phi|$ as a function of their bond dimension χ . Here, ρ is a $N = 30$ -qubit pure state generated from an ideal noiseless ($p = 0$) random quantum circuit of depth $d = 6$ and $|\phi\rangle$ are obtained by truncating ρ to bond dimension χ . In panel b), each gate in the circuit is perturbed by local depolarization noise with strength p resulting in a mixed state ρ . The prior state σ is the same as in a). For both panels, we compare CRM estimation (orange dots) with standard shadow estimation (blue dots). We fix $N_U = 15$ and $N_M = 10^5$. The error-bars are evaluated as standard errors of the mean over random unitaries. The black solid lines denote the exact fidelity \mathcal{F}_ϕ . The black dashed lines are guides to the eye for 0.5 and 1 respectively.

Fig. 6.1 shows the estimations $\widehat{\mathcal{F}}_\phi$ for a $N = 30$ qubit noiseless [$p = 0$, panel a)] and noisy state [$p = 10^{-3}, 10^{-4}$, panel b)], with error bars calculated as the standard error of the mean over random unitaries. When χ increases, the estimated fidelity \mathcal{F}_ϕ increases, and the error bars of the CRM estimations decrease as the CR shadows become more accurate ($\hat{\rho}^{(r)}$ becomes more positively correlated to $\sigma^{(r)}$). At small χ instead, the CR shadows fail to provide improved estimations and have larger error bars compared to (standard) classical shadows as seen in Fig. 6.1a). These features are similarly observed in the case of the noisy experimental state in Fig. 6.1b), where the pure state $|\phi\rangle$ remains always different from the mixed state ρ .

²With this data-set we can construct Pauli shadows as shown in the appendix of [64].

³We note that σ does not need to be a valid density matrix (does not need to satisfy $\sigma \geq 0$ and $\text{Tr}(\sigma) = 1$).

6.2.2 Purity estimations: common randomized vs importance sampling

We shall now move the discussion to investigate the performance of evaluating the purity of a quantum state with the CR estimation in comparison to the estimation of importance sampling (IS). Particularly, we will be interested to analyze the performance of ‘unitary-agnostic’ estimator of the purity. In order to simulate a realistic experimental scenario, we consider for convenience N -qubit noisy GHZ states $\rho(p) = (1 - p) |\psi_{\text{GHZ}}^N\rangle\langle\psi_{\text{GHZ}}^N| + p\mathbb{1}/2^N$ with p being the depolarization noise strength. As an approximation of the prepared state, we consider a priori the knowledge of the ideal GHZ state $\sigma = |\psi_{\text{GHZ}}^N\rangle\langle\psi_{\text{GHZ}}^N|$ for the case of the CRM and the IS protocol. Our goal is to gauge the general performance in terms of the scaling of the average statistical error $\mathcal{E} = |\hat{p}_2 - p_2|/p_2$ computed over 100 simulated experimental runs of the RM protocol. For both the standard and CRM protocol as mentioned earlier, the data acquisition remains the same as we sample *uniformly* N_U random unitaries from the circular unitary ensemble and apply them on the state ρ . On the other hand, in the case of importance sampling, we sample N_U random unitaries from the *importance sampling* distribution introduced in Eq. (3.3) of Chapter. 3 where we build $[X_2(U)]_{\text{IS}}$ from the knowledge of state σ at the pre-processing stage of the protocol. Note equally that the CRM protocol uses the same knowledge σ of the state only during the post-processing stage. After the unitary operations, the rotated state is then projected N_M times in the computational basis.

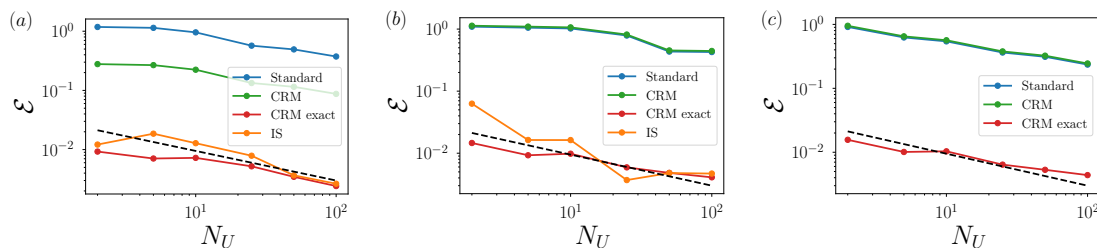


Figure 6.2: *Purity estimation for standard (uniform), CRM and IS estimators* — Panels (a) and (b) show the scaling of the average statistical error \mathcal{E} as function of the number of unitaries N_U for total system size of 24 qubits. The ‘experimental’ state $\rho(p)$ is taken for two different values of noise strengths of $p = 0.1$ and $p = 0.3$ for panel (a) and (b) respectively. Panel (c) shows the average statistical error for a 12-qubit reduced state taken from a total system of 24 qubits extracted for the CRM and standard (uniform) estimates from the same RM data-set as in panel (a) (where $p = 0.1$). We have considered here $N_M = 5 \cdot 10^7$. The black dashed line is a guide to the eye $\propto 1/\sqrt{N_U}$.

In Fig. 6.2, we consider $\rho(p)$ to be a 24-qubit noisy GHZ state and fix $N_M = 5 \cdot 10^7$. In particular, Fig. 6.2(a-b) shows the statistical error scaling for all the three protocols (standard or uniform, CRM, ‘CRM exact’ and IS) as a function of the number of applied random unitaries N_U for two different values of noise strength. In particular, the ‘CRM exact’ represents a scenario where we have a perfectly benchmarked quantum device in terms of a theoretical state σ that faithfully represents the ‘experimental’ state ρ including all its decoherence parameters. In our simulations for the CRM exact method, we take the theoretically modelled state to be $\sigma = \rho(p)$. Correspondingly, the purity of the state $\rho(p)$ was noted to be $p_2 \sim 0.81$ and $p_2 \sim 0.49$ for $p = 0.1$ and $p = 0.3$ respectively. We note that the purity decreases with an increase of the noise strength p and we get a mixed state $\rho(p)$.

At first, we observe clearly that both CRM and the IS protocol provide better estimations of the purity compared to uniform sampling while having a fidelity given by $\langle \psi_{\text{GHZ}}^N | \rho(p=0.1) | \psi_{\text{GHZ}}^N \rangle \sim 0.9$ and $\langle \psi_{\text{GHZ}}^N | \rho(p=0.3) | \psi_{\text{GHZ}}^N \rangle \sim 0.7$ with respect to the ideal GHZ state. Interestingly, we observe from Fig. 6.2(a-b) that the IS protocol outperforms the CRM protocol in terms of statistical error scalings. The ‘CRM exact’ performs equally well compared to the IS protocol while requiring an exact description of the prepared state. In realistic experiments, it could be challenging to obtain an exact theoretical model of the decoherence. If such a decoherence model is available (or would be available in the future), it can be readily used to obtain enhanced estimations of the purity based on the CRM framework⁴. On the contrary, we see that this knowledge (of the exact decoherence model) is not necessary for the IS protocol in order to obtain optimal performances compared to other methods.

We also observe from Fig. 6.2(c) that the CRM and ‘CRM exact’ frameworks equally allow us to obtain the enhanced estimations of the purity of sub-systems of interest from the *same* numerically recorded RM data-set of Fig. 6.2(a). Here, we have considered the half-partition reduced state $\rho_{\text{red}}(p) = \text{Tr}_{1,\dots,N/2}[\rho(p)]$ of 12 qubits of the full 24-qubit GHZ state for $p = 0.1$. We obtain the corresponding enhanced estimations with CRM (and CRM exact) by incorporating the knowledge of the state of the sub-system $\sigma_{\text{red}} = \text{Tr}_{1,\dots,N/2}(\sigma)$ ($\sigma_{\text{red}} = \text{Tr}_{1,\dots,N/2}[\rho(p)]$ respectively). We observe that, for a fixed measurement budget ($M = N_U N_M$), as the CRM protocol optimizes the purity estimation of the full system (24 qubits in Fig.6.2(a)), it equally guarantees the reduction of statistical errors in the estimates of the relevant sub-system purities. We note that this advantage is completely absent in the case of the IS protocol, which requires importance sampling new set of unitaries based on the distribution that depends on the relevant sub-system to obtain optimal purity estimations of the same (as illustrated for example in Sec. 3.4.4 of Chapter. 3). Lastly, we remind that, the IS protocol introduced in Chapter. 3 is restricted to quantities such as purities or cross platform fidelities [32] while the CRM protocol can be applied to probe arbitrary multi-copy functionals of the state via the classical shadow formalism. In the next section, we shall show the advantages of the CRM protocol for such quantities of interest.

6.2.3 Higher order estimations: common randomized vs standard shadows

For our last and final illustration, we take the example of the estimation of the QFI using the classical shadow formalism as previously discussed in Chapter. 4. We consider evaluating the first two bounds F_0 and F_1 using both the standard (uniform) and CR shadows and compare their respective performances. As introduced earlier in this chapter and recalling Eq.(4.13) in Chapter. 4, we can provide unbiased U-statistics estimators for the bounds F_0 and F_1 by constructing $r = 1, \dots, N_U$ CR

⁴This knowledge can also be used to perform a more accurate importance sampling of the random unitaries.

shadows as

$$\begin{aligned}\hat{F}_0 &= \frac{4}{2!} \binom{N_U}{2}^{-1} \sum_{r_1 \neq r_2} \text{Tr}(\hat{\rho}_\sigma^{(r_1)} [\hat{\rho}_\sigma^{(r_2)}, \mathcal{A}] \mathcal{A}), \\ \hat{F}_1 &= 2\hat{F}_0 - \frac{4}{3!} \binom{N_U}{3}^{-1} \sum_{r_1 \neq \dots \neq r_3} \text{Tr}(\hat{\rho}_\sigma^{(r_1)} \hat{\rho}_\sigma^{(r_2)} [\hat{\rho}_\sigma^{(r_3)}, \mathcal{A}] \mathcal{A})\end{aligned}\quad (6.11)$$

where we recall that \mathcal{A} is an Hermitian operator and $\hat{\rho}_\sigma^{(r)} = \hat{\rho}^{(r)} - \sigma^{(r)} + \sigma$. Note that by taking the approximate state $\sigma = 0$, one recovers the standard estimator of U-statistics as given in Eq. (4.13).

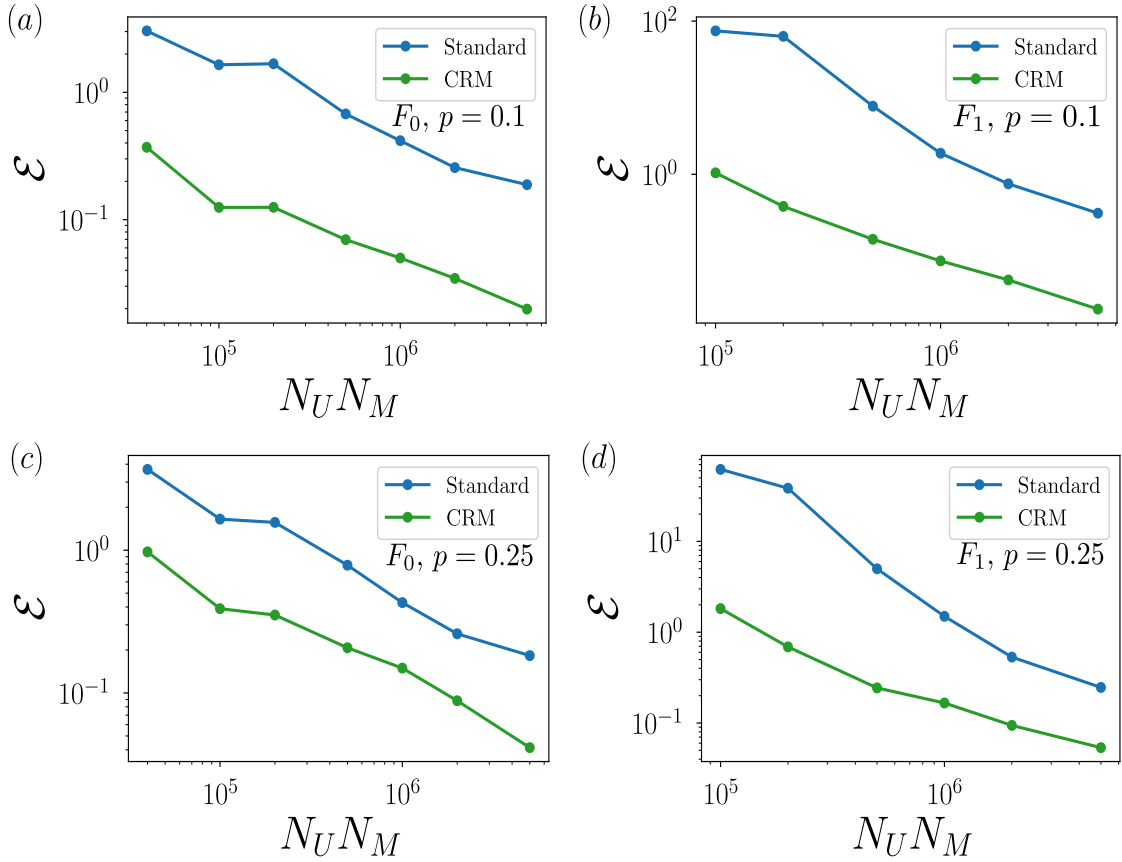


Figure 6.3: *Higher order function estimation for standard (uniform) and CRM estimators* — Panels (a-b) for $p = 0.1$ and panel (c-d) for $p = 0.25$, show the scaling of the average statistical error \mathcal{E} in the estimation of the lower bound F_0 (panels (a) and (c)) and F_1 (panels (b) and (d)) as function the number of measurements $N_U N_M$ for a 10-qubit noisy ground state $\rho_G(p)$. We have fixed $N_M = 2 \cdot 10^4$.

For our case study, we consider the ground state $|\psi_G\rangle$ of the transverse field Ising model (TFIM) at the critical point. We recall that the TFIM Hamiltonian reads as

$$H = -J \sum_i Z_i Z_{i+1} - h \sum_i X_i \quad (6.12)$$

with Z_i and X_i being the Pauli- z and Pauli- x matrices acting on the qubit i . Here h is the transverse field and we take $J = 1$. As described before this Hamiltonian

displays a quantum phase transition at $h = 1$ where it features non-trivial multipartite entanglement that can be probed using the QFI. In order to relate our numerical simulations to a real experimental scenario, we consider noisy prepared ground states where the noise is modelled by global depolarization. Thus we study states of the type $\rho_G(p) = (1 - p) |\psi_G\rangle\langle\psi_G| + p\mathbb{1}/2^N$ with p being the strength of the noise. This study is inspired by our prior experimental investigation in Sec. 4.3.2 of Chapter. 4 where we estimated the QFI (using the lower bounds) for the noisy ground states prepared via the QAOA algorithm. In particular, to effectively construct CR shadows, we consider having at hand the ideal theory state $\sigma = |\psi_G\rangle\langle\psi_G|$ unaffected by noise.

We perform 100 numerical simulations of the RM experimental protocol to calculate the average statistical error $\mathcal{E} = |\hat{F}_n - F_n|/F_n$ for $n = 0, 1$ as a function of different values of N_U and for two distinct values of the noise parameter p . We fix the number of measurements $N_M = 2 \cdot 10^4$. Fig. 6.3 displays the results on the average statistical error for a noisy $N = 10$ qubit ground state as a function of the measurement budget $N_U N_M$. In general, we clearly observe favorable statistical error scaling by using the CRM protocol to estimate higher order functionals compared to the standard shadow protocol. This implies that to achieve a fixed error accuracy in terms of \mathcal{E} , the CRM protocol requires less measurements compared to standard shadow protocol. The true values of the lower bound for the noisy ground states are $F_0 = 33.33$ and $F_1 = 36.66$ for $p = 0.1$ and $F_0 = 23.15$ and $F_1 = 28.92$ for $p = 0.25$ respectively. We can observe some interesting features from our numerical simulations. Fig. 6.3(a-b) (similarly for panels Fig. 6.3(c-d)) that has the fidelity $\langle\psi_G|\rho_G(p = 0.1)|\psi_G\rangle \sim 0.9$ greater than $\langle\psi_G|\rho_G(p = 0.25)|\psi_G\rangle \sim 0.75$, we see better improvement of statistical error scaling for both the lower bounds. This is due to the fact that the ideal state σ is more positively correlated to the ‘experimental’ ground state $\rho_G(p)$ when the noise strength p is lower. This is directly reflected by the values of the fidelity shown earlier.

Lastly, we also remark for a fixed noise strength p that by comparing Fig. 6.3(a) and (c) with the panels Fig. 6.3(b) and (d), the higher order bound F_1 suffers more from statistical errors compared to F_0 for both the standard and the CR estimator. Thus the CRM framework becomes essential in tackling and providing enhanced estimations of higher order functionals compared to the standard shadow protocol.

6.3 Conclusion

In this chapter, we introduced the common randomized measurement protocol that enables us to reduce statistical errors in the estimations of any multi-copy observables that can be estimated using the RM-data. The CRM protocol incorporates an approximate knowledge of the quantum state at the post-processing stage of the randomized measurement experiments. It perfectly captures the slogan of the RM toolbox “measure first, ask questions later” as it can be readily applied on past or future RM data in order to enhance estimations of quantum properties of interest.

We have studied its performance for multiple quantities starting from linear ob-

servable in the context of direct fidelity estimation, to the purity and also higher order functionals such as lower bounds to the QFI. We showed through our numerical experiments that the statistical errors were reduced compared to the standard (uniform) estimator for all the quantities mentioned above. In particular, we also discussed a potential advantage of the CRM protocol compared to that of the IS protocol. Though the IS protocol provides optimal performances even for noisy states probed from an ideal theoretical distribution, we see that the CRM protocol provides an added advantage to obtain enhanced estimation of the purity for all sub-systems of interest from the *same* experimental data at the post-processing stage. Additionally, inspired by our previous work on estimating the QFI [100], in our work [126], we also demonstrate the effectiveness of the CRM protocol to estimate the von Neumann entropy by extrapolating it in terms of a polynomial approximation of the density matrix ρ . This polynomial approximation allows us to implement the RM toolbox to measure and provide an alternate method to measure the von Neumann entropy without the need of quantum state tomography.

The CRM framework can also be applied for a wide range of applications such as gradient estimation in variational quantum algorithms [109], probing of quantum phases of matter [65, 78, 88] and also constructing improved robust shadows with finite measurement statistics as done in our work [129, Appendix. B3].

7

Conclusions and perspectives / Conclusions et perspectives en français

The principal objective of this thesis was to clearly present solutions to pertinent questions that surrounded the randomized measurement (RM) toolbox by using a combination of both analytical and numerical techniques which would help us investigate new properties associated to entanglement created in large quantum platforms of today. Here, we will briefly summarize the key results presented in this manuscript and end the discussion with some interesting existing problems that can be of interest to work on in the future.

The first objective that we addressed in this manuscript was to develop methods to fight against statistical errors encountered by the RM protocol to be able to estimate quantities of interest in larger system-sizes of interest. We provide two solutions to this problem that are described in Chapter. 3 and Chapter. 6. Firstly, as discussed in Chapter. 3 and in Ref. [99], we presented a protocol to reduce statistical errors in the estimation of the purity using the unitary agnostic approach of the RM toolbox [30, 11]. The previous proposed method can be used to measure the purity in (sub-)system sizes in the range of 10 – 15 qubits [11]. Our new method uses a prior *approximate knowledge* in terms of classically modelling the prepared quantum state to perform *importance sampling* of the local random unitaries. As we demonstrated analytically and also in various case studies by simulating the RM experiment numerically, this collection of unitaries reduced statistical errors compared to a collection of unitaries that were sampled uniformly from the Haar measure. Thus our method that is readily applicable in experiments allows one to probe the purity (or the second Rényi entropy) of (sub-)system sizes in the range of 25 – 30 qubits which was out of reach before.

Secondly, not restricting ourselves only to the purity, as shown in Chapter. 6 and in Ref. [126], we developed another method that helps us extend our previous results to be applicable to various other properties of interest that can be assessed in particular using the classical shadow formalism [64]. These quantities especially can be expressed as either polynomials $\text{Tr}(\rho^n)$ or multi-copy functionals $\text{Tr}(O^{(n)}\rho^{\otimes n})$

of the quantum state ρ . The method bases itself on the notion of *common random numbers* and thus is dubbed as *common randomized measurements*. It once again relies on a classical approximation of the quantum state prepared in the experiment. In contrast to the importance sampling method, here the additional ingredients of the procedure are applied only in the post-processing stage of the RM protocol (note that here the unitaries are sampled uniformly). Thus it can be readily used to boost quantities estimated in the past and also in the future from the RM data. Additionally, it also allows us to boost estimations for all sub-systems of interest of the quantum system. In terms of its practical use, this method can boost estimation of quantities of interest compared to the standard formalism of classical shadows for (sub-)system sizes upto 15 – 16 qubits depending on the available classical memory.

Another central work of this manuscript was to develop a protocol to access non-linear quantities that can not be explicitly expressed in terms of polynomials or multi-copy operators of the quantum state. In this context, we were interested to estimate the highly non-linear quantity known *quantum Fisher information* (QFI) and extend the RM toolbox to probe features associated to multipartite entanglement in quantum systems. The QFI is an important quantity for metrological applications [94] as it validates the presence of multipartite entanglement via the *entanglement depth* of the underlying quantum state [67, 122]. We circumvented the challenge to measure the QFI, which was earlier only possible either by using an expensive measurement method of quantum state tomography or could be effectively estimated in the case of a thermal state via dynamical susceptibilities [58]. This was discussed in Chapter. 4 and in Ref. [100]. We proposed a novel method to estimate the QFI by constructing a polynomial series of lower bounds in function of the density matrix that converges to the QFI. Each of these bounds can be estimated from the classical shadow formalism at a lower measurement cost in comparison to quantum state tomography. Additionally, this work also motivated the development of rigorous sample complexity bounds to gauge the required number of measurements needed to estimate arbitrary multi-copy functionals that are accessible via the classical shadow formalism.

In this manuscript, we also addressed a pertinent practical problem of the RM toolbox. The practical issue that we treat rose from the fact that the data treatment associated with the classical shadow formalism required an expensive classical post-processing cost. To evaluate the unbiased estimators of multi-copy functions of interest of higher order ($n > 3$) and for larger system-sizes via the U-statistics estimator soon presents a computational bottleneck as it requires summing over all possible combinations of n distinct classical shadows. As a solution to this problem developed in Chapter. 5 and in Ref. [101], we proposed an alternate formalism known as the *batch shadow formalism* to obtain unbiased estimators of arbitrary functions of interest and analytically provide sample complexity bounds to understand its performance. Given a RM dataset consisting of M random unitaries, the batch shadow formalism reduces the computational run-time cost of post-processing a n order function compared to the previous U-statistics estimator from $\mathcal{O}(M^n)$ (old) to $\mathcal{O}(M)$ (new) steps while providing similar statistical performances.

Lastly, as this manuscript is centered around protocols based on randomized measurements that can be experimentally implemented to measure interesting properties related to entanglement in quantum platforms; with the methods and protocols developed in this manuscript, we were able to experimentally observe and validate

novel entanglement properties prepared in two different types of quantum hardware: a quantum computer consisting of superconducting qubits and a trapped ion quantum simulator. Firstly, in Chapter. 4 and in Ref. [100], we measured the QFI by employing the RM toolbox via the converging series of lower bounds for two kinds of quantum states prepared on an IBM superconducting quantum device: GHZ states and ground state of the transverse field Ising model (TFIM) at the critical point using the QAOA algorithm. Using the batch shadow formalism and other advanced tools that included mitigating errors of the RM protocol [15, 76], we validated the presence of multipartite entanglement in all of our prepared quantum states upto system size consisting of 13 qubits. Secondly, in Chapter. 5 and in Ref. [101], again using the batch shadow formalism we re-analyzed the existing randomized measurement data of a prior experiment performed on a trapped ion quantum simulator in Ref. [11] to observe for the first time an interesting property associated to entanglement known as the *entanglement barrier*. We estimate the second Rényi operator entanglement entropy (Rényi 2-OE, a fourth order function) from the experimental data that presents the signature of the entanglement barrier. Additionally, we experimentally validate the presence of entanglement in mixed states with a new entanglement condition derived based on the CCNR criterion.

We believe that the work presented in this manuscript paves the way for the future to investigate interesting properties associated to entanglement to benchmark quantum states prepared in new experimental platforms. For the future, it would be interesting to study and work on various possible extensions of the randomized measurement protocol and methods that we have introduced during the course of this manuscript. From a wider perspective, one can say that there still exists two main bottlenecks that still prevent the RM toolbox to reach its full potential: (i) the RM protocol now suffers from a *reduced* exponential scaling of the required number of measurements due to statistical errors as a function of the system size, (ii) for the classical shadow formalism, the required classical memory prevents us from post-processing the *effective* batch shadow estimators for system-sizes more than $N \sim 16$. Possible solutions would require us to develop strategies to implement randomized measurements that would require *polynomial* number of measurements as a function of system-size. On the other hand, one could think of incorporating memory efficient framework of tensor networks to potentially solve the classical memory issue. This would lead to an efficient technique to post-process RM dataset of larger system-sizes on classical hardware in order to estimate classical shadow functionals of interest.

A possible direction of investigation could be to develop a formalism to perform importance sampling applicable for classical shadows that could present a new alternate method to fight against statistical errors in the estimation of multi-copy functionals. Based on the preliminary studies presented in Chapter. 6, one can perform a rigorous inspection to understand the performance improvements obtained by *separate or combination* of the proposed methods of importance sampling and common randomized measurements. It would be also interesting to consider a data-driven approach in the form of an adaptive scheme to iteratively adapt the importance sampling distribution on prior RM data taken in the experiment.

From the view point of entanglement detection, one can propose an optimal unifying criterion to detect entanglement solely based on the entanglement detection quantities accessible by the RM toolbox. This can help certify entangled states based

on a single experimental framework of randomized measurements and beyond the limitation of certain criteria. Lastly, I would like to acknowledge the support by Laboratoire d'excellence LANEF in Grenoble and from the Grenoble Nanoscience Foundation for this PhD work.

Conclusions et perspectives en français

L'objectif principal de cette thèse était de présenter clairement des solutions aux questions pertinentes qui entourent la boîte à outils de la mesure aléatoire (RM toolbox) en utilisant une combinaison de techniques analytiques et numériques qui nous aideraient à étudier de nouvelles propriétés associées à l'intrication créée dans les grandes plateformes quantiques d'aujourd'hui. Ici, nous résumerons brièvement les résultats clés présentés dans ce manuscrit et nous terminerons la discussion par quelques problèmes existants intéressants sur lesquels il pourrait être intéressant de travailler à l'avenir.

Le premier objectif que nous avons abordé dans ce manuscrit était de développer des méthodes pour lutter contre les erreurs statistiques rencontrées par le protocole RM pour estimer les quantités d'intérêt dans des systèmes de plus grande taille. Nous proposons deux solutions à ce problème qui sont décrites dans les chapitres. 3 et au chapitre. 6. Tout d'abord, comme indiqué au chapitre. 3 et dans Ref. [99], nous avons présenté un protocole visant à réduire les erreurs statistiques dans l'estimation de la pureté (purity estimations) en utilisant "l'approche agnostique unitaire" de la boîte à outils RM [30, 11]. La méthode courante proposée peut être seulement utilisée pour mesurer la pureté dans des tailles de (sous-)systèmes de l'ordre de 10 à 15 qubits [1]. Notre nouvelle méthode utilise *des connaissances approximatives* préalables en termes de modélisation classique de la structure de l'état quantique préparé pour effectuer *un échantillonnage d'importance* des unitaires aléatoires locaux. Comme nous l'avons démontré analytiquement et également dans diverses études de cas en simulant numériquement l'expérience RM, cette collection d'unitaires réduit les erreurs statistiques par rapport à une collection d'unitaires échantillonnés uniformément à partir de la mesure de Haar. Ainsi, notre méthode, qui est facilement applicable dans les expériences, permet de sonder la pureté (ou la seconde entropie de Rényi) de (sous-)systèmes de taille comprise entre 25 – 30 qubits, ce qui était hors de portée auparavant.

Deuxièmement, ne pas se limiter à la pureté, comme le montrent le chapitre. 6 et dans Ref. [126], nous avons mis au point une autre méthode qui nous permet d'étendre nos résultats précédents à diverses autres propriétés intéressantes qui peuvent être évaluées en particulier à l'aide du formalisme de classical shadows [64]. Ces quantités peuvent notamment être exprimées comme suit polynômes $\text{Tr}(\rho^n)$ ou des fonctionnelles multi-copies $\text{Tr}(O^{(n)}\rho^{\otimes n})$ de l'état quantique ρ . La méthode se base sur la notion de *nombres aléatoires communs* et est donc appelée *des mesures aléatoires communs*. Elle repose à nouveau sur une approximation classique de l'état quantique préparé dans l'expérience. Contrairement à la méthode de l'échantillonnage d'importance, les ingrédients supplémentaires de la procédure ne sont appliqués ici qu'au stade du post-traitement du protocole RM (notons qu'ici les unitaires sont échantillonnés uniformément). Elle peut donc être facilement utilisée pour améliorer les quantités estimées dans le passé et dans le futur à partir des données du RM. En outre, elle nous permet également de renforcer les estimations pour

tous les sous-systèmes d'intérêt du système quantique. En termes d'utilisation pratique, cette méthode peut améliorer l'estimation des quantités d'intérêt par rapport au formalisme standard des classical shadows pour des tailles de (sous-)systèmes allant jusqu'à 15 – 16 qubits en fonction de la mémoire classique disponible.

Un autre travail central de ce manuscrit a consisté à développer un protocole pour accéder à des données non linéaires des quantités qui ne peuvent pas être explicitement exprimées en termes de polynômes ou d'opérateurs multi-copies de l'état quantique. Dans ce contexte, nous nous sommes intéressés à l'estimation de la quantité hautement non linéaire connue sous le nom *d'information de Fisher quantique* (QFI) et à l'extension de la boîte à outils RM pour sonder les caractéristiques associées à l'intrication multipartite dans les systèmes quantiques. La QFI est une quantité importante pour les applications métrologiques [94] car elle valide la présence d'une intrication multipartite via la profondeur d'intrication de l'état quantique [67, 122]. Nous avons contourné le défi de la mesure du QFI, qui n'était auparavant possible qu'en utilisant une méthode de mesure coûteuse de tomographie de l'état quantique ou qui pouvait être estimée efficacement dans le cas d'un état thermique via les susceptibilités dynamiques [58]. Ce point a été discuté au chapitre 4 et dans Ref. [100]. Nous avons proposé une nouvelle méthode pour estimer le QFI en construisant une série polynomiale de limites inférieures en fonction de la matrice de densité qui converge vers le QFI. Chacune de ces bornes peut être estimée à partir du formalisme de classical shadows à un coût de mesure inférieur à celui de la tomographie de l'état quantique. En outre, ce travail a également motivé le développement de limites rigoureuses de complexité d'échantillonnage pour évaluer le nombre requis de mesures nécessaires pour estimer des fonctionnelles multi-copies arbitraires qui sont accessibles via le formalisme de classical shadows [64].

Dans ce manuscrit, nous avons également abordé un problème pratique pertinent de la boîte à outils RM. Le problème pratique que nous traitons provient du fait que le traitement des données associé au formalisme de classical shadows nécessite un post-traitement classique coûteux. L'évaluation des estimateurs non biaisés des fonctions multicopies d'intérêt d'ordre supérieur ($n > 3$) et pour des tailles de système plus importantes via l'estimateur U-statistique présente un problème rapidement, car elle nécessite de faire la somme de toutes les combinaisons possibles de M classical shadows distinctes. Une solution à ce problème, développée dans le chapitre 5 et dans Ref. [101], nous avons proposé un formalisme alternatif connu sous le nom de *formalisme de batch shadows* pour obtenir des estimateurs non biaisés de fonctions arbitraires d'intérêt et fournir analytiquement des limites de complexité d'échantillon pour comprendre sa performance. Étant donné un ensemble de données RM composé de M unitaires aléatoires, le formalisme de batch shadows réduit le coût d'exécution informatique du post-traitement d'une fonction d'ordre n par rapport à l'estimateur U-statistique précédent de $\mathcal{O}(M^n)$ (ancien) à $\mathcal{O}(M)$ (nouveau).

Enfin, avec les méthodes et les protocoles développés dans ce manuscrit, nous avons pu observer et valider expérimentalement de nouvelles propriétés d'intrication préparées dans deux types différents de plateforme quantique : un ordinateur quantique composé de qubits supraconducteurs et un simulateur quantique d'ions piégés. Tout d'abord, dans le chapitre 4 et dans Ref. [100], nous avons mesuré le QFI en utilisant la boîte à outils RM via la série convergente de limites inférieures pour deux types d'états quantiques préparés sur un dispositif quantique supraconducteur IBM

: Les états GHZ et l'état fondamental du modèle d'Ising à champ transverse (TFIM) au point critique en utilisant l'algorithme QAOA. En utilisant le formalisme de batch shadows et d'autres outils avancés [15, 76], nous avons validé la présence d'une intrication multipartite dans tous nos états quantiques préparés jusqu'à une taille de système de 13 qubits. Deuxièmement, dans le chapitre. 5 et dans Ref. [101], toujours en utilisant le formalisme de batch shadows, nous avons réanalysé les données de mesure aléatoires existantes d'une expérience antérieure réalisée Ref. [11] pour observer pour la première fois une propriété intéressante associée à l'intrication, connue sous le nom de barrière d'intrication. Nous estimons l'entropie d'intrication du second opérateur de Rényi (Rényi 2-OE, une fonction du quatrième ordre) à partir des données expérimentales qui présentent la signature de la barrière d'intrication. En outre, nous validons expérimentalement la présence d'intrication mixte par une nouvelle condition d'intrication basée sur le critère de la CCNR.

Pour l'avenir, il serait intéressant d'étudier et de travailler sur diverses extensions possibles du protocole de mesure aléatoire et des méthodes que nous avons introduites au cours de ce manuscrit. D'un point de vue plus large, on peut dire qu'il existe encore deux problèmes principaux qui empêchent la boîte à outils RM d'atteindre son plein potentiel : (i) le protocole RM souffre maintenant d'une échelle exponentielle *réduite* du nombre requis de mesures dues aux erreurs statistiques en fonction de la taille du système, (ii) pour le formalisme de classical shadows, la mémoire classique requise nous empêche de post-traiter les données de l'échantillon de mesure aléatoire par des estimateurs *efficaces* de batch shadows pour des tailles de système supérieures à $N \sim 16$. Les solutions possibles nécessiteraient que nous développions des stratégies pour mettre en œuvre des mesures aléatoires qui nécessitent un nombre polynomial de mesures en fonction de la taille du système. D'un autre côté, on pourrait envisager d'incorporer le cadre efficace de mémoire des réseaux tensoriels (tensor networks) pour résoudre potentiellement le problème de mémoire classique. Il en résulterait une technique efficace de post-traitement des ensembles de données RM de tailles de système plus importantes sur du matériel classique afin d'estimer les fonctionnelles de classical shadows qui nous intéressent.

Une direction possible de recherche pourrait être de développer un formalisme pour effectuer un échantillonnage par importance applicable aux classical shadows qui pourrait présenter une nouvelle méthode alternative pour lutter contre les erreurs statistiques. Sur la base des études préliminaires présentées au chapitre. 6, on peut procéder à une inspection rigoureuse pour comprendre les améliorations de performance obtenues par des méthodes *séparées ou combinées* d'échantillonnage d'importance et de mesures aléatoires communes. Il serait également intéressant d'envisager une approche guidée par les données sous la forme d'un schéma adaptatif pour adapter itérativement la distribution de l'échantillonnage d'importance sur les données RM antérieures prises dans l'expérience.

Du point de vue de la détection de l'intrication, on peut proposer un critère unificateur optimal pour détecter l'intrication en se basant uniquement sur les quantités de détection de l'intrication accessibles par la boîte à outils RM. Cela peut aider à certifier des états intriqués en utilisant un cadre général et au-delà de la limitation de certains critères.

8

Résumé en français

Nous présentons ici un bref résumé des travaux détaillés dans cette thèse. Dans le premier chapitre, l'objectif principal est de donner un résumé des quantités importantes qui nous intéressent dans cette thèse pour comprendre et valider la présence de l'intrication dans les systèmes quantiques. L'intrication quantique est actuellement une ressource vitale et joue un rôle clé dans les diverses applications, depuis la cryptographie quantique [28], la téléportation quantique [4], la métrologie quantique [94] et récemment dans le calcul et la simulation quantique [97]. Il existe diverses quantités, à commencer par les inégalités de Bell [10], les témoins d'intrication [120], les quantités entropiques et les fonctionnelles non linéaires de l'état quantique qui certifient la présence d'intrication dans un état quantique [53].

En Chapitre. 1, nous viserons à fournir un bref aperçu théorique de quelques quantificateurs d'intrication importants parmi la vaste gamme de quantités qui certifient l'intrication. En particulier, dans ce chapitre, nous nous concentrerons principalement sur l'introduction des quantités qui seront pertinentes pour ce manuscrit et qui seront discutées en détail dans les chapitres suivants. En particulier, nous nous intéresserons aux quantificateurs qui décrivent l'intrication bipartite (intrication entre deux constituants du système) dans le contexte des états *purs* tels que *la pureté*, *les entropies d'intrication* et les systèmes quantiques *mixtes* tels que les *critères PPT ou CCNR et l'entropies d'intrication de l'opérateur*. Nous discuterons également de l'intrication dans le scénario multipartite (intrication entre plusieurs parties du système) et en particulier d'une quantité telle que *l'information quantique de Fisher* (QFI) qui a une relation profonde avec les applications en métrologie quantique et qui peut témoigner la *profondeur d'intrication* (le nombre de particules qui sont non trivialement intriquées) d'un état quantique.

Ensuite, ces états quantiques maintenant peuvent-être préparés dans les plateformes quantiques bruyants à échelle intermédiaire qui vont de dizaines à des centaines de qubits [97]. Dernièrement, la caractérisation des propriétés quantiques préparées dans ces systèmes, indépendamment de l'architecture de la plateforme, a suscité un intérêt significatif parmi les théoriciens ainsi que les expérimentateurs construisant de tels dispositifs. Il est important de noter que la mesure des pro-

propriétés et des quantités associées à l'intrication, telle qu'elle a été présentée dans le chapitre précédent, devient pertinente pour comprendre la propriété quantique la plus élémentaire qui peut être utilisée pour évaluer les performances des ordinateurs et des simulateurs quantiques.

Dans chapitre. 2, on présente et discute trois candidats potentiels qui abordent ce problème pour sonder les propriétés associées à l'intrication préparées sur des matériels quantiques. Ces méthodes sont la *tomographie d'état quantique* [54], la mesure des propriétés avec des *copies physiques* [68, 123] du système quantique et les *mesures aléatoires* [31]. En particulier, nous introduisons formellement la méthode centrale de ce manuscrit connue sous le nom de *boîte à outils de mesures aléatoires* (boîte à outils RM) [31] et nous redéfinirons le formalisme dans le contexte de la *mesure de la pureté* d'un état quantique inconnu dans des plateformes quantiques génériques composées de qubits.

Le protocole de mesure aléatoire est basé sur l'exécution, sur un état quantique d'intérêt préparé, d'opérations unitaires aléatoires (au nombre de N_U) qui sont échantillonnées à partir d'un ensemble unitaire approprié, suivies par des mesures projective dans une base fixe (au nombre de N_M pour chaque unitaire aléatoire). Cette procédure, répétée plusieurs fois pour différents ensembles d'unitaires et de mesures projectives enregistrées, constitue un ensemble de données. Ensuite, un post-traitement classique efficace de ces données collectées nous permet d'accéder aux propriétés intéressantes associées à l'intrication du système quantique. En outre, nous discutons d'un ajout essentiel à la boîte à outils de la RM, appelé le *formalisme de classical shadows* [64]. Ce formalisme, qui utilise des mesures aléatoires, nous permet d'estimer d'autres quantités intéressantes sur la base des données de mesure aléatoires. Ces fonctions peuvent être exprimées sous forme de fonctions polynomiales telles que $\text{Tr}(\rho^n)$ ou de valeurs d'espérance d'opérateurs multicopies $\text{Tr}(O^{(n)}\rho^{\otimes n})$.

Optimisation du protocole de mesures aléatoires avec échantillonnage préférentiel

Dans Chapitre. 2, nous avons discuté de la façon dont nous pouvons mesurer la pureté d'un état quantique inconnu en effectuant des mesures aléatoires dans une expérience. Le budget de mesure $M = N_U N_M$, où N_U est le nombre d'unitaires aléatoires locales appliquées et N_M le nombre de mesures projectives effectuées pour chaque unitaire appliquée, définit le nombre total de répétitions effectuées dans l'expérience. Toutefois, comme les expériences sont répétées pour un budget de mesure fini, l'estimation de la pureté est entachée d'erreurs statistiques. En particulier, le nombre requis de mesures dans le cas de mesures aléatoires pour une tolérance donnée de l'échelle d'erreur statistique *exponentiellement* ($M \sim 2^{\alpha N}$ avec $\alpha \in [1, 1.5]$) en ce qui concerne le nombre de qubits N [29, 11, 125, 32]. Cela limite typiquement notre accès à l'estimation de la pureté dans les expériences pour des tailles de (sous-)systèmes dans le régime de 10 – 15 qubits.

La croissance de la taille des plateformes expérimentales actuelles nécessite le développement de méthodes afin d'évaluer la génération d'intrication dans tels dispositifs quantiques au-delà du régime restrictif actuel. Dans Chapitre. 3 sur la base des travaux de Ref. [99], nous proposons un protocole basé sur des mesures aléatoires qui nous permettra de mesurer la pureté des états quantiques dans des

(sous-)systèmes de taille significativement plus grande. Nous y parvenons en réduisant de manière prédominante les erreurs statistiques qui régissent l'estimation de la pureté à partir d'un ensemble fini de mesures.

Pour le détailler, la version précédente du protocole de mesure aléatoire introduit dans les travaux antérieurs de [30, 11] était basée sur une méthode *agnostique de l'état* pour mesurer la pureté. Elle mettait en œuvre un ensemble d'unitaires aléatoires qui étaient toujours choisies uniformément à partir de la mesure de Haar, quel que soit l'état préparé dans l'expérience. Mais dans les scénarios expérimentaux typiques, la première étape consiste toujours à décider de l'état parfait ρ que nous voulons préparer sur le dispositif quantique. Dans certains scénarios, ces états quantiques préparés peuvent être bien approximés à l'aide d'une simulation classique [89]. Notre proposition principale consiste donc en deux étapes principales. Tout d'abord, nous utilisons cette précieuse *connaissance préalable* pour construire une représentation classique de l'état quantique expérimental. L'état classique antérieur peut être considéré comme une *approximation* de l'état expérimental réalisé en raison d'effets de décohérence inconnus ou d'autres raisons fondamentales qui limitent les représentations classiques des états quantiques. Deuxièmement, sur la base des connaissances préalables, nous préparons la bonne *sélection* d'unitaires aléatoires locales pour l'expérience qui aiderait à réduire les erreurs statistiques. C'est l'esprit de l'échantillonnage préférentiel [96] où ces unitaires sont échantillonnés selon une distribution de probabilité appropriée définie en fonction de l'état classique approximatif à disposition et exploitent la structure de l'état quantique sous-jacent.

Estimation de l'information quantique de Fisher avec le formalisme de classical shadows

En Chapitre. 4, nous abordons la mesure de l'information quantique de Fisher (QFI). Comme nous l'avons vu avant dans le chapitre. 1, le QFI est un excellent exemple de quantité qui peut certifier, pour certaines applications, un avantage quantique potentiel par rapport à ses homologues classiques [94]. Par exemple, c'est la quantité centrale liée à la métrologie quantique [94, 93] car elle valide les états qui ont la ressource quantique adéquate pour fournir des sensibilités métrologiques améliorées [94, 93]. Il est important de noter que la ressource quantique responsable de l'amélioration des sensibilités métrologiques est *l'intrication multipartite*. Le QFI joue en outre un rôle important dans la mise en évidence de divers autres phénomènes quantiques associés à l'intrication multipartite dans la physique quantique des corps multiples. Il révèle les propriétés universelles de l'intrication pendant les transitions de phase à température finie [137] ou le rôle de l'intrication multipartite dans la transition de phase topologique [92].

Le défi actuel que nous abordons dans ce chapitre est de mesurer le QFI pour un état quantique inconnu préparé sur une plateforme quantique composé de qubits. La difficulté d'estimer le QFI provient du fait qu'il s'agit d'une fonction *non linéaire* de la matrice de densité ρ et qu'elle ne peut pas être transformée en une observable qui peut être mesurée facilement dans les expériences. La méthode la plus couramment utilisée pour estimer le QFI d'une manière indépendante de l'état semble être la tomographie d'état quantique. Cette méthode a un coût élevé en termes de nombre de mesures à exécuter sur la plateforme quantique. Dans ce chapitre et comme indiqué

dans nos travaux [100], nous fournirons une méthode alternative pour mesurer le QFI en construisant une série polynomiale de la matrice de densité sous la forme de bornes inférieures qui convergent vers le QFI. Chacune des bornes inférieures peut être mesurée de manière agnostique en utilisant le formalisme classique de l'ombre [64] sur les dispositifs expérimentaux actuels avec les mêmes données de mesure aléatoires. Nous montrons que chacune de ces bornes peut être estimée à partir du formalisme de classical shadows à un coût de mesure inférieur à celui de la tomographie d'état quantique. Nous mettons en évidence ses caractéristiques de convergence ainsi que des identités rigoureuses de complexité d'échantillon pour estimer le nombre requis de mesures pour les estimer avec une précision et un intervalle de confiance donnés. Nous généralisons ces calculs pour évaluer le nombre de mesures nécessaires pour estimer des fonctionnelles multi-copies arbitraires qui sont accessibles via le formalisme de classical shadows [64].

La dernière partie de ce chapitre est basée sur Ref. [129], où nous avons mesuré le QFI en employant la boîte à outils RM via la série convergente de limites inférieures pour deux types d'états quantiques préparés sur un dispositif quantique supraconducteur IBM : Les états GHZ et l'état fondamental du modèle d'Ising à champ transverse (TFIM) au point critique en utilisant l'algorithme QAOA. En utilisant le formalisme de batch shadows (introduit dans le chapitre suivant) et d'autres outils avancés de la boîte à outils de la RM, nous avons validé la présence d'un enchevêtrement multipartite dans tous nos états quantiques préparés jusqu'à une taille de système de 13 qubits.

Observation de la barrière d'intrication à l'aide de batch shadows

Dans les chapitres précédents nous avons vu que, l'ajout du formalisme de classical shadows à la boîte à outils de la RM permet d'accéder à de nombreuses quantités non linéaires intéressantes qui peuvent certifier l'intrication à partir de l'ensemble des données expérimentales de la RM. Plus précisément, ces quantités peuvent être écrites comme des valeurs d'espérance de l'opérateur multicopie $O^{(n)}$ de la matrice de densité ρ , c'est-à-dire $f_n = \text{Tr}(O^{(n)}\rho^{\otimes n})$. L'estimateur *U-statistique* relie directement les données RM à l'estimation de ces fonctions [59]. Une question pratique essentielle qui se pose est liée à notre capacité à post-traiter efficacement les données expérimentales sur un ordinateur classique afin d'obtenir ces estimateurs. L'estimateur actuel de la U-statistique constitue un goulot d'étranglement pour le post-traitement classique permettant d'extraire les quantités d'intérêt. L'évaluation des estimateurs non biaisés des fonctions multicopies d'intérêt d'ordre supérieur ($n > 3$) et pour des systèmes de plus grande taille via l'estimateur U-statistique présente rapidement un problème informatique, car elle nécessite de faire la somme de toutes les combinaisons possibles de n classical shadows distinctes. Jusqu'à présent, les fonctionnelles jusqu'à l'ordre $n \leq 3$ ont été extraites avec succès des données expérimentales [11, 34]. Dans chapitre. 5 et dans Ref. [101], nous proposons un autre formalisme connu sous le nom de *formalisme de batch shadows* pour obtenir des estimateurs non biaisés de fonctions arbitraires d'intérêt et fournir analytiquement des limites de complexité de l'échantillon pour comprendre sa performance. Étant donné un ensemble de données RM composé de M unitaires aléatoires, nous avons montré que le formalisme de l'ombre du lot réduit le coût d'exécution informatique du post-traitement d'une fonction d'ordre n par rapport à l'estimateur U-statistique

précédent de $\mathcal{O}(M^n)$ (ancien) à $\mathcal{O}(M)$ (nouveau) étapes.

En outre, ce nouveau formalisme nous permet de réanalyser les données de mesure aléatoires existantes d'une expérience antérieure réalisée en Ref. [11] pour observer pour la première fois une propriété intéressante associée à l'intrication connue sous le nom de *barrière d'intrication*. Nous estimons l'entropie d'intrication du second opérateur de Rényi (Rényi 2-OE, une fonction du quatrième ordre $n = 4$) à partir des données expérimentales qui présentent cette signature de la barrière d'intrication. Nous validons également expérimentalement la présence d'intrication dans les états mixtes avec une nouvelle condition d'intrication que nous dérivons sur la base du critère CCNR.

Common randomized measurements ou Mesures aléatoires communes

Dans Chapitre. 6 qui est basé sur Ref. [126], nous discutons d'une proposition récemment élaborée pour obtenir des estimations améliorées de quantités d'intérêt à partir de données de mesure aléatoires [126]. Comme nous l'avons montré précédemment dans le chapitre. 3, nous avons proposé une méthode basée sur l'échantillonnage préférentiel d'unitaires aléatoires locales pour réduire l'échelle exponentielle du nombre requis de mesures pour évaluer la pureté d'un état quantique inconnu. Cette méthode a notamment permis d'améliorer les performances et de réduire l'erreur statistique de l'estimation "unitaire agnostique" de la pureté (voir Eq. (2.28)). Une question générale importante que nous pouvons poser maintenant est la suivante : Comment pouvons-nous réduire le nombre de mesures nécessaires pour évaluer les quantités accessibles à l'aide du formalisme de classical shadows? En particulier, nous nous intéressons à la réduction de l'erreur statistique dans l'estimation de l'espérance des opérateurs multicopies (MCO) $f_n = \text{Tr}(O^{(n)}\rho^{\otimes n})$ qui souffrent également d'échelles exponentielles des mesures requises en fonction de la taille du système N [31]. Cette question a été abordée pour réduire les erreurs statistiques dans le contexte de l'évaluation des fonctions exprimées en tant qu'observable à copie unique, c'est-à-dire les fonctions du type $f_1 = \text{Tr}(O^{(1)}\rho)$ [63, 56, 55, 133, 123]. Ici, notre objectif principal est de fournir une méthode pour optimiser toutes les fonctions d'intérêt pour $n \geq 1$.

Dans ce chapitre, nous présentons d'abord l'idée principale de notre proposition visant à améliorer les estimations en réduisant les erreurs statistiques des MCO. Elle s'inspire des *nombre aléatoires communs* (common random numbers), largement utilisés en statistique pour réduire la variance, et nous aidera à présenter le protocole *mesures aléatoires communes* (common randomized measurements) (CRM). Sur la base de cette idée, nous proposons la construction d'estimateurs *boostés* de fonctionnels multicopies à l'aide des common randomized shadows (CR shadows) et introduisons en outre une nouvelle estimation CRM pour l'estimateur agnostique unitaire pour la pureté. Enfin, nous illustrons ses performances pour estimer de nombreuses propriétés quantiques intéressantes accessibles à partir de l'ensemble de données RM. Nous comparons les performances du protocole CRM avec celles du protocole RM standard (ou uniforme). En particulier, nous nous intéressons aux performances pour des quantités allant des observables linéaires ($f_1 = \text{Tr}(O^{(1)}\rho)$), à la pureté ($\text{Tr}(\rho^2)$) et aux fonctions d'ordre supérieur de la matrice densité telles que les limites du QFI (F_0 et F_1) introduites dans le chapitre. 4. En ce qui concerne la pureté évaluée pour des systèmes de plus grande taille avec l'estimateur "agnos-

tique", nous étudions les échelles d'erreur du protocole CRM par rapport à celle de l'échantillonnage d'importance introduite au chapitre. 3.

Appendices

A

Alternate expressions for the lower bounds and the quantum Fisher information

This appendix provides the alternate expressions of the lower bounds of the quantum Fisher information (QFI) that we introduced in Chapter. 4. In particular, we show that the converging series of lower bounds can be expressed in terms of multi-copy functionals as well as polynomials of the density matrix.

We have shown in Chapter. 4 an alternate expression for the QFI in Eq. (4.4). It involves polynomials of the eigenvalues of the density matrix ρ that form a converging series of lower bounds to the QFI. One could naively think that the introduction of this alternate expression has no additional benefits as once again we need quantum state tomography (QST) to estimate the eigenvalues to measure QFI. In this section we bridge this gap and show that Eq. (4.4) can indeed be expressed firstly in terms of polynomials of the density matrix and secondly also in terms of a multi-copy operator. Both these forms then allow us to estimate these bounds using the classical shadow formalism as we shall show in the next section.

Our starting point is to formulate the standard expression of the QFI [9, 8] given in Eq. (4.1) in an alternate form using the swap operator $\mathbb{S} = \sum_{i_1, i_2} |i_2, i_1\rangle\langle i_1, i_2|$:

$$F_Q = 2 \operatorname{Tr} \left(\frac{(\rho \otimes \mathbb{1} - \mathbb{1} \otimes \rho)^2}{\rho \otimes \mathbb{1} + \mathbb{1} \otimes \rho} \mathbb{S}(\mathcal{A} \otimes \mathcal{A}) \right). \quad (\text{A.1})$$

In the above expression, it might be that the denominator is not invertible, in that case it admits a multiplication by the Moore-Penrose pseudoinverse of the denominator that commutes with the numerator. To better understand the expression of QFI in the above equation, we can expand its numerator using the spectral decomposition $\rho = \sum_i \lambda_i |i\rangle\langle i|$

$$(\rho \otimes \mathbb{1} - \mathbb{1} \otimes \rho)^2 = \left(\sum_{i,j} (\lambda_i |i\rangle\langle i| \otimes |j\rangle\langle j| - \lambda_j |i\rangle\langle i| \otimes |j\rangle\langle j|) \right)^2 = \sum_{i,j} (\lambda_i - \lambda_j)^2 |i, j\rangle\langle i, j| \quad (\text{A.2})$$

and the (pseudo)inverse of the denominator of the fraction as

$$\begin{aligned} (\rho \otimes \mathbb{1} + \mathbb{1} \otimes \rho)^{-1} &= \left(\sum_{i,j} (\lambda_i |i\rangle\langle i| \otimes |j\rangle\langle j| + \lambda_j |i\rangle\langle i| \otimes |j\rangle\langle j|) \right)^{-1} \\ &= \sum_{i,j:\lambda_i+\lambda_j>0} (\lambda_i + \lambda_j)^{-1} |i, j\rangle\langle i, j|. \end{aligned} \quad (\text{A.3})$$

Noting additionally, we can express

$$|\langle i | \mathcal{A} | j \rangle|^2 = \langle j, i | \mathcal{A} \otimes \mathcal{A} | i, j \rangle = \text{Tr}(|i, j\rangle\langle i, j| \mathbb{S}(\mathcal{A} \otimes \mathcal{A})). \quad (\text{A.4})$$

With the combination of the previous results in Eq. (A.2) and Eq. (A.3) and the above equation we get the alternate expression of QFI as given in Eq. (A.1). In a similar spirit, we can also provide an alternate expression of our lower bounds in Eq. (4.4). Noting additionally that, we can express the expansion term in Eq. (4.3) as

$$\begin{aligned} &\sum_{\ell=0}^n \sum_{i,j} (1 - \lambda_i - \lambda_j)^\ell |i, j\rangle\langle i, j| \\ &= \sum_{\ell=0}^n \left(\sum_{i,j} (|i\rangle\langle i| \otimes |j\rangle\langle j| - \lambda_i |i\rangle\langle i| \otimes |j\rangle\langle j| - \lambda_j |i\rangle\langle i| \otimes |j\rangle\langle j|) \right)^\ell \\ &= \sum_{\ell=0}^n (\mathbb{1} \otimes \mathbb{1} - \rho \otimes \mathbb{1} - \mathbb{1} \otimes \rho)^\ell, \end{aligned} \quad (\text{A.5})$$

we similarly get the final alternate form of the lower bounds

$$F_n = 2 \text{Tr} \left[\sum_{\ell=0}^n (\rho \otimes \mathbb{1} - \mathbb{1} \otimes \rho)^2 (\mathbb{1} \otimes \mathbb{1} - \rho \otimes \mathbb{1} - \mathbb{1} \otimes \rho)^\ell \mathbb{S}(\mathcal{A} \otimes \mathcal{A}) \right]. \quad (\text{A.6})$$

Moreover, in order to see the expression of the lower bounds as polynomials of ρ , we start by expanding further the term

$$(\mathbb{1} \otimes \mathbb{1} - \rho \otimes \mathbb{1} - \mathbb{1} \otimes \rho)^\ell = \sum_{q=0}^{\ell} \binom{\ell}{q} (-1)^q (\rho \otimes \mathbb{1} + \mathbb{1} \otimes \rho)^q, \quad (\text{A.7})$$

by swapping the sums and using the *hockey-stick identity* $\sum_{\ell=q}^n \binom{\ell}{q} = \binom{n+1}{q+1}$, we can re-express the lower bound as

$$F_n = 2 \sum_{q=0}^n \binom{n+1}{q+1} (-1)^q \text{Tr} \left((\rho \otimes \mathbb{1} - \mathbb{1} \otimes \rho)^2 (\rho \otimes \mathbb{1} + \mathbb{1} \otimes \rho)^q \mathbb{S}(\mathcal{A} \otimes \mathcal{A}) \right) = \sum_{q=0}^n \binom{n+1}{q+1} (-1)^q P_{q+2}. \quad (\text{A.8})$$

Here we introduce the function P_{q+2} which contains an order $q+2$ in the density matrix ρ . By further expanding the terms inside the trace expression and using the cyclic property of the trace, we can directly relate P_{q+2} explicitly in terms of powers of ρ and the operator \mathcal{A}

$$P_{q+2} = 2 \sum_{\ell=0}^{q+2} C_\ell^{(q)} \text{Tr}(\rho^{q+2-\ell} \mathcal{A} \rho^\ell \mathcal{A}) \quad (\text{A.9})$$

where we have introduced the coefficients $C_\ell^{(q)} = \binom{q}{\ell} - 2\binom{q}{\ell-1} + \binom{q}{\ell-2}$ which are defined such that $\binom{q}{\ell'} = 0$ if $\ell' < 0$ or $\ell' > q$. Alternately, we can define the cyclic permutation operator

$$\Pi_{(q+2)} = \sum_{i_1, i_2, \dots, i_{q+2}} |i_2, \dots, i_{q+2}, i_1\rangle \langle i_1, i_2, \dots, i_{q+2}| \quad (\text{A.10})$$

with $|i_m\rangle$'s being the basis states for the Hilbert space that contains ρ . This operator acts on $q+2$ copies of the system and shifts them a single step backwards. Using this operator and rewriting Eq. (A.8) as shown in our work [100, Eq. A7], we get the following expression for the lower bounds F_n

$$\begin{aligned} F_n &= 2 \sum_{q=0}^n \binom{n+1}{q+1} (-1)^q \sum_{\ell=0}^{q+2} C_\ell^{(q)} \text{Tr}(\rho^{q+2-\ell} \mathcal{A} \rho^\ell \mathcal{A}) \\ &= 2 \sum_{q=0}^n \binom{n+1}{q+1} (-1)^q \text{Tr}[O^{(q+2)} \rho^{\otimes(q+2)}] \end{aligned} \quad (\text{A.11})$$

with the $(q+2)$ -copy operator defined as

$$O^{(q+2)} = \left[2 (\mathbb{1}^{\otimes(q+1)} \otimes \mathcal{A}^2) + \sum_{\ell=1}^{q+1} C_\ell^{(q)} (\mathbb{1}^{\otimes(q+1-\ell)} \otimes \mathcal{A} \otimes \mathbb{1}^{\otimes(\ell-1)} \otimes \mathcal{A}) \right] \Pi_{(q+2)}. \quad (\text{A.12})$$

We see that both the expressions in Eq. (A.8) and Eq. (A.11) are compatible to be estimated using the classical shadow formalism. In practice, when we want to extract effectively the estimations of the lower bounds from experimental data, it is easier to work with the expression of Eq. (A.8). Lastly, we can note for the sake of completeness as shown in our work [100], that we can also iteratively calculate each bound F_n from the previous ones by writing

$$F_n = (-1)^n \left[P_{n+2} - \sum_{r=0}^{n+1} \binom{n+1}{r+1} (-1)^r F_r \right]. \quad (\text{A.13})$$

With these expression, one can use the classical shadow formalism to evaluate the lower bounds of the QFI until the desired convergence is reached.

B

Variance computation for the batch shadow estimator

This appendix provides the derivation of the closed form of the variance for the batch shadow estimator that can be used to evaluate arbitrary multi-copy functionals of the density matrix. In particular, the expression of the variance is essential to obtain the sample complexity to estimate a function of interest using the batch shadow formalism.

We start by performing randomized measurements to construct classical shadows of an N -qubit state ρ . On each run of the protocol, we sample N single-qubit random unitaries from the CUE or a 2-design and apply them locally on each qubit. This is followed by a single computational-basis measurement on each qubit ($N_M = 1$). This procedure is repeated M times and allows us to construct M classical shadows $\hat{\rho}^{(r)}$ of ρ with $r = 1, \dots, M$ [64]. We know that the expectation value of the classical shadows is $\mathbb{E}[\hat{\rho}] = \rho$. The functions that we are interested to evaluate can be expressed as $f_n = \text{Tr}(O^{(n)}\rho^{\otimes n})$. To evaluate this function with a total of M measurements using the batch shadow formalism introduced in Chapter. 5, we can construct n' batch shadows as given in Eq. (5.7). The corresponding batch shadow estimator can be constructed as shown in Eq. (5.8) and is given by $\tilde{f}_n^{(n')}$. In this section as we shown in Ref. [101], we shall mainly focus on the simplest and computationally most efficient case of post-processing the batch shadow estimator which is obtained for $n' = n$. We write this more formally as a sum over all the permutations π ($i \mapsto \pi(i)$ for $i \in \{1 \dots, n\}$) which leads to

$$\tilde{f}_n^{(n)} = \frac{1}{n!} \sum_{b_1 \neq \dots \neq b_n} \text{Tr} \left(O^{(n)} \bigotimes_{i=1}^n \hat{\rho}^{(b_i)} \right) = \frac{1}{n!} \frac{n^n}{M^n} \sum_{\pi} \sum_{t_1 \in T_1, \dots, t_n \in T_n} \text{Tr} \left[O^{(n)} W_{\pi} \bigotimes_{i=1}^n \hat{\rho}^{(t_i)} W_{\pi}^{\dagger} \right] \quad (\text{B.1})$$

with W_{π} being the operator that permutes the n classical shadows correspondingly as $W_{\pi} = \sum_{j_1, \dots, j_n} |j_{\pi(1)}\rangle\langle j_1| \otimes \dots \otimes |j_{\pi(n)}\rangle\langle j_n|$ (where the $|j_i\rangle$'s are orthonormal basis states). Now our goal is to compute the variance term $\text{Var}[\tilde{f}_n^{(n)}]$ by a similar reasoning

as done shown in Chapter. 4 (to compute the variance of the U-statistics estimator using classical shadows). We can express the variance using the decomposition given in Eq. (B.1) as

$$\text{Var}[\hat{f}_n^{(n)}] = \left(\frac{1}{n!} \frac{n^n}{M^n} \right)^2 \sum_{\substack{\pi, \pi' \\ t_1, t'_1 \in T_1 \\ \vdots \\ t_n, t'_n \in T_n}} \text{Cov} \left[\text{Tr} \left(O^{(n)} W_\pi \otimes_{i=1}^n \hat{\rho}^{(t_i)} W_\pi^\dagger \right), \text{Tr} \left(O^{(n)} W_{\pi'} \otimes_{i=1}^n \hat{\rho}^{(t'_i)} W_{\pi'}^\dagger \right) \right] \quad (\text{B.2})$$

Note that all shadows that appear only once in the covariances above (i.e., those with indices $t_i \neq t'_i$) simply average to ρ (where the average is performed over the applied unitaries: $\mathbb{E}[\hat{\rho}^{(t_i)}] = \mathbb{E}[\hat{\rho}^{(t'_i)}] = \rho$). The shadows that appear twice (those with indices $t_i = t'_i$), on the other hand, contribute less trivially. Furthermore, because of the averaging over all permutations π, π' , the positions of the shadows appearing twice (i.e., the indices i such that $t_i = t'_i$) does not matter. Thus to compute the above sums over all the batch indices $t_i, t'_i \in T_i$, we can decompose these, depending on the number k of copies of shadows that are in common in the two terms inside the covariances—that is, with k values for the index i such that $t_i = t'_i$, and the remaining $(n - k)$ values such that $t_i \neq t'_i$. Hence we can explicitly write:

$$\begin{aligned} \text{Var}[\tilde{f}_n^{(n)}] &= \left(\frac{1}{n!} \frac{n^n}{M^n} \right)^2 \sum_{\pi, \pi'} \sum_{k=0}^n \binom{n}{k} \sum_{\substack{t_1 \in T_1 \\ \vdots \\ t_k \in T_k}} \sum_{\substack{\tau_{k+1} \neq \tau'_{k+1} \in T_{k+1} \\ \vdots \\ \tau_n \neq \tau'_n \in T_n}} \text{Cov} \left[\text{Tr} \left(W_\pi^\dagger O^{(n)} W_\pi [\otimes_{i=1}^k \hat{\rho}^{(t_i)} \otimes_{j=k+1}^n \hat{\rho}^{(\tau_j)}] \right), \right. \\ &\quad \left. \text{Tr} \left(W_{\pi'}^\dagger O^{(n)} W_{\pi'} [\otimes_{i=1}^k \hat{\rho}^{(t_i)} \otimes_{j=k+1}^n \hat{\rho}^{(\tau'_j)}] \right) \right] \\ &= \left(\frac{1}{n!} \frac{n^n}{M^n} \right)^2 \sum_{\pi, \pi'} \sum_{k=0}^n \binom{n}{k} \left(\frac{M}{n} \right)^k \left(\frac{M}{n} \left(\frac{M}{n} - 1 \right) \right)^{n-k} \text{Cov} [C_\pi, C_{\pi'}] \\ &= \sum_{k=0}^n \binom{n}{k} \left(\frac{n}{M} \right)^k \left(1 - \frac{n}{M} \right)^{n-k} \text{Var} \left[\frac{1}{n!} \sum_{\pi} \text{Tr} \left(W_\pi^\dagger O^{(n)} W_\pi [\otimes_{i=1}^k \hat{\rho}^{(i)} \otimes \rho^{\otimes(n-k)}] \right) \right], \end{aligned} \quad (\text{B.3})$$

with

$$C_\pi = \text{Tr} \left(W_\pi^\dagger O^{(n)} W_\pi [\otimes_{i=1}^k \hat{\rho}^{(i)} \otimes \rho^{\otimes(n-k)}] \right)$$

and

$$C_{\pi'} = \text{Tr} \left(W_{\pi'}^\dagger O^{(n)} W_{\pi'} [\otimes_{i=1}^k \hat{\rho}^{(i)} \otimes \rho^{\otimes(n-k)}] \right).$$

We notice from the first to the second lines in Eq. (B.3) (in addition to averaging the shadows $\hat{\rho}^{(\tau_j)}, \hat{\rho}^{(\tau'_j)}$ to ρ , see above) that all different shadows $\hat{\rho}^{(t_i)}$ give the same statistics (hence, the same covariances), so that we could without loss of generality replace the k shadows $\hat{\rho}^{(t_i)}$ by any other k shadows $\hat{\rho}^{(i)}$, e.g. those for $i = 1, \dots, k$. All $\frac{M}{n}$ terms from each of the k sums over $t_i \in T_i$, and all $\frac{M}{n} \left(\frac{M}{n} - 1 \right)$ terms from each of the $n - k$ sums over $\tau_j \neq \tau'_j \in T_j$ then give the same values. For the last line we just rearranged all prefactors and included the sums over π, π' inside the covariances, noticing that the two arguments of the covariances are then the same.

Let us note already that the variance term inside the sum of Eq. (B.3) cancels for $k = 0$: the sum can therefore be taken to start from $k = 1$. Simplifying further our notations by defining,

$$\mathcal{V}_k = \text{Var} \left[\frac{1}{n!} \sum_{\pi} \text{Tr} \left(W_\pi^\dagger O^{(n)} W_\pi [\otimes_{i=1}^k \hat{\rho}^{(i)} \otimes \rho^{\otimes(n-k)}] \right) \right], \quad (\text{B.4})$$

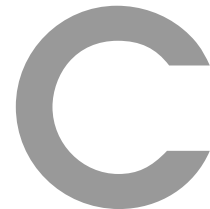
we obtain by using the binomial expansion

$$\begin{aligned}
\text{Var}[\tilde{f}_n^{(n)}] &= \sum_{k=1}^n \binom{n}{k} \left(\frac{n}{M}\right)^k \left(1 - \frac{n}{M}\right)^{n-k} \mathcal{V}_k \\
&= \sum_{\ell=1}^n \binom{n}{\ell} \left(\frac{n}{M}\right)^\ell \left[\sum_{k=1}^{\ell} \binom{\ell}{k} (-1)^{\ell-k} \mathcal{V}_k \right] \\
&= \frac{n^2}{M} \mathcal{V}_1 + \frac{n^3(n-1)}{2M^2} (\mathcal{V}_2 - 2\mathcal{V}_1) + \mathcal{O}\left(\frac{1}{M^2}\right). \tag{B.5}
\end{aligned}$$

By performing similar calculations, we can also provide analogous expression of Eq. (B.5) for any value of n' given by

$$\begin{aligned}
\text{Var}[\tilde{f}_n^{(n')}] &= \sum_{j=1}^n \binom{n}{j} \frac{\binom{n'-n}{n-j}}{\binom{n'}{n}} \sum_{k=1}^j \binom{j}{k} \left(\frac{n'}{M}\right)^k \left(1 - \frac{n'}{M}\right)^{j-k} \mathcal{V}_k \\
&= \sum_{\ell=1}^n \frac{\binom{n}{\ell}^2}{\binom{n'}{\ell}} \left(\frac{n'}{M}\right)^\ell \left[\sum_{k=1}^{\ell} \binom{\ell}{k} (-1)^{\ell-k} \mathcal{V}_k \right] \\
&= \frac{n^2}{M} \mathcal{V}_1 + \frac{n^2(n-1)^2 \frac{n'}{n'-1}}{2M^2} (\mathcal{V}_2 - 2\mathcal{V}_1) + \mathcal{O}\left(\frac{1}{M^2}\right). \tag{B.6}
\end{aligned}$$

Thus we have obtained explicit expressions of the variance that can be evaluated with the knowledge of the quantum state ρ and the multi-copy operator $O^{(n)}$.



Properties of classical shadows with local Pauli measurements

This appendix derives novel properties of Pauli shadows by exploiting the rich structure of Pauli-basis measurements and improves over other previous bounds on the trace overlap between different Pauli shadows.

Given a N qubit state prepared on a quantum device, we can construct a Haar classical shadow $\hat{\rho}^{(r)}$ (equivalently called a Haar shadow) of the state (with $N_M = 1$) [64]:

$$\hat{\rho}^{(r)} = \bigotimes_{i=1}^N \left(3 U_i^{(r)\dagger} \left| s_i^{(r)} \right\rangle \langle s_i^{(r)} \right| U_i^{(r)} - \mathbb{1}_2 \right) \quad (\text{C.1})$$

where the applied local random unitary is sampled from the CUE equivalently from the Haar measure (local CUE measurements). Alternatively we could consider random single-qubit operations that equivalently lead to measuring each qubit in one of the random Pauli basis of \mathcal{X} , \mathcal{Y} or \mathcal{Z} (local Pauli measurements).

These lead to six possible states that can be succinctly summarized as:

$$|\mathcal{B}, s\rangle \quad \text{with} \quad \mathcal{B} \in \{\mathcal{X}, \mathcal{Y}, \mathcal{Z}\}, \quad s \in \{\pm\} \quad (\text{C.2})$$

More precisely, these states correspond to the following six possibilities:

$$\begin{aligned} |0\rangle &= |\mathcal{Z}, +\rangle, & |1\rangle &= |\mathcal{Z}, -\rangle, \\ |+\rangle &= |\mathcal{X}, +\rangle, & |-\rangle &= |\mathcal{X}, -\rangle, \\ |i+\rangle &= |\mathcal{Y}, +\rangle, & |i-\rangle &= |\mathcal{Y}, -\rangle. \end{aligned} \quad (\text{C.3})$$

To construct a *Pauli shadow* $\hat{\rho}$, we choose randomly and uniformly for each single qubit i , a basis \mathcal{B}_i in \mathcal{X} , \mathcal{Y} or \mathcal{Z} which is subsequently followed by the resulting basis measurement that provides a string of signs $\mathbf{s} = (s_1, \dots, s_N) \in \{\pm\}$. With

this information and defining N chosen bases $\mathcal{B} = (\mathcal{B}_1, \dots, \mathcal{B}_N)$, we can provide an unbiased estimator of the density matrix ρ as [65]:

$$\hat{\rho}(\mathcal{B}, \mathbf{s}) = \bigotimes_{i=1}^N \left(3 |\mathcal{B}_i, s_i\rangle\langle\mathcal{B}_i, s_i| - \mathbb{1}_2 \right) \quad \text{such that} \quad \mathbb{E}[\hat{\rho}(\mathcal{B}, \mathbf{s})] = \rho \quad (\text{C.4})$$

Here, \mathbb{E} denotes the expectation value over the uniformly sampled random bases, as well as the resulting measurement outcomes. Note that the single qubit Pauli shadows have some interesting properties due to the fact that their chosen measurement bases are mutually unbiased [118]. For $\mathcal{B} \neq \mathcal{B}'$, we have

$$\text{Tr} \left[(3 |\mathcal{B}, s\rangle\langle\mathcal{B}, s| - \mathbb{1}_2) (3 |\mathcal{B}', s'\rangle\langle\mathcal{B}', s'| - \mathbb{1}_2) \right] = \frac{1}{2} \quad \forall s, s' \in \{\pm\} \quad (\text{C.5})$$

and for $\mathcal{B} = \mathcal{B}'$ we have

$$\text{Tr} \left[(3 |\mathcal{B}, s\rangle\langle\mathcal{B}, s| - \mathbb{1}_2) (3 |\mathcal{B}', s'\rangle\langle\mathcal{B}', s'| - \mathbb{1}_2) \right] = \begin{cases} -4 & \text{if } s \neq s'. \\ 5 & \text{if } s = s'. \end{cases} \quad (\text{C.6})$$

This rich geometric structure allows us to deduce streamlined upper bounds on the trace overlap between different Pauli shadows. The following Lemma is an important result that shall come in use in later computations.

Lemma 1. *Given two N -qubit basis strings $\mathcal{B}, \mathcal{B}' \in \{\mathcal{X}, \mathcal{Y}, \mathcal{Z}\}^{\times N}$, for any sign of the outcome strings $s, s' \in \{\pm\}^{\times N}$ the following two statements hold:*

$$\text{Tr} \left(\hat{\rho}(\mathcal{B}, \mathbf{s}) \hat{\rho}'(\mathcal{B}', \mathbf{s}') \right)^2 \leq \prod_{i=1}^N \left(5^2 \mathbf{1}\{\mathcal{B}_i = \mathcal{B}'_i\} + \left(\frac{1}{2}\right)^2 \mathbf{1}\{\mathcal{B}_i \neq \mathcal{B}'_i\} \right) \quad (\text{C.7})$$

and

$$\mathbb{E} \left[\prod_{i=1}^N \left(5^2 \mathbf{1}\{\mathcal{B}_i = \mathcal{B}'_i\} + \left(\frac{1}{2}\right)^2 \mathbf{1}\{\mathcal{B}_i \neq \mathcal{B}'_i\} \right) \right] = 8.5^N, \quad (\text{C.8})$$

where $\mathbf{1}\{\mathcal{B}_i = \mathcal{B}'_i\}$ and $\mathbf{1}\{\mathcal{B}_i \neq \mathcal{B}'_i\}$ denote the indicator function of the advertised events.

The proof strategy for this auxiliary statement is inspired by a recent analysis of classical shadows for single-qubit SIC POVMs, see [118, Appendix IX.B].

Proof. The proof of the first inequality follows from the observation that the single qubit states $|\mathcal{B}_i, s_i\rangle$ and $|\mathcal{B}'_i, s'_i\rangle$ are mutually unbiased whenever $\mathcal{B}_i \neq \mathcal{B}'_i$. If two bases coincide ($\mathcal{B}_i = \mathcal{B}'_i$), the squared overlap either contributes $(-4)^2$ ($s' \neq s$) or 5^2 ($s = s'$) and can be bounded by choosing the larger term amongst them. Eq. (C.7) now follows from applying this single-qubit argument to each contribution in the N -fold tensor product that make up the two shadows as the trace inner product of two shadows factorises into N single-qubit contributions from Eq. (C.4).

Secondly, noting that all random basis choices are independent, we can develop Eq. (C.8) as:

$$\begin{aligned} \mathbb{E} \left[\prod_{i=1}^N \left(5^2 \mathbf{1}\{\mathcal{B}_i = \mathcal{B}'_i\} + \left(\frac{1}{2}\right)^2 \mathbf{1}\{\mathcal{B}_i \neq \mathcal{B}'_i\} \right) \right] &= \left[\mathbb{E} \left(5^2 \mathbf{1}\{\mathcal{B}_i = \mathcal{B}'_i\} + \left(\frac{1}{2}\right)^2 \mathbf{1}\{\mathcal{B}_i \neq \mathcal{B}'_i\} \right) \right]^N \\ &= \left[5^2 \mathbb{E}[\mathbf{1}\{\mathcal{B}_i = \mathcal{B}'_i\}] + \left(\frac{1}{2}\right)^2 \mathbb{E}[\mathbf{1}\{\mathcal{B}_i \neq \mathcal{B}'_i\}] \right]^N = \left[5^2 \times \frac{1}{3} + \left(\frac{1}{2}\right)^2 \times \frac{2}{3} \right]^N = 8.5^N, \end{aligned} \quad (\text{C.9})$$

where we have used the fact that the expectation of an indicator function is the probability of the associated event. More precisely, $\mathbb{E}[\mathbf{1}\{\mathcal{B}_i = \mathcal{B}'_i\}] = \Pr[\mathcal{B}_i = \mathcal{B}'_i] = 1/3$, because there is a total of three basis choices to choose from. The same argument also ensures $\mathbb{E}[\mathbf{1}\{\mathcal{B}_i \neq \mathcal{B}'_i\}] = \Pr[\mathcal{B}_i \neq \mathcal{B}'_i] = 1 - \Pr[\mathcal{B}_i = \mathcal{B}'_i] = 1 - 1/3 = 2/3$. \square

We now collect a number of helpful auxiliary statements that will enable us to deduce tight bounds on the estimation protocol for function f_2 and f_4 as done in Chapter. 5. Some statements directly follow from the properties of classical shadows and are therefore valid for both Pauli and CUE shadows. Other results, however, do explicitly use the structure of Pauli basis measurements and are therefore only valid for Pauli shadows.

Lemma 2. *Given a Pauli or Haar shadow $\hat{\rho}$ that acts on N qubits and O be an observable on the same dimension. We have:*

$$\text{Var} \left[\text{Tr}(O\hat{\rho}) \right] \leq \mathbb{E} \left[\text{Tr}(O\hat{\rho})^2 \right] \leq \text{Tr}(O^2)2^N. \quad (\text{C.10})$$

Proof. The above statement follows from the proof of the original bound on the shadow norm of linear observables in Ref. [64] (proof of Proposition. 3). \square

Lemma 3. *Let $\hat{\rho}$ and $\hat{\rho}'$ be two independent Pauli shadows on N qubits. Then we have*

$$\text{Var} \left[\text{Tr}(\hat{\rho}\hat{\rho}') \right] \leq \mathbb{E} \left[\text{Tr}(\hat{\rho}\hat{\rho}')^2 \right] \leq 8.5^N. \quad (\text{C.11})$$

Proof. The proofs directly follows from Lemma. 1 by taking the expectation value of Eq. (C.7). \square

These properties will be explicitly used in Chapter. 5 in order to derive improved sample complexity bounds for functions of interest.

Bibliography

- [1] F. Arute et al. “Quantum supremacy using a programmable superconducting processor”. In: *Nature* 574.7779 (2019), pp. 505–510. ISSN: 1476-4687. DOI: [10.1038/s41586-019-1666-5](https://doi.org/10.1038/s41586-019-1666-5). URL: <https://doi.org/10.1038/s41586-019-1666-5>.
- [2] G. Barontini, L. Hohmann, F. Haas, J. Estève, and J. Reichel. “Deterministic generation of multiparticle entanglement by quantum Zeno dynamics”. In: *Science* 349.6254 (2015), pp. 1317–1321. ISSN: 0036-8075. DOI: [10.1126/science.aaa0754](https://doi.org/10.1126/science.aaa0754). URL: <https://science.sciencemag.org/content/349/6254/1317>.
- [3] J. L. Beckey, M. Cerezo, A. Sone, and P. J. Coles. “Variational quantum algorithm for estimating the quantum Fisher information”. In: *Phys. Rev. Res.* 4 (2022), p. 013083. DOI: [10.1103/PhysRevResearch.4.013083](https://doi.org/10.1103/PhysRevResearch.4.013083). URL: <https://link.aps.org/doi/10.1103/PhysRevResearch.4.013083>.
- [4] C. H. Bennett, G. Brassard, C. Crépeau, R. Jozsa, A. Peres, and W. K. Wootters. “Teleporting an unknown quantum state via dual classical and Einstein-Podolsky-Rosen channels”. In: *Phys. Rev. Lett.* 70 (13 1993), pp. 1895–1899. DOI: [10.1103/PhysRevLett.70.1895](https://doi.org/10.1103/PhysRevLett.70.1895). URL: <https://link.aps.org/doi/10.1103/PhysRevLett.70.1895>.
- [5] B. Bertini, P. Kos, and T. Prosen. “Operator Entanglement in Local Quantum Circuits I: Chaotic Dual-Unitary Circuits”. In: *SciPost Phys.* 8 (4 2020), p. 67. DOI: [10.21468/SciPostPhys.8.4.067](https://doi.org/10.21468/SciPostPhys.8.4.067). URL: <https://scipost.org/10.21468/SciPostPhys.8.4.067>.
- [6] D. Bluvstein et al. “A quantum processor based on coherent transport of entangled atom arrays”. In: *Nature* 604.7906 (2022), pp. 451–456. ISSN: 1476-4687. DOI: [10.1038/s41586-022-04592-6](https://doi.org/10.1038/s41586-022-04592-6). URL: <https://doi.org/10.1038/s41586-022-04592-6>.
- [7] J. G. Bohnet, B. C. Sawyer, J. W. Britton, M. L. Wall, A. M. Rey, M. Foss-Feig, and J. J. Bollinger. “Quantum spin dynamics and entanglement generation with hundreds of trapped ions”. In: *Science* 352.6291 (2016), pp. 1297–1301. ISSN: 0036-8075. DOI: [10.1126/science.aad9958](https://doi.org/10.1126/science.aad9958). URL: <https://science.sciencemag.org/content/352/6291/1297>.
- [8] S. L. Braunstein, C. M. Caves, and G. J. Milburn. “Generalized Uncertainty Relations: Theory, Examples, and Lorentz Invariance”. In: *Annals of Physics* 247.1 (1996), pp. 135–173. ISSN: 0003-4916. DOI: [10.1006/aphy.1996.0040](https://doi.org/10.1006/aphy.1996.0040). URL: <https://www.sciencedirect.com/science/article/pii/S0003491696900408>.

-
- [9] S. L. Braunstein and C. M. Caves. “Statistical distance and the geometry of quantum states”. In: *Phys. Rev. Lett.* 72 (1994), pp. 3439–3443. DOI: [10.1103/PhysRevLett.72.3439](https://doi.org/10.1103/PhysRevLett.72.3439). URL: <https://link.aps.org/doi/10.1103/PhysRevLett.72.3439>.
- [10] N. Brunner, D. Cavalcanti, S. Pironio, V. Scarani, and S. Wehner. “Bell nonlocality”. In: *Rev. Mod. Phys.* 86 (2014), pp. 419–478. DOI: [10.1103/RevModPhys.86.419](https://doi.org/10.1103/RevModPhys.86.419). URL: <https://link.aps.org/doi/10.1103/RevModPhys.86.419>.
- [11] T. Brydges, A. Elben, P. Jurcevic, B. Vermersch, C. Maier, B. P. Lanyon, P. Zoller, R. Blatt, and C. F. Roos. “Probing Rényi entanglement entropy via randomized measurements”. In: *Science* 364.6437 (2019), pp. 260–263. ISSN: 10959203. DOI: [10.1126/science.aau4963](https://doi.org/10.1126/science.aau4963). URL: <http://dx.doi.org/10.1126/science.aau4963>.
- [12] G. Burkard, T. D. Ladd, A. Pan, J. M. Nichol, and J. R. Petta. “Semiconductor spin qubits”. In: *Rev. Mod. Phys.* 95 (2023), p. 025003. DOI: [10.1103/RevModPhys.95.025003](https://doi.org/10.1103/RevModPhys.95.025003). URL: <https://link.aps.org/doi/10.1103/RevModPhys.95.025003>.
- [13] J. Carrasquilla, G. Torlai, R. G. Melko, and L. Aolita. “Reconstructing quantum states with generative models”. In: *Nature Machine Intelligence* 1.3 (2019), pp. 155–161. ISSN: 2522-5839. DOI: [10.1038/s42256-019-0028-1](https://doi.org/10.1038/s42256-019-0028-1). URL: <https://doi.org/10.1038/s42256-019-0028-1>.
- [14] M. Cerezo, A. Sone, J. L. Beckey, and P. J. Coles. “Sub-quantum Fisher information”. In: *Quantum Science and Technology* (2021). DOI: [10.1088/2058-9565/abfbef](https://doi.org/10.1088/2058-9565/abfbef). URL: <http://iopscience.iop.org/article/10.1088/2058-9565/abfbef>.
- [15] S. Chen, W. Yu, P. Zeng, and S. T. Flammia. “Robust Shadow Estimation”. In: *PRX Quantum* 2 (2021), p. 030348. DOI: [10.1103/PRXQuantum.2.030348](https://doi.org/10.1103/PRXQuantum.2.030348). URL: <https://link.aps.org/doi/10.1103/PRXQuantum.2.030348>.
- [16] M.-D. Choi. “Completely positive linear maps on complex matrices”. In: *Linear Algebra Appl.* 10 (1975), pp. 285–290. DOI: [10.1016/0024-3795\(75\)90075-0](https://doi.org/10.1016/0024-3795(75)90075-0). URL: [https://doi.org/10.1016/0024-3795\(75\)90075-0](https://doi.org/10.1016/0024-3795(75)90075-0).
- [17] Z.-P. Cian, H. Dehghani, A. Elben, B. Vermersch, G. Zhu, M. Barkeshli, P. Zoller, and M. Hafezi. “Many-Body Chern Number from Statistical Correlations of Randomized Measurements”. In: *Phys. Rev. Lett.* 126.5 (2021), p. 050501. DOI: [10.1103/PhysRevLett.126.050501](https://doi.org/10.1103/PhysRevLett.126.050501). URL: <https://link.aps.org/doi/10.1103/PhysRevLett.126.050501>.
- [18] J. Clarke and F. K. Wilhelm. “Superconducting quantum bits”. In: *Nature* 453.7198 (2008), pp. 1031–1042. ISSN: 1476-4687. DOI: [10.1038/nature07128](https://doi.org/10.1038/nature07128). URL: <https://doi.org/10.1038/nature07128>.
- [19] B. Collins. “Moments and Cumulants of Polynomial random variables on unitary groups, the Itzykson-Zuber integral and free probability”. In: *arXiv:math-ph/0205010* (2002). URL: <https://arxiv.org/abs/math-ph/0205010>.
-

-
- [20] B. Collins and I. Nechita. “Random matrix techniques in quantum information theory”. In: *Journal of Mathematical Physics* 57.1 (2015). 015215. ISSN: 0022-2488. DOI: [10.1063/1.4936880](https://doi.org/10.1063/1.4936880). URL: <https://doi.org/10.1063/1.4936880>.
- [21] M. Cramer, M. B. Plenio, S. T. Flammia, R. Somma, D. Gross, S. D. Bartlett, O. Landon-Cardinal, D. Poulin, and Y.-K. Liu. “Efficient quantum state tomography”. In: *Nature Communications* 1.1 (2010), p. 149. ISSN: 2041-1723. DOI: [10.1038/ncomms1147](https://doi.org/10.1038/ncomms1147). URL: <https://doi.org/10.1038/ncomms1147>.
- [22] I. H. Deutsch. “Harnessing the Power of the Second Quantum Revolution”. In: *PRX Quantum* 1 (2020), p. 020101. DOI: [10.1103/PRXQuantum.1.020101](https://doi.org/10.1103/PRXQuantum.1.020101). URL: <https://link.aps.org/doi/10.1103/PRXQuantum.1.020101>.
- [23] J. M. Deutsch. “Quantum statistical mechanics in a closed system”. In: *Phys. Rev. A* 43 (1991), pp. 2046–2049. DOI: [10.1103/PhysRevA.43.2046](https://doi.org/10.1103/PhysRevA.43.2046). URL: <https://link.aps.org/doi/10.1103/PhysRevA.43.2046>.
- [24] P. Diaconis and P. J. Forrester. “A. Hurwitz and the origins of random matrix theory in mathematics”. In: *arXiv:1512.09229* (2015). URL: <https://arxiv.org/abs/1512.09229>.
- [25] D. P. DiVincenzo. “Quantum Computation”. In: *Science* 270.5234 (1995), pp. 255–261. DOI: [10.1126/science.270.5234.255](https://doi.org/10.1126/science.270.5234.255). URL: <https://doi.org/10.1126/science.270.5234.255>.
- [26] J. Dubail. “Entanglement scaling of operators: a conformal field theory approach, with a glimpse of simulability of long-time dynamics in 1+1d”. In: *J. Phys. A* 50.23 (2017), p. 234001. DOI: [10.1088/1751-8121/aa6f38](https://doi.org/10.1088/1751-8121/aa6f38). URL: <https://doi.org/10.1088/1751-8121/aa6f38>.
- [27] J. Eisert, M. Cramer, and M. B. Plenio. “Colloquium: Area laws for the entanglement entropy”. In: *Rev. Mod. Phys.* 82 (2010), pp. 277–306. DOI: [10.1103/RevModPhys.82.277](https://doi.org/10.1103/RevModPhys.82.277). URL: <https://link.aps.org/doi/10.1103/RevModPhys.82.277>.
- [28] A. K. Ekert. “Quantum cryptography based on Bell’s theorem”. In: *Phys. Rev. Lett.* 67 (1991), pp. 661–663. DOI: [10.1103/PhysRevLett.67.661](https://doi.org/10.1103/PhysRevLett.67.661). URL: <https://link.aps.org/doi/10.1103/PhysRevLett.67.661>.
- [29] A. Elben, B. Vermersch, M. Dalmonte, J. I. Cirac, and P. Zoller. “Rényi Entropies from Random Quenches in Atomic Hubbard and Spin Models”. In: *Phys. Rev. Lett.* 120.5 (2018), p. 50406. ISSN: 10797114. DOI: [10.1103/PhysRevLett.120.050406](https://doi.org/10.1103/PhysRevLett.120.050406). URL: <https://link.aps.org/doi/10.1103/PhysRevLett.120.050406>.
- [30] A. Elben, B. Vermersch, C. F. Roos, and P. Zoller. “Statistical correlations between locally randomized measurements: A toolbox for probing entanglement in many-body quantum states”. In: *Phys. Rev. A* 99 (2019), p. 052323. DOI: [10.1103/PhysRevA.99.052323](https://doi.org/10.1103/PhysRevA.99.052323). URL: <https://link.aps.org/doi/10.1103/PhysRevA.99.052323>.
- [31] A. Elben, S. T. Flammia, H.-Y. Huang, R. Kueng, J. Preskill, B. Vermersch, and P. Zoller. “The randomized measurement toolbox”. In: *Nature Reviews Physics* 5.1 (2023), pp. 9–24. ISSN: 2522-5820. DOI: [10.1038/s42254-022-00535-2](https://doi.org/10.1038/s42254-022-00535-2). URL: <https://doi.org/10.1038/s42254-022-00535-2>.
-

-
- [32] A. Elben, B. Vermersch, R. Van Bijnen, C. Kokail, T. Brydges, C. Maier, M. K. Joshi, R. Blatt, C. F. Roos, and P. Zoller. “Cross-Platform Verification of Intermediate Scale Quantum Devices”. In: *Phys. Rev. Lett.* 124.1 (2020), p. 10504. ISSN: 10797114. DOI: [10.1103/PhysRevLett.124.010504](https://doi.org/10.1103/PhysRevLett.124.010504). URL: <https://link.aps.org/doi/10.1103/PhysRevLett.124.010504>.
- [33] A. Elben, J. Yu, G. Zhu, M. Hafezi, F. Pollmann, P. Zoller, and B. Vermersch. “Many-body topological invariants from randomized measurements in synthetic quantum matter”. In: *Science Advances* 6.15 (2020), eaaz3666. ISSN: 2375-2548. DOI: [10.1126/sciadv.aaz3666](https://doi.org/10.1126/sciadv.aaz3666). URL: <https://advances.sciencemag.org/lookup/doi/10.1126/sciadv.aaz3666>.
- [34] A. Elben et al. “Mixed-State Entanglement from Local Randomized Measurements”. In: *Phys. Rev. Lett.* 125 (2020), p. 200501. DOI: [10.1103/PhysRevLett.125.200501](https://doi.org/10.1103/PhysRevLett.125.200501). URL: <https://link.aps.org/doi/10.1103/PhysRevLett.125.200501>.
- [35] J. Emerson, Y. S. Weinstein, M. Saraceno, S. Lloyd, and D. G. Cory. “Pseudo-Random Unitary Operators for Quantum Information Processing”. In: *Science* 302.5653 (2003), pp. 2098–2100. DOI: [10.1126/science.1090790](https://doi.org/10.1126/science.1090790). URL: <https://www.science.org/doi/abs/10.1126/science.1090790>.
- [36] S. J. van Enk and C. W. J. Beenakker. “Measuring $\text{Tr}\rho^n$ on Single Copies of ρ Using Random Measurements”. In: *Phys. Rev. Lett.* 108 (2012), p. 110503. DOI: [10.1103/PhysRevLett.108.110503](https://doi.org/10.1103/PhysRevLett.108.110503). URL: <https://link.aps.org/doi/10.1103/PhysRevLett.108.110503>.
- [37] E. Farhi, J. Goldstone, and S. Gutmann. “A Quantum Approximate Optimization Algorithm”. In: *arXiv:1411.4028* (2014). URL: <https://arxiv.org/abs/1411.4028>.
- [38] R. P. Feynman. “Simulating physics with computers”. In: *International Journal of Theoretical Physics* 21.6 (1982), pp. 467–488. ISSN: 1572-9575. DOI: [10.1007/BF02650179](https://doi.org/10.1007/BF02650179). URL: <https://doi.org/10.1007/BF02650179>.
- [39] M. P. A. Fisher, V. Khemani, A. Nahum, and S. Vijay. “Random Quantum Circuits”. In: *arXiv:2207.14280* (2022). URL: <https://arxiv.org/abs/2207.14280>.
- [40] M. Fishman and G. Torlai. *PastaQ: A Package for Simulation, Tomography and Analysis of Quantum Computers*. 2020. URL: <https://github.com/GTorlai/PastaQ.jl/>.
- [41] S. T. Flammia and Y.-K. Liu. “Direct Fidelity Estimation from Few Pauli Measurements”. In: *Phys. Rev. Lett.* 106 (2011), p. 230501. DOI: [10.1103/PhysRevLett.106.230501](https://doi.org/10.1103/PhysRevLett.106.230501). URL: <https://link.aps.org/doi/10.1103/PhysRevLett.106.230501>.
- [42] I. Frérot, M. Fadel, and M. Lewenstein. “Probing quantum correlations in many-body systems: a review of scalable methods”. In: *arXiv:2302.00640* (2023). URL: <https://arxiv.org/abs/2302.00640>.
- [43] N. Friis et al. “Observation of Entangled States of a Fully Controlled 20-Qubit System”. In: *Phys. Rev. X* 8 (2018), p. 021012. DOI: [10.1103/PhysRevX.8.021012](https://doi.org/10.1103/PhysRevX.8.021012). URL: <https://link.aps.org/doi/10.1103/PhysRevX.8.021012>.
-

-
- [44] M. Gabbrielli, A. Smerzi, and L. Pezzè. “Multipartite Entanglement at Finite Temperature”. In: *Scientific Reports* 8.1 (2018), p. 15663. ISSN: 2045-2322. DOI: [10.1038/s41598-018-31761-3](https://doi.org/10.1038/s41598-018-31761-3). URL: <https://doi.org/10.1038/s41598-018-31761-3>.
- [45] M. Gärttner, P. Hauke, and A. M. Rey. “Relating Out-of-Time-Order Correlations to Entanglement via Multiple-Quantum Coherences”. In: *Phys. Rev. Lett.* 120 (2018), p. 040402. DOI: [10.1103/PhysRevLett.120.040402](https://link.aps.org/doi/10.1103/PhysRevLett.120.040402). URL: <https://link.aps.org/doi/10.1103/PhysRevLett.120.040402>.
- [46] I. M. Georgescu, S. Ashhab, and F. Nori. “Quantum simulation”. In: *Rev. Mod. Phys.* 86 (1 2014), pp. 153–185. DOI: [10.1103/RevModPhys.86.153](https://link.aps.org/doi/10.1103/RevModPhys.86.153). URL: <https://link.aps.org/doi/10.1103/RevModPhys.86.153>.
- [47] V. Giovannetti, S. Lloyd, and L. Maccone. “Quantum Metrology”. In: *Phys. Rev. Lett.* 96 (2006), p. 010401. DOI: [10.1103/PhysRevLett.96.010401](https://link.aps.org/doi/10.1103/PhysRevLett.96.010401). URL: <https://link.aps.org/doi/10.1103/PhysRevLett.96.010401>.
- [48] D. Girolami and B. Yadin. “Witnessing Multipartite Entanglement by Detecting Asymmetry”. In: *Entropy* 19.3 (2017), p. 124. ISSN: 1099-4300. DOI: [10.3390/e19030124](http://www.mdpi.com/1099-4300/19/3/124). URL: <http://www.mdpi.com/1099-4300/19/3/124>.
- [49] N. Gisin and R. Thew. “Quantum communication”. In: *Nature Photonics* 1.3 (2007), pp. 165–171. ISSN: 1749-4893. DOI: [10.1038/nphoton.2007.22](https://doi.org/10.1038/nphoton.2007.22). URL: <https://doi.org/10.1038/nphoton.2007.22>.
- [50] D. Gottesman. “The Heisenberg Representation of Quantum Computers”. In: *arXiv:quant-ph/9807006* (1998). URL: <https://arxiv.org/abs/quant-ph/9807006>.
- [51] D. Gross, K. Audenaert, and J. Eisert. “Evenly distributed unitaries: On the structure of unitary designs”. In: *Journal of Mathematical Physics* 48.5 (2007), p. 052104. DOI: [10.1063/1.2716992](https://doi.org/10.1063/1.2716992). URL: <https://doi.org/10.1063/1.2716992>.
- [52] D. Gross, Y.-K. Liu, S. T. Flammia, S. Becker, and J. Eisert. “Quantum State Tomography via Compressed Sensing”. In: *Phys. Rev. Lett.* 105.15 (2010), p. 150401. DOI: [10.1103/PhysRevLett.105.150401](https://link.aps.org/doi/10.1103/PhysRevLett.105.150401). URL: <https://link.aps.org/doi/10.1103/PhysRevLett.105.150401>.
- [53] O. Gühne and G. Tóth. “Entanglement detection”. In: *Phys. Rep.* 474.1 (2009), pp. 1–75. ISSN: 0370-1573. DOI: [10.1016/j.physrep.2009.02.004](https://www.sciencedirect.com/science/article/pii/S0370157309000623). URL: <https://www.sciencedirect.com/science/article/pii/S0370157309000623>.
- [54] J. Haah, A. W. Harrow, Z. Ji, X. Wu, and N. Yu. “Sample-Optimal Tomography of Quantum States”. In: *IEEE Transactions on Information Theory* 63.9 (2017), pp. 5628–5641. DOI: [10.1109/TIT.2017.2719044](https://ieeexplore.ieee.org/document/7956181). URL: <https://ieeexplore.ieee.org/document/7956181>.
- [55] C. Hadfield. “Adaptive Pauli Shadows for Energy Estimation”. In: *arXiv:2105.12207* (2021). URL: <https://arxiv.org/abs/2105.12207>.
-

-
- [56] C. Hadfield, S. Bravyi, R. Raymond, and A. Mezzacapo. “Measurements of Quantum Hamiltonians with Locally-Biased Classical Shadows”. In: *Communications in Mathematical Physics* 391.3 (2022), pp. 951–967. ISSN: 1432-0916. DOI: [10.1007/s00220-022-04343-8](https://doi.org/10.1007/s00220-022-04343-8). URL: <https://doi.org/10.1007/s00220-022-04343-8>.
- [57] A. Hamma, R. Ionicioiu, and P. Zanardi. “Ground state entanglement and geometric entropy in the Kitaev model”. In: *Physics Letters A* 337.1 (2005), pp. 22–28. ISSN: 0375-9601. DOI: [10.1016/j.physleta.2005.01.060](https://doi.org/10.1016/j.physleta.2005.01.060). URL: <https://www.sciencedirect.com/science/article/pii/S0375960105001544>.
- [58] P. Hauke, M. Heyl, L. Tagliacozzo, and P. Zoller. “Measuring multipartite entanglement through dynamic susceptibilities”. In: *Nature Physics* 12.8 (2016), pp. 778–782. ISSN: 1745-2481. DOI: [10.1038/nphys3700](https://doi.org/10.1038/nphys3700). URL: <https://doi.org/10.1038/nphys3700>.
- [59] W. Hoeffding. “A class of statistics with asymptotically normal distribution”. In: *Breakthroughs in Statistics*. Springer, 1992, pp. 308–334.
- [60] J. C. Hoke and et al. “Quantum information phases in space-time: measurement-induced entanglement and teleportation on a noisy quantum processor”. In: *arXiv:2303.04792* (2023). URL: <https://arxiv.org/abs/2303.04792>.
- [61] M. Horodecki, P. Horodecki, and R. Horodecki. “Separability of mixed states: necessary and sufficient conditions”. In: *Physics Letters A* 223.1 (1996), pp. 1–8. ISSN: 0375-9601. DOI: [https://doi.org/10.1016/S0375-9601\(96\)00706-2](https://doi.org/10.1016/S0375-9601(96)00706-2). URL: <https://www.sciencedirect.com/science/article/pii/S0375960196007062>.
- [62] R. Horodecki, P. Horodecki, M. Horodecki, and K. Horodecki. “Quantum entanglement”. In: *Rev. Mod. Phys.* 81 (2009), pp. 865–942. DOI: [10.1103/RevModPhys.81.865](https://doi.org/10.1103/RevModPhys.81.865). URL: <https://link.aps.org/doi/10.1103/RevModPhys.81.865>.
- [63] H.-Y. Huang, R. Kueng, and J. Preskill. “Efficient Estimation of Pauli Observables by Derandomization”. In: *Phys. Rev. Lett.* 127 (2021), p. 030503. DOI: [10.1103/PhysRevLett.127.030503](https://doi.org/10.1103/PhysRevLett.127.030503). URL: <https://link.aps.org/doi/10.1103/PhysRevLett.127.030503>.
- [64] H.-Y. Huang, R. Kueng, and J. Preskill. “Predicting many properties of a quantum system from very few measurements”. In: *Nature Physics* 16.10 (2020), pp. 1050–1057. ISSN: 1745-2473. DOI: [10.1038/s41567-020-0932-7](https://doi.org/10.1038/s41567-020-0932-7). URL: <http://www.nature.com/articles/s41567-020-0932-7>.
- [65] H.-Y. Huang, R. Kueng, G. Torlai, V. V. Albert, and J. Preskill. “Provably efficient machine learning for quantum many-body problems”. In: *Science* 377.6613 (2022), eabk3333. DOI: [10.1126/science.abk3333](https://doi.org/10.1126/science.abk3333). URL: <https://www.science.org/doi/abs/10.1126/science.abk3333>.
- [66] S. Humeniuk and T. Roscilde. “Quantum Monte Carlo calculation of entanglement Rényi entropies for generic quantum systems”. In: *Phys. Rev. B* 86 (2012), p. 235116. DOI: [10.1103/PhysRevB.86.235116](https://doi.org/10.1103/PhysRevB.86.235116). URL: <https://link.aps.org/doi/10.1103/PhysRevB.86.235116>.
-

-
- [67] P. Hyllus, W. Laskowski, R. Krischek, C. Schwemmer, W. Wieczorek, H. Weinfurter, L. Pezzé, and A. Smerzi. “Fisher information and multiparticle entanglement”. In: *Phys. Rev. A* 85.2 (2012), p. 22321. DOI: [10.1103/PhysRevA.85.022321](https://doi.org/10.1103/PhysRevA.85.022321). URL: <https://link.aps.org/doi/10.1103/PhysRevA.85.022321>.
- [68] R. Islam, R. Ma, P. M. Preiss, M. Eric Tai, A. Lukin, M. Rispoli, and M. Greiner. “Measuring entanglement entropy in a quantum many-body system”. In: *Nature* 528.7580 (2015), pp. 77–83. ISSN: 14764687. DOI: [10.1038/nature15750](https://doi.org/10.1038/nature15750). URL: <http://www.nature.com/doi/10.1038/nature15750>.
- [69] D. Jaksch, H.-J. Briegel, J. I. Cirac, C. W. Gardiner, and P. Zoller. “Entanglement of Atoms via Cold Controlled Collisions”. In: *Phys. Rev. Lett.* 82 (1999), pp. 1975–1978. DOI: [10.1103/PhysRevLett.82.1975](https://doi.org/10.1103/PhysRevLett.82.1975). URL: <https://link.aps.org/doi/10.1103/PhysRevLett.82.1975>.
- [70] D. Jaksch, J. I. Cirac, P. Zoller, S. L. Rolston, R. Côté, and M. D. Lukin. “Fast Quantum Gates for Neutral Atoms”. In: *Phys. Rev. Lett.* 85 (2000), pp. 2208–2211. DOI: [10.1103/PhysRevLett.85.2208](https://doi.org/10.1103/PhysRevLett.85.2208). URL: <https://link.aps.org/doi/10.1103/PhysRevLett.85.2208>.
- [71] A. Jamiolkowski. “Linear transformations which preserve trace and positive semidefiniteness of operators”. In: *Rep. Math. Phys.* 3 (1972), pp. 275–278. DOI: [10.1016/0034-4877\(72\)90011-0](https://doi.org/10.1016/0034-4877(72)90011-0). URL: <https://www.sciencedirect.com/science/article/pii/0034487772900110>.
- [72] M. K. Joshi, A. Elben, B. Vermersch, T. Brydges, C. Maier, P. Zoller, R. Blatt, and C. F. Roos. “Quantum Information Scrambling in a Trapped-Ion Quantum Simulator with Tunable Range Interactions”. In: *Phys. Rev. Lett.* 124 (2020), p. 240505. DOI: [10.1103/PhysRevLett.124.240505](https://doi.org/10.1103/PhysRevLett.124.240505). URL: <https://link.aps.org/doi/10.1103/PhysRevLett.124.240505>.
- [73] M. K. Joshi, C. Kokail, R. van Bijnen, F. Kranzl, T. V. Zache, R. Blatt, C. F. Roos, and P. Zoller. *Exploring Large-Scale Entanglement in Quantum Simulation*. 2023. URL: <https://arxiv.org/abs/2306.00057>.
- [74] V. Katariya and M. M. Wilde. “Geometric distinguishability measures limit quantum channel estimation and discrimination”. In: *Quantum Information Processing* 20.2 (2021). DOI: [10.1007/s11128-021-02992-7](https://doi.org/10.1007/s11128-021-02992-7). URL: <https://doi.org/10.1007/s11128-021-02992-7>.
- [75] A. Kitaev and J. Preskill. “Topological Entanglement Entropy”. In: *Phys. Rev. Lett.* 96 (2006), p. 110404. DOI: [10.1103/PhysRevLett.96.110404](https://doi.org/10.1103/PhysRevLett.96.110404). URL: <https://link.aps.org/doi/10.1103/PhysRevLett.96.110404>.
- [76] D. E. Koh and S. Grewal. “Classical Shadows With Noise”. In: *Quantum* 6 (2022), p. 776. ISSN: 2521-327X. DOI: [10.22331/q-2022-08-16-776](https://doi.org/10.22331/q-2022-08-16-776). URL: <https://doi.org/10.22331/q-2022-08-16-776>.
- [77] B. P. Lanyon et al. “Efficient tomography of a quantum many-body system”. In: *Nature Physics* 13.12 (2017), pp. 1158–1162. ISSN: 1745-2481. DOI: [10.1038/nphys4244](https://doi.org/10.1038/nphys4244). URL: <https://doi.org/10.1038/nphys4244>.
-

-
- [78] L. Lewis, H.-Y. Huang, V. T. Tran, S. Lehner, R. Kueng, and J. Preskill. “Improved machine learning algorithm for predicting ground state properties”. In: *arXiv:2301.13169* (2023). URL: <https://arxiv.org/abs/2301.13169>.
- [79] Y.-C. Liang, Y.-H. Yeh, P. E. M. F. Mendonça, R. Y. Teh, M. D. Reid, and P. D. Drummond. “Quantum fidelity measures for mixed states”. In: *Reports on Progress in Physics* 82.7 (2019), p. 076001. DOI: [10.1088/1361-6633/ab1ca4](https://doi.org/10.1088/1361-6633/ab1ca4). URL: <https://dx.doi.org/10.1088/1361-6633/ab1ca4>.
- [80] Z. Liu, Y. Tang, H. Dai, P. Liu, S. Chen, and X. Ma. “Detecting Entanglement in Quantum Many-Body Systems via Permutation Moments”. In: *Phys. Rev. Lett.* 129 (2022), p. 260501. DOI: [10.1103/PhysRevLett.129.260501](https://doi.org/10.1103/PhysRevLett.129.260501). URL: <https://link.aps.org/doi/10.1103/PhysRevLett.129.260501>.
- [81] K. Macieszczak, M. Ą. Gu Ą Ą, I. Lesanovsky, and J. P. Garrahan. “Dynamical phase transitions as a resource for quantum enhanced metrology”. In: *Phys. Rev. A* 93 (2016), p. 022103. DOI: [10.1103/PhysRevA.93.022103](https://doi.org/10.1103/PhysRevA.93.022103). URL: <https://link.aps.org/doi/10.1103/PhysRevA.93.022103>.
- [82] K. Mallayya, M. Rigol, and W. De Roeck. “Prethermalization and Thermalization in Isolated Quantum Systems”. In: *Phys. Rev. X* 9 (2019), p. 021027. DOI: [10.1103/PhysRevX.9.021027](https://doi.org/10.1103/PhysRevX.9.021027). URL: <https://link.aps.org/doi/10.1103/PhysRevX.9.021027>.
- [83] C. Monroe et al. “Programmable quantum simulations of spin systems with trapped ions”. In: *Rev. Mod. Phys.* 93 (2021), p. 025001. DOI: [10.1103/RevModPhys.93.025001](https://doi.org/10.1103/RevModPhys.93.025001). URL: <https://link.aps.org/doi/10.1103/RevModPhys.93.025001>.
- [84] T. Monz, P. Schindler, J. T. Barreiro, M. Chwalla, D. Nigg, W. A. Coish, M. Harlander, W. Hänsel, M. Hennrich, and R. Blatt. “14-Qubit Entanglement: Creation and Coherence”. In: *Phys. Rev. Lett.* 106 (2011), p. 130506. DOI: [10.1103/PhysRevLett.106.130506](https://doi.org/10.1103/PhysRevLett.106.130506). URL: <https://link.aps.org/doi/10.1103/PhysRevLett.106.130506>.
- [85] T. Mori, T. N. Ikeda, E. Kaminishi, and M. Ueda. “Thermalization and prethermalization in isolated quantum systems: a theoretical overview”. In: *J. Phys. B* 51.11 (2018), p. 112001. DOI: [10.1088/1361-6455/aabcdf](https://doi.org/10.1088/1361-6455/aabcdf). URL: <https://doi.org/10.1088/1361-6455/aabcdf>.
- [86] A. Neven et al. “Symmetry-resolved entanglement detection using partial transpose moments”. In: *npj Quantum Information* 7.1 (2021), p. 152. DOI: [10.1038/s41534-021-00487-y](https://doi.org/10.1038/s41534-021-00487-y). URL: <https://www.nature.com/articles/s41534-021-00487-y>.
- [87] M. Ohliger, V. Nesme, and J. Eisert. “Efficient and feasible state tomography of quantum many-body systems”. In: *New Journal of Physics* 15.1 (2013), p. 015024. DOI: [10.1088/1367-2630/15/1/015024](https://doi.org/10.1088/1367-2630/15/1/015024). URL: <https://dx.doi.org/10.1088/1367-2630/15/1/015024>.
- [88] E. Onorati, C. Rouze, D. S. Franca, and J. D. Watson. “Efficient learning of ground & thermal states within phases of matter”. In: *arXiv:2301.12946* (2023). URL: <https://arxiv.org/abs/2301.12946>.
-

-
- [89] R. Orús. “Tensor networks for complex quantum systems”. In: *Nature Reviews Physics* 1.9 (2019), pp. 538–550. ISSN: 2522-5820. DOI: [10.1038/s42254-019-0086-7](https://doi.org/10.1038/s42254-019-0086-7). URL: <https://doi.org/10.1038/s42254-019-0086-7>.
- [90] S. Pappalardi, A. Russomanno, A. Silva, and R. Fazio. “Multipartite entanglement after a quantum quench”. In: *Journal of Statistical Mechanics: Theory and Experiment* 2017.5 (2017), p. 053104. DOI: [10.1088/1742-5468/aa6809](https://dx.doi.org/10.1088/1742-5468/aa6809). URL: <https://dx.doi.org/10.1088/1742-5468/aa6809>.
- [91] A. Peres. “Separability Criterion for Density Matrices”. In: *Phys. Rev. Lett.* 77 (1996), pp. 1413–1415. DOI: [10.1103/PhysRevLett.77.1413](https://link.aps.org/doi/10.1103/PhysRevLett.77.1413). URL: <https://link.aps.org/doi/10.1103/PhysRevLett.77.1413>.
- [92] L. Pezzè, M. Gabbriellini, L. Lepori, and A. Smerzi. “Multipartite Entanglement in Topological Quantum Phases”. In: *Phys. Rev. Lett.* 119 (2017), p. 250401. DOI: [10.1103/PhysRevLett.119.250401](https://link.aps.org/doi/10.1103/PhysRevLett.119.250401). URL: <https://link.aps.org/doi/10.1103/PhysRevLett.119.250401>.
- [93] L. Pezzè and A. Smerzi. “Entanglement, Nonlinear Dynamics, and the Heisenberg Limit”. In: *Phys. Rev. Lett.* 102.10 (2009), p. 100401. ISSN: 0031-9007. DOI: [10.1103/PhysRevLett.102.100401](https://link.aps.org/doi/10.1103/PhysRevLett.102.100401). URL: <https://link.aps.org/doi/10.1103/PhysRevLett.102.100401>.
- [94] L. Pezzè, A. Smerzi, M. K. Oberthaler, R. Schmied, and P. Treutlein. “Quantum metrology with nonclassical states of atomic ensembles”. In: *Reviews of Modern Physics* 90.3 (2018), p. 35005. ISSN: 0034-6861. DOI: [10.1103/RevModPhys.90.035005](https://link.aps.org/doi/10.1103/RevModPhys.90.035005). URL: <https://link.aps.org/doi/10.1103/RevModPhys.90.035005>.
- [95] I. Pi žorn and T. Prosen. “Operator space entanglement entropy in XY spin chains”. In: *Phys. Rev. B* 79 (2009), p. 184416. DOI: [10.1103/PhysRevB.79.184416](https://link.aps.org/doi/10.1103/PhysRevB.79.184416). URL: <https://link.aps.org/doi/10.1103/PhysRevB.79.184416>.
- [96] M. Planitz, W. H. Press, B. P. Flannery, S. A. Teukolsky, and W. T. Vetterling. *Numerical Recipes: The Art of Scientific Computing*. 3rd ed. Vol. 71. 457. New York, NY, USA: Cambridge University Press, 1987. ISBN: 0521880688, 9780521880688. DOI: [10.2307/3616786](https://doi.org/10.2307/3616786).
- [97] J. Preskill. “Quantum Computing in the NISQ era and beyond”. In: *Quantum* 2 (2018), p. 79. ISSN: 2521-327X. DOI: [10.22331/q-2018-08-06-79](https://quantum-journal.org/papers/q-2018-08-06-79/). URL: <https://quantum-journal.org/papers/q-2018-08-06-79/>.
- [98] T. Prosen and I. Pi žorn. “Operator space entanglement entropy in a transverse Ising chain”. In: *Phys. Rev. A* 76 (2007), p. 032316. DOI: [10.1103/PhysRevA.76.032316](https://link.aps.org/doi/10.1103/PhysRevA.76.032316). URL: <https://link.aps.org/doi/10.1103/PhysRevA.76.032316>.
- [99] A. Rath, R. van Bijnen, A. Elben, P. Zoller, and B. Vermersch. “Importance Sampling of Randomized Measurements for Probing Entanglement”. In: *Phys. Rev. Lett.* 127 (2021), p. 200503. DOI: [10.1103/PhysRevLett.127.200503](https://link.aps.org/doi/10.1103/PhysRevLett.127.200503). URL: <https://link.aps.org/doi/10.1103/PhysRevLett.127.200503>.
- [100] A. Rath, C. Branciard, A. Minguzzi, and B. Vermersch. “Quantum Fisher Information from Randomized Measurements”. In: *Phys. Rev. Lett.* 127 (2021), p. 260501. DOI: [10.1103/PhysRevLett.127.260501](https://link.aps.org/doi/10.1103/PhysRevLett.127.260501). URL: <https://link.aps.org/doi/10.1103/PhysRevLett.127.260501>.
-

-
- [101] A. Rath, V. Vitale, S. Murciano, M. Votto, J. Dubail, R. Kueng, C. Branciard, P. Calabrese, and B. Vermersch. “Entanglement Barrier and its Symmetry Resolution: Theory and Experimental Observation”. In: *PRX Quantum* 4 (2023), p. 010318. DOI: [10.1103/PRXQuantum.4.010318](https://doi.org/10.1103/PRXQuantum.4.010318). URL: <https://link.aps.org/doi/10.1103/PRXQuantum.4.010318>.
- [102] Z. Ren, W. Li, A. Smerzi, and M. Gessner. “Metrological Detection of Multipartite Entanglement from Young Diagrams”. In: *Phys. Rev. Lett.* 126.8 (2021), p. 80502. DOI: [10.1103/PhysRevLett.126.080502](https://doi.org/10.1103/PhysRevLett.126.080502). URL: <https://link.aps.org/doi/10.1103/PhysRevLett.126.080502>.
- [103] M. Rigol, V. Dunjko, and M. Olshanii. “Thermalization and its mechanism for generic isolated quantum systems”. In: *Nature* 452.7189 (2008), pp. 854–858. ISSN: 1476-4687. DOI: [10.1038/nature06838](https://doi.org/10.1038/nature06838). URL: <https://doi.org/10.1038/nature06838>.
- [104] Á. Rivas and A. Luis. “Intrinsic metrological resolution as a distance measure and nonclassical light”. In: *Phys. Rev. A* 77 (2008), p. 063813. DOI: [10.1103/PhysRevA.77.063813](https://doi.org/10.1103/PhysRevA.77.063813). URL: <https://link.aps.org/doi/10.1103/PhysRevA.77.063813>.
- [105] Á. Rivas and A. Luis. “Precision Quantum Metrology and Nonclassicality in Linear and Nonlinear Detection Schemes”. In: *Phys. Rev. Lett.* 105 (2010), p. 010403. DOI: [10.1103/PhysRevLett.105.010403](https://doi.org/10.1103/PhysRevLett.105.010403). URL: <https://link.aps.org/doi/10.1103/PhysRevLett.105.010403>.
- [106] D. A. Roberts and B. Yoshida. “Chaos and complexity by design”. In: *Journal of High Energy Physics* 2017.4 (2017), p. 121. ISSN: 1029-8479. DOI: [10.1007/JHEP04\(2017\)121](https://doi.org/10.1007/JHEP04(2017)121). URL: [https://doi.org/10.1007/JHEP04\(2017\)121](https://doi.org/10.1007/JHEP04(2017)121).
- [107] O. Rudolph. “Computable Cross-norm Criterion for Separability”. In: *Letters in Mathematical Physics* 70.1 (2004), pp. 57–64. ISSN: 1573-0530. DOI: [10.1007/s11005-004-0767-7](https://doi.org/10.1007/s11005-004-0767-7). URL: <https://doi.org/10.1007/s11005-004-0767-7>.
- [108] O. Rudolph. “Further Results on the Cross Norm Criterion for Separability”. In: *Quantum Information Processing* 4.3 (2005), pp. 219–239. ISSN: 1573-1332. DOI: [10.1007/s11128-005-5664-1](https://doi.org/10.1007/s11128-005-5664-1). URL: <https://doi.org/10.1007/s11128-005-5664-1>.
- [109] S. H. Sack, R. A. Medina, A. A. Michailidis, R. Kueng, and M. Serbyn. “Avoiding Barren Plateaus Using Classical Shadows”. In: *PRX Quantum* 3 (2022), p. 020365. DOI: [10.1103/PRXQuantum.3.020365](https://doi.org/10.1103/PRXQuantum.3.020365). URL: <https://link.aps.org/doi/10.1103/PRXQuantum.3.020365>.
- [110] M. Saffman, T. G. Walker, and K. Mølmer. “Quantum information with Rydberg atoms”. In: *Rev. Mod. Phys.* 82 (2010), pp. 2313–2363. DOI: [10.1103/RevModPhys.82.2313](https://doi.org/10.1103/RevModPhys.82.2313). URL: <https://link.aps.org/doi/10.1103/RevModPhys.82.2313>.
- [111] K. J. Satzinger et al. “Realizing topologically ordered states on a quantum processor”. In: *Science* 374.6572 (2021), pp. 1237–1241. DOI: [10.1126/science.abi8378](https://doi.org/10.1126/science.abi8378). URL: <https://www.science.org/doi/abs/10.1126/science.abi8378>.
-

-
- [112] R. Schmied, J.-D. Bancal, B. Allard, M. Fadel, V. Scarani, P. Treutlein, and N. Sangouard. “Bell correlations in a Bose-Einstein condensate”. In: *Science* 352.6284 (2016), pp. 441–444. DOI: [10.1126/science.aad8665](https://doi.org/10.1126/science.aad8665). URL: <https://www.science.org/doi/abs/10.1126/science.aad8665>.
- [113] U. Schollwöck. “The density-matrix renormalization group in the age of matrix product states”. In: *Annals of Physics* 326.1 (2011), pp. 96–192. ISSN: 00034916. DOI: [10.1016/j.aop.2010.09.012](https://doi.org/10.1016/j.aop.2010.09.012). URL: <https://linkinghub.elsevier.com/retrieve/pii/S0003491610001752>.
- [114] M. P. da Silva, O. Landon-Cardinal, and D. Poulin. “Practical Characterization of Quantum Devices without Tomography”. In: *Phys. Rev. Lett.* 107 (2011), p. 210404. DOI: [10.1103/PhysRevLett.107.210404](https://doi.org/10.1103/PhysRevLett.107.210404). URL: <https://link.aps.org/doi/10.1103/PhysRevLett.107.210404>.
- [115] A. Smerzi. “Zeno Dynamics, Indistinguishability of State, and Entanglement”. In: *Phys. Rev. Lett.* 109 (2012), p. 150410. DOI: [10.1103/PhysRevLett.109.150410](https://doi.org/10.1103/PhysRevLett.109.150410). URL: <https://link.aps.org/doi/10.1103/PhysRevLett.109.150410>.
- [116] C. Song et al. “10-Qubit Entanglement and Parallel Logic Operations with a Superconducting Circuit”. In: *Phys. Rev. Lett.* 119 (2017), p. 180511. DOI: [10.1103/PhysRevLett.119.180511](https://doi.org/10.1103/PhysRevLett.119.180511). URL: <https://link.aps.org/doi/10.1103/PhysRevLett.119.180511>.
- [117] M. Srednicki. “Chaos and quantum thermalization”. In: *Phys. Rev. E* 50 (1994), pp. 888–901. DOI: [10.1103/PhysRevE.50.888](https://doi.org/10.1103/PhysRevE.50.888). URL: <https://link.aps.org/doi/10.1103/PhysRevE.50.888>.
- [118] R. Stricker, M. Meth, L. Postler, C. Edmunds, C. Ferrie, R. Blatt, P. Schindler, T. Monz, R. Kueng, and M. Ringbauer. “Experimental Single-Setting Quantum State Tomography”. In: *PRX Quantum* 3 (2022), p. 040310. DOI: [10.1103/PRXQuantum.3.040310](https://doi.org/10.1103/PRXQuantum.3.040310). URL: <https://link.aps.org/doi/10.1103/PRXQuantum.3.040310>.
- [119] H. Strobel, W. Muessel, D. Linnemann, T. Zibold, D. B. Hume, L. Pezzè, A. Smerzi, and M. K. Oberthaler. “Fisher information and entanglement of non-Gaussian spin states”. In: *Science* 345.6195 (2014), pp. 424–427. ISSN: 0036-8075. DOI: [10.1126/science.1250147](https://doi.org/10.1126/science.1250147). URL: <https://science.sciencemag.org/content/345/6195/424>.
- [120] B. M. Terhal. “Bell inequalities and the separability criterion”. In: *Physics Letters A* 271.5 (2000), pp. 319–326. ISSN: 0375-9601. DOI: [10.1016/S0375-9601\(00\)00401-1](https://doi.org/10.1016/S0375-9601(00)00401-1). URL: <https://www.sciencedirect.com/science/article/pii/S0375960100004011>.
- [121] G. Torlai, G. Mazzola, J. Carrasquilla, M. Troyer, R. Melko, and G. Carleo. “Neural-network quantum state tomography”. In: *Nature Physics* 14.5 (2018), pp. 447–450. ISSN: 17452481. DOI: [10.1038/s41567-018-0048-5](https://doi.org/10.1038/s41567-018-0048-5). URL: <http://www.nature.com/articles/s41567-018-0048-5>.
- [122] G. Tóth. “Multipartite entanglement and high-precision metrology”. In: *Phys. Rev. A* 85.2 (2012), p. 22322. DOI: [10.1103/PhysRevA.85.022322](https://doi.org/10.1103/PhysRevA.85.022322). URL: <https://link.aps.org/doi/10.1103/PhysRevA.85.022322>.
-

-
- [123] K. Van Kirk, J. Cotler, H.-Y. Huang, and M. D. Lukin. “Hardware-efficient learning of quantum many-body states”. In: *arXiv:2212.06084* (2022). URL: <https://arxiv.org/abs/2212.06084>.
- [124] B. Vermersch, A. Elben, M. Dalmonte, J. I. Cirac, and P. Zoller. “Unitary n-designs via random quenches in atomic Hubbard and spin models: Application to the measurement of Rényi entropies”. In: *Phys. Rev. A* 97.2 (2018), p. 23604. ISSN: 24699934. DOI: 10.1103/PhysRevA.97.023604. URL: <https://link.aps.org/doi/10.1103/PhysRevA.97.023604>.
- [125] B. Vermersch, A. Elben, L. M. Sieberer, N. Y. Yao, and P. Zoller. “Probing Scrambling Using Statistical Correlations between Randomized Measurements”. In: *Phys. Rev. X* 9.2 (2019), p. 21061. DOI: 10.1103/PhysRevX.9.021061. URL: <http://dx.doi.org/10.1103/PhysRevX.9.021061>.
- [126] B. Vermersch, A. Rath, B. Sundar, C. Branciard, J. Preskill, and A. Elben. “Enhanced estimation of quantum properties with common randomized measurements”. In: *arXiv:2304.12292* (2023). URL: <https://arxiv.org/abs/2304.12292>.
- [127] F. Verstraete, V. Murg, and J. Cirac. “Matrix product states, projected entangled pair states, and variational renormalization group methods for quantum spin systems”. In: *Adv. Phys.* 57 (2008), p. 143. DOI: 10.1080/14789940801912366. URL: <https://doi.org/10.1080/14789940801912366>.
- [128] G. Vidal and R. F. Werner. “Computable measure of entanglement”. In: *Phys. Rev. A* 65 (2002), p. 032314. DOI: 10.1103/PhysRevA.65.032314. URL: <https://link.aps.org/doi/10.1103/PhysRevA.65.032314>.
- [129] V. Vitale, A. Rath, P. Jurcevic, A. Elben, C. Branciard, and B. Vermersch. “Estimation of the Quantum Fisher Information on a quantum processor”. In: *arXiv:2307.16882* (2023). URL: <https://arxiv.org/abs/2307.16882>.
- [130] H. Wang and T. Zhou. “Barrier from chaos: operator entanglement dynamics of the reduced density matrix”. In: *Journal of High Energy Physics* 2019.12 (2019), p. 20. ISSN: 1029-8479. DOI: 10.1007/JHEP12(2019)020. URL: [https://doi.org/10.1007/JHEP12\(2019\)020](https://doi.org/10.1007/JHEP12(2019)020).
- [131] T.-L. Wang, L.-N. Wu, W. Yang, G.-R. Jin, N. Lambert, and F. Nori. “Quantum Fisher information as a signature of the superradiant quantum phase transition”. In: *New Journal of Physics* 16.6 (2014), p. 063039. DOI: 10.1088/1367-2630/16/6/063039. URL: <https://dx.doi.org/10.1088/1367-2630/16/6/063039>.
- [132] R. F. Werner. “Quantum states with Einstein-Podolsky-Rosen correlations admitting a hidden-variable model”. In: *Phys. Rev. A* 40 (1989), pp. 4277–4281. DOI: 10.1103/PhysRevA.40.4277. URL: <https://link.aps.org/doi/10.1103/PhysRevA.40.4277>.
- [133] T.-C. Yen, A. Ganeshram, and A. F. Izmaylov. “Deterministic improvements of quantum measurements with grouping of compatible operators, non-local transformations, and covariance estimates”. In: *npj Quantum Information* 9.1 (2023), p. 14. ISSN: 2056-6387. DOI: 10.1038/s41534-023-00683-y. URL: <https://doi.org/10.1038/s41534-023-00683-y>.
-

- [134] M. Yu, D. Li, J. Wang, Y. Chu, P. Yang, M. Gong, N. Goldman, and J. Cai. “Experimental estimation of the quantum Fisher information from randomized measurements”. In: *Phys. Rev. Res.* 3 (2021), p. 043122. DOI: [10.1103/PhysRevResearch.3.043122](https://doi.org/10.1103/PhysRevResearch.3.043122). URL: <https://link.aps.org/doi/10.1103/PhysRevResearch.3.043122>.
- [135] X.-D. Yu, S. Imai, and O. Gühne. “Optimal Entanglement Certification from Moments of the Partial Transpose”. In: *Phys. Rev. Lett.* 127 (2021), p. 060504. DOI: [10.1103/PhysRevLett.127.060504](https://doi.org/10.1103/PhysRevLett.127.060504). URL: <https://link.aps.org/doi/10.1103/PhysRevLett.127.060504>.
- [136] P. Zanardi. “Entanglement of quantum evolutions”. In: *Phys. Rev. A* 63 (4 2001), p. 040304. DOI: [10.1103/PhysRevA.63.040304](https://doi.org/10.1103/PhysRevA.63.040304). URL: <https://link.aps.org/doi/10.1103/PhysRevA.63.040304>.
- [137] P. Zanardi, M. G. A. Paris, and L. Campos Venuti. “Quantum criticality as a resource for quantum estimation”. In: *Phys. Rev. A* 78.4 (2008), p. 42105. DOI: [10.1103/PhysRevA.78.042105](https://doi.org/10.1103/PhysRevA.78.042105). URL: <https://link.aps.org/doi/10.1103/PhysRevA.78.042105>.
- [138] P. Zanardi, C. Zalka, and L. Faoro. “Entangling power of quantum evolutions”. In: *Phys. Rev. A* 62 (2000), p. 030301. DOI: [10.1103/PhysRevA.62.030301](https://doi.org/10.1103/PhysRevA.62.030301). URL: <https://link.aps.org/doi/10.1103/PhysRevA.62.030301>.
- [139] C. Zhang et al. “Detecting metrologically useful asymmetry and entanglement by a few local measurements”. In: *Phys. Rev. A* 96 (2017), p. 042327. DOI: [10.1103/PhysRevA.96.042327](https://doi.org/10.1103/PhysRevA.96.042327). URL: <https://link.aps.org/doi/10.1103/PhysRevA.96.042327>.
- [140] C.-J. Zhang, Y.-S. Zhang, S. Zhang, and G.-C. Guo. “Entanglement detection beyond the computable cross-norm or realignment criterion”. In: *Phys. Rev. A* 77 (2008), p. 060301. DOI: [10.1103/PhysRevA.77.060301](https://doi.org/10.1103/PhysRevA.77.060301). URL: <https://link.aps.org/doi/10.1103/PhysRevA.77.060301>.
- [141] T. Zhang, N. Jing, and S.-M. Fei. “Quantum separability criteria based on realignment moments”. In: *Quantum Information Processing* 21.8 (2022), p. 276. ISSN: 1573-1332. DOI: [10.1007/s11128-022-03630-6](https://doi.org/10.1007/s11128-022-03630-6). URL: <https://doi.org/10.1007/s11128-022-03630-6>.
- [142] D. Zhu et al. “Cross-platform comparison of arbitrary quantum states”. In: *Nature Communications* 13.1 (2022), p. 6620. ISSN: 2041-1723. DOI: [10.1038/s41467-022-34279-5](https://doi.org/10.1038/s41467-022-34279-5). URL: <https://doi.org/10.1038/s41467-022-34279-5>.
- [143] H. Zhu. “Multiqubit Clifford groups are unitary 3-designs”. In: *Phys. Rev. A* 96 (2017), p. 062336. DOI: [10.1103/PhysRevA.96.062336](https://doi.org/10.1103/PhysRevA.96.062336). URL: <https://link.aps.org/doi/10.1103/PhysRevA.96.062336>.
- [144] H. Zhu, R. Kueng, M. Grassl, and D. Gross. “The Clifford group fails gracefully to be a unitary 4-design”. In: *arXiv:1609.08172* (2016). URL: <https://arxiv.org/abs/1609.08172>.

